To the Graduate Council:

I am submitting herewith a thesis written by Christopher William Howard entitled "Investigating the evolution of two southern Appalachian terrane boundaries and a plutonic complex: Tectonic implications of structural, geochemical, and geochronologic studies in the central Georgia Inner Piedmont" I have examined the final electronic copy of this thesis for form and content and recommend that it be accepted in partial fulfillment of the requirements for the degree of Master of Science, with a major in Geology.

_____
Robert D. Hatcher, Jr., Major Professor

We have read this thesis
and recommend its acceptance:

_____
Harry Y. McSween

_____
Micah J. Jessup

Accepted for the Council

_____
Carolyn R. Hodges
Vice Provost and Dean of the Graduate School

Investigating the evolution of two southern Appalachian terrane boundaries and a plutonic complex: Tectonic implications of structural, geochemical, and geochronologic studies in the central Georgia Inner Piedmont

A Thesis
Presented for the
Master of Science Degree
University of Tennessee, Knoxville

Christopher William Howard
August 2012

Acknowledgements

Completion of this project would not have been possible without a great deal of mentoring, encouragement, and patience from my advisor Robert D. Hatcher, Jr.. His passion for Appalachian tectonics and geologic field work is contagious, and I believe I may have caught more than a little. I would like to thank Dr. Hap McSween for his guidance in understanding granite geochemistry and pluton emplacement in the southern Appalachians. Dr. Micah Jessup provided advice on interpreting quartz microstructures as well as compelling discussions about Himalayan geology. Working in the root of an orogenic belt is challenging, so it was always nice to talk with someone who works in an active collision zone.

Nancy Meadows truly deserves her own paragraph here. Nancy was a constant source of encouragement, chocolate, and psychiatric help when necessary. She reviewed every chapter in this thesis and probably sacrificed at least half a box of red pens while doing it. She was also always available to discuss the art of proper citation in scientific papers.

Thanks to Mike Higgins, Ralph Crawford, John Costello, Joe Hill, and Arthur Merschat for taking the time to participate in my field review. Thanks to the EDMAP program, The UT Science Alliance Center of Excellence, ExxonMobil, and the MAYO Foundation for financial support. None of my research would have been possible without their generous aid.

The Hatchery: Matt and Justin, thanks for being excellent field partners for two mapping seasons in lovely central Georgia. Matt, thanks for taking me under your wing during my first field season and showing the newbie how to map in polydeformed crystalline rocks. Arthur, Phillip, Annie, Kathleen, Mary, Brittany, and Heather thanks for helping me feel welcome and providing stimulating conversations about all things

geology (and sometimes not) related. Also, special thanks to Andrew Wunderlich for all of his cartography assistance. I don't think I would have been able to complete my map without you.

I would also like to thank the many landowners of Butts, Lamar, and Monroe Counties, Georgia, who graciously allowed me to wander around on their property in search of the ever elusive outcrop. A special thanks to Tommy Vaughn for access to his property and his enthusiasm for my project. Thanks to Dr. Randy Kath of the University of West Georgia who generously shared unpublished structural and lithologic data he has collected from two parcels within my study area.

Finally, I will be ever grateful to my family. Tonya, there is no way I would have been able to make it through all of this without your love, understanding, and encouragement. Yes, we are finally going to go on honeymoon. Torin and Logan, you two have sacrificed far too much personal time without even knowing it. Thanks to my parents, siblings, and in-laws for all of their encouragement. I will also be forever grateful to my "little" brother Andrew who has sacrificed floor space for me to sleep on for the better part of 14 months throughout this entire process. May I never have to sleep on your floor again.

Abstract

Detailed geologic mapping in the central Georgia Inner Piedmont has revealed a plutonic complex in the Cat Square terrane (CST) between the Brindle Creek and Towaliga faults ~80 km SE of Atlanta. The complex has an area ~235 km^2 and is composed of two distinct mappable granitoids. The High Falls Granite (HFG) is a Siluro-Devonian (424-380 Ma) porphyritic granite with characteristic blocky microcline megacrysts. The Indian Springs Granite (ISG, 313-299 Ma) has an equigranular, fine- to medium-grained texture. Some foliation in the HFG is concordant with regional trends, but a relict magmatic or secondary tectonic foliation was also observed in many parts of the pluton.

The location of two terrane boundaries was delineated during field mapping. The Brindle Creek fault and terrane boundary is a narrow (<30 m) mylonite zone that accommodated oblique-dextral strike-slip displacement likely during the Neoacadian orogeny. The Towaliga fault zone and terrane boundary formed as a dextral strike-slip fault, producing a wide (up to 1 km) mylonite zone during the Alleghanian orogeny. The Walker Top Granite (WTG, 407-357 Ma) in the North Carolina CST is roughly the same age, and is mineralogically, texturally, and geochemically similar to the HFG. This suggests the HFG and WTG may be consanguineous. Crystallization ages of the Walker Top Granite have been used as a proxy for the closure of the Cat Square remnant ocean basin in the northern Inner Piedmont.

Geochemical and geochronologic data suggest that the emplacement of the oldest portion of the HFG may not be coeval with the closing of the southern end of the Cat Square basin. Instead, the oldest portions of the HFG may have been generated above a subduction zone prior to the Acadian/Neoacadian collisional event, while the youngest portions of the HFG could have been generated by crustal anatexis when the Carolina superterrane was obducted onto the Laurentian + Taconian margin. If the

entire HFG batholith was generated by anatexis, obduction of the Carolina superterrane must have occurred well before the 424 Ma crystallization age of the oldest sample of HFG, requiring revision of tectonic models for the southern Appalachians.

Table of Contents

Chapter 1: Introduction.....1

Methodology.....2

Objectives.....3

Location.....3

Previous work.....8

Chapter 2: Rock Unit Descriptions.....10

Introduction.....10

Methodology.....10

Tugaloo Terrane.....11

Lower Tallulah Falls Formation.....11

Lithonia Gneiss.....12

Amphibolite.....13

Gondite.....14

Cat Square terrane.....14

Biotite gneiss.....17

Sillimanite schist.....20

High Falls Granite.....23

Indian Springs Granite.....25

Pine Mountain window.....27

Woodland gneiss.....27

Fault Rocks.....30

Towaliga mylonite.....30

Siliceous cataclasite.....32

Brindle Creek Fault mylonite.....35

Diabase dikes....36

Chapter 3: Geochemistry and Geochronology....37

Introduction....37

Granitoid Geochemistry....37

Major element chemistry....40

Trace element abundances....46

REE chemistry....48

Tectonic discrimination diagrams....50

Comparison of geochemistry of the High Falls and Walker Top Granites....58

Summary and interpretation of granite geochemistry....59

Granite geochronology....61

Geochronologic methodology....61

Zircon morphology....63

Geochronologic results....76

Zircon REE concentrations....78

Summary and results of granite geochronology....78

Synthesis of granite geochemistry and geochronology....80

Chapter 4: Metamorphism....83

Introduction....83

Field and petrographic evidence of metamorphism....85

Thermobarometry of selected samples....88

Garnet-biotite thermometry....89

Zircon saturation thermometry....90

Garnet-plagioclase-hornblende-quartz barometry....90

Conclusions....92

Chapter 5: Structure and Tectonics....93

Introduction....93

Tectonic Framework....96

Major structures in the research area....98

Brindle Creek fault....98

Towaliga fault....98

Tectonic evolution of the southern Appalachians....102

Tectonostratigraphic terranes in the project area....108

Tugaloo terrane....106

Cat Square terrane....107

Pine Mountain window....108

Structural observations....110

Fabrics....110

Folds....115

Microstructures....115

Interpretation of structural data....120

D_1....126

D_2....128

D_3....130

D_4....131

D_5....131

D_6....132

Chapter 6: Conclusions.....133

Synthesis of structural, geochronologic, and geochemical analysis.....133

Important points.....136

References cited.....138

Appendices.....152

List of Figures

Chapter 1

Figure 1-1. Location map of the project area....4
Figure 1-2. Mapped area and quadrangle boundaries....5
Figure 1-3. Physiographic provinces of the southern Appalachians....7
Figure 1-4. Nearby mapping credit....9

Chapter 2

Figure 2-1. Lithonia gneiss....13
Figure 2-2. Outcrop and hand sample of amphibolite....15
Figure 2-3. Thin section images of amphibolite....16
Figure 2-4. Biotite gneiss outcrop photographs....18
Figure 2-5. Biotite gneiss thin section images....19
Figure 2-6. SIllimanite schist saprolite outcrop and hand sample photograph....21
Figure 2-7. Schist thin section images....22
Figure 2-8. High Falls Granite outcrop photographs....24
Figure 2-9. High Falls Granite thin section images....26
Figure 2-10. Modal abundances of Indian Springs Granite and Strekeisen diagram....27
Figure 2-11. Indian Springs Granite outcrop and hand sample photos....28
Figure 2-12. Indian Springs Granite thin section images....29
Figure 2-13. Woodland Gneiss outcrop photographs....31
Figure 2-14. Towaliga mylonite outcrop and thin section photographs....33
Figure 2-15. Siliceous cataclasite outcrop and hand sample photographs....34

Chapter 3

Figure 3-1. Simplified geologic map showing location of geochemical samples.....39
Figure 3-2. Granitoid classification “feldspar triangle”.....43
Figure 3-3. Harker diagrams of major elements.....45
Figure 3-4. Harker diagrams of trace elements.....47
Figure 3-5. Spider diagram of mantle-normalized trace elements.....49
Figure 3-6. Spider diagram of chondrite normalized REE.....50
Figure 3-7. Tectonic discrimination diagrams after Pearce et al. (1984).....52
Figure 3-8. Tectonic discrimination diagram after Harris et al. (1986).....53
Figure 3-9. Tectonic discrimination diagrams after Frost et al. (2001).....56
Figure 3-10. Simplified geologic map showing location of geochronology samples.....62
Figure 3-11. Geochronologic data for High Falls Granite sample BG18.....65
Figure 3-12. Geochronologic data for High Falls Granite sample HHF.....67
Figure 3-13. Geochronologic data for High Falls Granite sample HFSP.....70
Figure 3-14. Geochronologic data for High Falls Granite sample S123.....72
Figure 3-15. Geochronologic data for High Falls Granite sample FRHF.....74
Figure 3-16. Representative REE concentrations of zircons analyzed.....79

Chapter 4

Figure 4-1. Metamorphic timing map.....84
Figure 4-2. Stromatic migmatite outcrop photograph.....86
Figure 4-3. Chloritized biotite thin section image.....88
Figure 4-4. Garnet-biotite thermometry locations for IS370.....90
Figure 4-5. Pavement outcrop of High Falls Granite.....91

Chapter 5

Figure 5-1. Tectonic assembly diagram for the southern and central Appalachians....95
Figure 5-2. Physiographic provinces of the southern Appalachians....96
Figure 5-3. Nearby mapping credit....99
Figure 5-4. Simplified geologic map of the project area....100
Figure 5-5. Large rhomb of cataclasite along the Towaliga fault....102
Figure 5-6. Geologic map of the Pine Mountain window....109
Figure 5-7. Examples of foliation....111
Figure 5-8. Outcrop photographs showing mineral stretching lineations....113
Figure 5-9. Outcrop photographs of Brindle Creek mylonite....114
Figure 5-10. Stereonets of foliation and lineation data....116
Figure 5-11. Outcrop photographs of folds....117
Figure 5-12. Outcrop photographs of folds in schist....118
Figure 5-13. Stereonets of fold data....119
Figure 5-14. Schistose metagraywacke thin section images....121
Figure 5-15. Towaliga mylonite and high temperature mylonite thin section images....123
Figure 5-16. Form line map....125
Figure 5-17. Summary of timing of deformation....127

List of Tables

Table 3-1. Geochemical data....41
Table 3-2. CIPW normative compositions for High Falls and Indian Springs Granites....43

Table 3-3. Classification of granitoids rocks after Frost et al. (2001).....55
Table 3-4. Zircon morphologies.....64

List of Attachments

Plate 1: Detailed Geologic Map of the High Falls, and Portions of the Indian Springs and Locust Grove 7.5-Minute Quadrangles, Georgia.

Chapter 1: Introduction

The Appalachians have been the subject of intense geologic study since the middle of the 19th Century. Then and now, this orogen is studied to unravel its developmental history, and to locate valuable resources to improve society. The Appalachians emerge from beneath the Coastal Plain in central Alabama and define a sinuous trace northward to the coasts of Newfoundland. The chain has been characterized as “the most elegant on Earth” (King, 1970). The orogen has a history that begins with the breakup of the supercontinent Rodinia in the Neoproterozoic and ends with formation of supercontinent Pangea during the Permian (Hatcher et al., 2007a). Three orogenies occurred between the times of the supercontinents, and were characterized by accretion of suspect and exotic terranes to the passive margin of eastern North America. While this is indeed a complex history, much of the evidence is preserved in the internides and sediment-filled basins along its flanks. The Inner Piedmont is home to the polydeformed Neoacadian core of the Appalachians. The rocks here have been uplifted from depths that produced sillimanite-grade metamorphism.

Detailed field mapping is a cornerstone to understanding the geologic history of any area, and is even more critical when the area has undergone several orogenies. Field mapping alone, however, is not enough to truly understand the complex history of these rocks. Techniques of modern geochemical and geochronologic analysis must also be employed to help formulate and refine models, and test hypotheses that are developed in the field. One of the most valuable lessons I have learned while studying geology is that even when things do not make sense initially, the relationships of structure and lithologies will become clear with continued collection of quality data. Producing a detailed geologic map in the Inner Piedmont of Georgia at 1:24,000 scale

was a major portion of my thesis work (Plate 1). While the map is only one component of the thesis, it provides a most valuable context for the other components. Without this context, petrologic, geochemical, and geochronologic analyses would merely plot points on graphs. The intent of this thesis is to integrate detailed geologic mapping and structural analysis with laboratory data to thoroughly describe the geology of my study area, and to discuss my results and their impact on our understanding of the tectonic history of the Inner Piedmont and the southern Appalachians.

Methodology

The field mapping component of my thesis work took place over ~10 months during the winter and springs of 2010 and 2011. A detailed geologic map of the High Falls and portions of the Indian Springs and Locust Grove quadrangles covering ~180 km^2 of the Georgia Inner Piedmont was the final product of the mapping component of my thesis (Plate 1). Structural measurements were stored in a Trimble GeoXT™ handheld differential GPS unit. With the exception of the Trimble™, mapping was accomplished using the same tools field geologists have employed for the past 100 years: a Brunton™ compass, rock hammer, hand lens, field book, topographic map, and good field boots. Station data were compiled using ESRI ArcMap™ GIS software. Geologic data were exported from ArcMap and compiled in Adobe Illustrator™ to complete the geologic map. Rock specimens transported to Knoxville were selected for representative hand samples, thin sections, and geochemical and geochronologic analysis. Sample processing took place at The University of Tennessee-Knoxville, The University of North Carolina–Chapel Hill, Vanderbilt University, and Stanford University. U-Pb age dating of zircons was conducted with the Sensitive High Resolution Ion Microprobe Reverse Geometry (SHRIMP-RG) lab at Stanford University. Detailed descriptions of sample preparations are included in pertinent chapters in this thesis.

Objectives

The following major goals were formulated for my research.

1. Produce a detailed geologic map of portions of the High Falls, Indian Springs, and Locust Grove quadrangles in central Georgia.
2. Trace the Brindle Creek and Towaliga faults southwest of areas previously mapped in the Georgia Inner Piedmont through the study area.
3. Analyze structural data collected during mapping and interpret deformation history of the project area.
4. Collect representative samples of major units in the Cat Square terrane for petrographic analysis.
5. Conduct bulk chemical analysis of High Falls Granite and Indian Springs Granite.
6. Date samples of the High Falls Granite using the USGS-Stanford-SHRIMP lab at Stanford University.
7. Determine if the High Falls Granite in my study area may be equivalent to the Walker Top Granite in North Carolina.
8. Compare my findings with previous work from the Cat Square terrane in Georgia and North Carolina to attempt to refine tectonic models of the Inner Piedmont and southern Appalachians.

Location

The project area is located ~82 km southeast of Atlanta, Georgia (Fig. 1-1), is centered around High Falls State Park, and covers portions of Butts, Lamar, and Monroe Counties. Interstate 75, GA Hwy 36, GA Hwy 42, and GA Hwy 16 provide easy access to the field area. Indian Springs State Park and Dauset Trails Nature Center

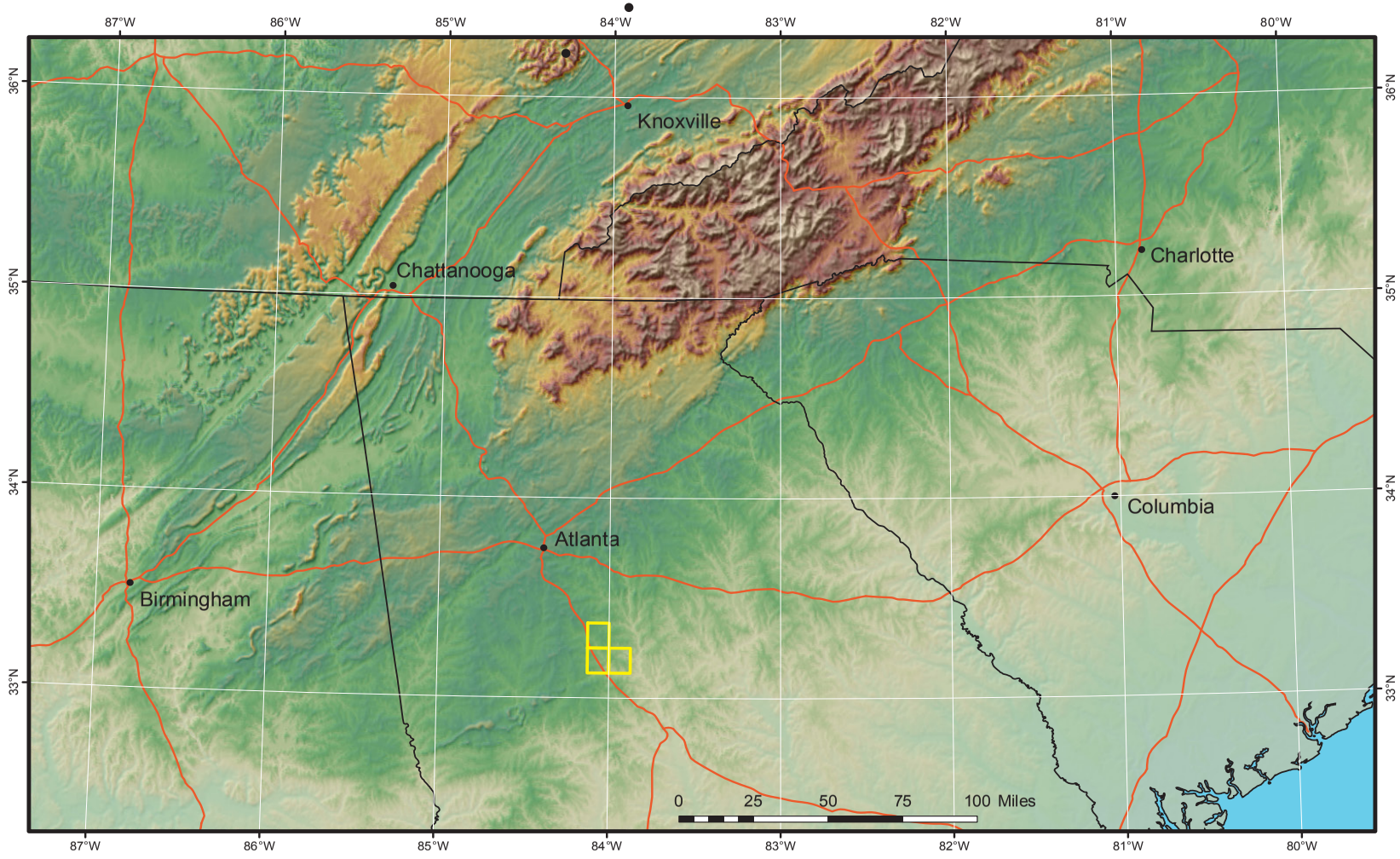


Figure 1-1. A location map of the project area. Quadrangles involved in this project are outlined in yellow (counterclockwise from NE; Locust Grove, High Falls, and Indian Springs quadrangles).

occur in the northeastern part of the study area. The Towaliga River flows from the northwest to southeast across the middle of the field area and is impounded to form High Falls Lake. High Falls State Park surrounds the southeastern portion of the lake and the region immediately downstream of the dam. The project area was originally restricted to the High Falls quadrangle, but was subsequently modified to include the unmapped NW portion of the Indian Springs quadrangle (R.D. Hatcher, Jr., unpublished data). The northwestern corner of the High Falls quadrangle was eliminated from the project area, while portions of the Indian Springs and Locust Grove quadrangles were added (Fig. 1-2). After modification, the completed project area covers ~180 km^2 (~70 mi^2) and adjoins another project area recently mapped at 1:24,000-scale in the Georgia Inner Piedmont immediately to the northeast in the Jackson quadrangle (M.T. Huebner). Additional mapping is in progress southwest of my project area (J.R. Rehrer,

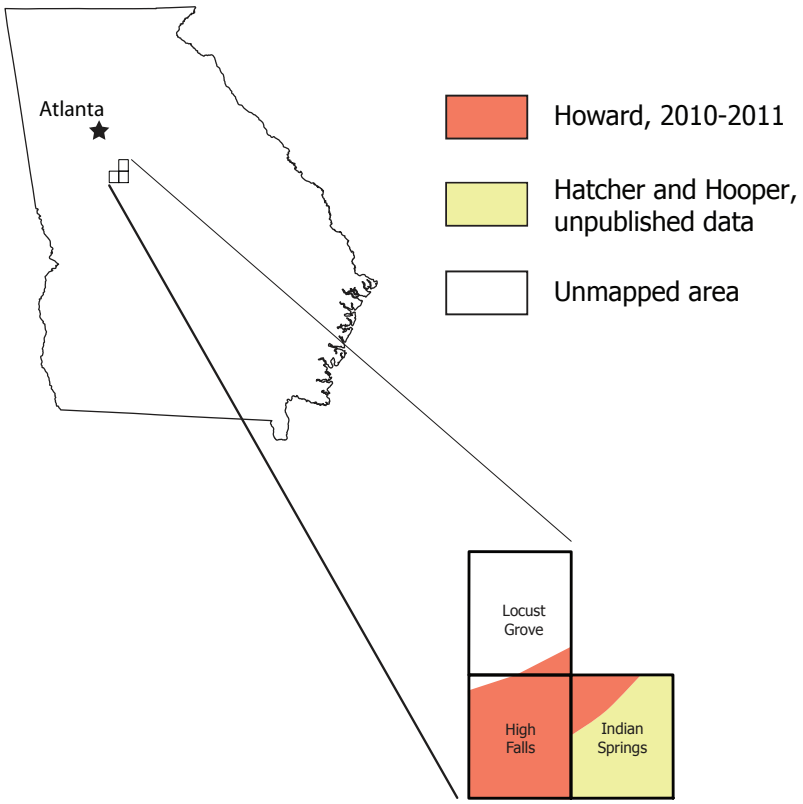


Figure 1-2. The mapped area is highlighted in red. The quadrangle boundaries abut previously mapped or unmapped areas.

in progress).

This project was conducted in the southern Appalachians. The Appalachian orogen was created by a series of at least three diachronous, accretionary, and collisional events along the eastern Laurentian margin after the breakup of supercontinent Rodinia (960-565 Ma) (Aleinikoff et al., 1995; Graybill, 2012). The Piedmont is a physiographic province in the southern Appalachians, which extends from the southeastern edge of mountainous (Blue Ridge) topography to the Coastal Plain, although Piedmont rocks continue eastward beneath the Coastal Plain (Fig 1-3). The Tugaloo terrane (eastern Blue Ridge and Inner Piedmont) and Carolina superterrane compose the Piedmont. The Carolina superterrane is made up of Perigondwanan Neoproterozoic to Cambrian volcanic-arc rocks that were accreted to the Laurentian-Taconian continental margin during the Devonian-Mississippian Acadian-Neoacadian orogeny. The Inner Piedmont consists of the eastern Tugaloo terrane (all Tugaloo terrane rocks east of the Brevard fault zone), Cat Square terrane, and Pine Mountain window, and is continuous from central Alabama to near Winston-Salem, North Carolina (Merschat and Hatcher, 2007). Inner Piedmont rocks are the Neoacadian metamorphic core, and are exposed for approximately 700 km along strike and for approximately 100 km from the Brevard fault zone to the northwest to the central Piedmont suture to the southeast. Peak metamorphism in the core of the Inner Piedmont reached upper amphibolite facies, making the Appalachian Inner Piedmont one of the largest areas of exposed sillimanite-grade rocks in the world (Hatcher, 2004). The Inner Piedmont can be further subdivided into eastern and western segments that are juxtaposed along the Brindle Creek fault. The Pine Mountain window, which exposes an uplifted block of Grenville basement and Paleozoic(?) cover (Steltenpohl et al., 2010), is also located in the eastern Inner Piedmont from ~8 km south of Flovilla, Georgia, to central Alabama (Steltenpohl et al., 2010). A more detailed summary of southern Appalachian tectonics is

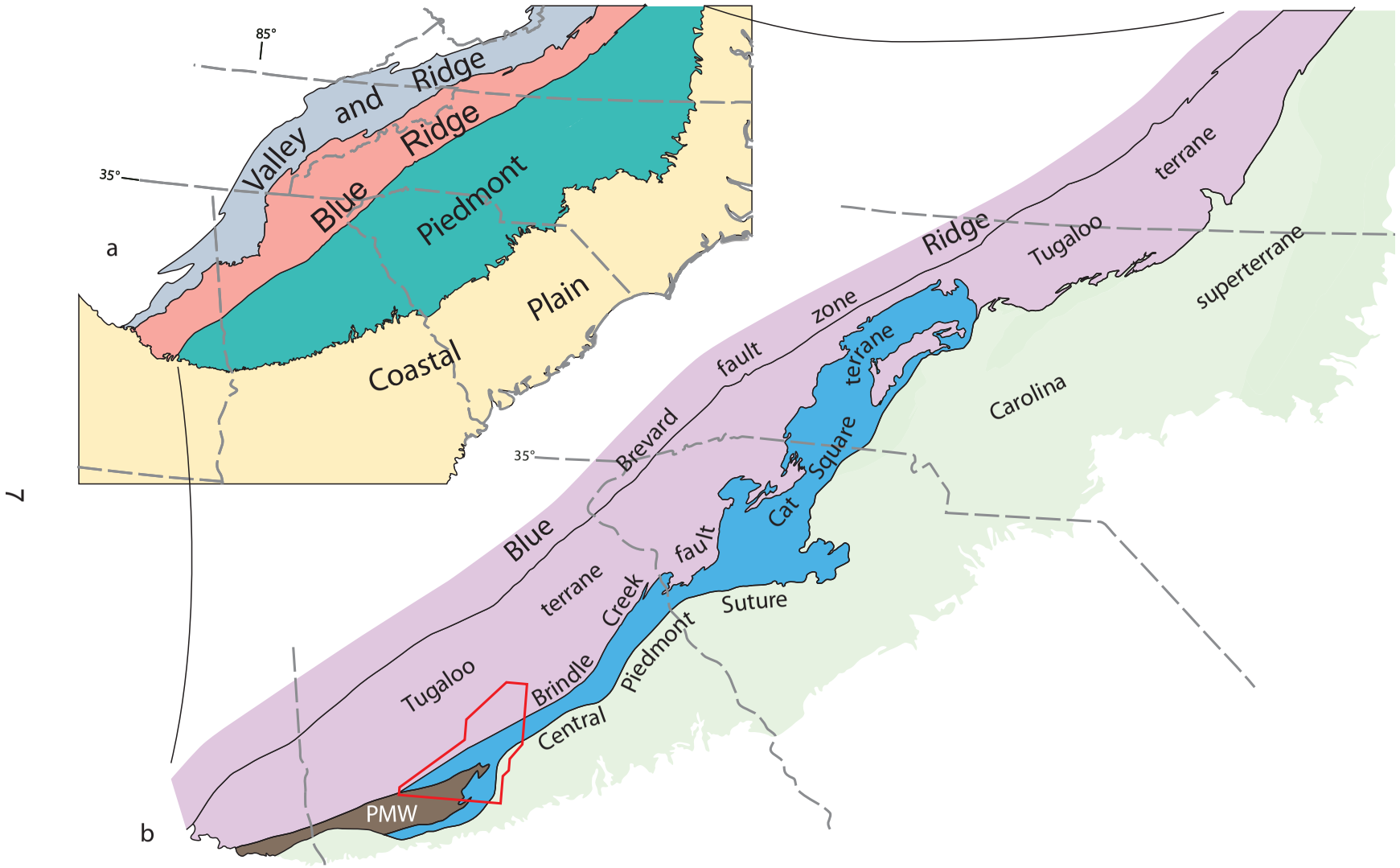


Figure 1-3. Index maps of the southern Appalachians showing the location of the study region. (a) Small scale physiographic map of the composite Piedmont and eastern Blue Ridge geologic provinces. (b) Tectonic map showing the terranes in the vicinity of the study area. Compiled mapped area in Figure 1-4 outlined in red. PMW—Pine Mountain window. Area outlined in red is the extent of Figure 1-4. Both images modified from Huebner et al. (2011).

included at the beginning of Chapter 5**.**

Previous work

Historically, detailed geologic mapping in the Inner Piedmont was largely avoided because of a perceived lack of exposure. While exposure in the central Georgia Inner Piedmont is not as good as exposure in the U.S. desert southwest (aside from Quaternary-sediment-filled basins), outcrops are still possible to locate and are more than adequate to produce high-quality geologic maps. Data can be collected for a geologic map from sources other than solid rock outcrops. Lithologic and structural data can be collected from saprolite outcrops, and it is possible to map contacts using float as well as variations in soil type. Large quantities of data have been collected in and around my field area. Watson (1902) compiled descriptions of granites and gneisses across Georgia. His report contained descriptions of the Lithonia Gneiss, which has been mapped in the Tugaloo terrane in my field area. McConnell and Abrams (1984) produced a small-scale geologic map of a large area around Atlanta that extended southward into Butts County to just north of my project area. Hatcher and Hooper (1989, unpublished data) produced a detailed geologic map from the Towaliga fault southward in the Indian Springs quadrangle. Atkins and Lineback (1992) produced a small-scale map of the Cedar Rock complex. This map covered portions of 18 7.5-minute quadrangles northwest of the Towaliga fault (including High Falls, Indian Springs, and Locust Grove), and the High Falls Granite was named in their study. Atkins and Lineback (1992) concluded that all of the metasedimentary rocks in my field area are part of a contact aureole created by the emplacement of the High Falls Granite. Davis (2010) mapped the Farrar and a portion of the Mansfield 7.5-minute quadrangles, and Huebner (unpublished data) mapped portions of the Jackson, Lloyd Shoals Dam, Stewart, and Worthville 7.5-minute quadrangles at 1:24,000 scale. Additional sources of

nearby mapping data are shown in Figure 1-4.

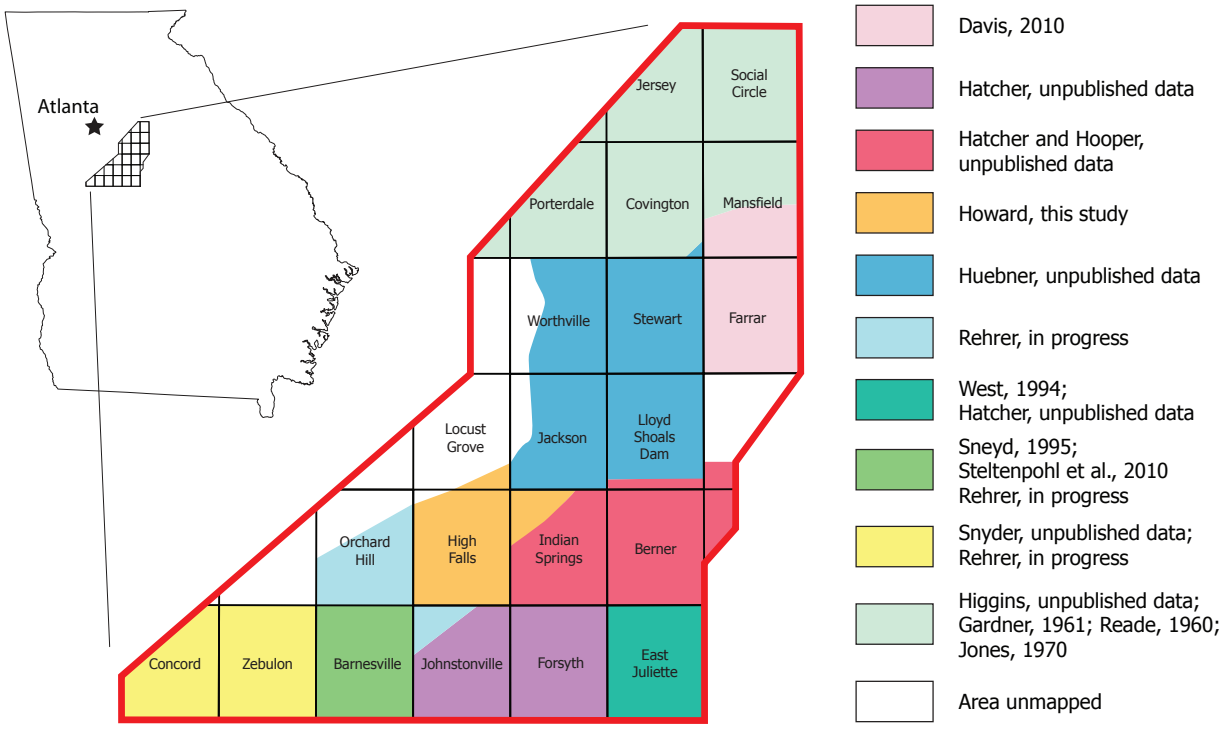


Figure 1-4. Mapping credit map (modified from Huebner et al., 2011).

Chapter 2: Rock Unit Descriptions

Introduction

Portions of the Tugaloo terrane, Cat Square terrane, and Pine Mountain window terrane were mapped as a part of this study (Plate I). The Neoproterozoic-Cambrian(?) lower Talullah Falls Formation and the Ordovician Lithonia gneiss were mapped in the Tugaloo terrane. The Cat Square terrane is composed of two Siluro-Devonian metasedimentary units, sillimanite schist and biotite gneiss. These metasedimentary rocks were intruded by the Siluro-Devonian High Falls Granite and the Pennsylvanian-Permian Indian Springs Granite. The Middle Proterozoic Woodland Gneiss is the only unit mapped inside the Pine Mountain window as a part of this study. The Brindle Creek fault separates the Tugaloo terrane from the Cat Square terrane, and the Towaliga fault zone is the boundary between the Cat Square terrane and the northwestern corner of the Pine Mountain window. These boundaries were delineated by identifying characteristic fault rocks.

Methodology

I described major phases, rock texture, and soil color at outcrops of each mappable unit; characteristic soil color helped identifiy rock units when outcrops of fresh material or saprolite were not available. I collected hand samples of each mappable unit in the project area for study at The University of Tennessee. High resolution photographs of outcrops and hand samples were taken with an 8.0 mega pixel digital camera. Many of the photographs in this chapter were enhanced using Adobe Photoshop™.

Billets were cut from hand samples and were shipped to Idaho Petrographics where 26 thin sections were made. Most thin sections were covered with glass slips, but several were left uncovered and double polished for scrutiny in the electron microprobe

laboratory at The University of Tennessee. Thin section photographs were taken with a Nikon digital camera attached to the Leitz Orthoplan Pol petrographic microscope. These photographs were then color- and contrast-balanced using Nikon image enhancement software. Point counts of two thin sections of Indian Springs Granite were made with a mechanical stage and using a 0.6 mm step on the petrographic microscope.

Tugaloo Terrane

The Tugaloo terrane consists of metamorphosed sedimentary rocks that were originally deposited on the Laurentian passive margin from the Neoproterozoic in the Ordovician (Hatcher et al., 2007a). The eastern part of the terrane is made up of the Tallulah Falls Formation. In northeastern Georgia Hatcher (1971a) identified a four-part stratigraphy in the Tallulah Falls Formation: basal graywacke-schist-amphibolite, garnet-aluminous schist, graywacke-pelitic schist, and an upper quartzite-schist member; the latter subsequently separated from the main unit. The lower member of the Tallulah Falls Formation is exposed in the study area, and consists of metagraywacke and sillimanite schist with interlayered amphibolite. The rocks were metamorphosed and intruded by granitoids during the Ordovician Taconian orogeny. In the study area, the Tallulah Falls Formation has been intruded by the Lithonia Gneiss (Watson, 1902).

Lower Tallulah Falls Formation

Only the lower member of the Tallulah Falls Formation is present in the Tugaloo terrane in the project area and makes up approximately two-thirds of the Tugaloo terrane. It consists of strongly foliated metagraywacke with interlayered sillimanite schist and amphibolite. Sillimanite schist and amphibolite in the field area do not form bodies large enough to map as separate units at 1:24,000 scale. Outcrops typically weather

to a deep red soil where the material is primarily metagraywacke, but tend to be red-brown or red-orange where schist is more abundant. A deep purple hue is common in zones where sillimanite is concentrated in the metasedimentary units. In the study area, metagraywacke layers range from 1 cm to over 10 m thick, vary from medium- to coarse-grained, and have a strong foliation defined by the orientation of quartz, feldspar An_{25-30} (Davis, 2010) porphyroclasts, and phyllosilicates. The primary phases are quartz, plagioclase, potassium feldspar, biotite, and muscovite. Rounded feldspar porphyroclasts up to 1 cm in size are common. Accessory phases include garnet, zircon, and opaques. Chlorite is also common in weathered samples and is assumed to be a product of retrograde metamorphism. Migmatitic metagraywacke is common throughout the unit, and is most abundant near the Brindle Creek fault. The migmatite is characterized by melt of roughly granitic composition that is interlayered with the metasedimentary material.

Lithonia Gneiss

The Lithonia Gneiss has been described as “highly contorted granite-biotite gneiss” (Watson, 1902) and its exposures constitute the additional one-third of the area mapped in the Tugaloo terrane as part of this research. Lithonia Gneiss typically forms pavement outcrops, which vary from one meter to tens of meters wide. Kilometer-scale outcrops can be found northeast of the study area (e.g., Arabia Mountain State Park), and fresh roadcuts can reveal rounded boulders up to 1.5 m. Biotite schlieren form obvious compositional layering and the characteristic deformed foliation in the Lithonia Gneiss is easily observed. Foliation can vary from moderate to very strong (Fig. 2-1) from one outcrop to another. The soil weathers red-orange to yellow-orange color, and relict feldspar megacrysts can sometimes be identified. The Lithonia Gneiss is a medium- to coarse-grained, massively layered granitoid with rounded to blocky feldspar

megacrysts up to 3 cm in length. Quartz, feldspar, biotite, muscovite, and occasional garnet make up the major phases visible in hand sample. Garnetiferous zones parallel to foliation composed of fine-grained garnet up to 5 cm wide and 50 cm long are also present locally.

Amphibolite

One of the distinguishing characteristics of the lower Tallulah Falls Formation is the relative abundance of amphibolite. Boudins ranging from 10 cm to 5 m are present throughout the lower Tallulah Falls Formation. Hornblende, biotite, garnet, and quartz are visible in hand specimen. Amphibolite is susceptible to rapid chemical weathering



Figure 2-1. Lithonia Gneiss with foliation defined by aligned quartz-feldspar layers and biotite-rich schlieren.

and typically produces a deep red saprolite. Amphibolite bodies in the Cat Square terrane (Fig. 2-2) are not as common, but appear to be very similar texturally and mineralogically in hand sample to those in the Tugaloo terrane. Thin sections (Fig. 2-3) reveal poorly developed foliation and a matrix of hornblende, plagioclase, potassium feldspar, biotite, muscovite, quartz, and garnet.

Gondite

Gondite consists of metamorphosed manganese silicate (Roy and Purkait, 1968), and typically occurs as isolated interlayers and boudins less than 0.5 m wide. Gondite boudins were noted, but they did not constitute enough material to warrant being mapped as a separate unit in the study area. In contrast, M.T. Huebner (personal comm.) mapped continuous “beds” of gondite in the Jackson, Stewart, and Worthville quadrangles farther northeast. Gondite is either not as abundant or not well enough exposed to be mapped as a continuous unit in the Locust Grove and High Falls quadrangles. Boudins of gondite are brown to red-brown and are quite dense and tenacious. Once a fresh surface is exposed it is obvious that the gondite is composed almost entirely of quartz and garnet.

Cat Square Terrane

The contact between the Tugaloo and Cat Square terranes is the Brindle Creek fault, which was first recognized in the North Carolina Inner Piedmont (Giorgis, 1999), and age dating of detrital zircon samples from southeast of the fault confirmed it was a terrane boundary (Bream et al., 2001). Major units exposed in the Cat Square terrane of central Georgia include Silurian-Devonian metasedimentary rocks and a plutonic complex made up of the Silurian-Devonian High Falls Granite and Mississippian-Permian Indian Springs Granite. The High Falls Granite covers an area of at least 235



Figure 2-2. (a) Looking northeast, an outcrop of garnet-amphibolite in the Towaliga River in High Falls State Park ~400 m downstream of High Falls Road; note interlayered pegmatite and contact with High Falls Granite in lower left of photograph, and GPS unit in upper center. (b) Hand sample of amphibolite from the same location as photograph (a).

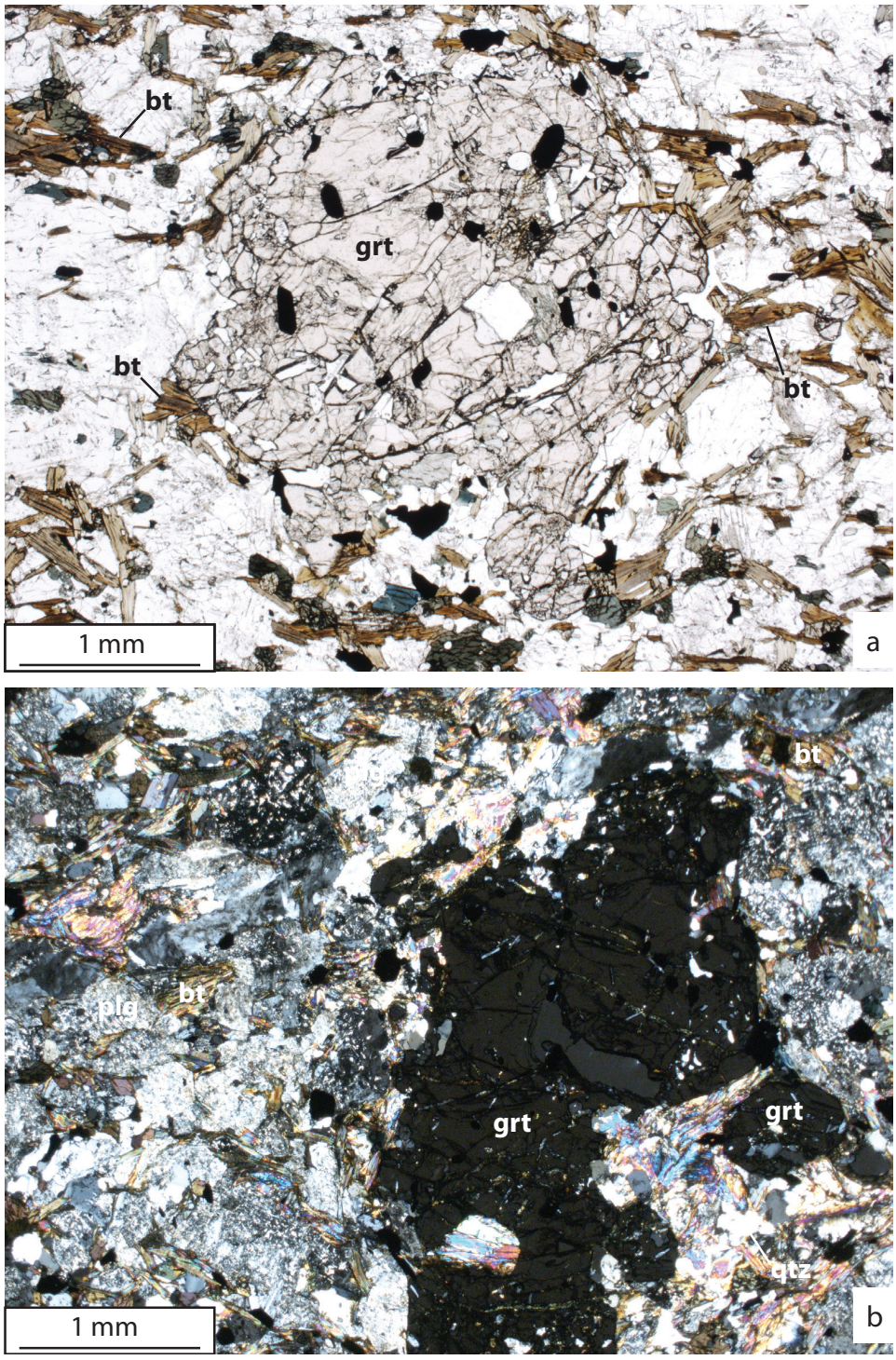


Figure 2-3. Thin section images of Cat Square terrane garnet-amphibolite. (a) Garnet with numerous opaque inclusions. Plane light. (b) Thin section showing garnet with opaque inclusions, biotite, and sericitized plagioclase An_{50}. bt-biotite; grt-garnet; plg-plagioclase; qtz-quartz. Both samples collected from exposure in Towaliga River ~400 m downstream of High Falls Road in High Falls State Park Road. Crossed nicols.

km^2, and geochemical and geochronologic analyses (Chapter 3) suggest that it is a composite pluton. The metasedimentary rocks of the Cat Square terrane are unique in the Inner Piedmont, because they contain zircons with provenance from both Laurentian and peri-Gondwanan sources.

Biotite Gneiss

Biotite gneiss (Fig. 2-4) is one of two metasedimentary units mapped in the Cat Square terrane, and outcrops cover approximately 10 percent of the project area between the Brindle Creek and Towaliga faults. Outcrops of relatively fresh biotite gneiss are commonly found in streams but are occasionally exposed in fresh roadcuts. Biotite gneiss xenoliths are also common in the High Falls Granite and range from a few cm to several m. These xenoliths typically have been partially melted. Biotite gneiss is usually strongly foliated and varies from fine- to medium-grained metagraywacke and medium- to coarse-grained migmatite in the Cat Square terrane. Like the lower Talullah Falls, migmatization of the biotite gneiss appears to increase near faults and contacts shared with the High Falls Granite. Textural variations are related to the degree of partial melting that affected the rock during metamorphism. Weathering produces soil with a characteristic deep red color, which is a product of high iron content. The biotite gneiss is primarily composed of quartz, biotite, plagioclase An_{24-31}, and K-feldspar. The accessory minerals, garnet, muscovite, and chlorite can also be identified in hand sample. Feldspar porphyroclasts are commonly well rounded and often have tails produced by simple shear that occurred throughout the metasedimentary units in the Cat Square terrane. Biotite gneiss protomylonite is often found near major ductile faults and S-C fabric is present in thin sections of these rocks (Fig. 2-5). Pegmatite veins also crosscut across bodies of biotite gneiss in and around zones of intense migmatization. These were likely produced by fluids released from breakdown of phyllosilicates during

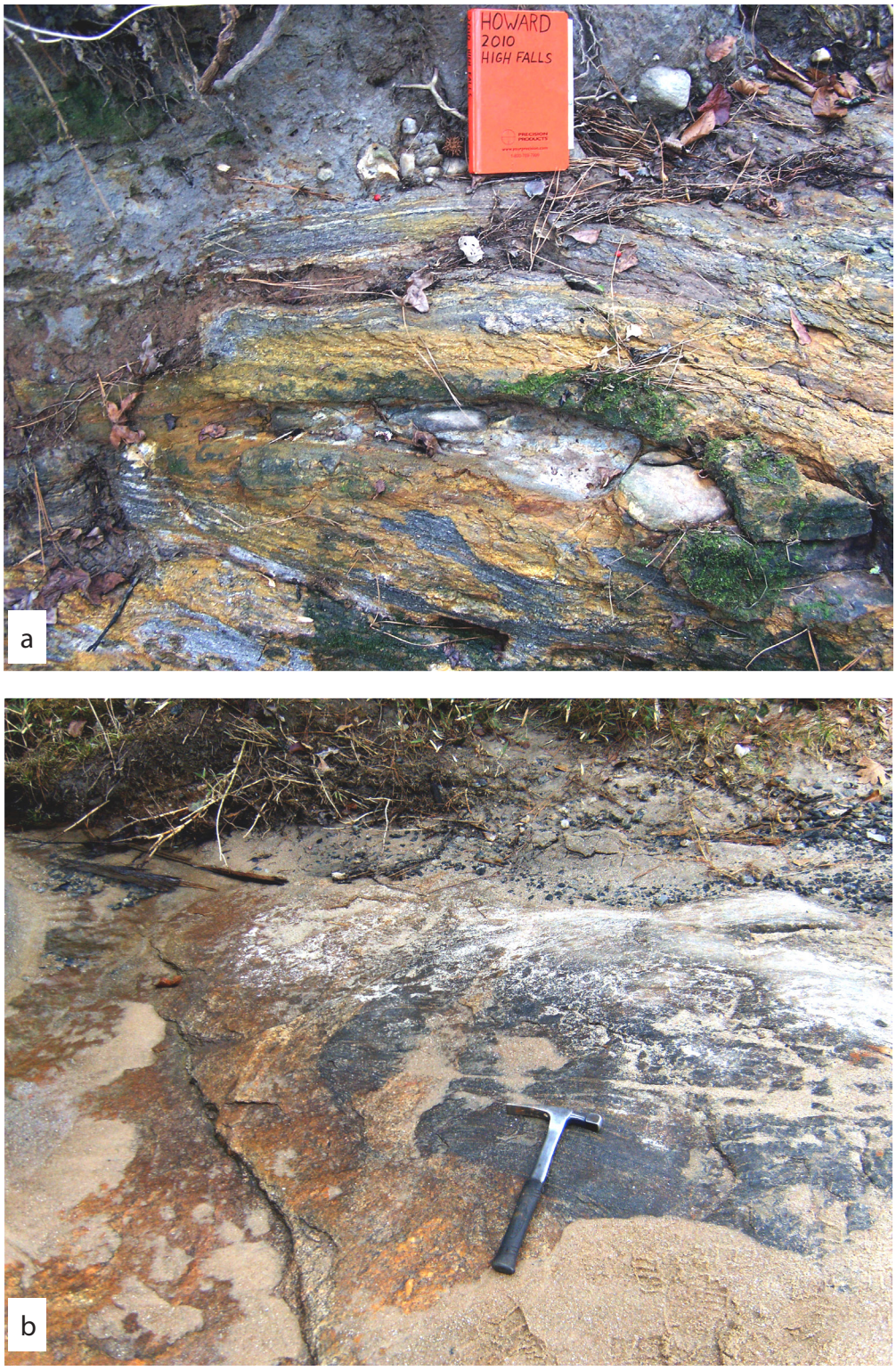


Figure 2-4. (a) Tightly folded biotite gneiss ~450 m west of intersection of I-75 and Buck Creek, looking northeast. (b) Biotite gneiss xenolith in a large body of High Falls Granite at the intersection of Hickory Ridge Road and Horseshoe Bend, looking north.

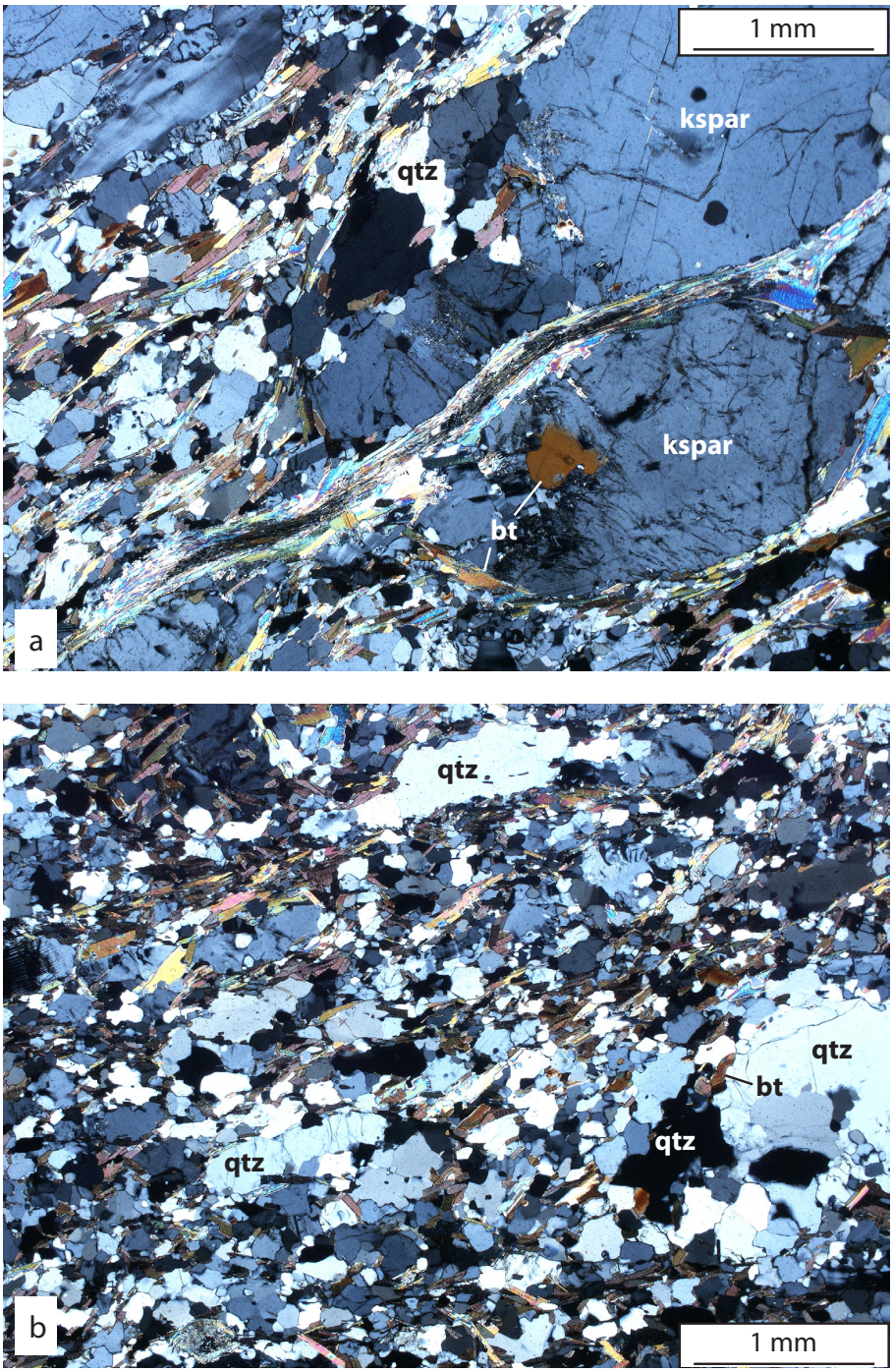


Figure 2-5. Biotite gneiss thin sections from sample collected ~550 m west of intersection of Buck Creek and Chappel Mill Road. Crossed nicols. (a) Rounded K-feldspar porphyroclasts surrounded by a matrix of quartz, potassium feldspar, and biotite. Quartz grains appear to have undergone grain boundary migration. (b) Annealed quartz grains surround biotite crystals that define an S-C fabric. bt-biotite; kspar-potassium feldspar; qtz-quartz.

metamorphism or by magmatic fluids from nearby intrusive bodies.

Sillimanite Schist

The second metasedimentary unit in the Cat Square terrane is sillimanite schist. A large body of sillimanite schist has been mapped in the High Falls quadrangle, and trends southwest to northeast parallel to regional foliation (Plate I). Outcrops of this unit (Fig. 2-6) make up approximately one quarter of the area mapped in the Cat Square terrane. Hand samples reveal muscovite, biotite, quartz, feldspar, garnet, and sillimanite in varying amounts. Interlayers of biotite gneiss and lenses of granitic melt are also common (Fig. 2-6). There is a fine line between classifying a specimen as schistose metagraywacke or as quartz-rich schist, even with fresh samples. Outcrops of fresh schist are rare in the mapped area because the rock is highly susceptible to chemical weathering. High annual rainfall in the Georgia Inner Piedmont combined with low topographic relief produces a deep weathering profile in metapelite bodies. Outcrops in deeply eroded streams expose the freshest material, but thin sections of samples collected in these locations reveal decomposition of micas and feldspars. The schist weathers to a variety of brown soils in the field area. Medium- and orange-brown soils are common if the schist contains little sillimanite or biotite. Elevated biotite concentrations result in the addition of a red hue, while sillimanite produces an iridescent purple soil (Fig. 2-6). Muscovite, garnet, and sillimanite are more resistant to chemical weathering and are preferentially preserved in the soil. The schist is very strongly foliated, and saprolite outcrops in ditches and unpaved roadbeds are still very useful for collecting structural data. Several hundred structural measurements were collected from this type of exposure. Thin sections of sillimanite schist (Fig. 2-7) reveal complex textures formed by intense deformation and dynamic recrystallization of quartz.

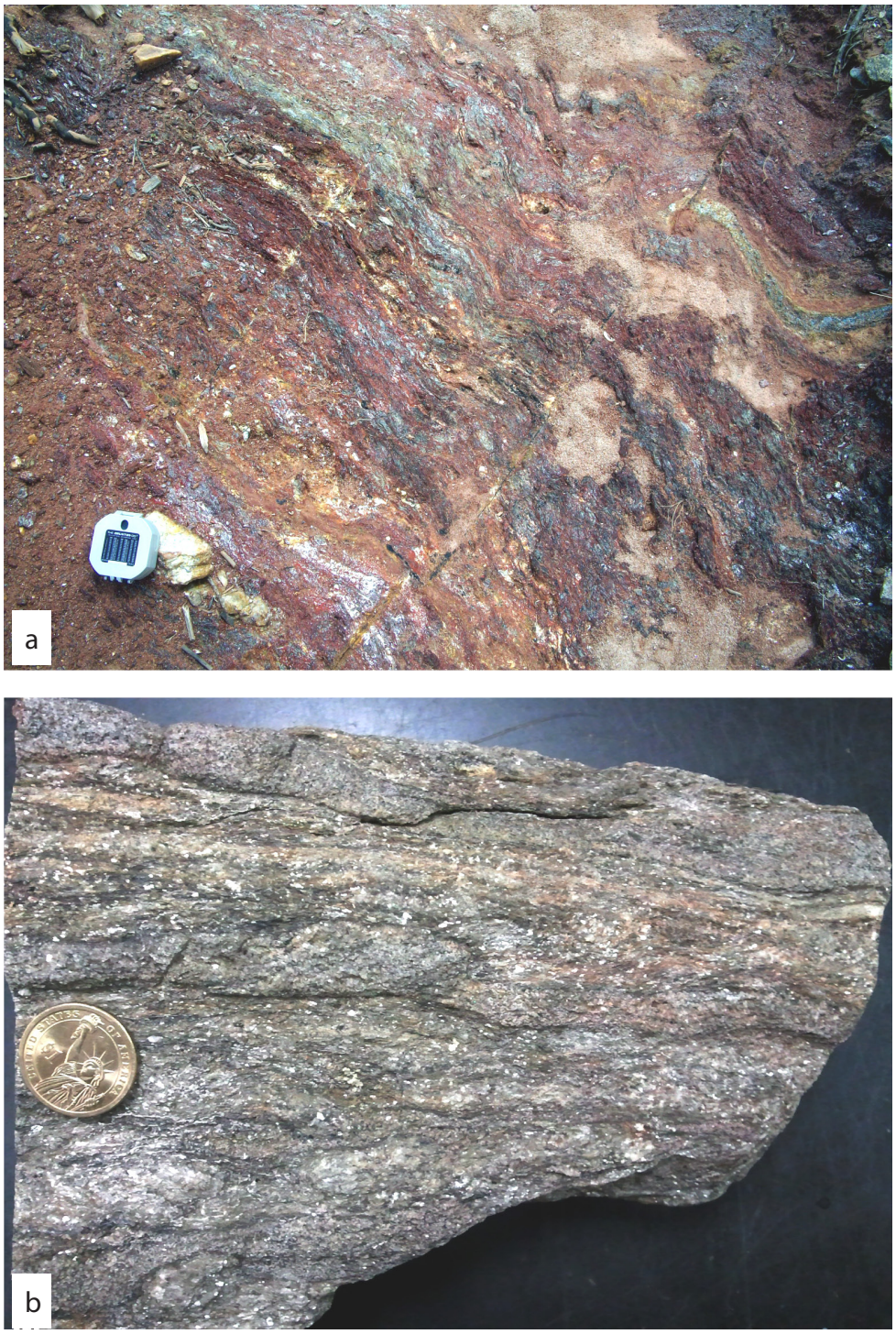


Figure 2-6. (a) Weathered sillimanite schist. A sillimanite-rich layer is just above and to the right of the Brunton™ compass from Possum Trot Road in the High Falls quadrangle, looking east. (b) Strongly foliated sillimanite schist and interlayered quartzo-feldspathic melt collected from Dauset Trails Nature Center in the Indian Springs quadrangle.

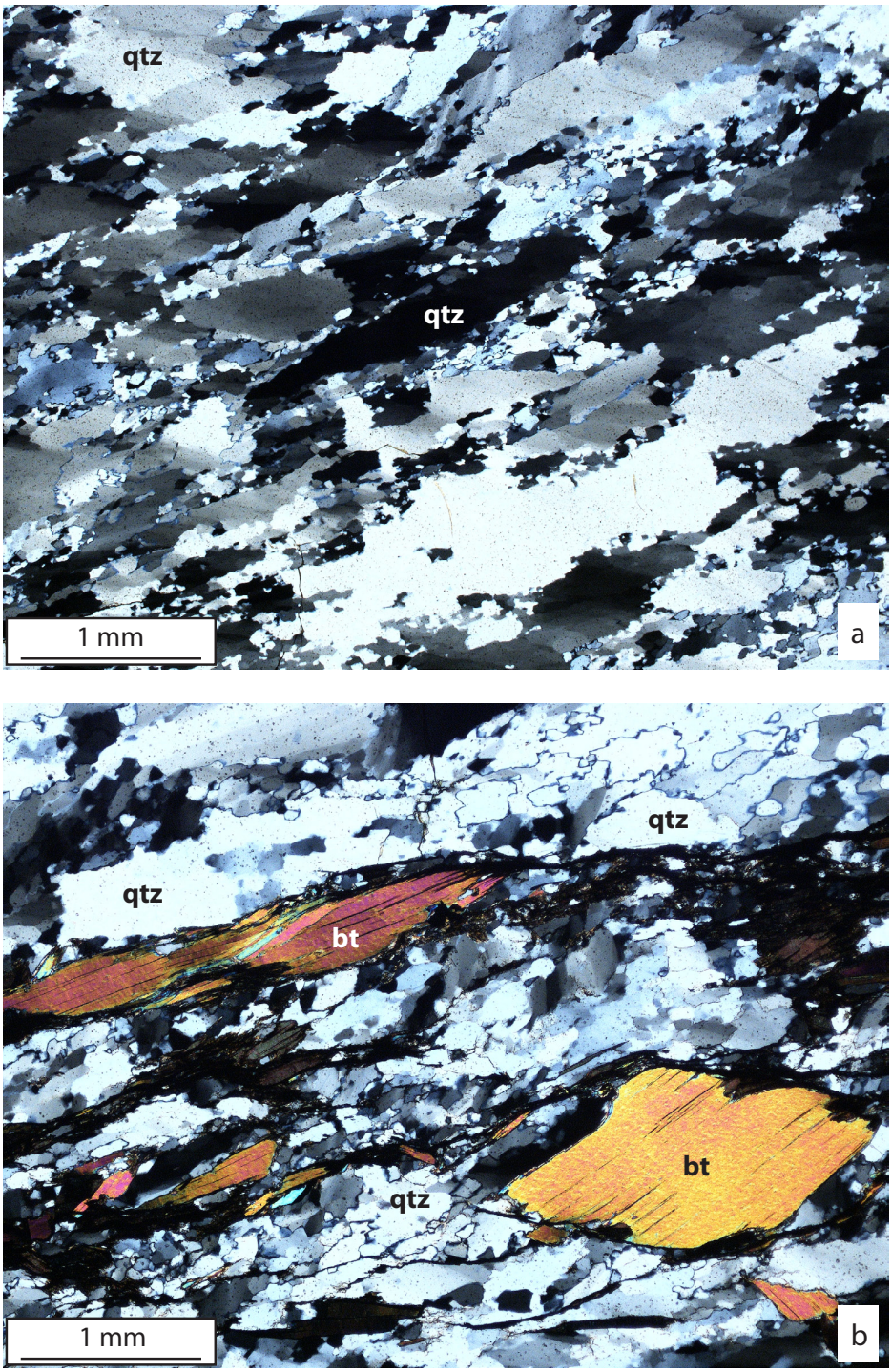


Figure 2-7. Thin sections revealing quartz textures from Unionville Road in High Falls quadrangle. Crossed nicols. (a) Elongate quartz grains with evidence of bulging and recrystallization around the perimeter; the interiors of the larger grains display undulatory extinction. (b) Biotite crystals define a well-developed S-C fabric and quartz grains with bulging grain boundaries. bt-biotite; qtz-quartz.

High Falls Granite

The High Falls Granite was named for excellent exposures within and around High Falls State Park (Atkins and Lineback, 1992). Previous work northeast of the study area referred to porphyritic granite with blocky megacrysts as the Murder Creek granite (Davis, 2010), but in this thesis all megacrystic granite in the Cat Square terrane is called High Falls Granite since that name has precedence. Mapping to the northeast of the project area revealed a nearly equal distribution of High Falls, Indian Springs, and the Dow's Pulpit Granites. The High Falls Granite in the Jackson quadrangle becomes the dominant igneous rock between the Brindle Creek and Towaliga faults (M. T. Huebner, personal commun.). Mapping in the study area confirmed this trend continues southwest through the Indian Springs and High Falls quadrangles. Preliminary results from an additional mapping project even farther southwest in the Barnesville quadrangle suggest that this trend may continue as far southwest as the intersection of the Brindle Creek and Towaliga faults (J. R. Rehrer, personal commun.). Exposures of the High Falls Granite constitute approximately 60 percent of the mapped area in the Cat Square terrane, and a large elongate body of High Falls Granite is exposed immediately northwest of nearly the entire length of the Towaliga fault in the study area (Plate I). Another large body of this unit is exposed on the western side of the High Falls quadrangle. Atkins and Lineback (1992) conducted reconnaissance mapping of portions of the High Falls quadrangle and called the westernmost granite body Hollonvile Granite. This body of granite was mapped as High Falls Granite as part of this study. Pavement outcrops of High Falls Granite (Fig. 2-8) are common but rounded boulders ranging from 0.5 to 10 m across are also found in the mapping area. High Falls Granite weathers to yellow-orange or orange-red soil; its characteristic blocky megacrysts can often be recognized in saprolite outcrops, and have often been used to collect structural data from ditches and washouts in the project area. Exposures of High Falls Granite are



Figure 2-8. (a) Small pavement outcrop of High Falls Granite with strongly aligned microcline megacrysts from ~550 m northwest of the intersection of City Pond Road and Mann Road in the High Falls quadrangle, looking down at pavement outcrop. (b) Large outcrop of High Falls Granite at the type locality in High Falls State Park; note dike of Indian Springs Granite behind Torin Howard, looking southwest.

moderate to strongly foliated porphyritic biotite granite that is characterized by blocky microcline megacrysts 1 to 7 cm long (Fig. 2-8), which commonly display Carlsbad twinning. Other major phases identifiable in hand sample are subhedral to anhedral plagioclase up to 1.5 cm, subhedral biotite up to 3 mm, and anhedral quartz crystals. Garnet, myrmekite, and epidote are also common, but are not ubiquitous. Foliation in the High Falls Granite is typically concordant with regional foliation. Exceptions occur in isolated zones in outcrop and map scale and are most likely related to nappe-style folding of the pluton. Submeter-scale xenoliths of biotite gneiss are not uncommon. This unit is also commonly crosscut by dikes and small pods of Indian Springs Granite. In thin section (Fig. 2-9) myrmekite is common as well as undulatory extinction in quartz crystals. Both of these features are a result of unrecovered strain.

Indian Springs Granite

The Indian Springs Granite is a fine- to medium-grained equigranular granite that is named for a large exposure in the shoals at Indian Springs State Park. Previous work northeast of the study area referred to this unit as the Rocky Creek granodiorite (Davis, 2010), but petrographic modal analyses performed during this study (Fig. 2-10) classify it as a granite. Indian Springs Granite forms pavement outcrops as well as rounded boulders up to 5 m in diameter. Mappable bodies of this unit make up approximately 5 percent of the exposure in the Cat Square terrane in the study area. Dikes and bodies of Indian Springs Granite too small to map at 1:24,000 scale cut through country rock and High Falls Granite throughout the Cat Square terrane. Major phases visible in hand sample (Fig. 2-11) are quartz, plagioclase, potassium feldspar, biotite, and muscovite. The Indian Springs Granite weathers to a yellow-orange or red-orange soil with a popcorn texture created by relict feldspar crystals. This unit is normally weakly foliated and is not concordant with regional foliation. Analysis of thin sections (Fig. 2-12) reveals

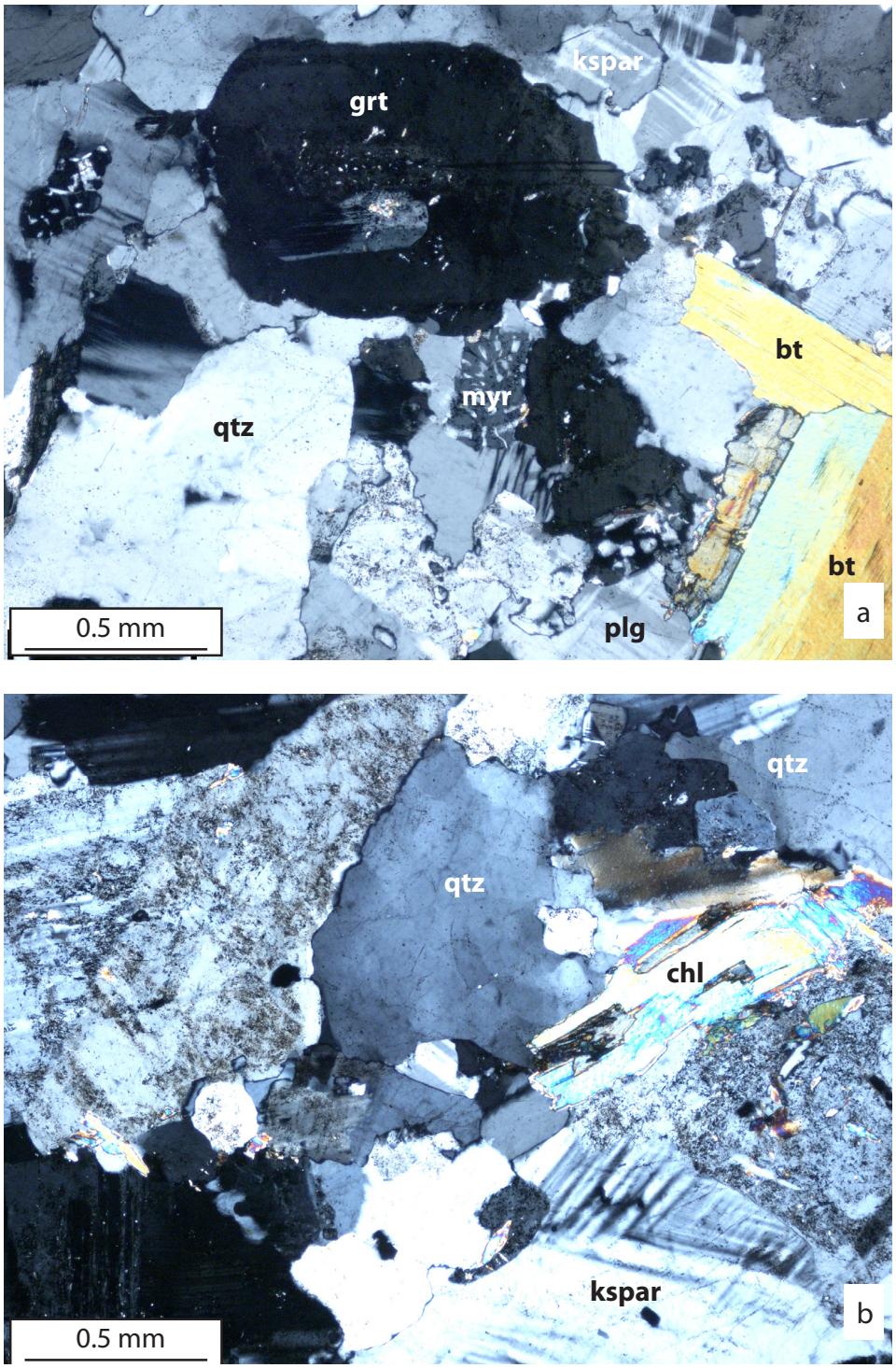


Figure 2-9. Thin sections of High Falls Granite collected from Gilmore Branch in the Indian Springs quadrangle. Crossed nicols. (a) Small garnet (~0.5mm) surrounded by a matrix of quartz, plagioclase feldspar and boitite. Note myrmekite just below garnet. (b) Sericitized plagioclase with strained quartz crystals (note undulatory extinction) and chlorite; bt-biotite; chl-chlorite; grt-garnet; kspar-K-feldspar; qtz-quartz; myr-myrmekite.

Sample	HF862	IS470
Quartz	34%	37.2%
Plagioclase	22.4%	29.0%
K-spar	18.2%	27.2%
Biotite	19.7%	2.6%
Muscovite	4.2%	3.2%
Apatite	0.2%	0.2%
Myrmekite	0.8%	0.6%
Garnet	0.3%	-
Total	100%	100%

(a)

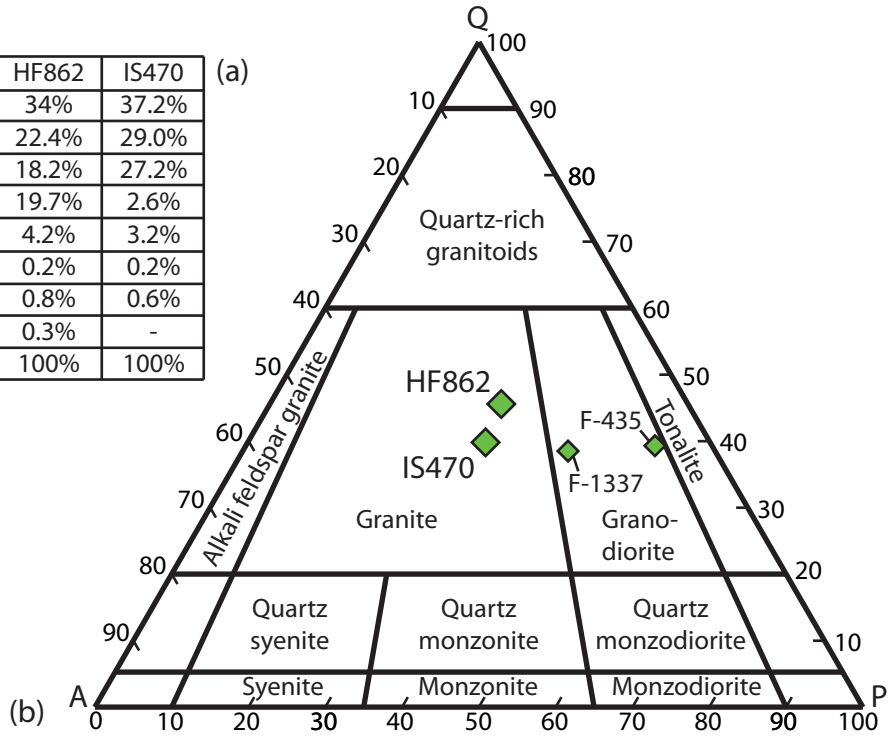


Figure 2-10. (a) Modal abundances of Indian Springs Granite. (b) Compositions of Indian Springs Granite samples are shown in the Strekeisen diagram. F-435 and F-1337 are from Davis (2010).

quartz grains that are not as strained as those seen in the High Falls Granite.

Pine Mountain Window

The Towaliga fault zone is the contact between the Cat Square terrane and Pine Mountain window. The Pine Mountain window is surrounded by the Towaliga, Box Ankle, Goat Rock, and Dean Creek faults (Hatcher et al., 2007a), and the window exposes a large allochthonous block of Grenville basement in the southernmost Appalachians.

Woodland Gneiss

The Woodland Gneiss is 1.1 Ga (Heatherington et al., 2006) Grenville basement gneiss that is exposed in the Pine Mountain window. Woodland Gneiss

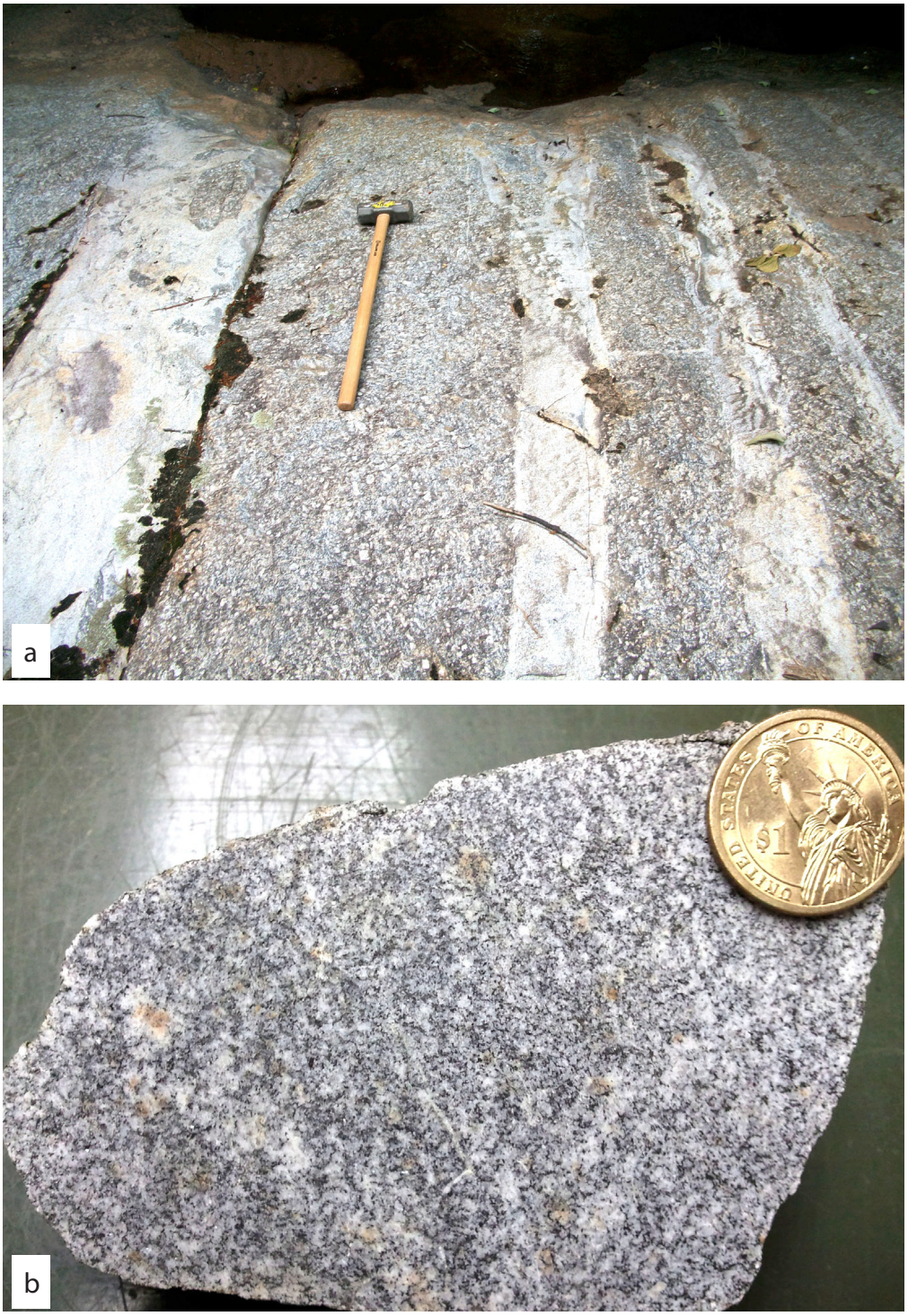


Figure 2-11. (a) Large dikes of Indian Springs Granite crosscut a larger body of High Falls Granite in Gilmore Branch in the Indian Springs quadrangle, looking southwest. Note the xenolith of High Falls Granite in the largest dike, to the left of the head of the sledge hammer. (b) Sawed specimen of Indian Springs Granite collected from location pictured in (a).

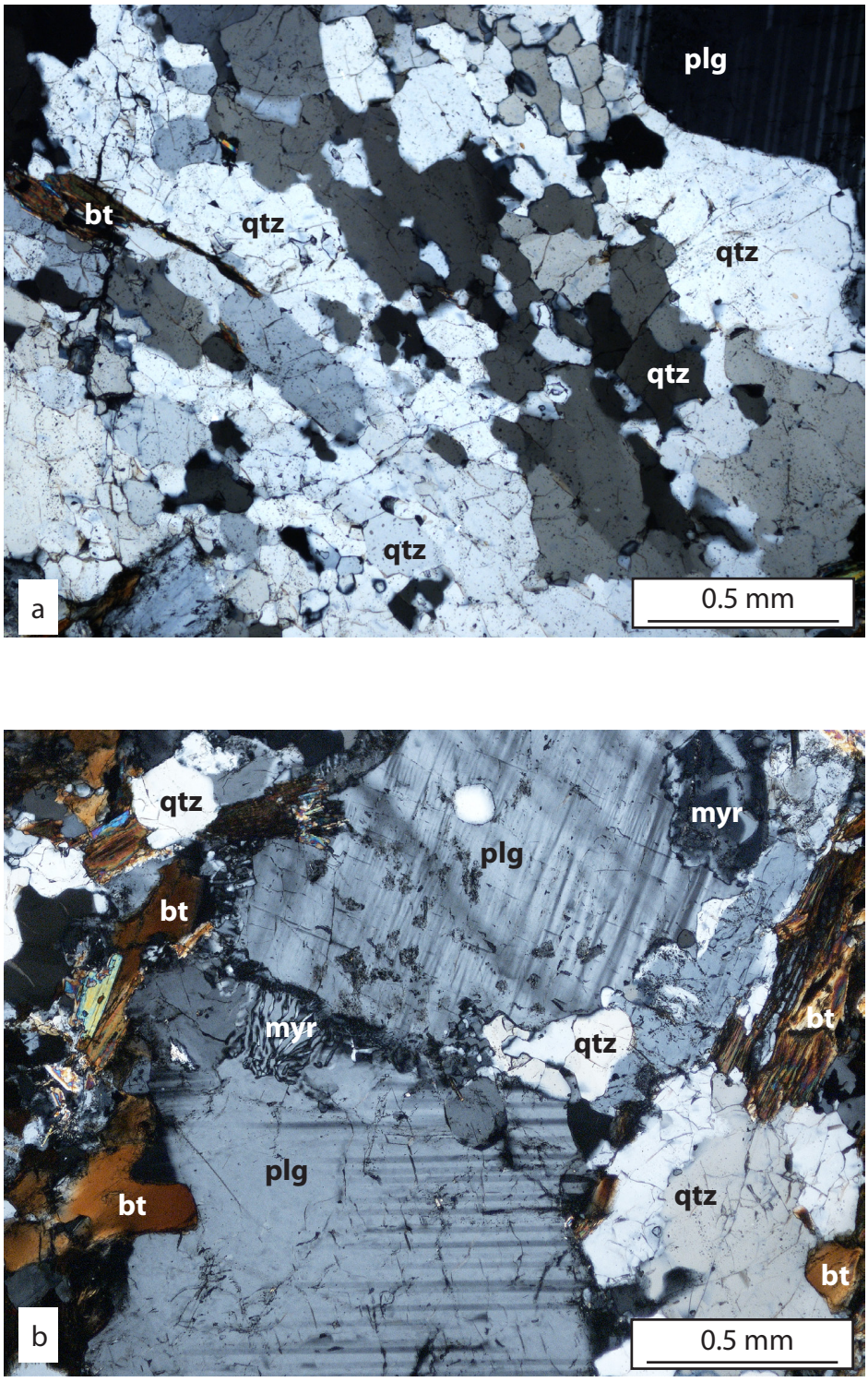


Figure 2-12. Thin sections of Indian Springs Granite from location pictured in Figure 2-10a. Crossed nicols. (a) Quartz appears to be less strained than in thin section of High Falls Granite (Fig. 2-10). (b) Myrmekite developed along the boundary between two plagioclase crystals. bt-biotite, myr-myrmekite, plg-plagioclase, qtz-quartz.

was mapped by Hatcher (unpublished data) across a large area in the Indian Springs quadrangle immediately southeast of the Towaliga fault. The unit continues through the southeastern corner of the High Falls quadrangle. Woodland Gneiss weathers to a red-brown soil containing relict feldspar megacrysts. Blocky feldspar megacrysts and abundant garnet characterizing this unit are readily visible in pavement outcrops (Fig. 2-13).

Fault Rocks

Like metamorphic rocks, fault rocks may have a variety of protoliths, and are typically subdivided by their texture and mineralogy. In addition to protolith composition, texture and mineralogy are related to presence of fluids, temperature, and strain rate along the fault. The study area contains two terrane boundaries, the Brindle Creek and Towaliga faults. The Brindle Creek fault is a narrow (10-30 m wide) mylonite zone that experienced oblique dextral strike-slip movement during the Neoacadian orogeny. The Towaliga fault zone is a wide dextral mylonite zone (1-9 km wide) (Bentley and Neathery, 1970; Hooper and Hatcher, 1988a) that formed during the late Paleozoic Alleghanian orogeny. This wide zone of plastic deformation was cut by brittle faults during the Mesozoic and pods of siliceous cataclasite formed along this thin band of brittle deformation. The Towaliga fault zone contains rocks that have enjoyed brittle and ductile deformation. The field area also contains several bands of ribbon quartz mylonite that formed in zones of intense shearing. These mylonites are not associated with either of the terrane boundaries discussed above.

Towaliga Mylonite

The Towaliga fault zone contains ductilely deformed rocks that range from mylonite to ultramylonite. Many specimens of High Falls Granite and Cat Square terrane



Figure 2-13. (a) Large exposure of Woodland Gneiss in shoals of the Little Towaliga River downstream of Higgins Mill, looking southwest. (b) Pavement outcrop of Woodland Gneiss along the Little Towaliga River ~100 m downstream of Unionville Road bridge, looking south; note large feldspar porphyroclasts.

metasedimentary rocks could be considered protomylonite, so the boundary between these rocks and Towaliga fault mylonite is demarked by evidence of significant ductile deformation. Rocks in the fault zone are characterized by a very strong mylonitic fabric and plastic grain size reduction in hand sample (Fig. 2-14). S-C fabrics may be visible in hand sample, but are almost always recognizable in thin section. Porphyroclasts of more resistant material often have tails that can be used as shear sense indicators. In many cases these are theta porphyroclasts (after Hooper and Hatcher, 1988b) and the tails area formed by disruptions in the flow of matrix material around the porphyroclasts. Common porphyroclasts are plagioclase, potassium feldspar, and garnet. In thin section, the mylonite matrix is composed of dynamically recrystallized quartz and biotite.

Siliceous Cataclasite

Rhomb-shaped pods of siliceous cataclasite can be found along the Towaliga fault throughout the study area. One especially large pod can be easily recognized in the southwestern corner of the High Falls quadrangle immediately southeast of the intersection of Mann Road and City Pond Road. This large hill (1000 m x 250 m and 35 m high) is composed entirely of siliceous cataclasite. Large white angular boulders and pebbles (Fig. 2-15) cover the entire surface of the hill. These boulders appear to be almost pure microcrystalline quartz crosscut by numerous joints that have been healed with quartz. Many of these joints offset each other, which indicates quartz precipitation was punctuated by several phases of brittle deformation. Cataclasite weathers to a light tan or yellow soil that can contain angular pebbles of microcrystalline quartz.

Ribbon Quartz Mylonite

Ribbon quartz mylonites are a strongly foliated rocks composed predominantly of quartz, and are found throughout the Cat Square terrane in the study area. Deformation

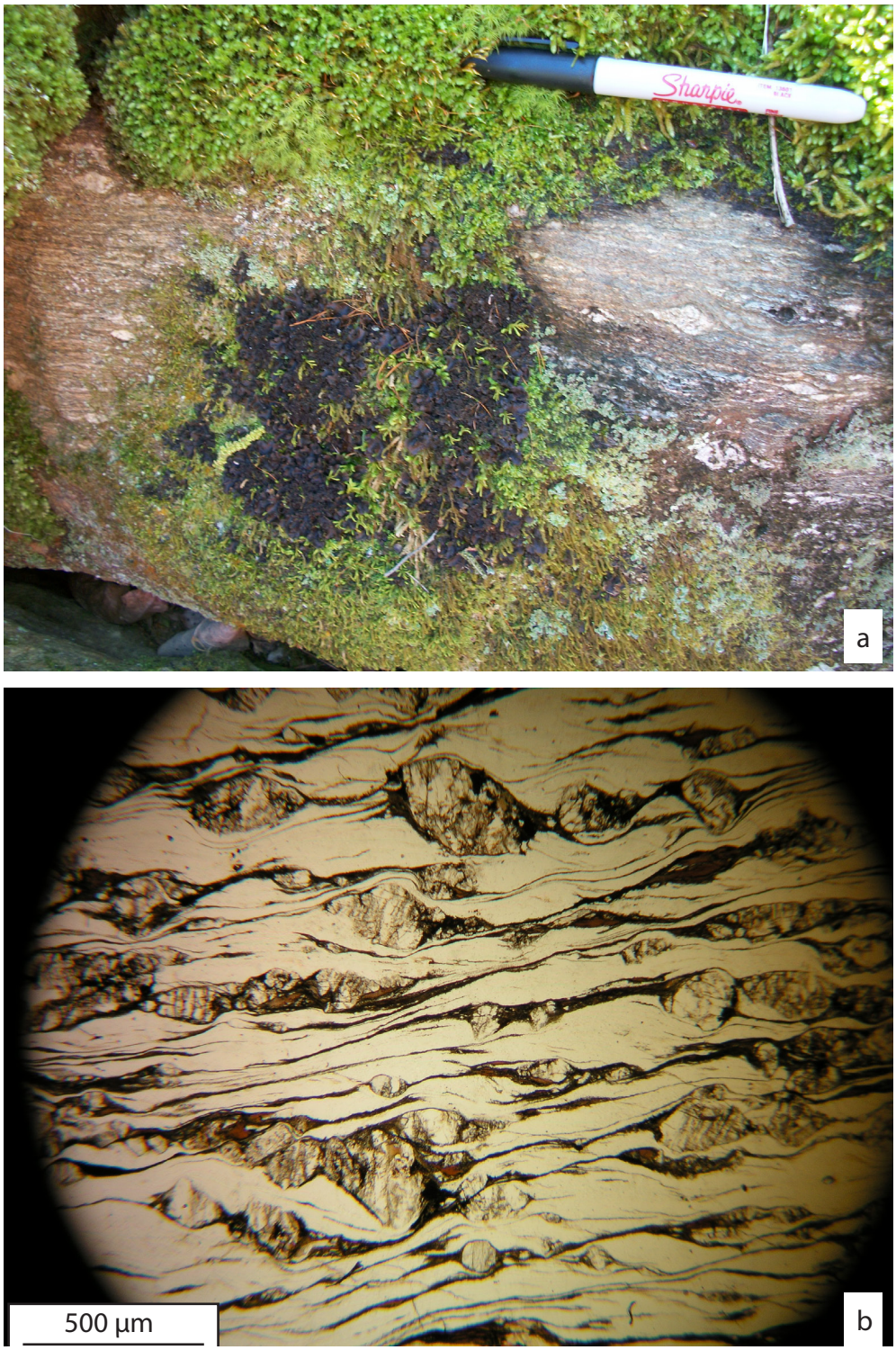


Figure 2-14.(a) Outcrop of mylonite from the Towaliga fault zone along Fambro Creek in the Indian Springs quadrangle, looking southeast. (b) Mylonite from float collected in the Towaliga fault zone along City Pond Road; note elongate feldspar porphyroclasts. Plane light.



Figure 2-15. (a) Blocks of siliceous cataclasite from a large rhomb southeast of Mann Road in the High Falls quadrangle, looking southwest. (b) Pebble of cataclasite with quartz-healed joints formed by several phases of brittle deformation.

in the Cat Square terrane formed discrete bands of intense shearing. In these bands, ribbon quartz mylonite was produced as a product of concentrated strain. Rocks of the Cat Square terrane were sheared *en masse* during Neoacadian deformation. This strain was not distributed throughout the rock mass homogeneously, but instead became concentrated in certain areas due to predisposed weaknesses. The weaknesses may have been a result of a concentration of quartz (which deforms plastically at a relatively low temperature). The mylonites are characterized by a composition of nearly 100 percent quartz that has been ductilely deformed into anastomosing ribbons and then annealed. This texture suggests that temperatures remained high enough for quartz crystallization to occur but there is little evidence of dynamic recrystallization. The quartz ribbons identified in the study area range from 20 to 50 cm wide. The outcrops are resistant to weathering and in some cases produce small waterfalls where creeks crossed the outcrops. Ribbon quartz mylonite float was also identified at several locations. Outcrops commonly developed a dark brown or black patina when in a creek bed but revealed a cream or light yellow on a fresh surface. This type of mylonite was only found in metasedimentary rocks of the Cat Square terrane.

Brindle Creek Fault Mylonite

Fault rocks along the Brindle Creek fault are similar in texture to those found in the Towaliga fault zone. The mylonite zone associated with the Brindle Creek fault is narrow (~30 m) compared to the Towaliga fault zone, which makes it more difficult to locate in the field. Rocks in the footwall of the Brindle Creek fault are usually highly migmatized, however, which was useful when tracing the fault. In thin section, S-C fabric is common in Brindle Creek mylonite, and deformed quartz grains have been annealed. No one soil type is associated with the Brindle Creek fault, which is a result of several protoliths being incorporated into the mylonite zone.

Diabase Dikes

Mesozoic diabase dikes were emplaced during the breakup of Pangea, and have been mapped in many portions of the southern Appalachian Piedmont. Davis (2010) and Huebner (personal commun.) mapped numerous diabase dikes during their field work. A few short (less than 500 m long) dikes were located and mapped in the northwestern part of the High Falls quadrangle, but these were the only diabase dikes identified in the project area. Diabase float is easy to recognize in the field since it forms rounded boulders and cobbles, and develops a distinct orange weathering rind. Fresh surfaces reveal a fine- to medium-grained mafic rock of basaltic composition.

Chapter 3: Geochemistry and Geochronology

Introduction

Bulk geochemical analysis can reveal subtle characteristics that cannot be observed in hand specimen or thin section. Geochemical signatures can be used to determine much about the origin and tectonic history of igneous rocks (Rollinson, 1993). Source material can be determined in addition to the degree that magma may have been altered by surrounding country rock during its ascent into the middle or upper crust. Special consideration must be given to igneous rocks that have also been metamorphosed. Partial melting and hydrothermal alteration can affect bulk rock geochemistry. Finally, geochemical signatures of igneous rocks can be compared to highlight similarities and differences in the origin and tectonic history of different plutons. The geochemistry and U-Pb isotopic ages of the High Falls Granite in central Georgia will be compared with the Walker Top Granite in North Carolina at the end of this chapter to examine the possible consanguinity of these megacrystic granites. Analyses of Indian Springs Granite will provide additional insight into its generation and emplacement during the Alleghanian orogeny. The tectonic implications of these results will help refine our understanding of southern Appalachian orogenesis. Bulk-rock geochemical data from Walker Top Granite of the North Carolina Inner Piedmont were collected by Giorgis (1999), Vinson (1999), Mapes (2002), Gatewood (2007), and Byars (2010), and are incorporated into this discussion for comparison.

Granitoid Geochemistry

Methodology

Representative samples of both the High Falls Granite (HF862 and IS370) and Indian Springs Granite (HF1465 and IS470) were collected for geochemical analysis

(Fig. 3-1). Saprolite is common in the southern Inner Piedmont, so a great deal of care was taken to collect the most fresh samples possible. Samples were broken down into 10-15 cm diameter pieces and placed in cloth sample bags. Fragments that were obviously weathered were discarded. The samples were further processed for geochemical analysis at The University of Tennessee. Equipment used was cleaned with acetone and precontaminated with a small amount of each sample. The specimens were broken down further using a “chipmunk” jaw crusher, and finally reduced to powder with a Shatterbox™ equipped with an alumina ceramic mill. Enough Indian Springs granodiorite was powdered to fill a 15 dram vial from each sample. Larger quantities (approximately 750 ml) of each specimen of High Falls Granite were powdered and split to insure that a representative sample was submitted for major and trace element geochemical analysis. The processed samples were analyzed at Activation Laboratories in Ancaster, Ontario. Activation Laboratories used inductively coupled plasma mass spectrometry (ICP-MS), total digestion inductively coupled plasma (TD-ICP), fusion methods mass spectrometry (FU-MS), and instrumental neutron activation analysis (INAA) to determine the major, trace, and rare earth element compositions of the four samples. CIPW norms were calculated; plots of geochemical data were generated with Geochemical Data Toolkit (GCDkit) in R for Windows™ version 3.0 (Janoušek et al., 2006).

B.A. Davis (2010) reported the results of geochemical analysis of additional samples of High Falls and Indian Springs Granites from the Farrar quadrangle; previously unpublished geochemical data from the Stewart and Lloyd Shoals Dam quadrangles (Fig. 3-1) were graciously provided by Matthew T. Huebner. These data (M.T. Huebner, unpublished data; Davis, 2010) have been incorporated into this chapter for comparison. Sample selection criteria and preparation methodology was similar to that used for my samples.

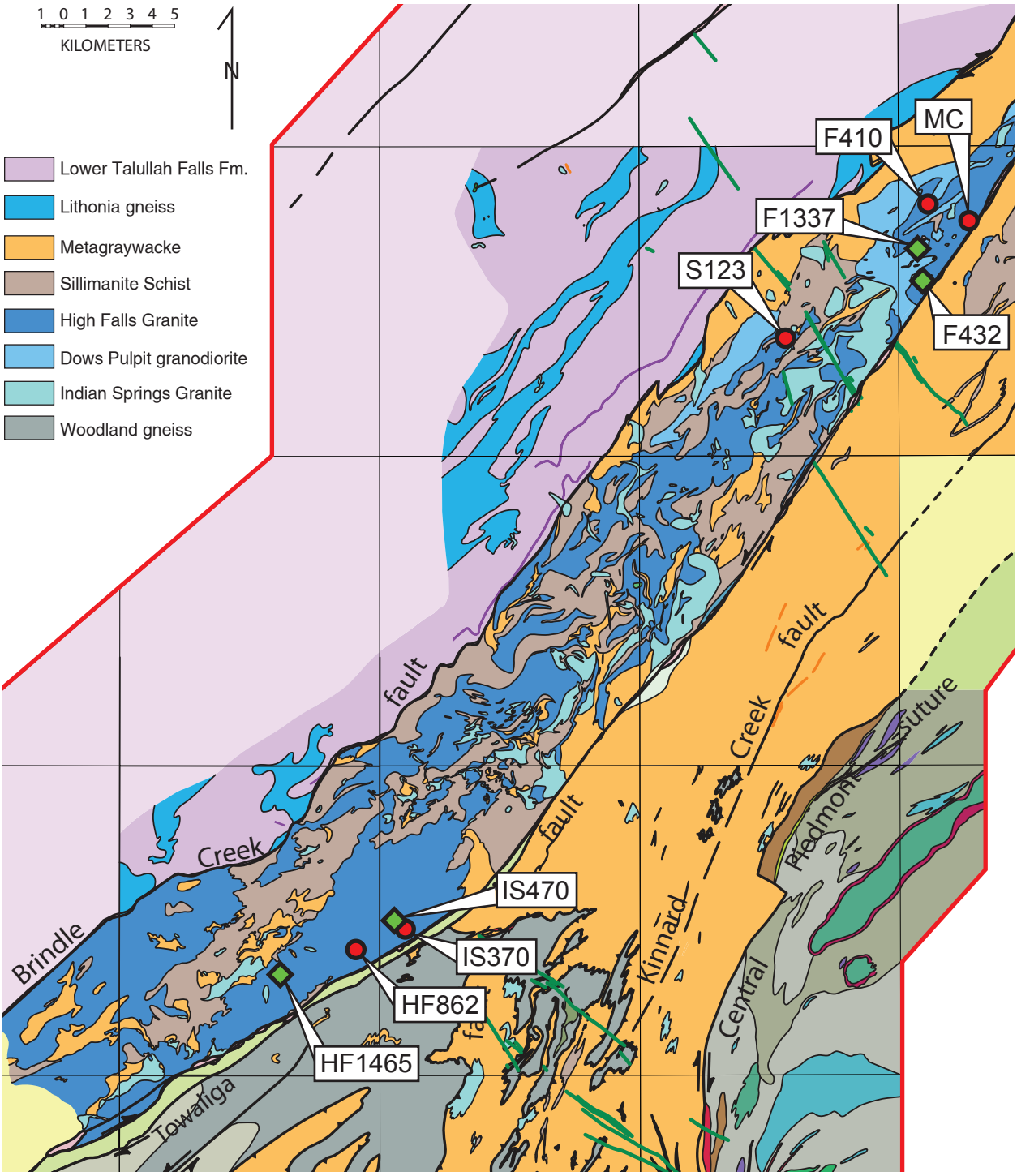


Figure 3-1. Simplified detailed geologic map of the area showing the location of geochemial samples in my mapped area to the southwest and in the area mapped by B.A. Davis (2010) to the northeast. Map compiled by M.T. Huebner from Davis (2010); Huebner (unpublished); Hatcher (unpublished); Hooper (1986) and my own data. Red circles are High Falls Granite and green diamonds are Indian Springs Granite.

Major-Element Chemistry

Ten elements (Si, Ti, Al, Fe, Mn, Mg, Ca, Na, K, and P) traditionally comprise the major elements (Rollinson, 1993). Abundances are typically reported as weight percent (wt percent) oxides in whole-rock analyses. Results of geochemical analyses of the four samples from my study area are compiled in Table 3-1 and reveal large variations in the concentrations of several major elements. For example, the average SiO_2 concentration in High Falls Granite is 66.97 wt percent with the standard deviation of 3.66 wt percent. Al_2O_3 concentration has an average of 15.86 wt percent with a standard deviation of 1.84 wt percent. Average total iron (Fe_2O_3total) is 3.62 with a standard deviation of 1.13. Standard deviations of all other major element oxides (TiO_2, MnO, MgO, CaO, Na_2O, and K_2O) for High Falls Granite samples are less than 1.00 wt percent.

The largest variation in major element concentration in Indian Springs Granite is in SiO_2 (avg. 69.27 wt percent, std. dev. 3.99 wt percent), Al_2O_3 (avg. 15.90 wt percent, std. dev. 1.12), and Fe_2O_3total (avg. 1.82 wt percent, std. dev. 1.19 wt percent). CIPW norms were calculated for each of the four samples listed above (Table 3-2). Calculated norms for all four samples contain corundum, which indicates the samples are peraluminous. Abundances of normative quartz are above 10 percent, which means they can be plotted in the albite-anorthite-orthoclase ternary diagram (Fig. 3-2). A quartz content above 10 percent has a negligible effect on classification based on feldspar abundances (O'Connor, 1965). Samples of High Falls and Indian Springs Granites collected as part of this study plot in the granite field. Other samples of High Falls Granite (Davis, 2010; Huebner, unpublished data) also plot in the granite field. Two samples of Indian Springs Granite from Davis (2010) contain smaller amounts of normative potassium feldspar and sodic plagioclase, and plot in the granodiorite field. It should be noted that Davis (2010) referred to this unit as the Indian Springs Granite.

Table 3-1. Geochemical data.

Sample ID		HF862	IS370	HF1465	IS470
Rock Unit		High Falls Granite	High Falls Granite	Indian Springs Granite	Indian Springs Granite
Analysis Type	Detection Limit				
FUS-ICP					
SiO_2	0.01%	61.6	65.8	72.28	74.36
Al_2O_3	0.01%	18.89	15.83	15.25	14.72
Fe_2O_3(total)	0.01%	5.38	5.38	1.38	0.57
MnO	0.0010%	0.093	0.116	0.028	0.019
MgO	0.01%	1.14	1.14	0.38	0.09
CaO	0.01%	2.99	2.4	1.59	1.08
Na_2O	0.01%	3.82	2.74	3.86	3.99
K_2O	0.01%	4.76	4.15	4.19	4.27
TiO_2	0.0010%	0.718	0.689	0.208	0.052
P_2O_5	0.01%	0.15	0.23	0.05	0.04
LOI		0.6	1.18	0.57	0.51
	Totals	100.1	99.66	99.78	99.7
Ba	1 ppm	851	905	911	391
Be	1 ppm	4	2	3	5
Sr	2 ppm	190	187	485	162
V	5 ppm	63	63	23	<5
Y	1 ppm	34	31	4	8
INAA					
Au	1 ppb	< 1	< 1	6	< 1
As	1 ppm	< 1	6		4
Br	0.5 ppm	< 0.5	< 0.5	< 0.5	< 0.5
Co	0.1 ppm	9.1	11.7	2.9	2.6
Cr	0.5 ppm	14.9	21.7	5.3	< 0.5
Hg	1 ppm	< 1	< 1	< 1	< 1
Ir	1 ppb	< 1	< 1	< 1	< 1
Sb	0.1 ppm	< 0.1	< 0.1	< 0.1	< 0.1
Sc	0.01 ppm	13.2	11.5	3.7	2
Se	0.5 ppm	< 0.5	< 0.5	< 0.5	< 0.5
W	1 ppm	9	5	6	3
FUS-MS					
Bi	0.1 ppm	< 0.1	0.2	< 0.1	1.6
Cs	0.1 ppm	4.5	1.9	2.5	2.6
Ga	1 ppm	23	21	19	19
Ge	0.5 ppm	2	1.6	1.2	1.5
Hf	0.1 ppm	8.4	7.1	3.4	1.7
In	0.1 ppm	< 0.1	< 0.1	< 0.1	< 0.1

Table 3-1. Geochemical data (continued)

Mo	2 ppm	< 2	< 2	< 2	< 2
Nb	0.2 ppm	14.6	14.7	5.4	3.2
Rb	2 ppm	155	144	114	159
Sn	1 ppm	3	2	2	2
Ta	0.1 ppm	1	1	0.33	0.99
Th	0.05 ppm	24.1	20.1	5.51	3.26
U	0.05 ppm	2.29	2.53	2.09	2.59
Zr	1 ppm	303	260	110	34
La	0.05 ppm	55.7	49	13.9	4.37
Ce	0.1 ppm	116	105	25.9	8.44
Pr	0.02 ppm	13.4	12.2	2.86	1.01
Nd	0.05 ppm	52.3	49.4	10.6	3.96
Sm	0.01 ppm	10.2	10.3	1.9	1.07
Eu	0.005 ppm	1.89	1.68	0.766	0.307
Gd	0.02 ppm	7.48	7.73	1.25	1.12
Tb	0.01 ppm	1.1	1.15	0.14	0.2
Dy	0.02 ppm	6.12	6.01	0.64	1.26
Ho	0.01 ppm	1.22	1.14	0.11	0.25
Er	0.01 ppm	3.46	3.15	0.29	0.74
Tl	0.05 ppm	0.97	0.92	0.7	0.99
Tm	0.005 ppm	0.512	0.47	0.04	0.117
Yb	0.01 ppm	3.3	3.14	0.26	0.76
Lu	0.002 ppm	0.526	0.516	0.045	0.114
TD-ICP					
Ag	0.5 ppm	< 0.5	< 0.5	< 0.5	< 0.5
Cd	0.5 ppm	< 0.5	< 0.5	< 0.5	< 0.5
Cu	1 ppm	2	17	5	2
Ni	1 ppm	14	17	5	2
Pb	5 ppm	35	30	39	41
S	0.00%	0.002	0.044	0.003	0.001
Zn	1 ppm	91	91	39	14

Table 3-2. CIPW normative compositions of High Falls and Indian Springs Granites. Norms calculated using GCDkit (Janoušek et al., 2006).

Sample ID	HF862	IS370	HF1465	IS470
Rock Unit	High Falls Granite	High Falls Granite	Indian Springs Granite	Indian Springs Granite
Normative mineralogy				
Quartz	13.479	27.786	29.959	32.474
Corundum	2.376	3.017	1.593	1.666
Orthoclase	28.13	24.525	24.762	25.234
Albite	32.324	23.185	32.662	33.762
Anorthite	13.854	10.404	7.562	5.097
Hypersthene	2.84	2.84	0.947	0.224
Ilmenite	0.194	0.144	0.053	0.038
Rutile	0.616	0.613	0.18	0.032
Apatite	0.355	0.545	0.118	0.095
Pr?	0.004	0.082	0.006	0.002
Total	94.172	93.141	97.842	98.624

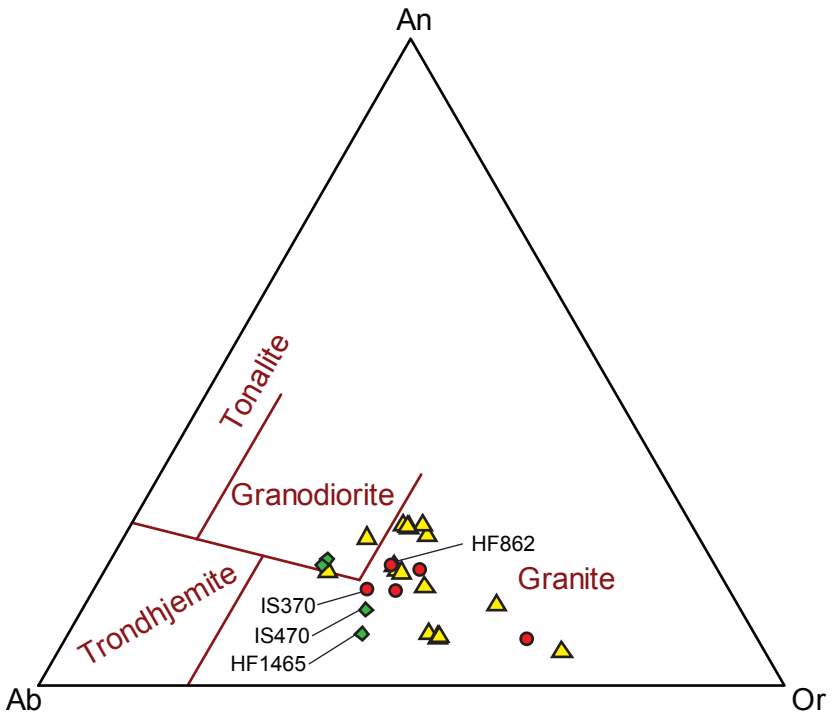


Figure 3-2. Granitoid classification “feldspar triangle” using fields of Barker (1979). Red circles are High Falls Granite, green diamonds are Indian Springs Granite, and yellow triangles are Walker Top Granite from North Carolina. (Ab = albite, Or = orthoclase, An = anorthite)

Harker diagrams have been utilized by others who have done geochemical work on Inner Piedmont granitoids in the Cat Square terrane (Giorgis, 1999; Mapes, 2002; Gatewood, 2007; Byars, 2010; Davis, 2010). The same kinds of diagrams have been used here to facilitate comparisons with previous work (Fig. 3-3), although Rollinson (1993) cautioned against making spurious correlations using major element variation diagrams. Percentages (including the abundances of major oxides used in geochemical analysis) are forced to be dependent on one another; as the percentage of one element increases, the percentage of others must decrease for the sum to be 100 percent. The dependent variables frequently produce a strong negative correlation in variation diagrams of both major and trace elements. The potential problems with how the geologic community has chosen to display geochemical data does not mean that this type of variation diagram should not be used, but it suggests that apparent correlations seen in the data may be a product of how the data were compiled as opposed to being related to geologic processes.

In general, a negative linear trend is present in several of the Harker diagrams (Al_2O_3, P_2O_5, MgO, TiO_2, CaO, and Fe_2O_3total) (Fig. 3-3). These trends are visible in data from High Falls and Indian Springs Granites samples. A non-linear scatter of data points for Na_2O and K_2O may be caused by one of (or even a combination of) several variables such as alteration during metamorphism, magma production in more than one tectonic setting, or a lengthy crystallization time (53-33 Ma for High Falls Granite, see below). It seems reasonable to assume that magmatic chemistry varied during this time. This is particularly true if the body of High Falls Granite is a composite pluton. In addition, a scatter of data may be the related to either over- or under-sampling megacrysts in the High Falls Granite. Variation in abundance of microcline megacrysts in the samples could easily affect the relative abundance of K_2O, Al_2O_3, and SiO_2.The bulk chemistry in a cooling magma chamber in which large number of phenocrysts

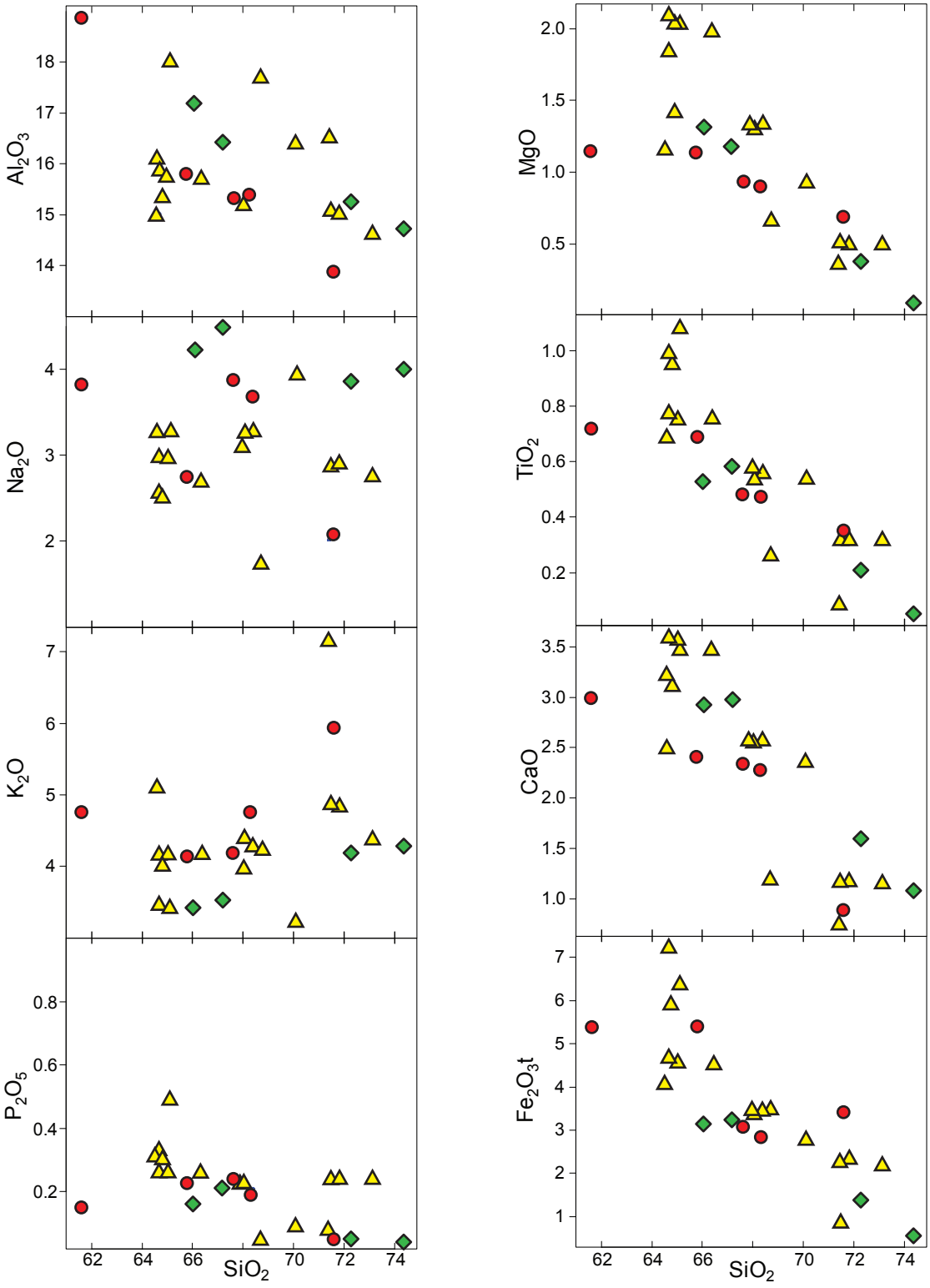


Figure 3-3. Harker diagrams of major elements. Red circles are High Fall Granite, green diamonds are Indian Springs Granite, and yellow triangles are Walker Top Granite.

have accumulated may not be an accurate representation of the chemistry of the entire magma chamber. In the High Falls Granite, the large number of microcline megacrysts could certainly affect the abundance of potassium and aluminum. Finally, metamorphism can overprint the geochemical signature of a protolith, producing increasing scatter in a variation diagram (Rollinson, 1993).

Trace Element Abundance

Trace elements are defined as any element that constitutes less than 0.1 wt percent of a bulk rock sample. The chemical properties (ionic radius, charge, etc.) of trace elements are the primary factor controlling their distribution in a rock sample. Trace elements are incorporated into the crystal lattice of minerals by substitution for major elements with similar chemical characteristics, or as interstitial atoms. These elements are also grouped either by their position in the Periodic Table or by their behavior in magmatic systems, and can be broadly defined as compatible or incompatible, based on their behavior in melts. Compatible elements preferentially remain in the crystal phase during melt generation, while incompatible elements are readily incorporated into the melt (Rollinson, 1993). While most major elements become mobile during metamorphism, the relative abundance of trace elements are typically much less affected. Trace-element signatures therefore reliably indicate the conditions under which a rock was formed. In addition, many trace elements (especially rare-earth elements) remain immobile under metamorphic conditions up to upper-amphibolite facies, and thus are not significantly affected by metamorphism or hydrothermal alteration.

Trace elements tend to depend less on major element abundance, as described above. Their abundance should also not be affected by under- or over-sampling of megacrysts during sample processing. After examining the plots in Figure 3-4, obvious

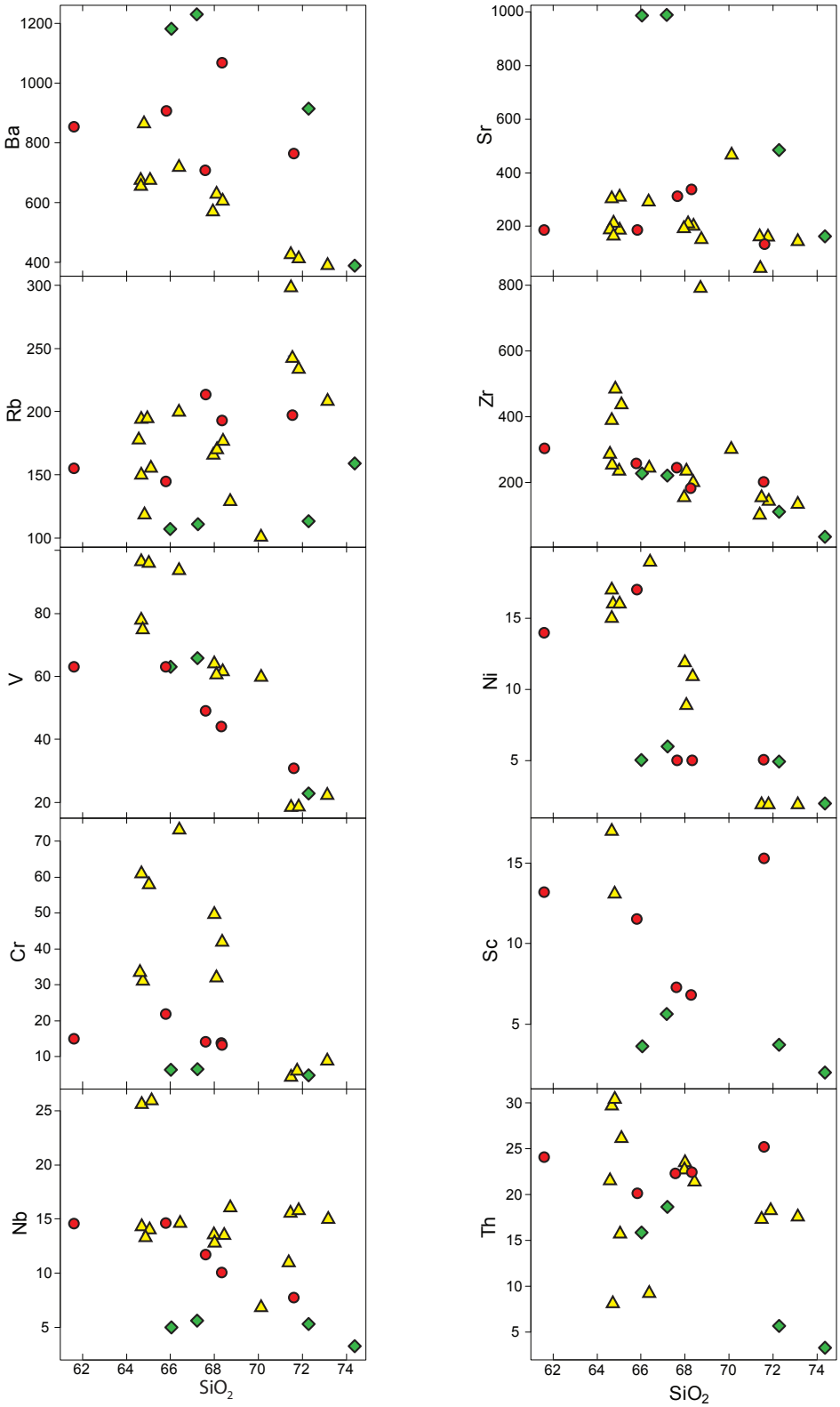


Figure 3-4. Harker diagrams of trace elements. Red circles are High Fall Granite, green diamonds are Indian Springs Granite, and yellow triangles are Walker Top Granite.

negative linear trends are much less common compared with those in the major element variation diagrams. Negative correlations are still present in V, Cr, Nb, and Zr for samples of High Falls and Indian Springs Granites. A negative correlation in Indian Springs data can be seen in Sr as well. A positive trend occurs in both granites for Rb, and a positive correlation is present in High Falls Granite. It is worth noting that Ba, Sr, and Rb are potentially mobile when rocks are hydrothermally altered, so trends (or a lack thereof) visible on Harker diagrams of these elements should be considered suspect (Rollinson, 1993). In contrast, trace-element abundance are much less susceptible to alteration by metamorphism.

Trace element abundance of the High Falls, Indian Springs, and Walker Top Granites have also been normalized to primitive mantle using the values of Sun and McDonough (1989) (Fig. 3-5). In general, each of these granites is enriched in large ion lithophile (LIL) elements, and depleted in high field strength (HFS) elements, which are small highly charged cations (Rollinson, 1993). These relationships are shown by an overall negative trend in the spider diagram (Fig. 3-5). This trend is expected during generation of a felsic melt, since the LIL elements are the most incompatible, while the HFS elements are relatively more compatible. Negative anomalies in Nb, P, and Ti are visible in all three granites. A significant positive anomaly in Pb is apparent in each granite as well. The High Falls and Walker Top Granites samples also have a negative anomaly in Sr.

REE Chemistry

Rare earth elements (REE) (La-Lu, ±Y) are particularly useful to interpret the genesis and alteration of a wide variety of rock types. All of these elements form stable 3+ ions and share nearly identical physical and chemical characteristics. Ionic radius consistently decreases as atomic number increases, so any differences in chemical

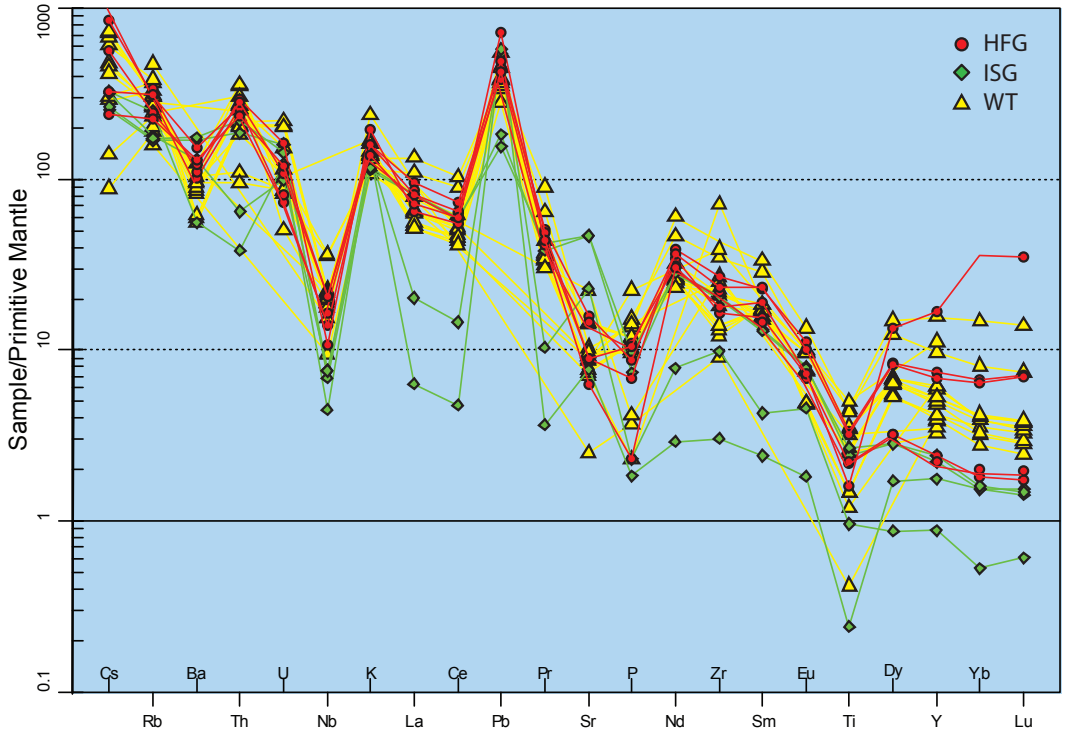


Figure 3-5. Spider diagram of mantle-normalized trace elements (after Sun and McDonough, 1989).

behavior are assumed to be related to these slight changes in atomic radius. These minor differences in radius cause the ions to be fractionated as a result of a variety of geologic processes, which produce characteristic REE signatures (Rollinson, 1993).

The large ionic radii and strong charge of REE make them highly incompatible. The light REE (La-Gd) are the largest, and are therefore the most incompatible (Hanchar and van Westrenen, 2007), so REE are preferentially concentrated in accessory minerals that crystallize during the final magmatic cooling. Monazite and xenotime are minerals that incorporate REE as major structural components. In fact, some workers (Wark and Miller, 1993) have suggested concentrations of REE occur primarily in accessory phases in granitic rocks.

The overall negative trend of REE abundances is a result of their relative incompatibilities. My samples are enriched in the most incompatible REE. A negative Eu anomaly is also present in the spider diagram (Fig. 3-6). Eu is normally trivalent, but under reducing conditions it can exist as a divalent ion. In its divalent state, Eu preferentially substitutes for Sr in feldspar. This typically results in a positive Eu anomaly in rocks that contain abundant feldspar (Sinha, 1983).

Tectonic Discrimination Diagrams

It is difficult to use major element concentrations to determine the tectonic setting of granites, because discrimination diagrams depend on only a few elements. Pearce et al. (1984) developed a set of discrimination diagrams for granites by analysis of 600 granitoid samples that formed in well-understood tectonic settings. These diagrams

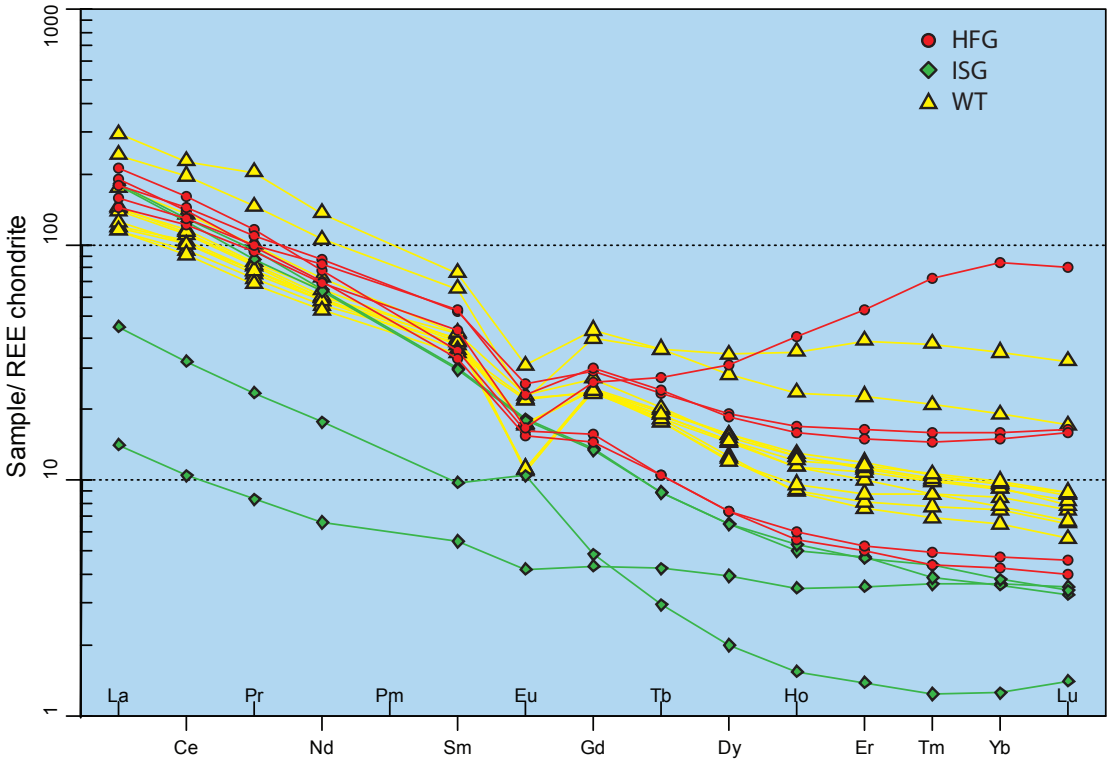


Figure 3-6. REE using chondrite normalization of Boynton (1984).

(Fig. 3-7) plot trace elements (or combinations of trace elements) against one another to assess the tectonic setting in which a particular granite formed. Some of these diagrams employ Rb, but Rb mobility has been documented in geochemical analysis of hydrothermally altered granitic rocks and can produce erroneous results in tectonic discrimination diagrams (Mukasa and Henry, 1990). Small compositional differences are somewhat exaggerated since these diagrams use logarithmic scales. Samples of High Falls Granite plot consistently in two pairs with one outlier, similar to the Walker Top samples. Specimens from the southwestern end of the study area (HF862 and IS370) plot very closely together on all four trace element plots of Pearce et al. (1984), and the values always fall in the field populated by volcanic-arc granite. Of course, this field is also populated by syn-collisional granites on the plot of Nb versus Y. Samples MC and F410 were collected in the northeastern part of the study area and also plot as a pair, but they plot in either the syn-collisional or within-plate granite fields in contrast to HF862 and IS370. S123 is an outlier and plots well inside the orogenic and within-plate fields (Fig. 3-7). These results suggest that the High Falls Granite may be the product of different mechanisms. Volcanic-arc granites are produced above a subducting slab of oceanic crust. Water is released from the downgoing slab and the overlying mantle partially melts, producing magma that ascends through the overlying crust. Syn-collisional granites are produced during orogenesis as continental crust is overthickened. These different mechanisms of magma generation apparently had very little effect on the mineralogy and texture of the High Falls Granite, because samples from across the field area are strikingly similar. While there is variability in the trace element abundances in samples of Indian Springs Granite, all of the specimens plot within the volcanic-arc granite field (Fig. 3-7).

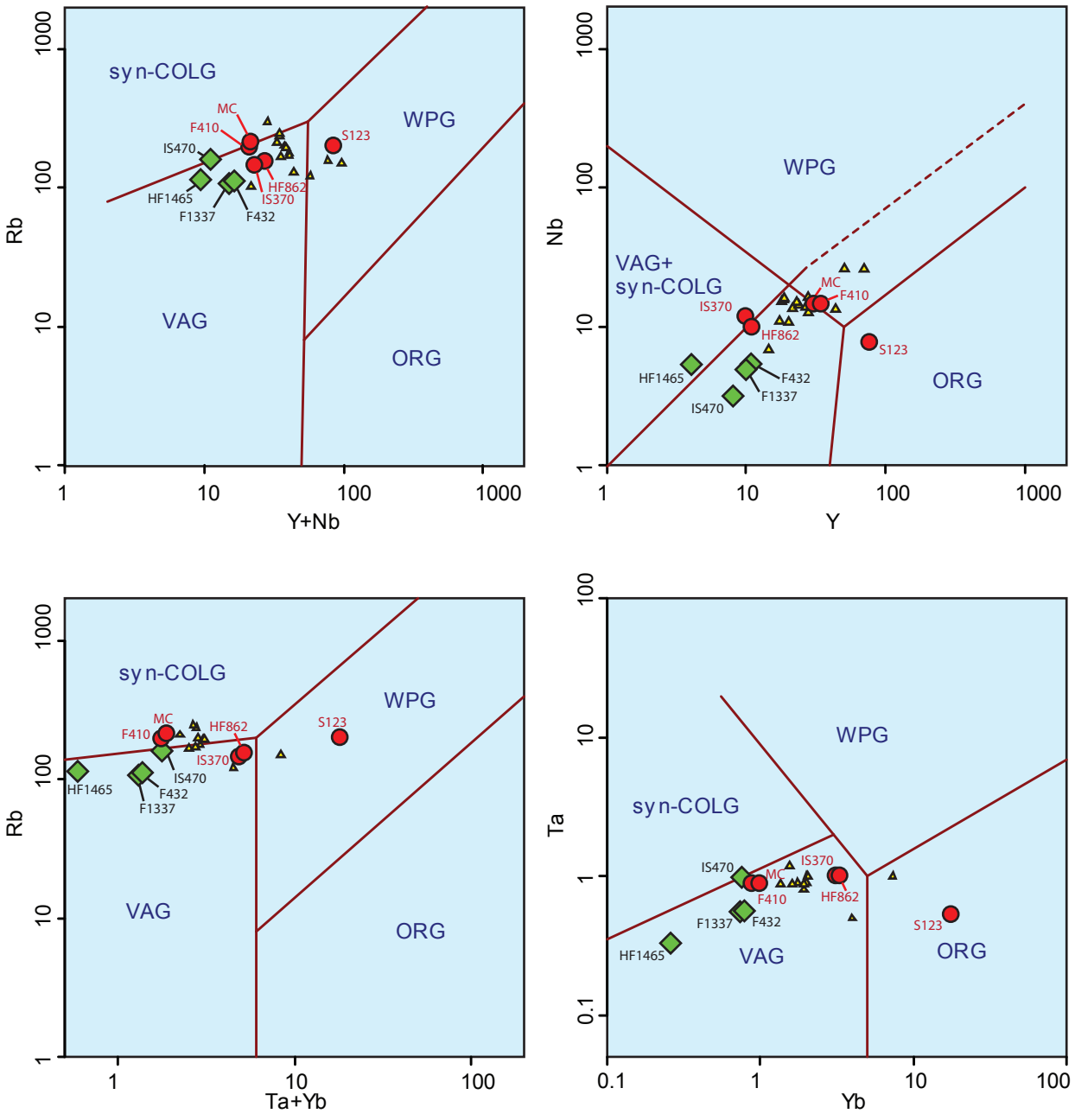


Figure 3-7. Tectonic discrimination diagrams after Pearce et al. (1984). Note logarithmic scale on both vertical and horizontal axes. ORG-orogenic granite. syn-COLG-syn-collisional granite. VAG- volcanic arc granite. WPG-within-plate granite.

Potential Rb mobility should be considered when interpreting Hf-Rb/30-Ta X 3 diagram (Fig. 3-8), but Hf and Ta are HFS elements and are considered immobile (Rollinson, 1993). All samples of High Falls Granite plot well within the volcanic-arc granite field. A significant increase in Rb content due to hydrothermal alteration would be necessary to move these data points out of the within-plate field into the volcanic-arc field. Mukasa and Henry (1990) documented Rb mobility in granite samples from the San Nicholas batholith in central and southern Peru that they attributed to deuteric alteration in which K replaces Rb. A similar reaction in samples from the study area would only move the data points closer to the within-plate granite field. Samples of Indian Springs Granite also plot in the volcanic-arc granite field with the exception of IS470, which plots in the syn-collisional field, but there is little petrographic evidence of hydrothermal alteration in my samples.

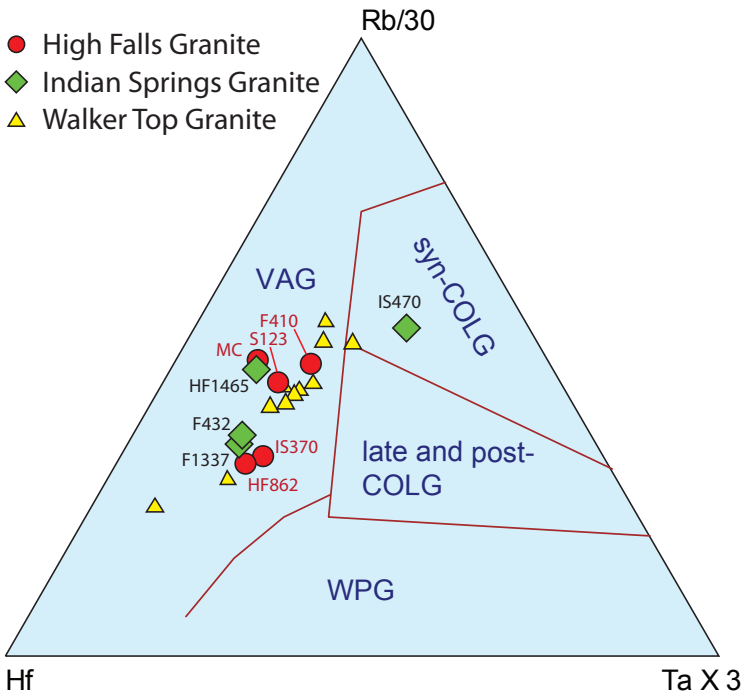


Figure 3-8. Tectonic discrimination diagram (after Harris et al.,1986). All samples plot in the volcanic-arc field except for one Indian Springs Granite and one Walker Top Granite sample.late and post-COLG- late- and post-collisional granite. syn-COLG-syn-collisional granite. VAG-volcanic arc granite. WPG-within plate granite.

The use of the tectonic discrimination diagrams developed by Pearce et al. (1984) and Harris et al. (1986) is summarized by Mukasa and Henry (1990). The volcanic-arc granites they described would have been generated in a subduction zone along a continental margin. In this scenario, the majority of magma would be generated in the mantle and would have been enriched in LIL elements by fluids associated with the down-going slab of oceanic crust. Syn-collisional granites are a product of melting continental crust. These granites are typically peraluminous and have “high Rb/Zr and Ta/Nb and low K/Rb ratios” (Mukasa and Henry, 1990). Late or post-collision granites are thought to be generated in the mantle, but have been heavily contaminated by continental crust during emplacement. The last group, post-collision granites, is also likely “derived from mantle lithosphere beneath collision zones” (Mukasa and Henry, 1990), and is very difficult to distinguish geochemically from within-plate granites.

Frost et al. (2001) developed a three-tiered system for classification of granitic rocks using major element chemistry (Table 3-3). They concluded that trace elements are not completely immobile in granitic rocks, and therefore discrimination systems should be based on major elements. They agreed, however, that the majority of trace elements reside in accessory phases, and trace-element concentration is likely a primary function of the abundance of these phases. Samples of the Siluro-Devonian High Falls Granite were certainly subjected to amphibolite facies metamorphism and, because of this, discrimination diagrams based on trace-element abundances are likely much more reliable. However, previous workers (Byars, 2010; Davis, 2010) used the classification scheme of Frost et al. (2001), so it is used in this discussion for the sake of comparison. The first tier of classification is based on the Fe number [FeO/(FeO+MgO)], which is related to the differentiation history of the granitic magma. Samples may be classified as ferroan or magnesian (Fig. 3-9) based on the relative abundance of Fe and Mg.The second tier is related to the type and abundance of feldspars in the sample.

Table 3-3. Classification of granitoid rocks (from Frost et al., 2001).

Fe-no. or Fe*:	magnesian							
MALI:	calcic		calc-alkalic		alkali-calcic		alkalic	
ASI:	metaluminous	peraluminous	metaluminous	peraluminous	metaluminous	peraluminous	metaluminous	peralkaline
Rock types	diorite, quartz diorite tonalite		diorite, monzodiorite, granodiorite		monzonite, syenite high K-granite		monzonite syenite granite	alkali fsp. syenite alkali fsp. granite
Occurrences	plutons on the outboard portions of Cordilleran batholiths plutons in island arcs plagiogranites		plutons in the main portion of Corderillan batholiths		plutons inboard from Cordilleran batholiths plutons associated with delamination of overthickened crust		plutons inboard from Cordilleran batholiths	
Examples	La Posta pluton (Walawender et al., 1990)	Cornucopia stock (Johnson et al., 1997)	Tuolumne suite (Bateman & Chappell, 1979)	N. Idaho batholith (Hyndman, 1984)	Ben Nevis (Haslam, 1968)	portions of the Vosges granites (Altherr et al., 2000)	Yamato Mtns (Zhao et al., 1995)	Shonkin Sag (Nash & Wilkinson, 1970)
Fe-no. or Fe*:	ferroan							
MALI:	calcic		calc-alkalic		alkali-calcic		alkalic	
ASI:	metaluminous	peraluminous	metaluminous	peraluminous	metaluminous	peraluminous	metaluminous	peralkaline
Rock types	none known	none known	granite	two-mica granite	ferrodiorite syenite, granite	two-mica granite	anorthosite ferrodiorite monzonite granite	alkali gabbro syenite alkali granite
Occurrences			some A-type plutons some granophyres in mafic plutons	some A-type plutons	A-type granites, granophyres associated with mafic dikes and plutons		within-plate plutons, plutons in cores of alkalic volcanoes	
Examples			Bunger Hills (Sheraton et al., 1992)	some Lachlan A-type granites (King et al., 1997)	Sherman batholith (Frost et al., 1999)	St. Vrain, Silver Plume (Anderson & Thomas, 1985)	Bjerkreim–Sokndal (Duchesne & Wilmart, 1997)	Na series of Pikes Peak (Smith et al., 1999)

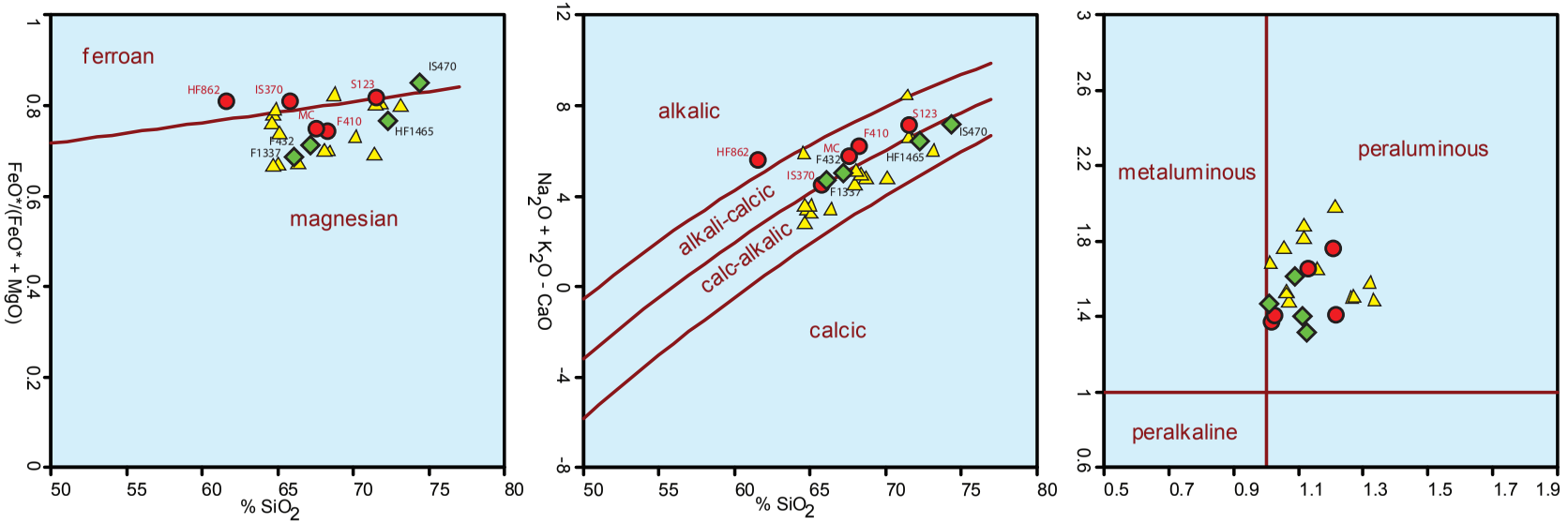


Figure 3-9. Tectonic discrimination diagrams (from Frost et al., 2001). Red circles are High Falls Granite, green diamonds are Indian Springs Granite, and yellow triangles are Walker Top Granite from North Carolina.

The modified alkali-lime index (MALI) (Na_2O+K_2O-CaO) can be used to determine the granitic magma source. Finally, the third tier is the aluminum saturation index (ASI), which is primarily influenced by micas and accessory minerals, and is also related to the magma source (Frost et al., 2001).

These quantities (Fe number, MALI, and ASI) have been plotted versus corresponding silica content (Fig. 3-9). High Falls Granite samples are evenly split between the ferroan and magnesian fields on the Fe#/SiO_2 diagram, while all but one specimen of Indian Springs Granite plots in the magnesian field. The magnesian field is typically populated by “Cordilleran-type” granitoids (Frost et al., 2001). The plot of MALI/SiO_2 shows the High Falls Granite plots predominantly in the alkali-calcic field, while Indian Springs samples straddle the boundary between the alkali-calcic and calcic-alkali fields. Finally, the ASI/SiO_2 plot for the High Falls and Indian Springs Granites indicates all of the samples plot in the peraluminous field. Table 5-3 shows how the three stages of classification subdivide granitic rocks. Using the criteria of Frost et al. (2001), the High Falls Granite is magnesian/ferroan alkali-calcic and peraluminous, Indian Springs Granite is magnesian alkali-calcic/calcic-alkali and peraluminous, and the Walker Top Granite is magnesian calc-alkalic and peraluminous. The High Falls Granite would have formed as either an A-type granite (for the ferroan samples) or inboard from the main portion of a batholith associated with a continental volcanic arc (magnesian samples) using this scheme. The Indian Springs Granite was emplaced in the main batholith of a continental arc system. Sample F410 is an exception because it plots in the ferroan field, which classifies it as an A-type granite. It is worth noting again that major elements are much more susceptible to alteration during metamorphism and chemical weathering, so this classification should be employed with care. However, it is interesting that, based on this classification scheme, the High Falls Granite may be associated with either a continental subduction zone or anorogenic generation of

magma. The rubric used for granitoid classification (Table 3-3) by Frost et al. (2001) does not include any S-type granites so all results must be either I-type or A-type.

Comparison of Geochemistry of the High Falls and Walker Top Granites

The Walker Top Granite in North Carolina is texturally and mineralogically similar to the High Falls Granite. Davis (2010) suggested the granites may have formed by the same processes at the same time. If equivalent, these plutons could help refine the tectonic history of the Siluro-Devonian docking of the Carolina superterrane with the Laurentian + Taconian margin.

All but two of the Walker Top samples plot in the granite field using the normative mineralogy criteria of Barker (1979) (Fig. 3-2). Major element Harker diagrams (Fig. 3-3) reveal similar trends in Walker Top data when compared to the High Falls Granite. One exception occurs in the plot of Al_2O_3 versus SiO_2 where the Walker Top Granite data scatter over a much larger area than the High Falls Granite, but there still is an overall negative trend in the Walker Top data. Trace-element Harker diagrams (Fig. 3-4) show that Cr and Th data for Walker Top samples have significant scatter when compared to data from High Falls Granite. There is also a well-defined negative linear correlation in the Ba versus SiO_2 plot for Walker Top samples. The remaining trace element Harker diagrams reveal similar trends between the Walker Top and High Falls Granites. REE data for both Walker Top and High Falls Granites show a negative linear trend as well as a negative Eu anomaly (Fig. 3-6). The High Falls Granite reveals a slight concave upward trend between Gd and Lu that does not appear in the Walker Top data. The presence of garnet, zircon, or xenotime can produce heavy REE enrichment (Best, 2003).

Walker Top Granite data have been plotted in the same tectonic discrimination diagrams developed by Pearce et al. (1984), Harris et al. (1986), and Frost et al. (2001)

that were employed for the High Falls Granite. The data are spread across the volcanic-arc, syn-collisional, and within-plate granite fields in much the same way as the High Falls Granite (Figs. 3-7, Fig. 3-8). With one exception, the Walker Top data plot in the volcanic-arc field in the ternary diagram (Fig. 3-8) of Harris et al. (1986).

Summary and Interpretation of Granite Geochemistry

Several variables make difficult any geochemical analysis of samples from the study area. First, the High Falls Granite crystallized over a period between 53 and 33 Ma (see below). The chemical makeup in the magma chamber could have been modified by pulses of new melt or the assimilation of crust during this period. Second, the High Falls Granite was metamorphosed during the Alleghanian orogeny. Finally, it is difficult to find unweathered samples of both the High Falls and Indian Springs Granites in the study area. Care was taken to analyze fresh material, but weathering may still have had an effect on sample chemistry. The High Falls and Walker Top Granites appear to be equivalent based on normative mineralogy (Barker, 1979), and the majority of major and trace elements trends on Harker diagrams, and REE patterns. Davis (2010) also came to this conclusion.

Tectonic discrimination diagrams were used in an attempt to determine the tectonic setting in which the High Falls and Walker Top Granites were generated; these methods also suggest genetic equivalency between the two granites. Ideally, the data points for each granitoid plot in tight clusters close to each other. The results compiled here indicate that both granitoids may have been produced in complex tectonic settings. The variables discussed above, which may complicate geochemical analysis, must be kept in mind when applying tectonic discrimination techniques. While Rb is potentially mobile, it is reassuring that the same two pairs (MC/F410 and HF862/IS370) plot together on all of the trace element discrimination diagrams (Figs. 3-7, Fig.

3-8), including those that do not rely on Rb abundance. The diagrams of Pearce et al. (1984) suggest that the High Falls Granite could be the product of at least two tectonic processes (discussed below). Based on these plots, samples HF862 and IS370 may have formed in a continental-arc setting, while MC and F410 may have been produced in a syn-collisional setting. Sample S123 consistently plots well within the orogenic or within-plate field, which suggests it was not produced by an arc system. The Walker Top Granite data plot across the same fields as the High Falls samples on the discrimination diagrams (Pearce et al., 1984; Harris et al., 1986). This indicates the Walker Top Granite may also have a complex tectonic history. Trace element discrimination diagrams indicate the likelihood that the Indian Springs Granite was formed by subduction beneath the Laurentian + Taconian margin.

The major element discrimination diagrams of Frost et al. (2001) (Fig. 3-9) also suggest that a complex (possibly transitional) tectonic setting produced the High Falls and Walker Top Granites, but the High Falls Granite data points do not pair up as consistently as they do in the trace element diagrams. These diagrams are only being used for comparison of the High Falls and Walker Top Granites. It is particularly noteworthy that all three of the granites analyzed in this study are peraluminous based on the classification of Frost et al. (2001) which is typically associated with S-type granites (Chappell and White, 1974); however, it is possible to generate peraluminous melts by melting of biotite-bearing metaluminous felsic rocks (Miller, 1985) or even by water-excess melting of mafic rocks (Ellis and Thompson, 1986).

Granite Geochronology

Geochronologic Methodology

Samples were collected for geochronologic analysis in the field area as well as from adjacent quadrangles. Two specimens of High Falls Granite (HFSP and HHF) were collected in the project area. Specimens from the Barnesville (BG18), Stewart (S123), and Farrar (FRHF) quadrangles (Fig. 3-10) were also analyzed at the Stanford University-U.S. Geological Survey Micro Analysis Center (SUMAC) facillty. Matt Huebner, Phillip Derryberry, and Carissa Snyder helped collect data that are used in this chapter at the SUMAC facility. This assistance is very much appreciated. Samples were only collected from large, well mapped bodies of High Falls Granite. Effort was made to collect fresh material in order to perform both geochemical and geochronologic analyses on the same specimen. While at the outcrop samples were typically broken up into pieces ~5 cm in diameter to prevent contamination between samples in the lab. Preliminary sample processing was conducted at The University of Tennessee-Knoxville, the University of North Carolina-Chapel Hill, and Vanderbilt University. The preliminary phase included crushing the specimens with a “chipmunk” jaw crusher and pulverizing the samples with a disc mill. The pulverized material was separated into light and heavy constituents using a Wilfley table. After thorough drying, magnetite in the heavy separates was removed with a hand magnet. Additional separations were made using methelyne iodide in a separatory funnel and then a Franz magnetic separator. The material that passed through the magnetic separator was taken to the SUMAC. Here, zircons were picked and mounted on polycarbonate pucks that were subsequently gold-plated. Cathodoluminescence (CL) images were made using a JEOL 5600 LV scanning electron microscope, after which the gold coating was removed. A digital camera mounted on a reflected light microscope was used to photograph each sample. The CL

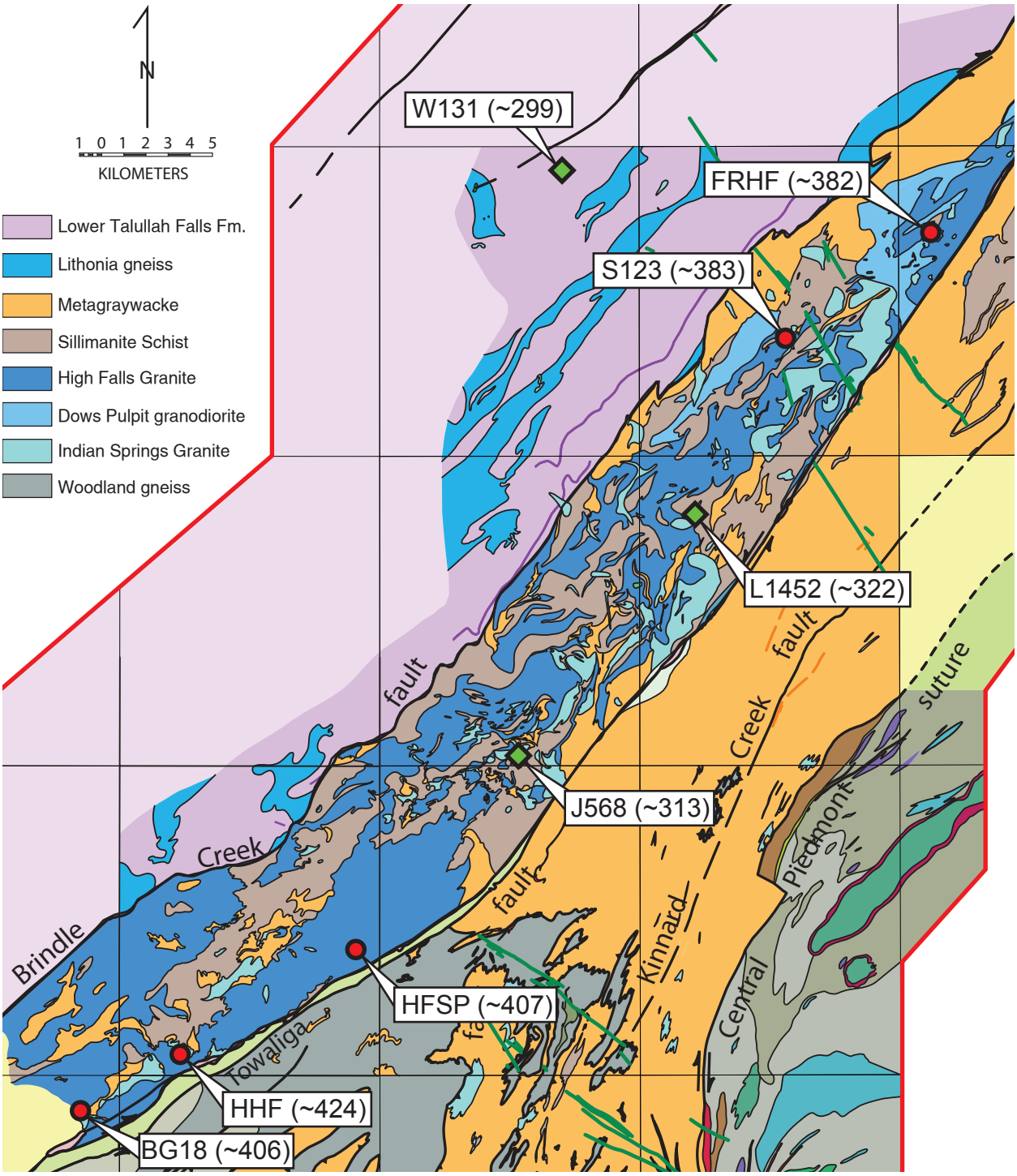


Figure 3-10. Simplified detailed geologic map of the area showing the location of geochronology samples in my mapped area to the southwest, in the area mapped by B.A. Davis (2010) to the northeast and in the area mapped by M.T. Huebner at center. Map compiled by M.T. Huebner from Davis (2010); Huebner (unpublished); Hatcher (unpublished); Hooper (1986) and my own data. Red circles are HIgh Falls Granite samples and green diamonds are Indian Springs Granite samples.

and reflected light images were examined to select optimum locations from SHRIMP-RG analysis. These locations included obvious inherited cores and metamorphic rims, but cracked or discolored areas within the zircons were avoided. The specimens were re-coated with gold and placed in the SHRIMP for analysis. During testing, a zircon standard (R-33, ~419 Ma), which was provided by the SUMAC facility, was analyzed after every fourth analysis to insure accurate data reduction. The raw data were processed by SUMAC staff using SQUID v. 1.03 (Ludwig, 2001). SUMAC staff also generated plots of age data with Isoplot v. 3.0 (Ludwig, 2003).

Zircon Morphology

The major axes of High Falls Granite zircons that were analyzed range from 80-406 μm long, while the minor axes of the crystals range from 41-122 μm wide. The aspect ratios of the zircons lie between 1:1.5 and 1:6.6. A more detailed description of the sizes and shapes of zircons in each sample can be found in Table 3-4. Longer, more acicular zircons are typically interpreted to have crystallized rapidly in volcanic or shallow intrusive rocks, while “stubbier” crystals with a lower aspect ratio (sometimes approaching 1) are associated with magmas that cooled slowly at a lower level in the crust (Corfu et al., 2003).

Zircons from sample BG18 (Barnesville) display a wide variation in albedo, which is commonly related to uranium content. Zircons, or zones within zircons low in uranium, commonly produce a lighter relative color in CL images when compared to uranium-rich zircons (Fig. 3-11). This contrast is not only evident when comparing the cores and rims of individual zircons, but also when comparing magmatic zircons. Zircons in BG18 show oscillatory zoning (repeated compositional variations) and sector zoning (compositional variation controlled by crystal structure) that is visible in CL images. This zonation is caused by compositional variation from nearly pure zircon (depleted in trace elements)

to contaminated zircon (enriched in trace elements). Several zircons in sample BG18 have inherited cores showing evidence of resorption that are encased by nearly euhedral recrystallized zircon rims (Fig. 3-11a).

Acicular zircons with high aspect ratios are common in sample HHF (Fig. 3-12a). These crystals typically have one or two visible inclusions in their cores but display only minor resorption embayments, which suggests that the majority of these zircons may have crystallized rapidly. Zircons with a lower aspect ratio have cores that may have been inherited, but isotopic analysis determined that only one of these (HHF-1) was actually inherited. This well-rounded core is also embayed, and is surrounded by a Neoacadian metamorphic rim. Oscillatory zoning is visible in all specimens analyzed from this sample.

Table 3-4. Zircon morphologies

	BG18	**HHF**	**HFSP**	**S123**	**FRHF**
Average Aspect Ratio	2.7	3.6	2.9	2.9	3.3
Maximum Aspect Ratio	3.8	6.6	4.4	4.0	4.4
Minimum Aspect Ratio	1.6	1.8	1.5	1.8	2.0
Maximum Major Axis	272.6	405.8	363.2	350.2	388.6
Minimum Major Axis	80.8	135.0	140.1	140.7	133.9
Maximum Minor Axis	112.9	87.3	107.6	106.1	121.5
Minimum Minor Axis	41.8	43.6	56.6	51.2	65.8

Figure 3-11. Geochronologic data for High Falls Granite sample BG18. (a) CL image of representative zircon crystals with locations of SHRIMP-RG analysis and ages based on $^{238}U/^{206}Pb$ abundances. (b) Isoplot calculated age. (c) Probability frequency plot with counts shown as blue rectangles and relative probability in red. (d) Concordia diagram with sample ages as green diamonds and error ellipses in red. Data courtesy of Justin R. Rehrer.

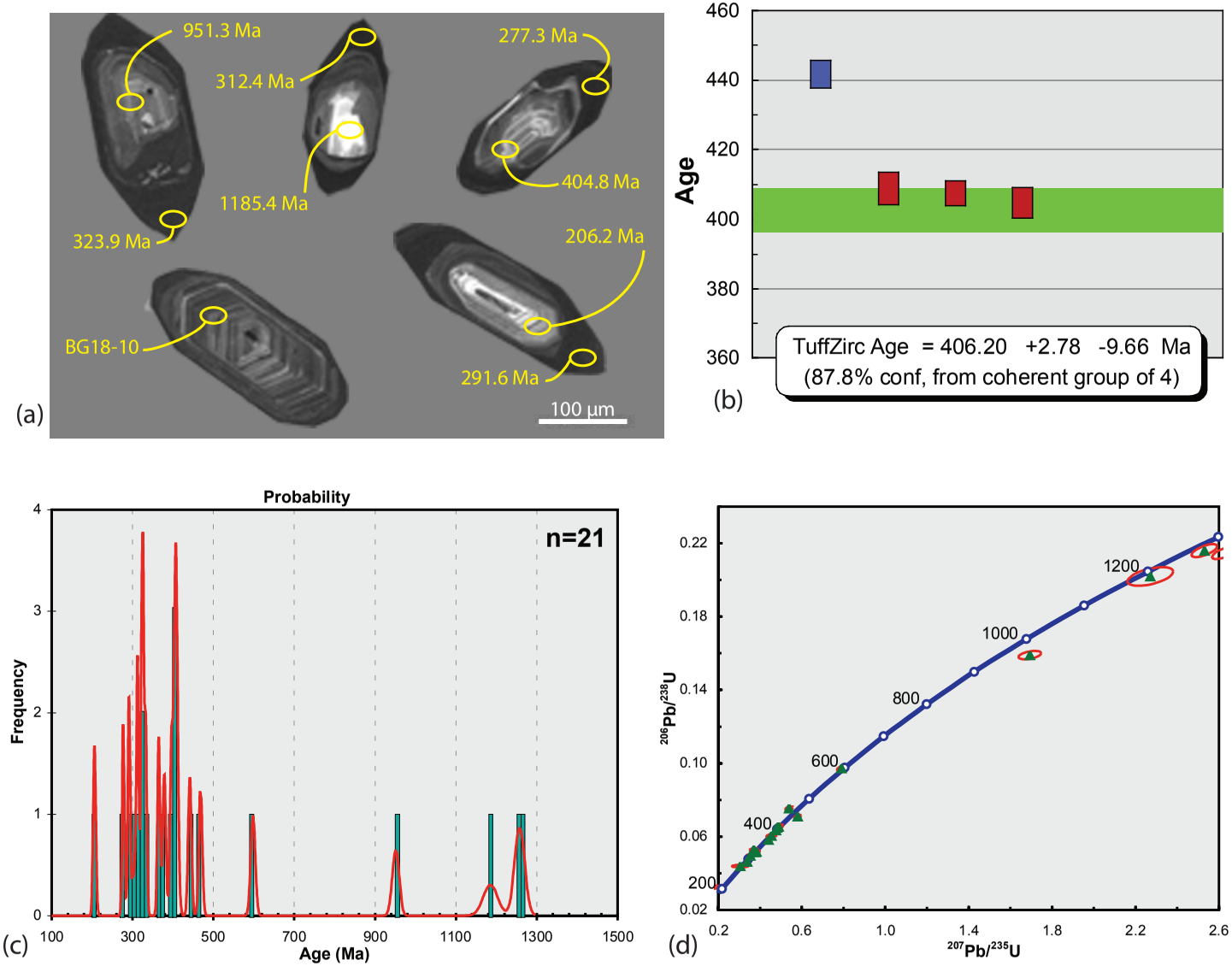
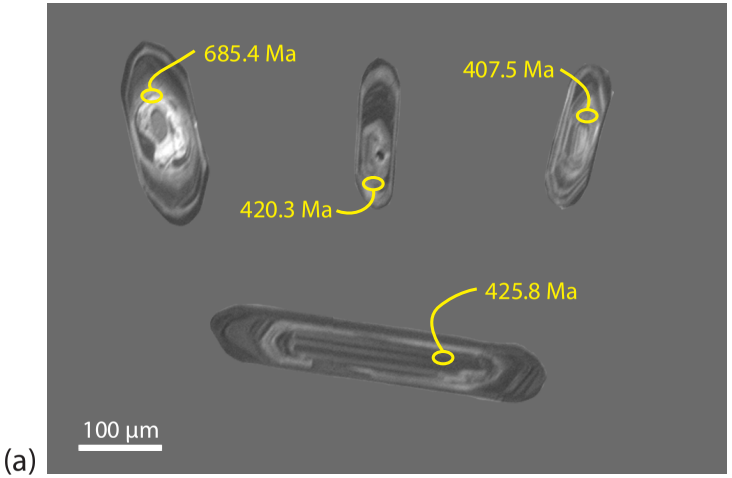
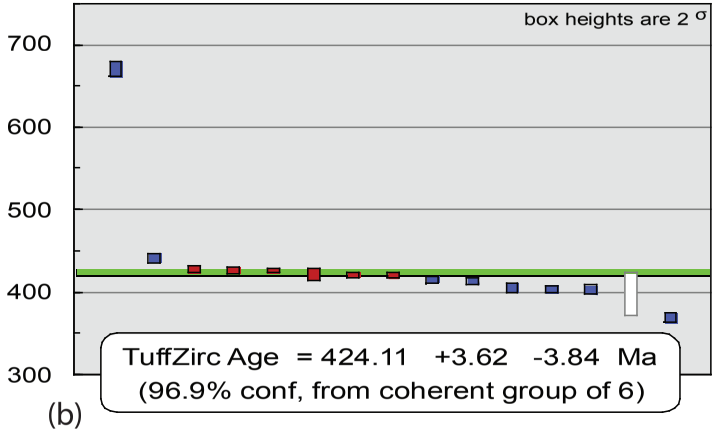

951.3 Ma
312.4 Ma
277.3 Ma
1185.4 Ma
404.8 Ma
323.9 Ma
206.2 Ma
BG18-10
291.6 Ma
100 µm
(a)
Age
460
440
420
400
380
360
TuffZirc Age = 406.20 +2.78 -9.66 Ma
(87.8% conf, from coherent group of 4)
(b)
Probability
n=21
Frequency
Age (Ma)
(c)
$^{206}Pb/^{238}U$
$^{207}Pb/^{235}U$
1200
1000
800
600
400
200
(d)

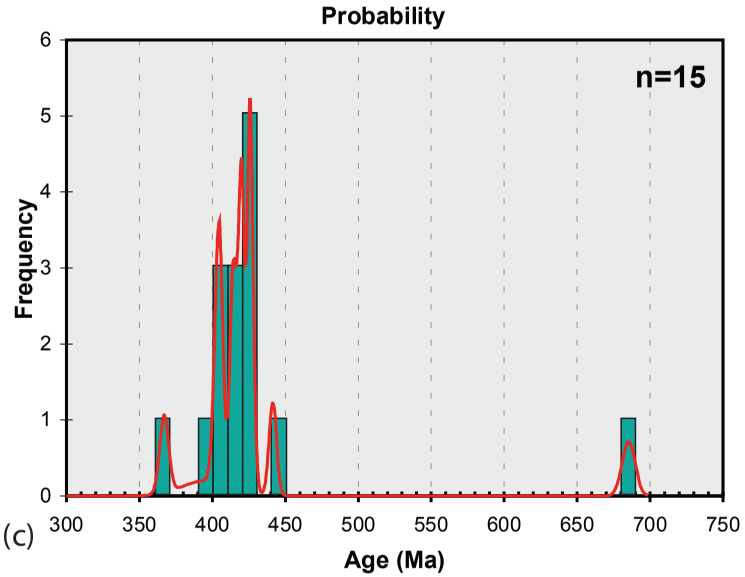
Figure 3-12. Geochronologic data for High Falls Granite sample HHF. (a) CL image of representative zircon crystals with locations of SHRIMP-RG analysis and ages based on $^{238}U/^{206}Pb$ abundances. (b) Isoplot calculated age. (c) Probability frequency plot with counts shown as blue rectangles and relative probability in red. (d) Concordia diagram with sample ages as green diamonds and error ellipses in red.


685.4 Ma
407.5 Ma
420.3 Ma
425.8 Ma
100 µm

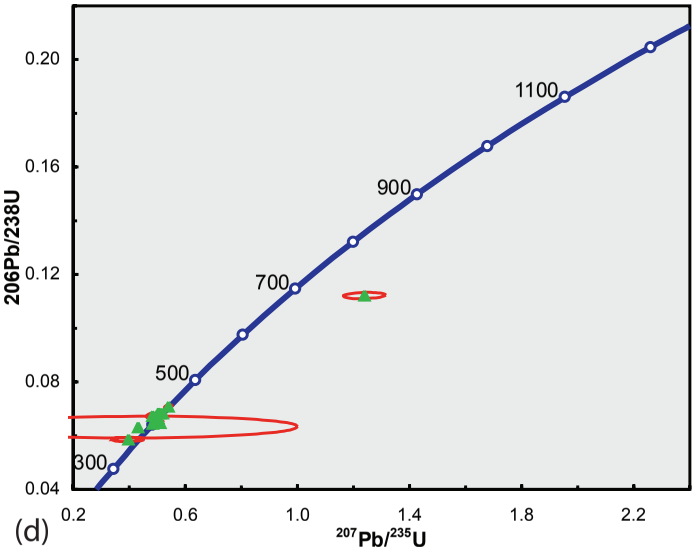
(a)


box heights are 2 σ
700
600
500
400
300
TuffZirc Age = 424.11 +3.62 -3.84 Ma
(96.9% conf, from coherent group of 6)

(b)


Probability
n=15
Frequency
Age (Ma)
0
1
2
3
4
5
6
300
350
400
450
500
550
600
650
700
750

(c)


206Pb/238U
207Pb/235U
0.04
0.08
0.12
0.16
0.20
0.2
0.6
1.0
1.4
1.8
2.2
300
500
700
900
1100

(d)

Zircons analyzed from the HFSP specimen are characterized by grains with aspect ratios that vary between 4.4 and 1.5. Zircons with relatively high aspect ratios generally show signs of resorption, but the grains with the lowest aspect ratios possess significant embayments caused by partial resorption (Fig. 3-13a). Significant resorption would logically be related to a lengthy cooling period; this is supported by age dating of cores and rims that produce dates several million years apart. Results of age dating are discussed in detail below. Several grains from HFSP also contain inherited cores. Inherited cores are typically much lighter in color (due to lower uranium content and thus older calculated age), and contain numerous inclusions when compared with other zircons from this sample.

Sample S123 from the Stewart quadrangle (Huebner, unpublished data) contains zircons that have relatively high aspect ratios; however, many of the analyzed zircons are broken with fractured ends. Incomplete zircons were not included in size and aspect ratio calculations (Table 3-4). While many of the crystals selected from sample S123 appeared to have inherited cores, age determinations indicate that only one core is truly inherited. Several zircons tested show signs of dissolution and recrystallization during cooling, and many crystals contain oscillatory zoning (Fig. 3-14a).

Zircons from sample FRHF (Fig. 3-15a) from the Farrar quadrangle (Davis, 2010) have the greatest amount of variability in morphology. Grains have a wide range of aspect ratios, and inclusions are abundant throughout some zircons while absent in others. Approximately half of the zircons analyzed contain signs of alteration during crystallization, and several crystals contain fractured cores surrounded by relatively intact material.

Generally, the morphology of the zircons analyzed as part of this study appears to correspond to slow cooling in a deep-seated magma chamber, but acicular crystals with high aspect ratios are present in most of the samples. Zircons produced by

Figure 3-13. Geochronologic data for High Falls Granite sample HFSP. (a) CL image of representative zircon crystals with locations of SHRIMP-RG analysis and ages based on $^{238}U/^{206}Pb$ abundances. (b) Isoplot calculated age. (c) Probability frequency plot with counts shown as blue rectangles and relative probability in red. (d) Concordia diagram with sample ages as green diamonds and error ellipses in red.

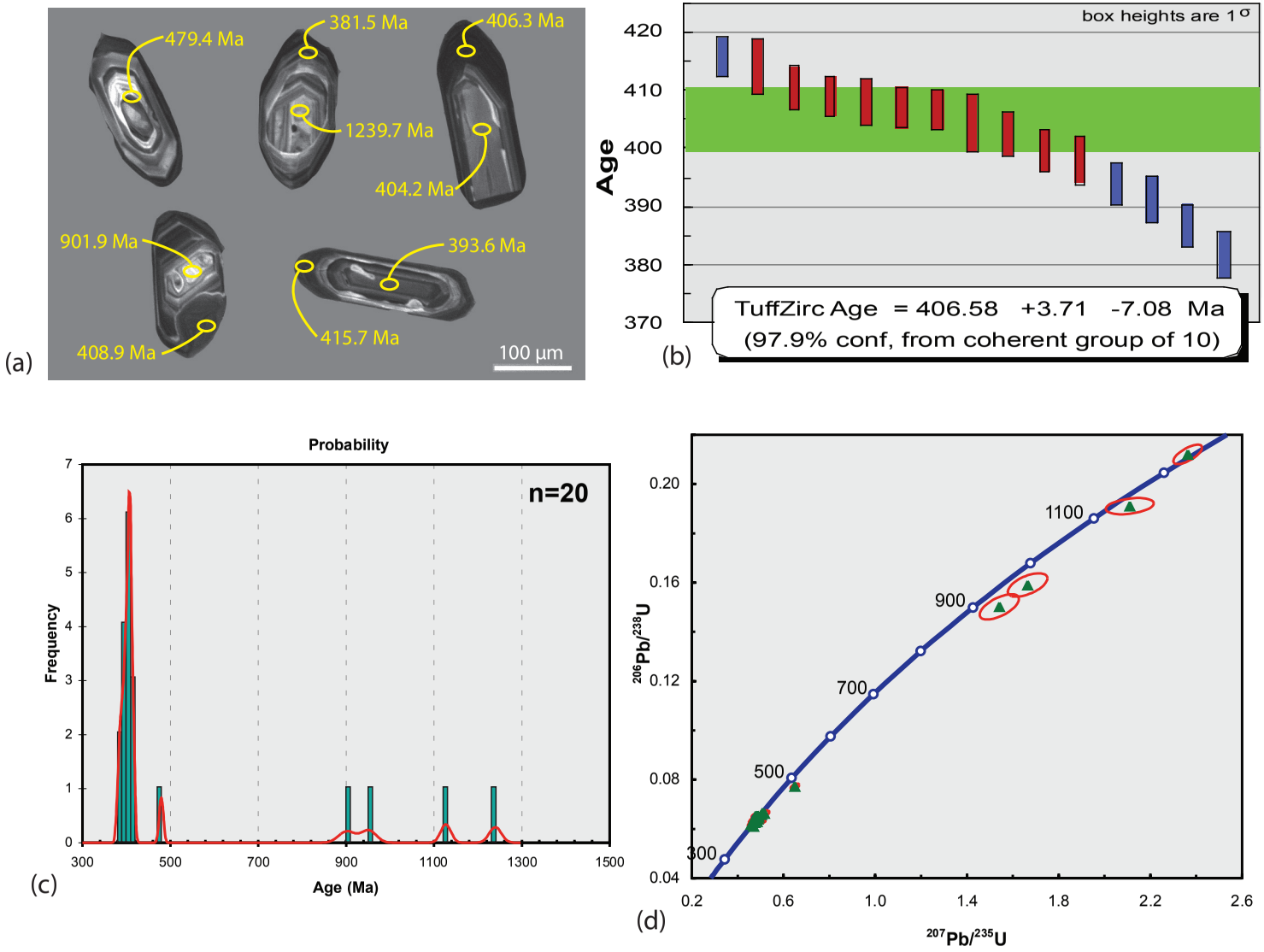

(a)
479.4 Ma
381.5 Ma
406.3 Ma
1239.7 Ma
404.2 Ma
901.9 Ma
393.6 Ma
415.7 Ma
408.9 Ma
100 µm
(b)
box heights are 1σ
Age
420
410
400
390
380
370
TuffZirc Age = 406.58 +3.71 -7.08 Ma
(97.9% conf, from coherent group of 10)
(c)
Probability
n=20
Frequency
Age (Ma)
(d)
206Pb/238U
207Pb/235U
300
500
700
900
1100

Figure 3-14. Geochronologic data for High Falls Granite sample S123. (a) CL image of representative zircon crystals with locations of SHRIMP-RG analysis and ages based on $^{238}U/^{206}Pb$ abundances. (b) Isoplot calculated age. (c) Probability frequency plot with counts shown as blue rectangles and relative probability in red. (d) Concordia diagram with sample ages as green diamonds and error ellipses in red. Data courtesy of Matthew T. Huebner.

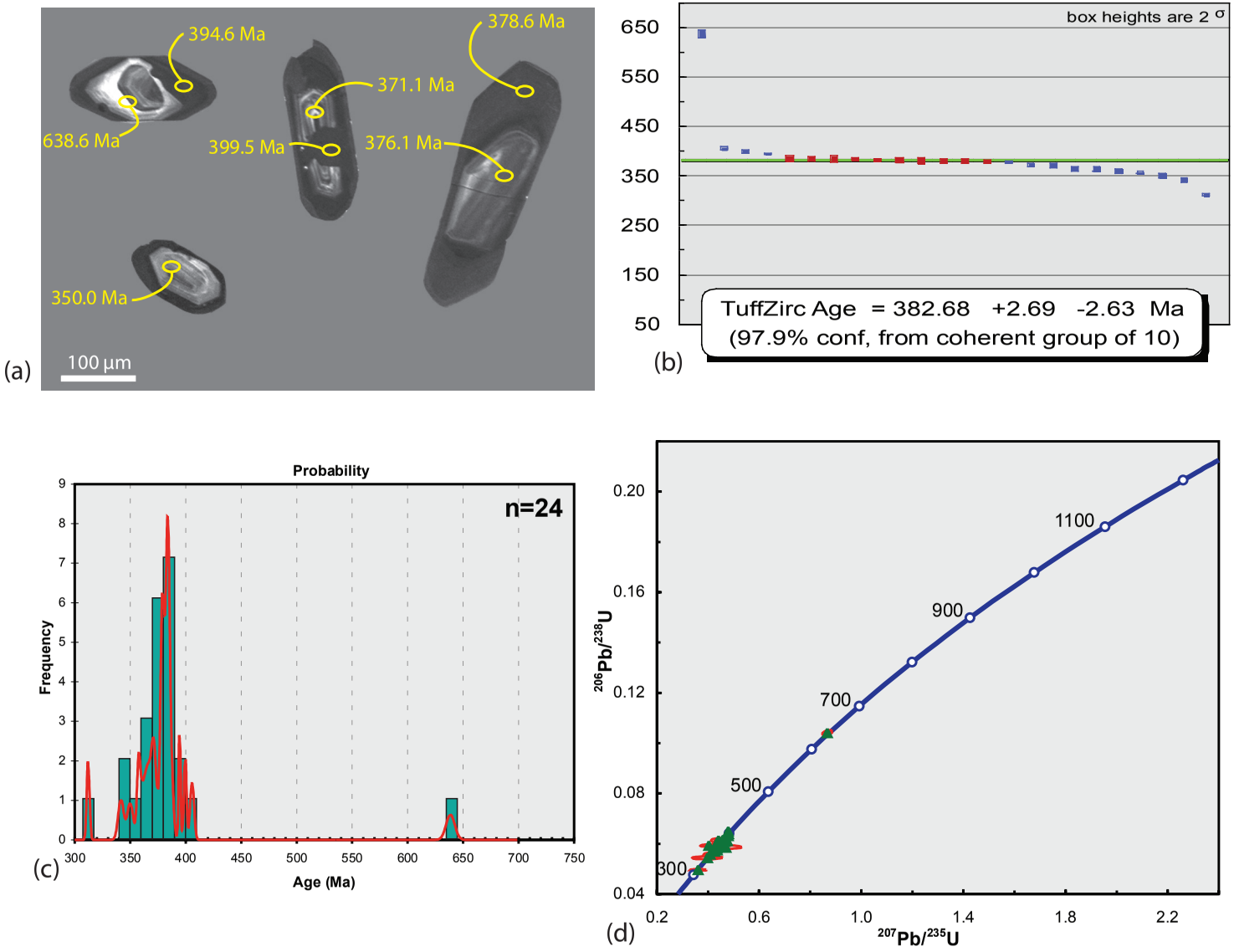
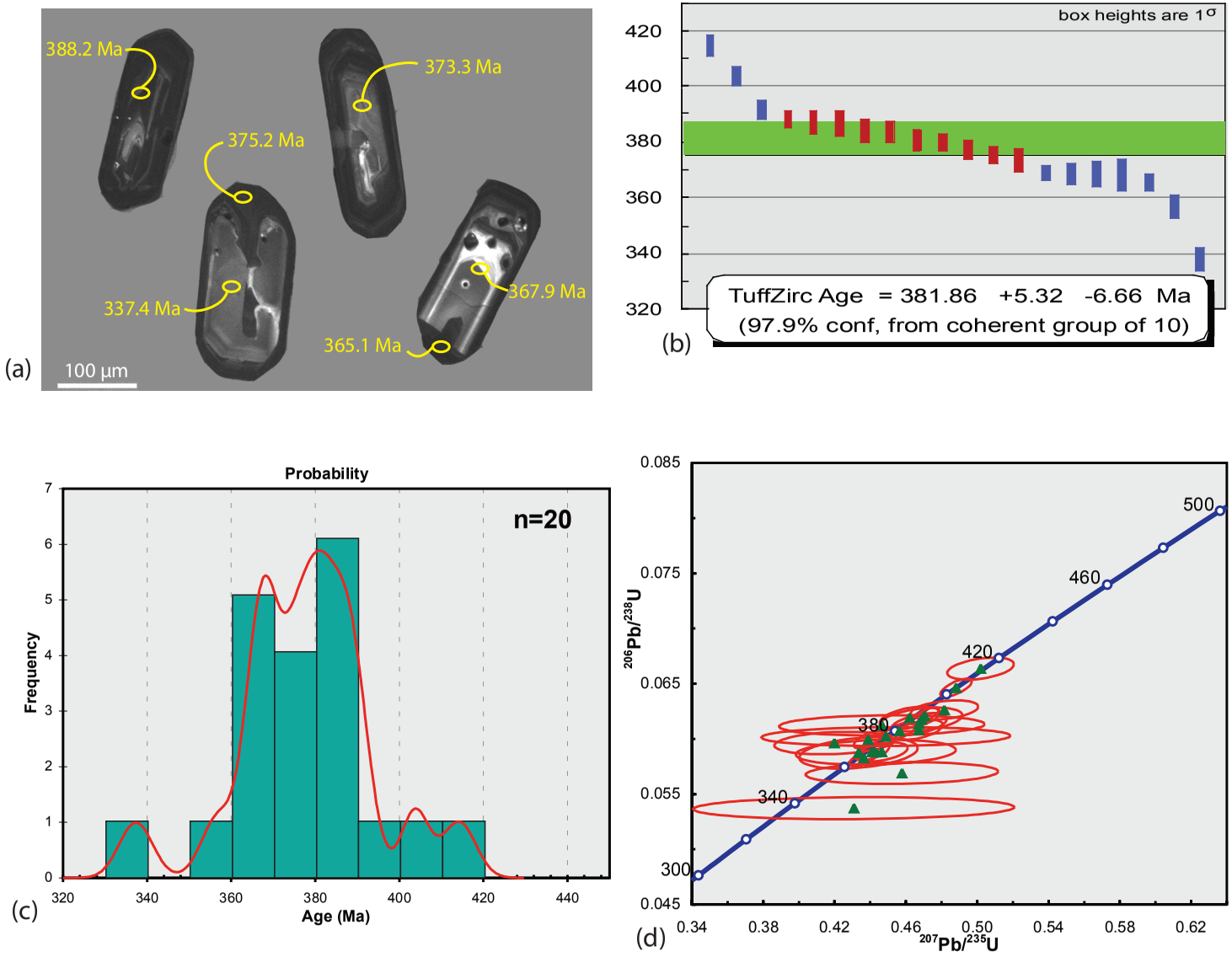

394.6 Ma
378.6 Ma
371.1 Ma
638.6 Ma
399.5 Ma
376.1 Ma
350.0 Ma
100 µm
(a)
box heights are 2 σ
650
550
450
350
250
150
50
TuffZirc Age = 382.68 +2.69 -2.63 Ma
(97.9% conf, from coherent group of 10)
(b)
Probability
n=24
Frequency
Age (Ma)
(c)
0.20
0.16
0.12
0.08
0.04
1100
900
700
500
300
0.2
0.6
1.0
1.4
1.8
2.2
$^{206}Pb/^{238}U$
$^{207}Pb/^{235}U$
(d)

Figure 3-15. Geochronologic data for High Falls Granite sample FRHF. (a) CL image of representative zircon crystals with locations of SHRIMP-RG analysis and ages based on $^{238}U/^{206}Pb$ abundances. (b) Isoplot calculated age. (c) Probability frequency plot with counts shown as blue rectangles and relative probability in red. (d) Concordia diagram with sample ages as green diamonds and error ellipses in red. Data courtesy of Matthew T. Huebner.


388.2 Ma
373.3 Ma
375.2 Ma
337.4 Ma
367.9 Ma
365.1 Ma
100 µm
(a)
box heights are 1σ
420
400
380
360
340
320
TuffZirc Age = 381.86 +5.32 -6.66 Ma
(97.9% conf, from coherent group of 10)
(b)
Probability
n=20
Frequency
Age (Ma)
(c)
0.085
0.075
0.065
0.055
0.045
500
460
420
380
340
300
$^{206}Pb/^{238}U$
$^{207}Pb/^{235}U$
(d)

metamorphism typically show evidence of significant resorption, but magmatic fluids derived from mica schists and migmatites (specifically in amphibolite facies terranes) yield euhedral zircons (Corfu et al., 2003). The numerous examples of resorption textures in individual crystals indicate that zircon crystallization phases were punctuated by periods of dissolution during Neoacadian emplacement of the High Falls Granite. Fluctuations in temperature, magmatic chemistry, and influx of magmatic fluids can affect the solubility of zircon (Corfu et al., 2003).

Geochronologic Results

The zircon age plot for BG18 produced an age of 406 +2.78 -9.66 Ma, but there is a second horizontal trend in the data plot at ~323 Ma. rims (Fig. 3-11b). Zircons that were analyzed in this sample make up a younger cluster of ages, which suggests metamorphic rims crystallized during an Alleghanian overprint. The probability-frequency plot (Fig. 3-11c) clearly reveals one inherited core with Pan-african affinity (~600 Ma) and 4 cores with Grenville ages (1260-950 Ma). The 600 Ma core is concordant, which supports the idea that this data point was not “accidentally” generated by focusing the ion beam on part of a Grenville core as well as a portion of Neoacadian overgrowth. Data suggest that this “accidental overlap” produced a similar age for one location analyzed for sample HHF; that scenario is discussed below. Thin peaks on the probability diagrams result from the two clusters of ages discussed above. The concordia diagrams (Fig. 3-11d) for this sample reveal the inherited cores are somewhat discordant, while the two clusters of Neoacadian and Alleghanian ages are much more concordant. The age dates of spot analyses of sample BG18 revealed that inherited cores are present (Fig. 3-11a). The age dates for these cores (BG18-13, 9.1, 7.1, and 4.1) agree with the interpretation that they are inherited, based on their morphology.

The calculated age for sample HHF (High Falls quadrangle) is 424 +3.62 -3.84 Ma, and all the data points except one cluster around this date (Fig. 3-12b). The High Falls Granite sample HHF is the oldest granitoid that has been dated so far anywhere in the Cat Square terrane. The relative probability plot (Fig. 3-12c) excludes point HHF-1. The other ages produce a narrow peak centered around the 424 Ma age. HHF-1 contains one zircon that yielded an age of ~682 Ma, but that data point is significantly discordant when compared with other ages from this sample in the concordia plot (Fig. 3-12d). It is likely that the analyzed spot overlapped an inherited core and Neoacadian overgrowth.

Isoplot calculated an Acadian age (407 +3.71 -7.08 Ma) for sample HFSP. Ages derived from non-inherited zircon components form a sharp peak at ~407 Ma in the probability plot (Fig. 3-13b). Several cores were visually identified in sample HFSP. The calculated ages of these cores confirm that they are inherited based on textural relationships and morphology. HFSP-5 produced an age of ~480 Ma, but lies on a chord that passes through the other inherited cores and would cross the concordia at ~1.0 Ga. This relationship suggests that all of the inherited cores have a Laurentian affinity.

Sample S123 (Stewart quadrangle) has a calculated age of 383 +2.69 -2.63 Ma. One Pan-African inherited core yielded an ~639 Ma age. The probability plot (Fig. 3-14c) reveals a slightly right-skewed peak. The vast majority of data points (including the ~639 Ma core) plot very close to the concordia curve for this sample. When compared to other High Falls Granite samples, this specimen has a small amount of inheritance.

FRHF (Farrar quadrangle) lies the farthest to the NE in the recently mapped portion of the Georgia Inner Piedmont (Davis, 2010) (Fig. 3-10). Interestingly, no inherited cores were observed in this sample. The probability plot (Fig. 3-15c) contains a fairly broad peak around the calculated age for this sample, 382 +5.32 -6.66 Ma, and

one age (Alleghanian) metamorphic rim from FRHF-13. The error ellipses plotted in this concordia diagram are larger than those of other samples discussed in this chapter.

Zircon REE Concentrations

The SHRIMP collected additional REE data for each zircon analyzed during geochronologic analysis. Representative concentrations have been chondrite-normalized (Fig. 3-16) and plotted for comparison. As expected, the zircon REE patterns from analyzed samples of High Falls Granite have a nearly identical shape. Others (e.g., Hoskin and Ireland, 2000) have concluded there is a surprisingly small variation in the overall REE chemistry of zircons from a wide range of rock types. Such consistency between samples has been attributed to the fact that, at the point of zircon saturation, the melt had granitic composition. The charge-balance requirements of the zircon crystal lattice may also tightly limit the possibilities for substitution (Hoskin and Ireland, 2000). The positive Ce anamoly and negative Eu anamoly seen in these samples is common in crustal zircon and "is consistent with formation under variable yet relatively oxidized conditions (Hoskin and Schaltegger, 2003)."

Summary and Implications of Granite Geochronology

Results of U-Pb dating reveal an overall younging trend from southwest to northeast in the Cat Square terrane in central Georgia. Four of the High Falls Granite samples have Acadian ages (407-382 Ma) and one sample (HHF) has an even older Silurian age (424 Ma). There are also interesting coincidences between High Falls Granite age and zircon inheritance. Inherited peri-Gondwanan and Laurentian cores are abundant in specimens collected from the southwest part of the study area (BG18, HHF, and HFSP), which also coincides with the oldest samples. Only one inherited core yielded an age between the two younger samples (S123 and FRHF) of

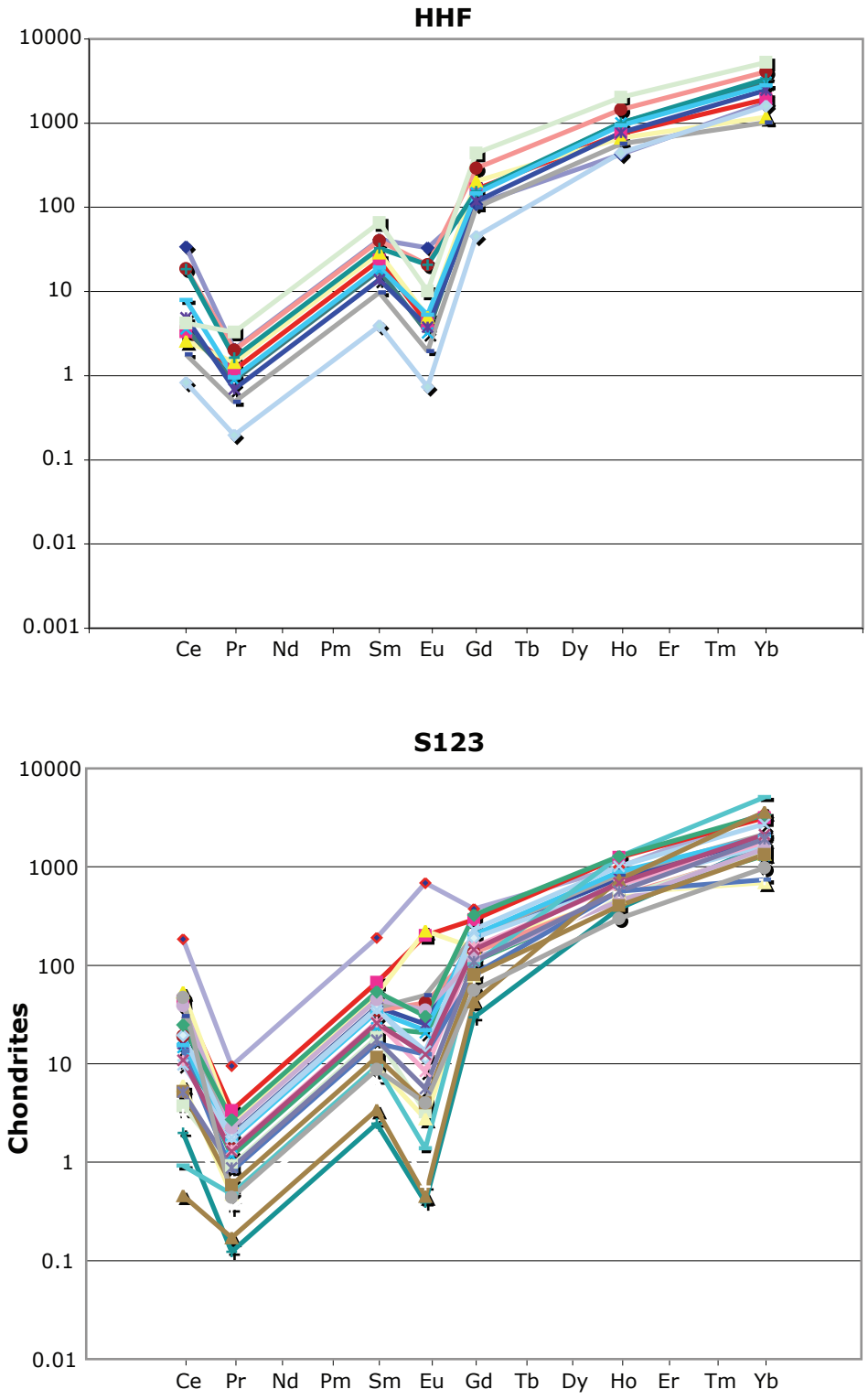


Figure 3-16. Representative REE concentrations of zircons analyzed from samples HHF and S123. Each colored line represents an individual SHRIMP-RG analysis.

High Falls Granite in the northeast part of the study area. High Falls Granite magma containing inherited cores must have been contaminated during emplacement by a crust containing both Laurentian and peri-Gondwanan zircons. Samples with few or no inherited cores were either not contaminated during emplacement or characteristics of that melt (temperature, water content, etc.) must have been conducive to resorption and subsequent recrystallization of zircon during cooling, thus erasing any evidence of inheritance.

Synthesis of Granite Geochemistry and Geochronolgy

Tectonic discrimination diagrams suggest that the High Falls Granite may have been produced in at least two tectonic settings: a continental-arc system formed by the subduction of oceanic crust, and syn-collisional melting of crustal material. However, if the High Falls Granite is solely the product of anatexis of sediment in the Cat Square terrane, the source of those sediments must be considered. Merschat and Hatcher (2007) suggested that sediments in the Cat square terrane were a mixture of Laurentian and peri-Gondwanan material deposited as the Rheic Ocean closed prior to the Acadian orogeny. If this hypothesis is correct, anatexis of these sediments would likely have generated a melt from a heterogeneous mixuture of mature continental sediment (sourced from Laurentia) and relatively immature volcanic island arc sediment (derived from the Carolina superterrane). A melt produced from such a mixture could have crystallized into a pluton of varying chemistry as seen on the tectonic discrimination diagrams above in this chapter.

U-Pb zircon dates have revealed a lengthy crystallization process for the High Falls Granite (53-33 Ma) as well as contrasting patterns of zircon inheritance within the granite body. High Falls Granite samples from the southwestern end of the study area (BG18, HHF, HFSP, HF862, and IS370) are the oldest, contain the most inherited zircon

cores, and consistently plot in the volcanic-arc granite field in trace element tectonic discrimination diagrams. Samples collected at the northeastern end of the study area (S123, FRHF, F410, and MC) are the youngest, contain few or no inherited zircon cores, and typically plot in the syn-collisional, within-plate, or orogenic granite fields. Taken together, these data suggest that the High Falls Granite may be a composite pluton that was generated either in two different tectonic settings or perhaps produced by a transitional tectonic environment as the Carolina superterrane approached and was obducted onto the Laurentian + Taconic margin. Possibilities include a westward-dipping subduction beneath the Laurentian + Taconian margin that reversed polarity to facilitate obduction of the Carolina superterrane, eastward- and westward-dipping subduction that produced the oldest High Falls Granite plutons, and then obducted the Carolina superterrane. The Carolina superterrane also may have accreted in several pieces in the southern Appalachians. Finally, the High Falls Granite may have been emplaced as one batholith that was subsequently turned onto its side. These possibilities will be discussed in detail in chapter six. Like the Sierra Nevada batholith (Glazner et al., 2004), the High Falls Granite may also be made up of several plutons. Low resolution of geochemical data coupled with the amount of exposure in the study area makes this hypothesis difficult to test.

The Walker Top Granite in the North Carolina Cat Square terrane also has a lengthy crystallization history (407-355 Ma) as separate plutons and trace element data from these rocks plot across volcanic-arc, syn-collisional, within-plate, and orogenic granite fields in tectonic discrimination diagrams (Byars, 2010). These facts, coupled with similarities in mineralogy, texture, and bulk rock geochemistry (REE patterns and trends on Harker diagrams), strongly suggest that the Walker Top and High Falls Granites are consanguineous. The data also suggest that both of these granites were emplaced by complex tectonic processes. Previous workers (Merschat, 2009; Byars,

2010; Davis, 2010) concluded the oldest Silurian crystallization ages of these granites act as a proxy for the Cat Square remnant ocean basin, having already been closed and buried to depths causing anatexis of Cat Square sediments. If the oldest portions of the High Falls batholith were produced above a subduction zone, the Cat Square basin could have closed later than 424 or even 406 Ma. The possibility of piecemeal accretion of peri-Gondwanan island arcs, opening of a back-arc basin, and other tectonic scenarios will be discussed in Chapter 6.

Chapter 4 - Metamorphism

Introduction

Interelationships between structural and metamorphic data can provide valuable insight into the tectonic history of any orogenic belt. The timing of deformation and the timing of peak metamorphism are keys to understanding the evolution of metamorphic terranes. The relationships of structures formed under known metamorphic conditions can be used to refine tectonic models.

Peak metamorphism in the Inner Piedmont occurred during the Devonian-Mississippian Neoacadian orogeny and the early Alleghanian as the eastern Tugaloo and Cat Square terranes were subducted beneath the Carolina superterrane, inducing large-scale migmatization and metamorphism reaching upper-amphibolite facies (Merschat, 2009). Erosional unroofing of the Inner Piedmont followed peak metamorphism, but the late Mississippian-Permian Alleghanian orogeny subsequently produced a metamorphic overprint (Huebner et al., 2011). Metamorphic isograd maps compiled by Merschat (2009) summarize data collected from decades of detailed geologic mapping in North Carolina, South Carolina, Georgia, and Tennessee, and extrapolate isograds to the southwest into central Georgia and Alabama, based on reconnaissance mapping (Fig. 4-1). A large sample of metamorphic zircon rims (n=123) were used in conjunction with the isograd maps to divide the southern Appalachians into metamorphic domains (Fig. 4-1). The Inner Piedmont is characterized by a core of sillimanite I-II facies rocks bounded by zones of lower-grade rocks that define a Barrovian sequence from garnet-staurolite-kyanite-sillimanite (Mershat, 2009). These isograds are generally parallel with regional structures in the Inner Piedmont, which suggests Neoacadian deformation was pre- or syn-metamorphic (Byars, 2010). In addition, metamorphic accessory minerals (garnet, biotite, hornblende,

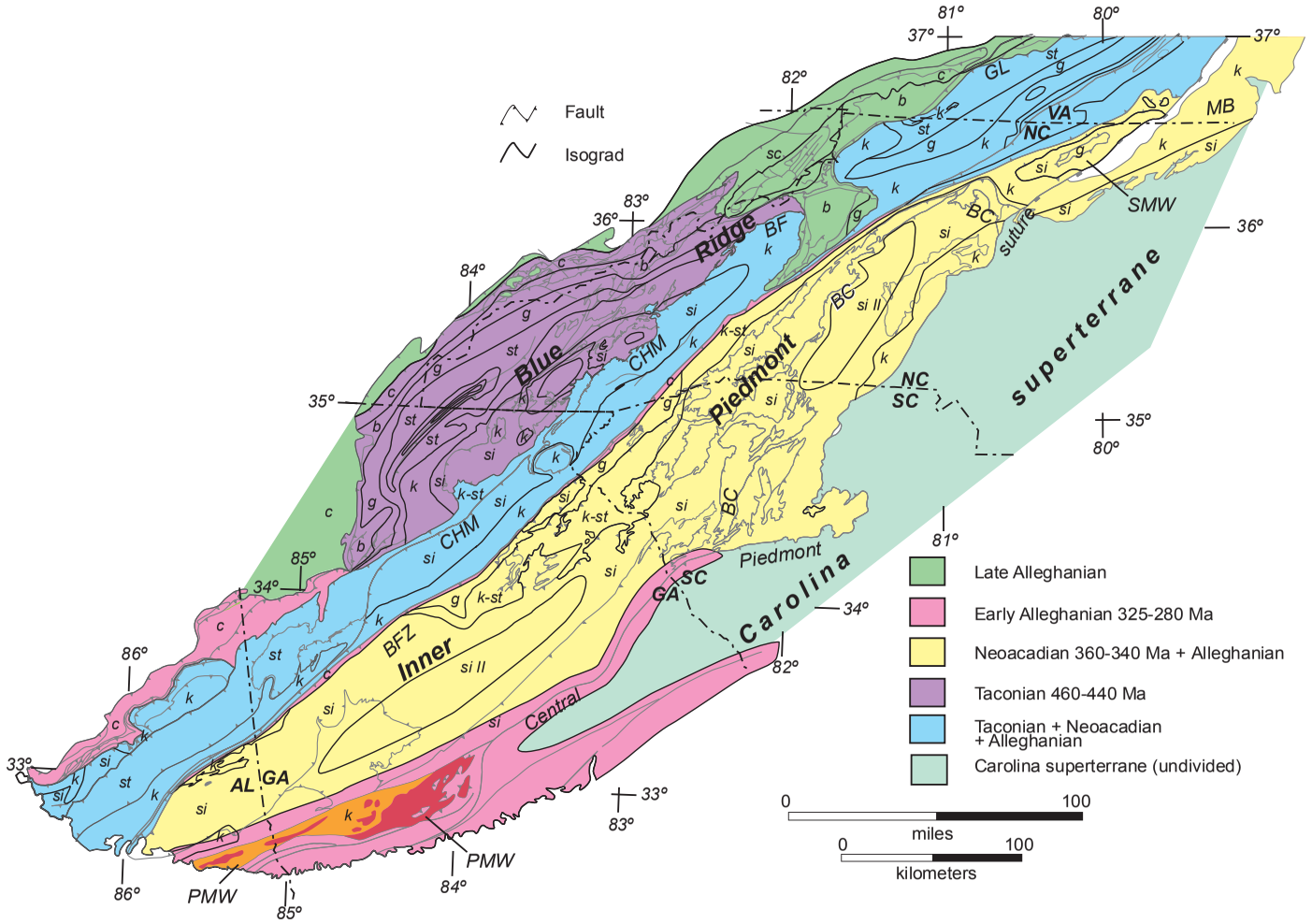


Figure 4-1. Metamorphic timing map with index mineral isograds of the southern Appalachians. Metamorphic zones assigned based on timing of metamorphism using compiled U-Pb zircon analyses. Index mineral abbreviations: sc–sub-chlorite. c–chlorite. b–biotite. g–garnet. st–staurolite. k-st–kyanite+staurolite. k–kyanite. si–sillimanite. si II–sillimanite II. BC–Brindle Creek fault. BFZ–Brevard fault zone. BF–Burnsville fault. CHM–Chattahoochee-Holland Mountain fault. GL–Gossan Lead fault. MB-Milton belt. PMW–Pine Mountain window. SMW–Sauratown Mountain window. (Modified from Merschat, 2009).

and muscovite) have been identified in the Tugaloo and Cat Square terranes on both sides of the Brindle Creek fault, suggesting pre- or syn-metamorphic emplacement of the Brindle Creek thrust sheet (Gilliam, 2010). Estimates of the pressure and temperature conditions during metamorphic events are also critical to understanding the petrogenesis of metamorphic rocks. Other workers (Bier, 2001; Bier et al., 2002; Merschat, 2003; Wilson, 2006; Gatewood, 2007) reported a wide range of estimated pressures and temperatures (3-8.7 kbar and 500-840°C) in the South and Brushy Mountains in North Carolina (Byars, 2010). Gilliam (2010) estimated that burial of the North Carolina eastern Tugaloo and Cat Square terranes occurred at a rate of approximately 1 km per 1.75 Ma.

Field and Petrographic Evidence of Metamorphism

The Cat Square terrane in the mapped area lies entirely within the sillimanite isograd delimited by Merschat (2009), which is supported by field observations. Abundant evidence of metamorphism is present in the mapped area. Metamorphic textures and index minerals are easily recognized. The effects of migmatization are visible in the field area and are especially prevalent within a few hundred meters of the Brindle Creek fault (Fig. 4-2). Phase changes due to metamorphism have produced garnet, kyanite, and sillimanite. These index minerals are part of the classic Barrovian facies series, and each of these phases can be readily identified in hand specimen. In this series garnet is formed by the continuous reaction:

$$\text{chlorite + muscovite} \rightarrow \text{garnet + biotite + quartz + } H_2O \text{ (Yardley, 1989)}$$

The next mineral in the Barrovian facies series is staurolite. No staurolite was



Figure 4-2. Stromatic migmatite exposed in the footwall of the Brindle Creek fault in dry creek bed approximately 600 m east of Fill Bridge Road, Butts County, Georgia.

identified during field work or petrographic analysis. Any staurolite present in the field area must have been consumed by metamorphic reactions as pressures and temperatures increased sufficiently to produce kyanite, or the bulk compostion of some rocks did not allow an aluminum silicate to crystallize. Kyanite was identified only in one outcrop in the northwestern corner of the Indian Springs quadrangle during detailed mapping. Sillimanite is the dominant high-grade index mineral in the mapped area. The change from kyanite to sillimanite is a polymorphic transition and requires no additional chemical input or output (Yardley, 1989). The coexistence of kyanite and sillimanite is not uncommon, because the reaction that produces sillimanite from kyanite is relatively sluggish (Yardley, 1989).

$$Al_2SiO_5 \rightarrow Al_2SiO_5$$

kyanite sillimanite

Sillimanite is most often identified in Cat Square and Tugaloo terrane metapelites. Davis (2010) divided the pelitic schist in the central Georgia Cat Square terrane into three prograde assemblages (shown below) that produce sillimanite, and all of these assemblages were identified in the field area. Chlorite is assumed to be retrograde in these assemblages.

(1) Muscovite + plagioclase + sillimanite + biotite + quartz ± chlorite ± opaques

(2) Muscovite + plagioclase + sillimanite + garnet + quartz + biotite ± chlorite ± apatite ± epidote ± opaques

(3) Plagioclase + sillimanite + garnet + quartz + biotite + K-feldspar ± opaques

Petrographic analysis of thin sections provided additional evidence of metamorphism. Metamorphic index minerals were observed in some specimens where hand sample identification of these phases was not possible. Evidence of retrograde metamorphism was also identified during petrographic analysis. The most common retrograde reaction was biotite → chlorite (Fig. 4-3). While it is possible that chlorite may persist under very high temperatures (sillimanite zone), chlorite may not exist in equilibrium with K-feldspar at these temperatures (Yardley, 1989). Peak P-T conditions in the Cat Square terrane of central Georgia reached 4-7.6 kbars and 630-715°C, confirming that this portion of the Inner Piedmont reached upper amphibolite facies (Davis, 2010).

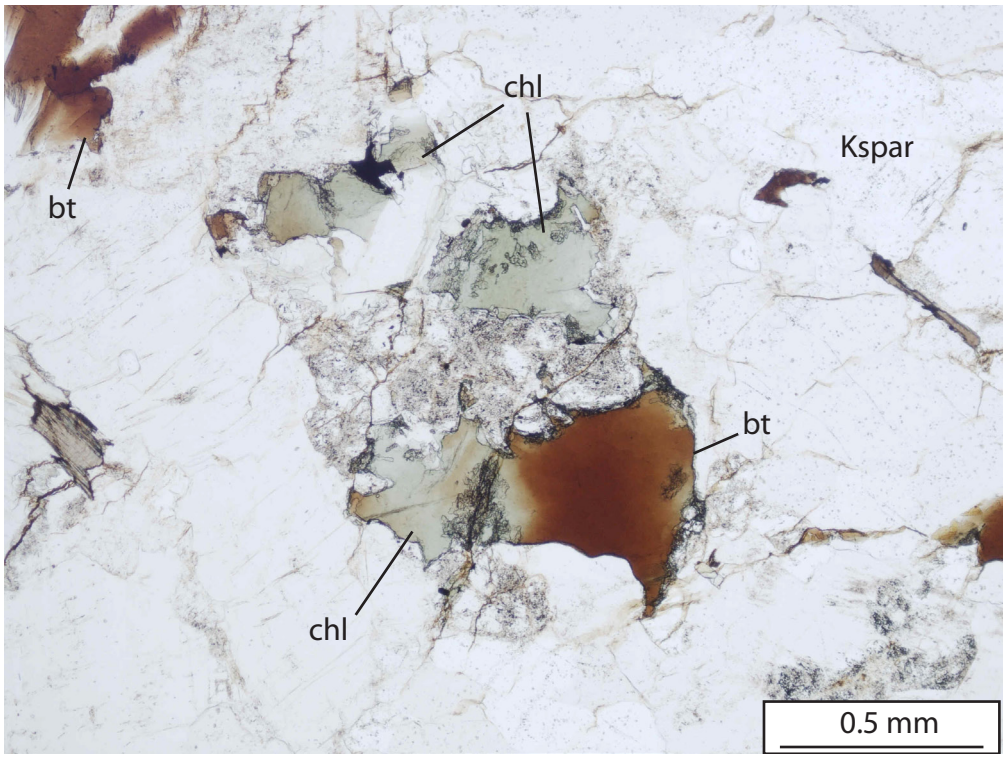


Figure 4-3. Chloritized biotite visible in thin section from sample of High Falls Granite collected approximately 1 km south of the intersection of English Road and City Pond Road in Lamar County, Georgia. bt-biotite. chl-chlorite. Kspar-K-feldspar. Plane light.

Thermobarometry of Selected Samples

Estimates of the pressure and temperature conditions to which a rock has been subjected can be useful when trying to deduce the metamorphic history of a region. A multitude of techniques have been developed by geochemists and metamorphic petrologists to estimate temperature and pressure. Good thermometers are measureable reactions that occur within a narrow range of temperatures of a large range of pressures. Good barometers have the inverse relationship between stability in relation to pressure and temperature (Yardley, 1989). Chemical data were collected using the electron microprobe at The University of Tennessee-Knoxville,

and thermobarometric calculations were conducted using software written by Spear and Kohn (1999). The results of this analysis have been compiled and are attached in Appendix 1.

Garnet-Biotite Thermometry

Fe^{II} and Mg^{II} cation exchange reactions between garnet and biotite have been experimentally calibrated and are often used as an accurate geothermometer in many rock types. The calibration of Holdaway et al. (1997) was used for temperature estimation and a pressure of 5 kbar was assumed. Davis (2010) estimated pressures in the Georgia Cat Square terrane peaked between 4-7.6 kbar. This geothermometer was used on sample IS370. Estimated temperatures for this sample range from 690-770°C (Fig. 4-4). These estimates places the sample in the sillimanite zone on P-T diagrams at the assumed pressure. This temperature estimate is higher than that for the thermobarometry data collected by Davis (2010) who reported peak temperatures from 630-715°C. The same thermometer was applied to another sample of High Falls Granite (HFSP) but the results were from 850-965°C, which seem unreasonable.

Zircon Saturation Thermometry

Zircon saturation thermometry is an alternative method often used to determine the temperature of emplacement of felsic plutonic rocks (Watson and Harrison, 1983). The accuracy of zircon saturation thermometry is dependent on zircon crystallizing in contact with the original melt (Hanchar and Watson, 2003). Early crystallization of phenocrysts in a magma chamber can produce fractionation of the melt and result in zircon crystallizing in contact with a melt that does not represent the original magma

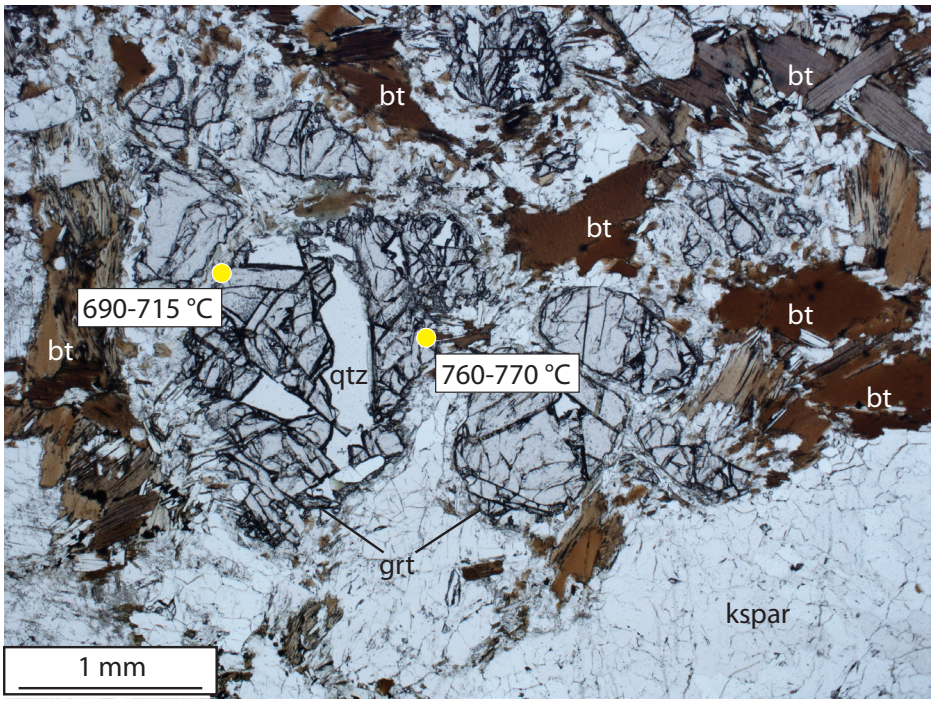


Figure 4-4. Locations used for garnet-biotite geothermometry for High Falls Granite sample IS370 (yellow circles). bt-biotite. grt-garnet. kspar-K-feldspar. q-quartz. Sample from Gilmore Creek ~1 km north of Blount Road, Monroe County, Georgia.

chamber chemistry. Fractionation caused by the crystallization of feldspar often results in depletion of Eu and Sr (Miller et al., 2003), and this can be seen in plots of bulk High Falls Granite chemistry (cf. Chapter 3). Therefore, the High Falls Granite is not a good candidate for application of zircon saturation thermometry.

Garnet-Plagioclase-Hornblende-Quartz Barometry

Determining the depth of emplacement of the High Falls Granite using a barometer would help refine tectonic reconstructions of the Neoacadian orogeny in the central Georgia Inner Piedmont. Unfortunately, conducting geobarometry on granites is notoriously difficult (H.Y. McSween, personal commun. 2011). Most geobarometers utilize net equilibrium reactions of phases that are not typically found in granites. A large



Figure 4-5. Pavement outcrop of High Falls Granite ~600 m downstream of High Falls Road along the Towaliga River, Monroe County, Georgia. Note interlayered dark concordant bands of garnet-amphibolite. Trimble™ GeoXT for scale.

body of garnet amphibolite (~100 m) was identified in the High Falls Granite (Fig. 4-5). Contact between the amphibolite and the High Falls Granite is concordant with foliation; and there is no evidence of contact metamorphism in the High Falls Granite or a chilled margin in the amphibolite. This suggests that the amphibolite is actually a large xenolith that was incorporated into the High Falls Granite during emplacement. The location of this xenolith and freshness of the material make it a good candidate for geobarometry, and the results could be used as a proxy for the body of High Falls Granite.

Two barometers were considered that use calibrated equilibrium reactions for garnet + hornblende + plagioclase + quartz in garnet amphibolites (Kohn and Spear, 1989, 1990). Unfortunately, electron microprobe analysis revealed the Fe content of the amphibole falls outside the compositional limits for both barometers. Using

geobarometers that have not been calibrated to the composition of a sample can produce unpredictable results.

Conclusions

Field observations confirm that peak metamorphism in the central Georgia Inner Piedmont produced upper-amphibolite facies conditions. Evidence includes abundant sillimanite identified in hand sample, and in thin section, and frequently observed migmatization of metasedimentary rocks. Evidence of retrograde metamorphism (chloritization of biotite) was identified in thin section. Timing of metamorphism has been delimited by U-Pb SHRIMP-RG geochronology. Metamorphic rims on zircon from central Georgia have identified a population Acadian-Neoacadian metamorphic rims (420-365 Ma) and a suite of Alleghanian rims (320-300 Ma) (M.T. Huebner, personal commun.). Electron microprobe analyses of thin sections collected from the mapped area indicate temperatures in the sample of High Falls Granite range from 690-770°C based on garnet-biotite Fe-Mg exchange geothermometry.

Chapter 5: Structure and Tectonics

Introduction

Geochemical and geochronologic data from granitoid rocks in the study area provide clues about the conditions of emplacement and provenance, but robust structural analysis of these plutonic and associated metasedimentary units produces data that can be used to determine how these rocks were deformed before, during, and after peak metamorphism in the Inner Piedmont. Detailed structural data collected areally in high-grade metamorphic terranes can be used to extrapolate the tectonic history of the region in 3-D (Plate 1). Griffin (1974) collected and analyzed structural data to build models of the Inner Piedmont that incorporated stacks of thrust nappes. Merschat et al. (2005) utilized structural data collected from the northern Inner Piedmont to hypothesize that the crystalline core had been extruded to the southwest in a mid-crustal orogenic channel during the Neoacadian event. It would be extremely difficult to visualize (let alone prove) this sort of complex kinematic history using only geochemical analysis or the best modern age-dating techniques. Detailed geologic mapping, coupled with structural analysis, then amalgamated with geochronologic and geochemical data, can produce insightful reconstructions of local and regional deformation, and tectonics.

Structural data (1,044 foliations, 93 lineations, 45 fold hinges and axial surfaces) were collected in the mapped area with a Brunton™ compass and recorded in a Trimble GeoXT™ handheld differential GPS unit. Station data were compiled in ESRI ArcMap™ GIS software. Geologic data were then exported from ArcMap to Adobe Illustrator™. Additional structural data (453 foliations and 18 lineations) from southwest of the Towaliga fault in the Indian Springs quadrangle (R.D. Hatcher, Jr., unpublished data) were added to the data set used for structural analysis. Stereonets were generated using Stereonet™ software written by Allmendinger (2011).

Tectonic Framework

The southern and central Appalachians stretch over 1,300 km from just south of New York City to the Coastal Plain of central Alabama. The Appalachian orogen was created by a series of at least three diachronous, accretionary, and collisional events along the eastern Laurentian margin after the breakup of supercontinent Rodinia (960-565 Ma) (Aleinikoff et al., 1995; Graybill, 2012) (Fig. 5-1). During the Ordovician Taconian orogeny volcanic island arcs were obducted onto the Laurentian margin. The Carolina superterrane was accreted to the Laurentian + Taconian margin during the Devonian-Acadian and late Devonian-early Mississippian Neoacadian orogenies. Finally, construction of the Appalachians was completed by the collision of Laurentia and Gondwana during the late Mississippian-Permian Alleghanian orogeny (Hatcher et al., 2007a). The sinuous trace of the Appalachians is a direct descendant of the geometry of the Laurentian rifted margin and the shape of the Gondwanan indenter that collided to form supercontinent Pangea during the Alleghanian orogeny. Promontories and embayments that formed during the breakup of Rodinia became recesses and salients, respectively, during the assembly of Pangea through tectonic inheritance (Thomas, 2006).

The Piedmont is the physiographic province southeast of the Blue Ridge, because it forms the modern topographic foothills and lower topography of the southern Appalachian Mountains; however, the exposed rocks, like those of the Blue Ridge Province to the west, are also part of the Neoacadian metamorphic core. The Piedmont physiographic province extends from the southeastern edge of mountainous (Blue Ridge) topography to the Coastal Plain, although Piedmont rocks continue eastward beneath the Coastal Plain (Fig. 5-2). The Tugaloo terrane (eastern Blue Ridge and Inner Piedmont) and Carolina superterrane compose the Piedmont. The Carolina

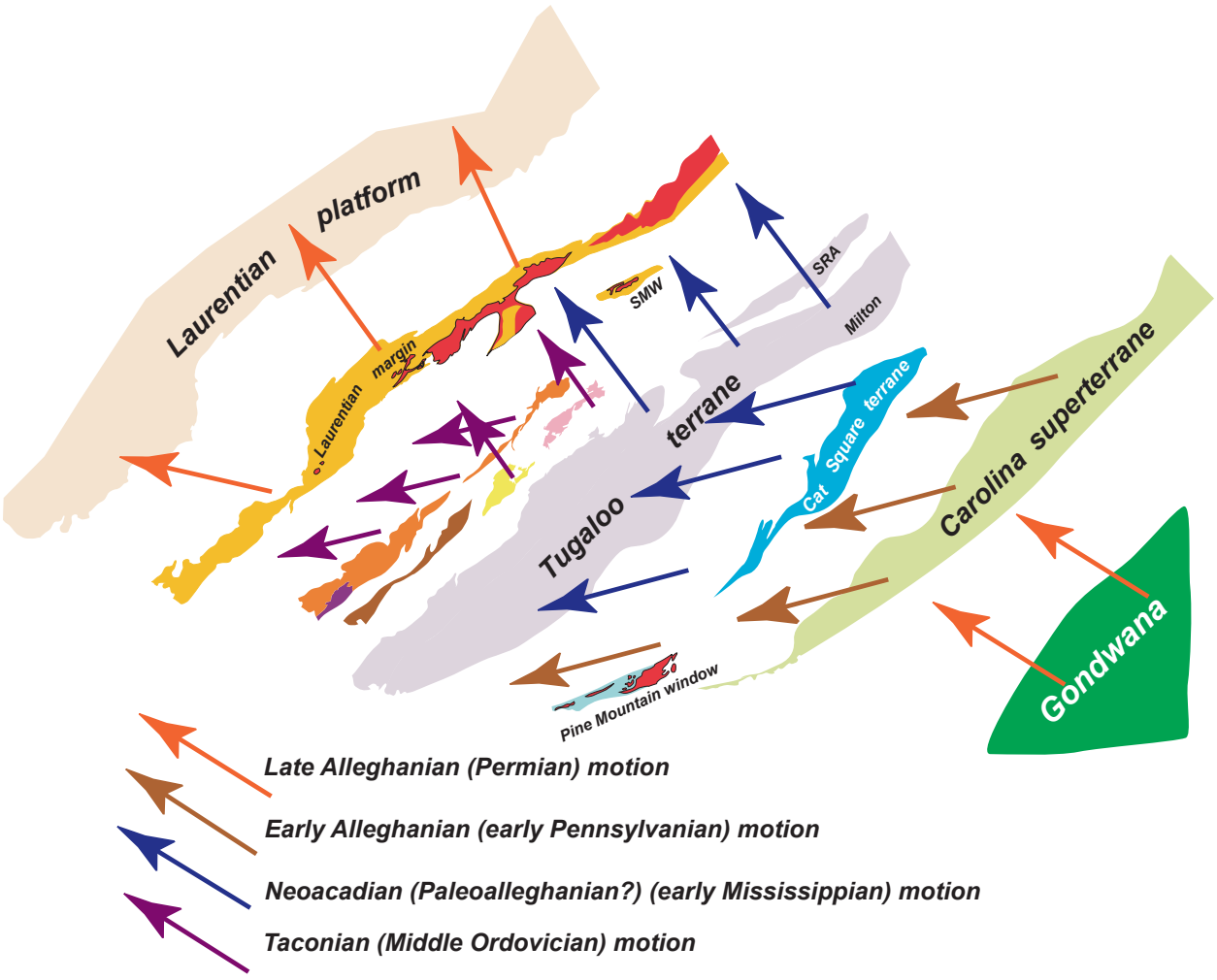


Figure 5-1. Tectonic assembly diagram of the central and southern Appalachians (modified from Hatcher et al., 2007a). SMW—Sauratown Mountains window, SRA—Smith River allochthon.

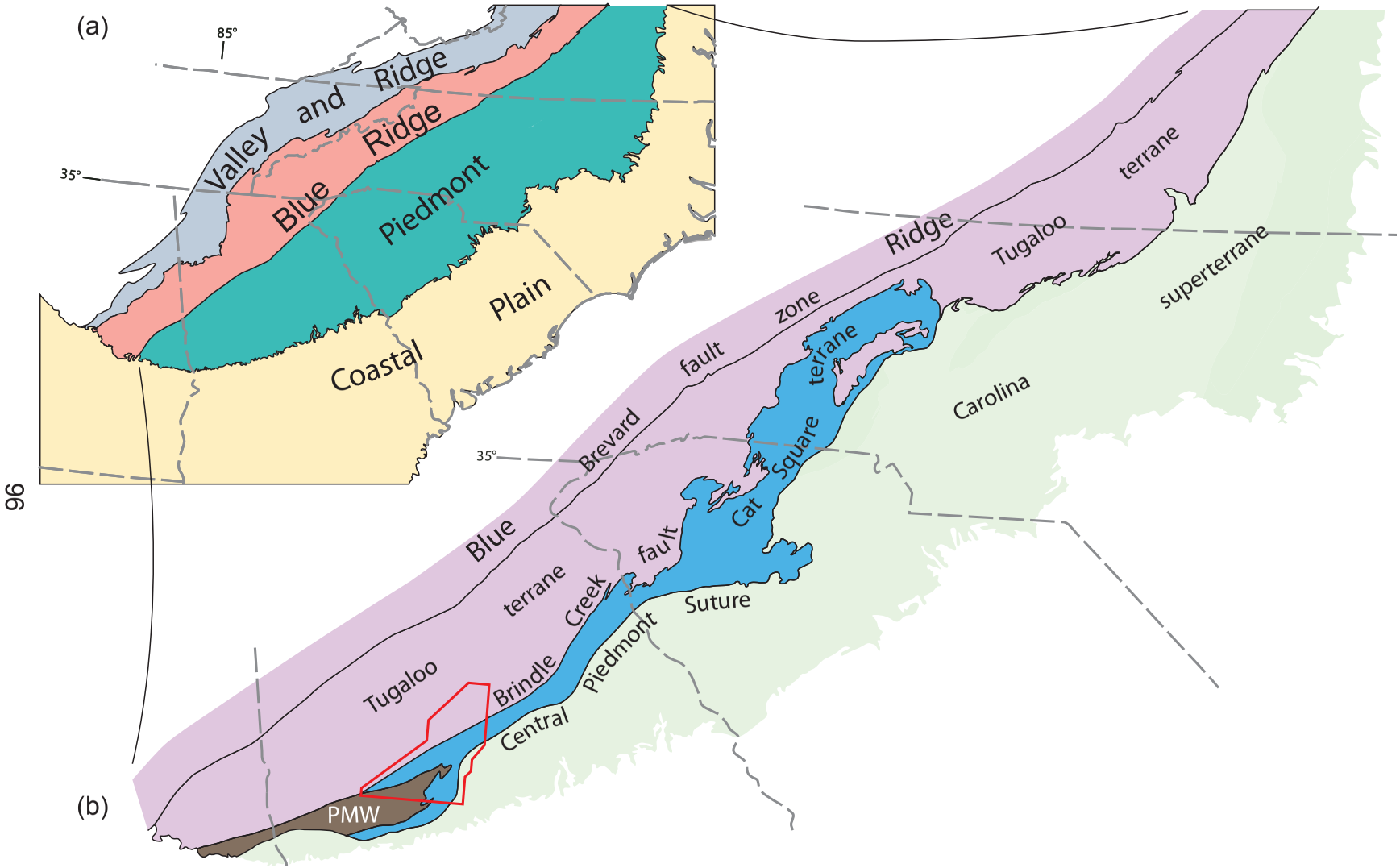


Figure 5-2. Index maps of the southern Appalachians showing the location of the study region. (a) Small scale physiographic map of the composite Piedmont and eastern Blue Ridge geologic provinces. (b) Tectonic map showing the terranes in the vicinity of the study area. Compiled mapped area in Figure 5-3 outlined in red. PMW—Pine Mountain window. Area outlined in red is the extent of Figure 1-4. Both images modified from Huebner et al. (2011).

superterrane is made up of Perigondwanan Neoproterozoic to Cambrian volcanic-arc rocks that were accreted to the Laurentian-Taconian continental margin during the Devonian-Mississippian Acadian-Neoacadian orogeny. The Carolina superterrane extends eastward from the central Pidemont suture, beneath Mesozoic-Cenozoic Coastal Plain sediments, to the Alleghanian suture. Regional aeromagnetic and gravity maps suggest that the Suwannee-Wiggins suture represents the boundary between material accreted to the eastern margin of Laurentia and Gondwanan (African) crust (Hatcher et al., 2007a).

The Inner Piedmont consists of the eastern Tugaloo terrane (all Tugaloo terrane rocks east of the Brevard fault zone), Cat Square terrane, and Pine Mountain window, and is continuous from central Alabama to near Winston-Salem, North Carolina (Merschat and Hatcher, 2007). Inner Piedmont rocks are exposed for approximately 700 km along strike and for approximately 100 km from the Brevard fault zone to the northwest to the central Piedmont suture to the southeast. The Inner Piedmont is made up of a stack of nappe-style (type F) crystalline thrust sheets that dip shallowly to the southeast (Griffin, 1971, 1974; Hatcher and Hooper, 1992). Peak metamorphism in the Inner Piedmont core reached upper amphibolite facies, making the Appalachian Inner Piedmont one of the largest areas of exposed sillimanite-grade rocks in the world (Hatcher, 2004). The Inner Piedmont can be further subdivided into eastern and western segments that are juxtaposed along the Brindle Creek fault. The western Inner Piedmont is characterized by migmatitic metagraywacke and pelitic schist interlayered with amphibolite, which were intruded by Ordovician, Silurian, and younger granitoids. Interlayered migmatitic aluminous schist and graywacke with minor amphibolite are found in the eastern Inner Piedmont. The Pine Mountain window, which exposes an uplifted block of Grenville basement and Paleozoic(?) cover (Steltenpohl et al., 2010), is also located in the eastern Inner Piedmont from ~8 km south of Flovilla, Georgia,

to central Alabama (Steltenpohl et al., 2010). Basement is defined as “crystalline rock that is the product of an earlier orogenic cycle and underlies a less deformed and less metamorphosed cover” (Hatcher, 1990).

Major structures in the research area

Brindle Creek fault

The Brindle Creek fault was initially mapped in the northern Inner Piedmont of North Carolina, but has also been identified and mapped in central Georgia. Continued detailed geologic mapping (Fig. 5-3) identified a narrow (<100 m) steeply dipping (70-88º) mylonite zone in central Georgia that was originally identified as a regional aeromagnetic anomaly. Shear-sense indicators in the mylonite zone (S-C fabrics, rotated porphyroclasts, and sheath fold axes) indicate the fault is dextral (Davis, 2010). U-Pb isotopic geochronologic analyses of metasedimentary rocks from both sides of the mylonite zone confirmed that the structure is the Brindle Creek fault and terrane boundary (Huebner and Hatcher, 2011). The trace of the Brindle Creek fault is sinuous in the mapped area (Fig. 5-4). The fault was mapped by locating outcrops of mylonite or delimiting easily identifiable units that are truncated by the fault (Lithonia Gneiss and High Falls Granite).

Towaliga fault

The Towaliga fault zone is a significant structure in the southern Appalachians. It has been mapped by reconnaissance from northeastern Georgia to central Alabama where it disappears beneath the Coastal Plain. The Towaliga fault zone is one of several faults in the eastern Piedmont fault system (including Goat Rock and Bartletts Ferry) (Hatcher et al., 1977) that underwent retrograde dextral ductile deformation during the

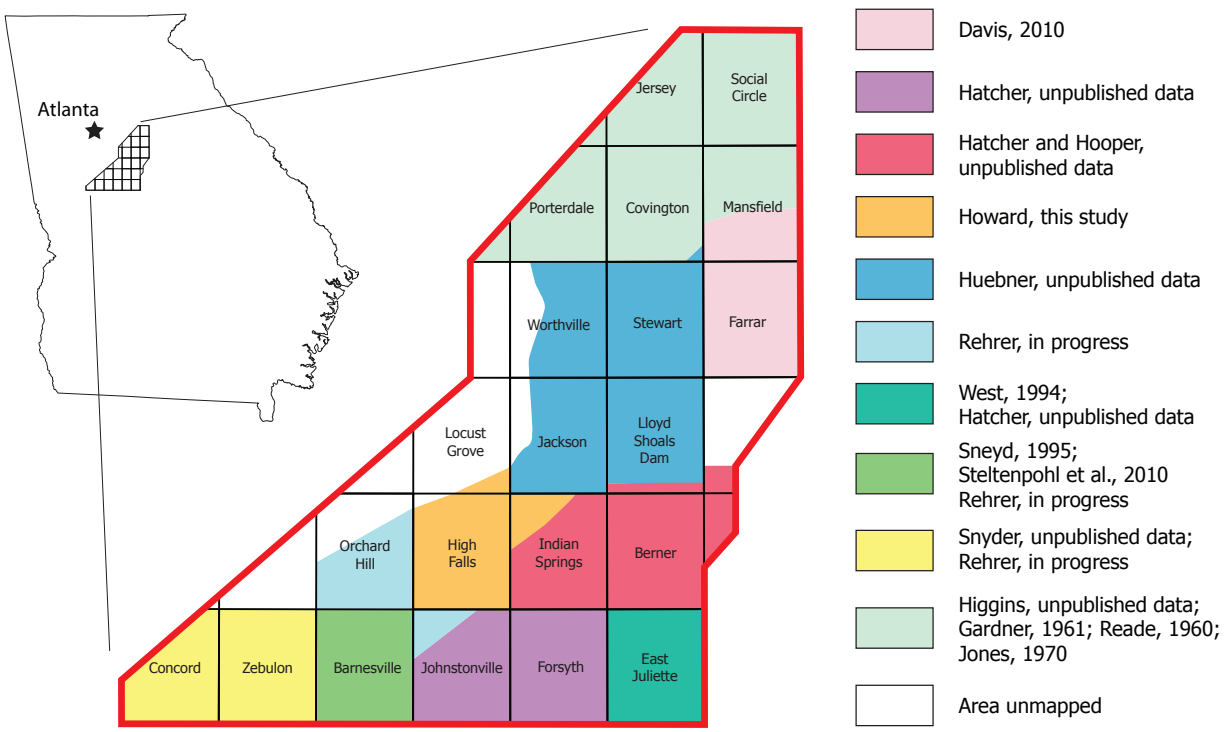


Figure 5-3. Nearby mapping credit (modified from Huebner et al., 2011).

Alleghanian orogeny. The Towaliga fault was later brittely reactivated under low- to medium-grade conditions (Huebner and Hatcher, 2011). Previous workers agree the Alleghanian ductile deformation was oblique dextral strike-slip with a minor normal dip-slip component in the Towaliga fault zone in Alabama and central Georgia (Hooper and Hatcher, 1988a; Steltenpohl, 1988; Steltenpol et al., 2010). Hooper and Hatcher (1988a) utilized microstructural shear sense indicators (σ, δ, and θ porphyroclasts; asymmetric microfolds; and inclined subgrain fabrics) in the Towaliga fault zone to determine that movement was primarily dextral strike slip. Hooper and Hatcher (1988a) described microscale interlayering of mylonite and ultramylonite, which also indicates heterogeneous strain and strain partitioning in the fault zone. Further investigations revealed shear sense indicators in other parts of the Towaliga fault zone consistently recorded dextral movement (Hadizahdeh et al., 1991; Davis, 2010; Huebner and

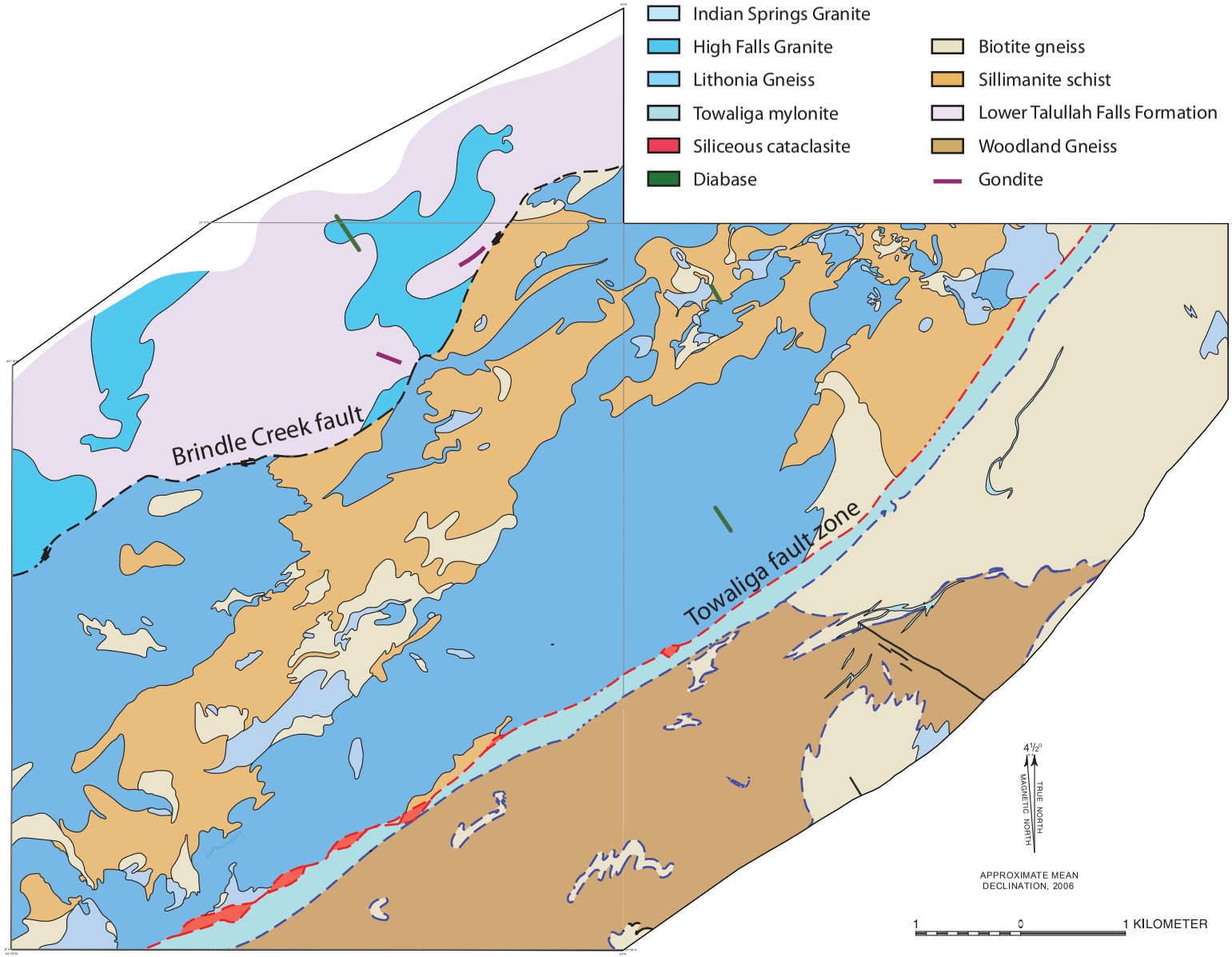


Figure 5-4. Simplified geologic map of the project area.

Hatcher, in review).

Hadizahdeh et al. (1991) observed evidence of both brittle and ductile deformation in the Towaliga fault zone, and that ductile quartz mylonites were juxtaposed by cataclasite generated by brittle deformation in the fault zone. Hadizahdeh et al. (1991) observed mm-sized bands of cataclasite that are parallel to the mylonitic foliation in the fault zone, brecciated mylonite, and large bodies of silicified breccia. Microstructural analysis of mylonite from the fault zone revealed thin (0.5-2 mm) discontinuous layers of brecciated mylonite. Thicker zones of brecciated mylonite (~7 m thick) are also interlayerd with quartz ultramylonite. The rock transitions from protomylonite to crushed breccia and to protocataclasite over a distance of approximately 1 m. Hadizahdeh et al. (1991) concluded that some healed quartz fabrics in the cataclasite zones indicate sinistral strike-slip displacement, which is opposite of the shear sense in mylonitic fabrics. Hadizahdeh et al. (1991) proposed two possible mechanisms that could have produced this unusual combination of plastic and brittle deformation in the Towaliga fault zone: (1) the mylonite zone could have been overprinted by a later phase of brittle deformation, which formed the cataclasite; and (2) the fault may have experienced both brittle and plastic deformation during a single phase of deformation near the brittle-ductile transition.

Rhombohedral pods of siliceous cataclasite (Fig. 5-5) (some 100s of m long and 10s of m high) can be found along the trace of the Towaliga fault zone (Schamel et al., 1980; Higgins et al., 1988; Hadizahdeh et al., 1991; Babaie et al., 1991a, 1991b; Huebner and Hatcher, 2011) and are indisputable evidence of brittle deformation. Huebner and Hatcher (in review) suggest the Towaliga fault was reactivated during the Mesozoic, and the cataclasite pods are dilational stepovers. Interestingly, the geometry of the cataclasite bodies and the offset of ~200 Ma diabase dikes that

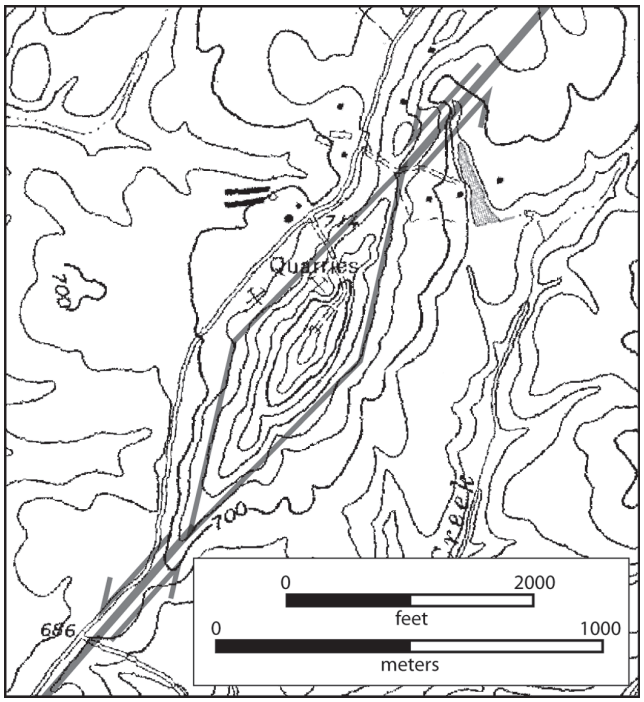


Figure 5-5. A large rhomb-shaped body of cataclasite along the Towaliga fault in the Stewart quadrangle. (From Huebner et al., 2011)

crosscut the Towaliga fault indicate Mesozoic displacement was sinistral. Both the ~N30ºE and ~N70ºE segments of the Towaliga fault contain cataclasite pods, indicating the segments were reactivated close to the same time by separate brittle faults. As the dilational stepovers formed, the pore-fluid pressure inside the stepovers would have dropped radically, causing an influx of hydrothermal fluids from the surrounding area. This explains the extensive mineralization that formed the cataclasite rhombs (Huebner and Hatcher, in review). The sinistral reactivation hypothesis of Huebner and Hatcher (in review) precludes the model of Hadizahdeh et al. (1991) that suggested the Towaliga fault was deformed brittlely and ductilely during a single event. Ductile structures in the Towaliga fault zone clearly indicate dextral shear sense.

Tectonic Evolution of the Southern Appalachians

Supercontinent Rodinia was formed during the Grenville orogeny. This Middle

Proterozoic orogeny affected continental crust worldwide (Hoffman, 1988). Successful rifting of Rodinia occurred in western and northeastern North American at 750 Ma or possibly as early as ~960 Ma in the central Appalachians (Graybill, 2012). An extensional event (~735 Ma) began in the central and southern Appalachians, but failed to achieve complete rifting (Aleinikoff et al., 1995). Alkalic plutonism and volcanism accompanied the attempted rifting. Rift basins were formed and received sediment (Mt. Rogers and Grandfather Mountain Formations and Ocoee Supergroup) (Hatcher et al., 2007a). Successful rifting in the central and southern Appalachians began ~565 Ma (Aleinikoff et al., 1995) and basin development resumed. The Ocoee Supergroup was deposited in these basins in Tennessee, North Carolina, and Georgia (Hatcher et al., 2007a). Rifting gradually transitioned to drifting during the Early Cambrian, and is recorded by deposition of the marine sedimentary units in the Chilhowee Group. These rocks consist of alternating sandstone and shale-sandstone that matured over time, beginning with immature graywacke and ending with calcareous shale that was likely deposited along a margin facing an open ocean (King and Ferguson, 1960). Sedimentation continued along the continental margin, while carbonates were deposited along with clastic sediments that were eroded from the Grenville mountains (Hatcher et al., 2007a). A craton-scale transgression flooded most of Laurentia during the Early Ordovician and produced carbonate sedimentation from the continental margin to modern New Mexico and Utah (Sloss, 1988).

The Taconic orogeny began when the Sevier foredeep basin formed in response to volcanic island arcs and sediments being obducted onto the continental margin of eastern Laurentia during the Middle Ordovician. Continuous volcanic activity to the east deposited K-bentonite beds throughout the eastern United States while mafic/felsic volcanic rocks and granitoids were emplaced in the Milton and Tugaloo terranes. The Neoproterozoic to Cambrian Laurentian rifted margin sediments

and crust were A-subducted beneath the obducting Taconic island arcs and were penetratively deformed while undergoing up to granulite facies metamorphism (Absher and McSween, 1985; Eckert et al., 1989; Mirante and Patino-Douce, 2000). Hatcher et al. (2007a) and Hatcher (2010) provided summaries and robust discussion of the Taconic orogeny in the central and southern Appalachians. A-subduction of the Laurentian margin was accompanied by accrection of several terranes, including the Tugaloo terrane in the southern Appalachians. The Taconic orogeny was the peak tectonothermal event in the Tugaloo terrane west of the Brevard fault zone (Merschat et al., 2010). This event provided the minimum age of deposition for Tugaloo sedimentary rocks, which must have been deposited before Taconic metamorphism occurred in the Late Ordovician.

Sediments accumulated east of the Laurentian-Taconic continental margin in the Rheic ocean. The Rheic ocean gradually grew narrower as an amalgamation of island arcs approached the Laurentian-Taconic continental margin from the east. These amalgamated peri-Gondwanan arcs formed outboard of Gondwana contemporaneously with the rifting of Rodinia, and are characterized by a suite of 600-500 Ma zircons (Hatcher et al., 2007a). Merschat and Hatcher (2007) proposed that, as the Rheic ocean narrowed, the Cat Square basin formed and received clastic sediments derived from the Laurentian-Taconian margin, the approaching Carolina superterrane, and Precambrian crust. The provenance of detrital zircons in the Cat Square terrane was critical in defining these rocks as a separate terrane (Bream, 2003).

Hatcher and Merschat (2006) suggested the Neoacadian orogeny began in the southern Appalachians as the Carolina superterrane accreted to and was obducted onto the Laurentian-Taconic accretionary margin. Timing of these events is delimited by several lines of evidence. The youngest detrital zircons found in the Cat Square terrane are ~430 Ma (Bream et al., 2004). This is the maximum age for the Cat Square basin.

An igneous zircon that crystallized at 430 Ma still must be exhumed, weathered from an igneous body, and transported before it is deposited in a basin. The Cat Square basin must therefore have remained open for some time later than ~430 Ma crystallization age (Hatcher et al., 2007a). The Inner Piedmont reached peak regional metamorphic conditions from 360-340 Ma based on U-Pb isotopic dating of zircon metamorphic rims from North Carolina, South Carolina, and Georgia (Merschat, 2009). The tectonothermal peak was reached as the Laurentian-Taconic continental margin and Cat Square basin sediments were A-subducted beneath the Carolina superterrane. This burial resulted in extensive migmatization of the Inner Piedmont (Hatcher et al., 2007a), and burial depths in the eastern Tugaloo terrane and Cat Square basin were sufficient to produce crustal anatexis. The melts coalesced to form the Walker Top Granite in North Carolina. Crystallization ages of the Walker Top Granite are 407-366 Ma (Gatewood, 2007; Byars, 2010). If these granites are anatectic, the 407 Ma U-Pb age is the current best minimum age for the Cat Square basin. Sediment in the basin must have been buried to depths of 15-20 km to produce anatexis (Merschat, 2009) and the melt must have cooled sufficiently to crystallize zircon by ~407 Ma. Analysis of geochemical data from the Walker Top and High Falls Granites presented herein (Chapter 3) indicates some Acadian-Neoacadian plutonism in the Inner Piedmont may be arc-related.

Structural data collected from the North Carolina Inner Piedmont suggest a unique kinematic history during the Neoacadian orogeny. A series of thrust sheets was directed northwest across the Inner Piedmont. Near the Brevard fault zone, the thrust sheets become southwest directed. Merschat et al. (2005) concluded the collision between the Laurentian-Taconian margin and the Carolina superterrane was likely an oblique transpressional event that zippered closed from north to south. Northwest-directed thrust sheets were buttressed against the Brevard fault zone, and the entire Inner Piedmont is hypothesized to have been extruded southwest in an orogenic

channel (Hatcher and Merschat, 2006).

The final phase of Appalachian orogenesis took place during the late Mississippian to Permian Alleghanian orogeny. The Alleghanian orogeny began with an oblique, transpressive, rotational, north-to-south zippered collision of Gondwana and assembled Laurentian margin, which included terranes accreted during the previous Paleozoic orogenies (Hatcher, 2002). Components of the eastern Piedmont fault system (including the Towaliga fault) formed and allowed blocks of crust to escape to the southwest as the collision progressed. Plutonic suites were emplaced across the eastern Blue Ridge, Inner Piedmont, and Carolina superterrane. The internides of the mountain chain were uplifted beginning in the late Mississippian, producing an exterior clastic wedge to the northwest (Hatcher et al., 1989). Finally, the orogeny transitioned into a head-on southeast-northwest-directed collision that transported the Blue Ridge Piedmont megathrust sheet a minimum of 350 km into the continental interior and formed the Appalachian foreland fold-thrust belt (Hatcher et al., 2007b).The still-weak Brevard fault zone was reactivated during this final phase of deformation as a brittle out-of-sequence thrust in the megathrust sheet (Hatcher et al., 2007a).

Tectonostratigraphic Terranes in the Project Area

Tugaloo Terrane

The Tugaloo terrane extends from the Chattahoochee-Holland Mountain fault in the eastern Blue Ridge to the Brindle Creek fault in the Inner Piedmont and consists of interlayered metasedimentary and metavolcanic units (Hatcher et al., 2007a). The metasedimentary rocks were initially deposited on the distal Laurentian passive margin following the breakup of Rodinia and the opening of Iapetus. They were subsequently metamorphosed during the Ordovician Taconic orogeny. Amphibolite is also abundant

in the Tugaloo terrane. Geochemical analyses were conducted on nine samples of amphibolite collected in the Newton window in North Carolina, and it was concluded the samples had either MORB or volcanic-arc tholeiite chemical signatures (Merschat, 2009). Regardless of origin, mappable bodies of amphibolite are found throughout the Tugaloo terrane. The Tugaloo terrane has been intruded by numerous plutons that range in age from Ordovician to Pennsylvanian-Permian (Hatcher et al., 2007a). It also contains the boundary—the Brevard fault zone—between the eastern Blue Ridge and western Inner Piedmont. The Brevard fault zone is traceable for over 750 km from Alabama to Virginia and is recognized as a mylonite zone over 1 km wide. For years it was assumed that the Brevard fault zone might be a terrane boundary or suture, because it was recognizable on topographic and aeromagnetic maps and has a complex structural history (as summarized by Hatcher 2001). However, the same stratigraphy is recognizable on both sides of the Brevard fault zone, and detrital zircon dating from both sides of the fault has revealed that both sides have the same stratigraphy and provenance, eliminating the possibility that it is a terrane boundary or suture (Hatcher et al., 2007a).

Cat Square Terrane

Migmatitic aluminous schist and metagraywacke are the dominant lithologies exposed in the Cat Square terrane from North Carolina to central Georgia. These rocks were recognized as a distinct terrane in the Inner Piedmont using modern zircon geochronology (Bream, 2003). In addition to the mixed Laurentian and peri-Gondwanan detrital zircons, a significant number of Cat Square terrane detrital zircons were dated at ~430 Ma, which is unique in the Inner Piedmont (Bream, 2003). The mixed affinity of detrital zircons, location between the Laurentian + Taconian margin and an exotic Neoproterozoic island arc, a relatively short lifespan, and incorporation of ocean crust

in the terrane itself are all characteristics of a modern remnant ocean basin (Ingersoll et al., 1995; Merschat and Hatcher, 2007; Merschat et al., 2010). The Cat Square terrane in North Carolina shares these characteristics and was most likely a remnant ocean basin that formed near modern-day New England, between the Laurentian + Taconian margin and approaching Carolina superterrane prior to the Neoacadian orogeny in the southern Appalachians (Merschat, 2009). The metasedimentary units in the Cat Square terrane in North Carolina were also intruded by the Walker Top Granite, which has a maximum U-Pb age of ~407 Ma (Gatewood, 2007). The youngest detrital zircons (~430 Ma) provide a maximum age for the ocean basin in which they were deposited, while the oldest crosscutting pluton (Walker Top, ~407 Ma) has been used to determine the minimum age of the basin. These data indicate that the northern part of the Cat Square basin was open from mid-Silurian to the Early Devonian off southern New England (Merschat, 2009). Interestingly, Walker Top Granite ages are younger from northeast to southwest in the North Carolina Cat Square terrane, suggesting that the basin closed diachronously from north to south during the Neoacadian orogeny (Merschat and Hatcher, 2007).

Pine Mountain Window

The Pine Mountain window is the southernmost basement massif exposed in the Appalachians (Steltenpohl et al., 2010). It has been called an allochthonous block of Grenville basement (Hatcher et al., 2007a), and is framed by several major faults (Fig. 5-6). The Towaliga fault forms the northwestern boundary between the Pine Mountain window and Cat Square terranes. The Goat Rock and Dean Creek faults form the southeastern boundary between the Pine Mountain window and the Carolina superterrane (Steltenpohl et al., 2010). The low-angle, folded Box Ankle fault transported Inner Piedmont rocks of the Cat Square terrane northwestward over the

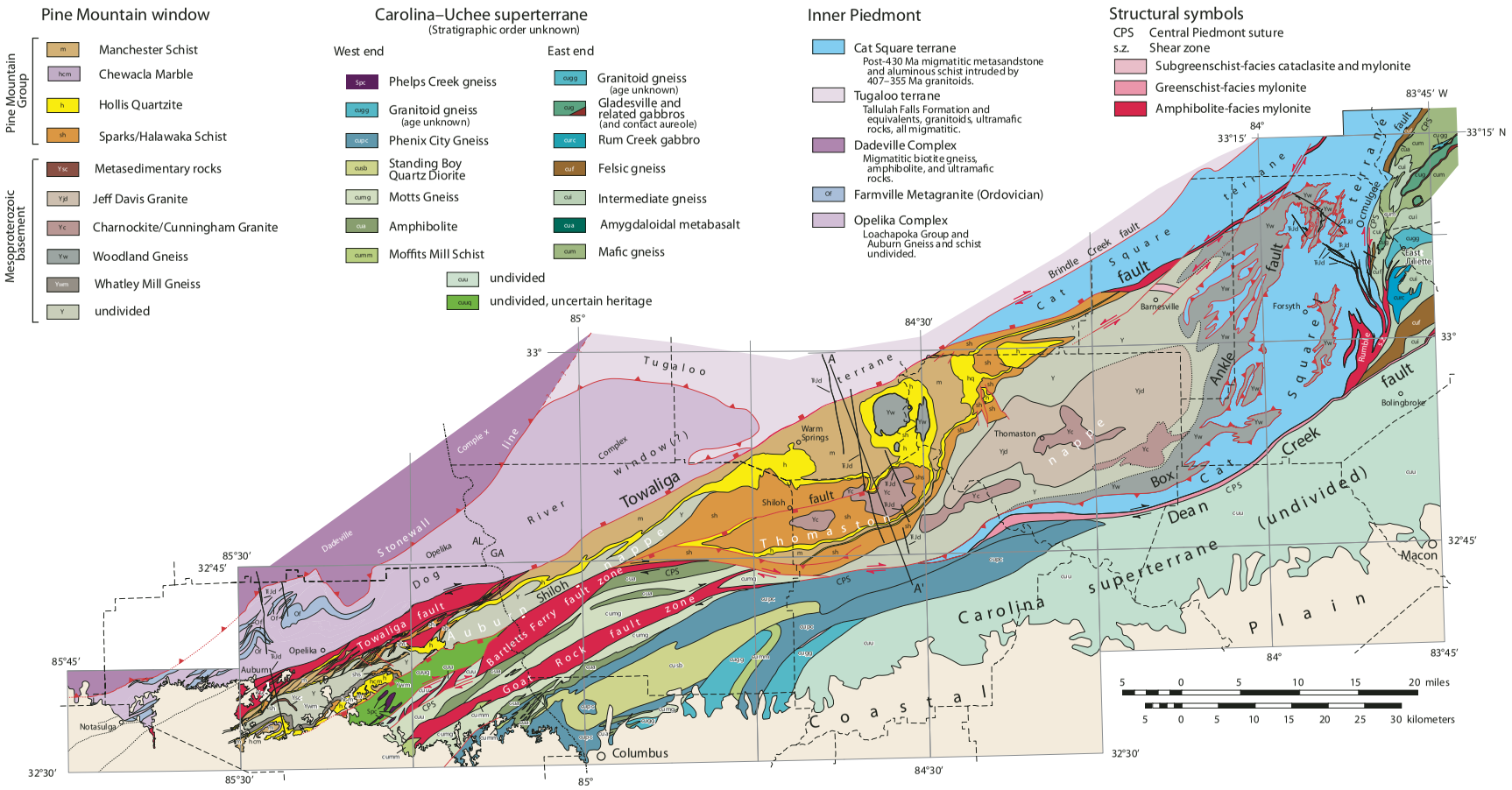


Figure 5-6. Geologic map of the Pine Mountain window (from Steltenpohl et al., 2010)

basement massif and forms the northeastern terminus of the window (Hooper and Hatcher, 1988b). The southwestern terminus of the Pine Mountain window is obscured by Coastal Plain sediments in Alabama (Steltenpohl et al., 2010). Recent U-Pb isotopic dating has produced ages of 1074 ± 24 Ma for Whatley Mill basement gneiss (Steltenpohl et al., 2010). Woodland Gneiss is the crystalline basement exposed in the study area and has produced an age of ~1.1 Ga (Steltenpohl et al., 2004). Large bodies of allochthonous basement are characteristic of orogenic belts. The Pine Mountain window is of particular interest for interpreting regional tectonic history, because it is the only internal Appalachian basement massif in contact with the peri-Gondwanan Carolina superterrane, and because its palinspastic location prior to the Alleghanian orogeny is still an enigma (Steltenphol et al., 2010).

Structural Obeservations

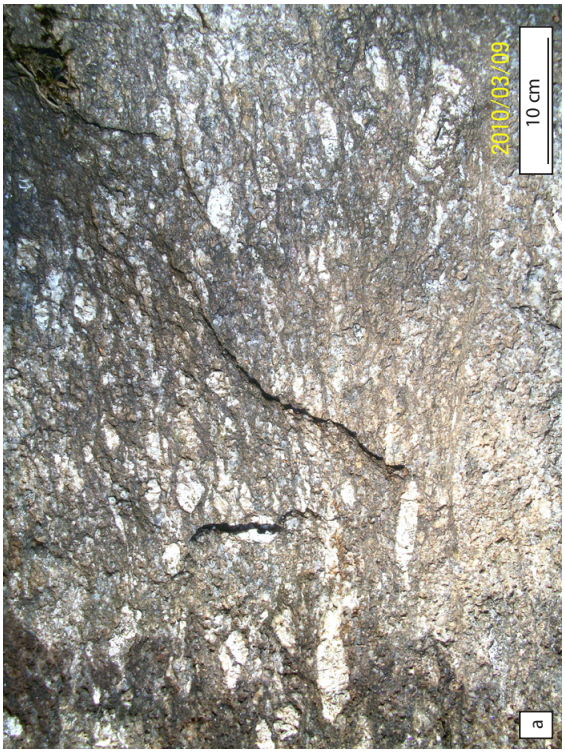
Fabrics

Foliation measurements were collected from a variety of sources in the field area. In fresh rock and saprolite outcrops, foliation is defined by the preferred alignment of elongate quartz grains, tabular feldspar, and platy phyllosilicates; sillimanite crystals; compositional layering; and mylonitic fabric (Fig. 5-7). A total of 1,044 foliations were collected from outcrops in the project area. The trend and plunge of 93 mineral stretching lineations were also recorded where available in the mapped area. These lineations are defined by elongated minerals (quartz, feldspar, phyllosilicates, sillimanite) that typically lie in the plane of foliation, although this relationship is not required (Fig. 5-8). Mylonitic rocks from the mapped area (Fig. 5-9) have strongly defined S and C fabrics. In most cases, the fabric is defined by compositional layering and alignment of minerals that have experienced plastic grain-size reduction (typically feldspar and

Figure 5-7. Examples of foliation from a variety of rock types in the project area. (a) Strong foliation defined by the alignment of microcline megacrysts (168°, 38°) in a High Falls Granite outcrop ~800 m north of Mann Road in the High Falls quadrangle. Looking southwest. (b) Irregular foliation defined by alignment of biotite and feldspar (173°, 68°) in Indian Springs Granite ~700 m north of Mann Road in the High Falls quadrangle. Looking southwest (c) Contact between High Falls Granite and a metagraywacke xenolith ~700 m southwest of the Towaliga River in High Falls State Park. Strong foliation in the metagraywacke is defined by the orientation of biotite crystals and compositional layering, while weaker foliation in the High Falls Granite is defined by discrete layers of biotite <30 mm long. Foliation between the two units is concordant (244°, 54°). Looking northwest. (d) Outcrop of migmatitic biotite gneiss ~1 km east of the Georgia Diagnostic Prison in Butts County, Georgia. The field of view is ~3 m wide and foliation here is defined by compositional layering in the biotite gneiss (140°, 59°). Looking southwest with Brunton for scale.


2010/02/27
20 mm
b


2010/04/29
d


2010/03/09
10 cm
a


2010/04/26
20 mm
c

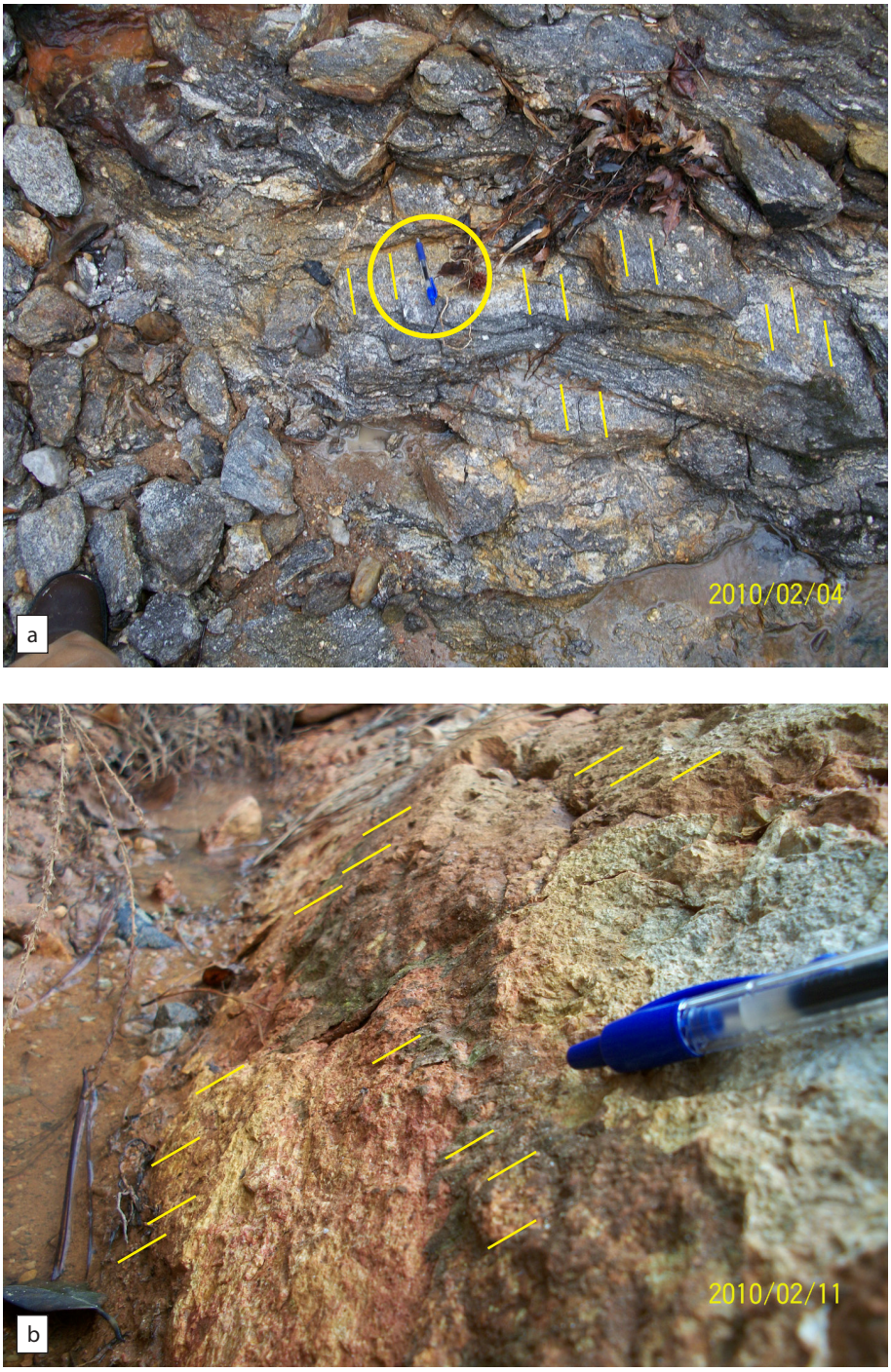


Figure 5-8. (a) An outcrop of biotite gneiss ~640 m east of High Ridge Trail in the High Falls quadrangle. Penetrative mineral stretching lineations (238°, 14°) in the plane of foliation (120°, 28°) are highlighted by the blue pen in the center of the photograph and the yellow lines, looking southwest. (b) Mineral stretching lineations (354°, 30°), highlighted by yellow lines, in a body of granite with mylonitic fabric (227°, 44°) ~300 m west of the intersection of Mann Road and City Pond Road in Lamar County, Georgia. Looking northeast.

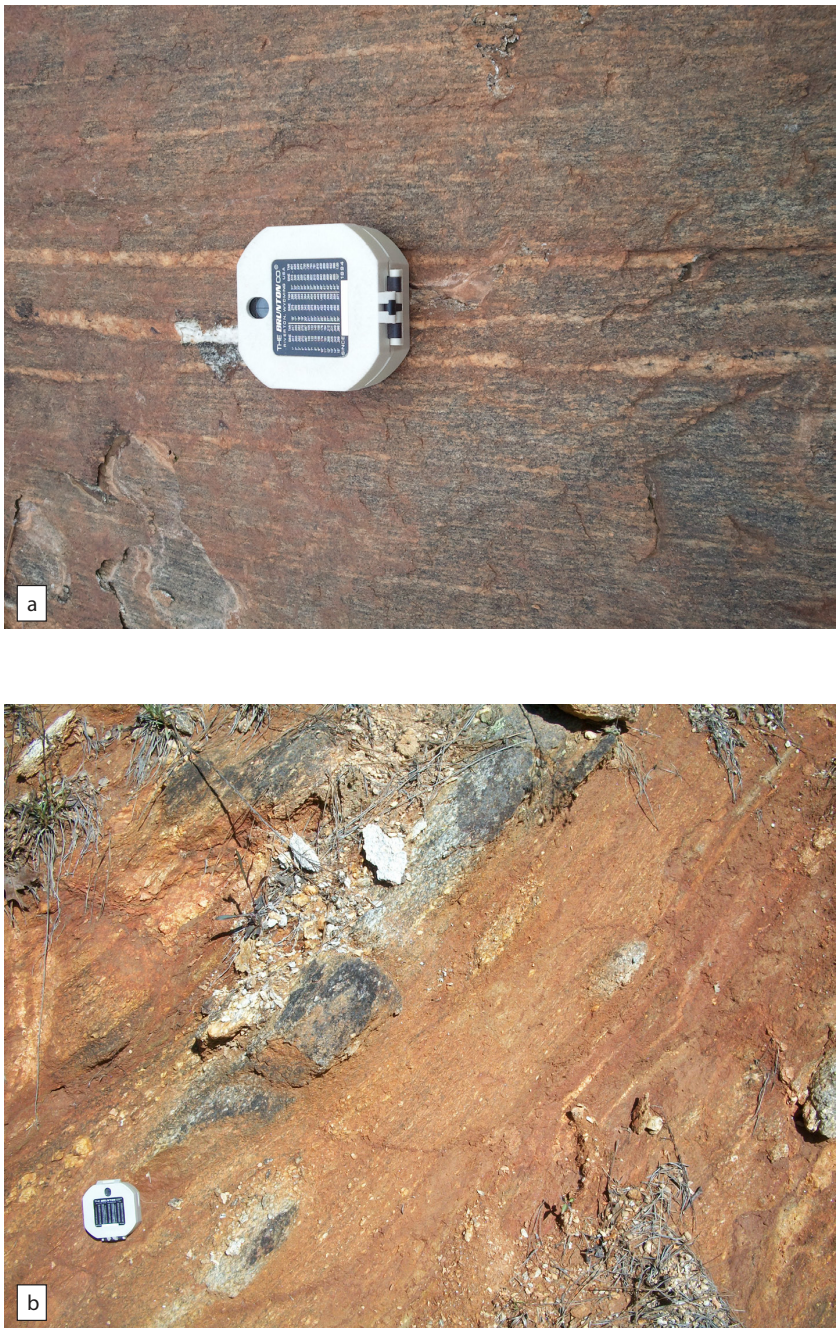


Figure 5-9. (a) Outcrop of Brindle Creek fault mylonite ~500 m northwest of the intersection of Georgia Highway 36 and Levi Barnes Road, Butts County, Georgia. Mylonitic fabric strikes 049° northeast and dips 76° southeast. Mylonitization has dramatically stretched quartz and feldspar grains so they appear as lenses up to 0.5 m long. Looking northeast. Photograph has been rotated 90° counterclockwise. b) Brindle Creek fault exposed in a saprolite outcrop ~50 m north of the intersection of Old Scout Road and Tall Tree Lane in Lamar County, Georgia. Elongate quartz grains and rotated feldspar porphyroclasts define the mylonitic fabric (174°, 65°) here, although not as strongly as those shown in (a). Looking northwest.

garnet) or elongation and some degree of recrystallization (quartz). Compositional layering is produced by segregation of quartz, phyllosilicates, sillimanite, and accessory phases into anastamosing layers in the mylonite. Inspection of hand samples and thin sections reveals several rock types have been incorporated into mylonite zones in the study area. The orientation of poles to foliations and lineations have been plotted using Stereonet™ (Fig. 5-10) . After plotting the data, Stereonet™ was used to create one percent area contour maps for both poles to foliation and lineation data (Fig. 5-10a and b). A π diagram was also generated for poles to foliation.

Folds

A variety of fold types were observed and measured in the mapped area, and these can be grouped into three general styles: tight to isoclinal folds, broad to open folds, and refolded folds. Tight to isoclinal folds and broad to open folds are subdivided on the basis of the fold's interlimb angle. Refolded folds are those whose axial surface has been folded. In general, folds observed in metasedimentary units in the study area can fit into all three styles (Figs. 5-11 and 5-12). Folds in plutonic rock in the study area were observed less frequently than in metasedimentary units, and these were typically broad to open folds. Another observation was that bodies of schist in the field had been much more intensely deformed than biotite gniess or granite, based on the frequency of folds. Refolded isoclinal folds and crenulation cleavage were commonly observed in schist units, while biotite gneiss and granitoids rarely revealed this style of deformation. Data collected from folds have been plotted using Stereonet™ (Fig. 5-13).

Microstructures

Thin sections were made from representative samples collected in the field area. Microstructures observed in these thin sections include well-developed S-C fabrics in

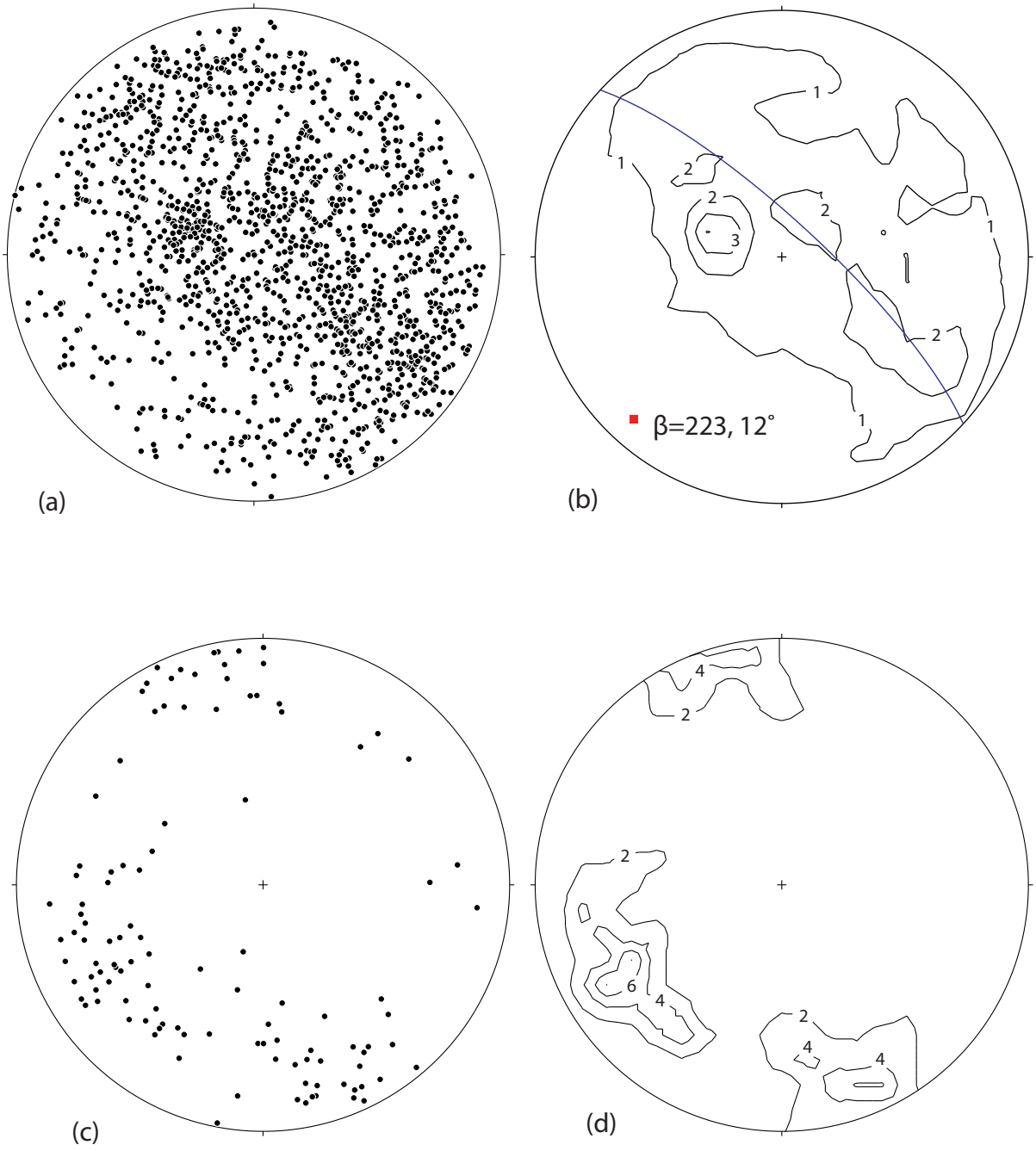


Figure 5-10. Lower hemisphere equal-area plots of mesofabric data collected in the study area with additional unpublished data from the Indian Springs quadrangle. (a) 1530 poles to foliation. (b) One percent per one percent area contours of poles to foliation. (c) 112 mineral stretching lineation measurements. (d) One percent per one percent area contours of lineation data. Contours on c and d represent the percent of data in one percent of the area on the stereonet.



Figure 5-11. (a) Folded biotite schist ~450 m south of Buck Creek in Lamar County, Georgia. Axial surface of isoclinal fold, outlined by the dashed yellow line, (axial surface 326°, 63°, hinge line 306°,33°) appears to be refolded. Head of rock hammer for scale. Looking down and northwest. (b) Tight fold in muscovite-biotite schist (axial surface 222°,74°, fold hinge 16°, 33°) exposed ~640 m south of Chief McIntosh Lake, Butts County, Georgia. GPS unit for scale. Looking down hinge line. Solid yellow lines in both (a) and (b) outline the dominant foliation there.

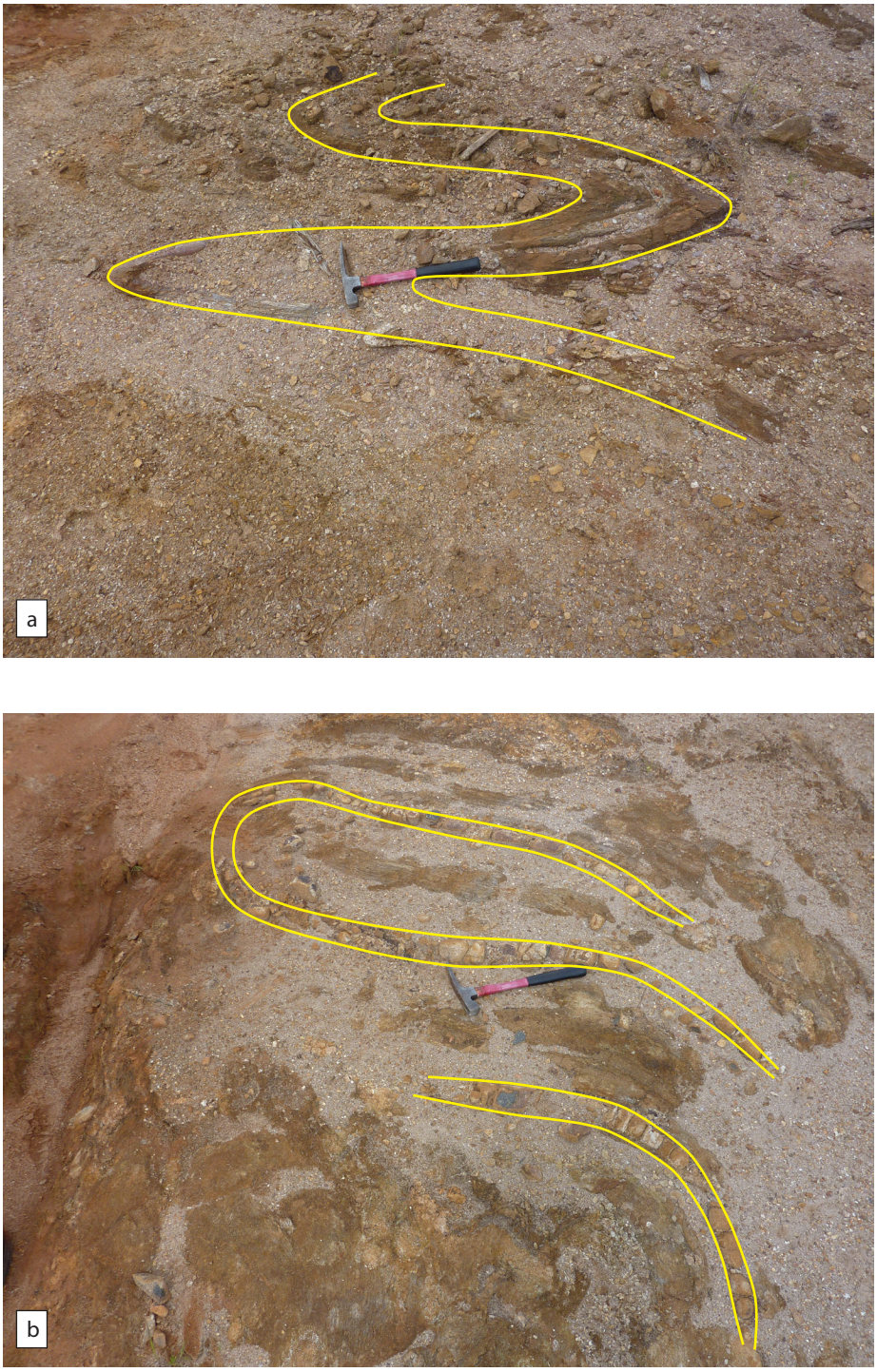


Figure 5-12. Folds in muscovite-biotite schist, with dominant foliation oulined by yellow lines, exposed ~150 m northeast of the intersection of Interstate 75 and High Falls Road, Lamar County, Georgia. (a) Series of tight folds with thickened hinges indicating passive flow. (b) Folded calc-silicate layer in the larger body of muscovite-biotite schist. Both photos courtesy of R.D. Hatcher Jr.

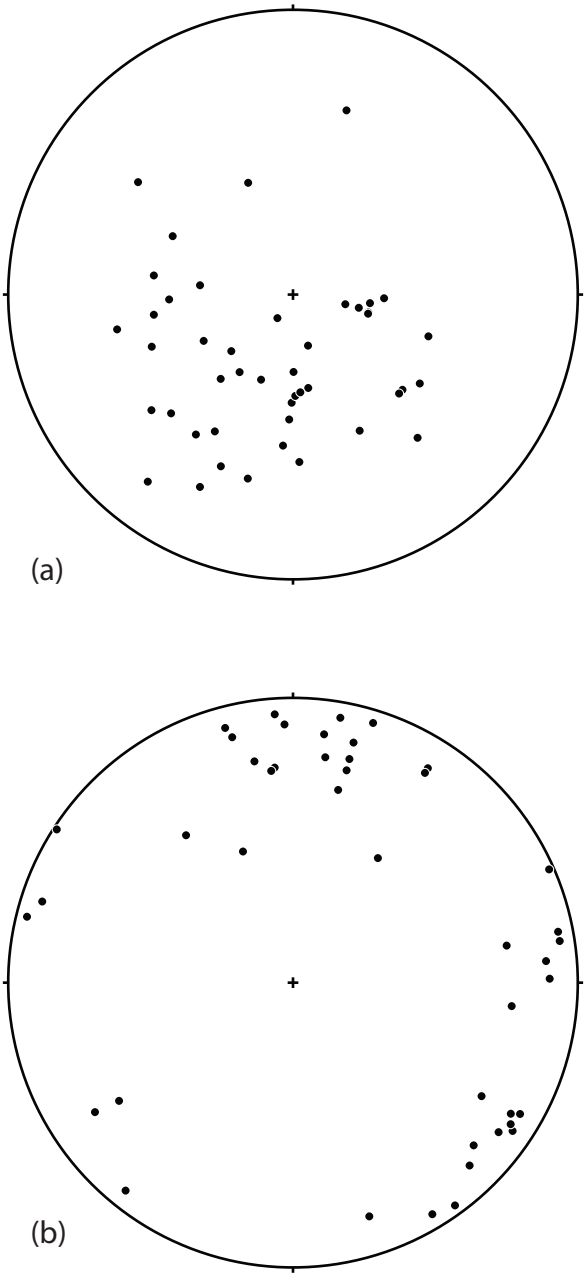


Figure 5-13. Stereonets of fold data collected from the project area. (a) 45 fold hinges. There is considerable variability in the trend of fold hinge lines, and the majority of hinge lines plunge either southeast or southwest. (b) 45 poles to fold axial surfaces. The majority of axial surfaces have a shallow dip and strike either east-west or northeast-southwest.

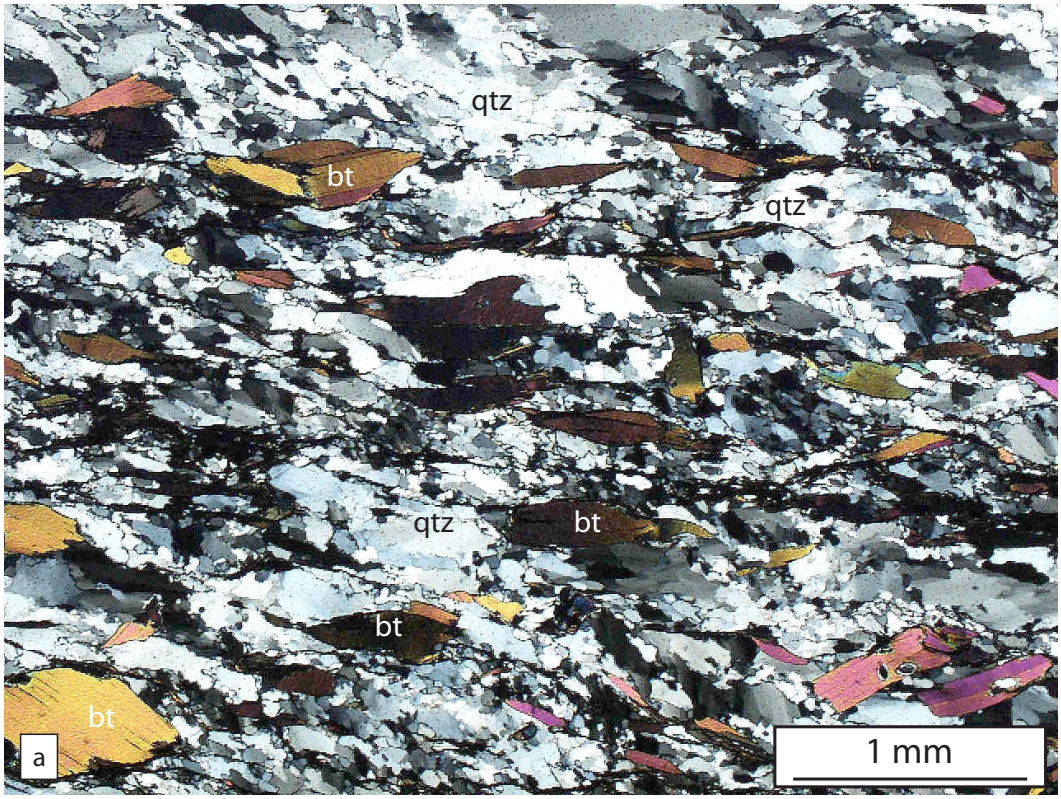
metasedimentary rocks; foliation delineated by the preferred orientation of elongate minerals in all rock types; rotated prophyroclasts; and bulging and annealed quartz crystals (Figs. 5-14 and 5-15). Well-developed mylonitic fabric was observed in thin sections of specimens from the Towaliga fault zone, Brindle Creek fault, and discrete shear zones in the Cat Square terrane. Quartz microstructures were also examined in thin section. Thin sections from rock units that are not proximal to a shear zone (major fault or otherwise) revealed quartz with undulose extinction and bulging at grain boundaries, indicating that recovered and unrecovered strain in quartz is common in most rocks in the field area.

Interpretation of Structural Data

Collecting structural data in the field has very little to do with interpretation. The strike and dip of foliations measured at an outcrop should be reproduceable within the error of the instrument (a Brunton™ compass) used to gather the data. In contrast, locations of contacts on a geologic map are an approximation in areas that do not have near 100 percent exposure. As the amount of exposure decreases and the complexity of the geology being mapped increases, the amount of approximation increases. Contacts on the geologic map (Plate 1) reflect the accuracy of location by solid (observed), long-dashed (located within 15 m), and dotted (concealed) lines.

A form line map of the strike of foliations in the study area was generated to help identify patterns in structural data (Fig. 5-16). If this type of figure generates consistent patterns in large areas of detailed mapping, the geologic map may be divided into structural domains. The form-line map of the study area produced a contorted mass of contours containing only one area with a consistent orientation in the region immediately north of the Towaliga fault zone where foliation strikes strongly northeast, parallel with

Figure 5-14. (a) Thin section of schistose metagraywacke from ~700 m north of the intersection of Mann Road and City Pond Road in Lamar County, Georgia. Foliation in this sample is delineated by the parallel orientation of elongate quartz grains and biotite crystals. An S-C fabric is also visible in thin section. Evidence of unrecovered strain is visible in many of the larger quartz grains as undulose extinction. Evidence of partially recovered strain is visible as bulging texture around the boundaries of some of these larger quartz grains. Thin section not oriented. (b) Thin section of High Falls Granite from Gilmore Creek ~1 km north of Blount Road, Monroe County, Georgia. Foliation in this thin section is also defined by elongate quartz grains and the preferred orientation of clusters of biotite crystals. Bulging at quartz grain boundaries is clearly visible in this thin section. Thin section not oriented. bt-biotite; qtz-quartz.


qtz
bt
qtz
qtz
bt
bt
bt
a
1 mm

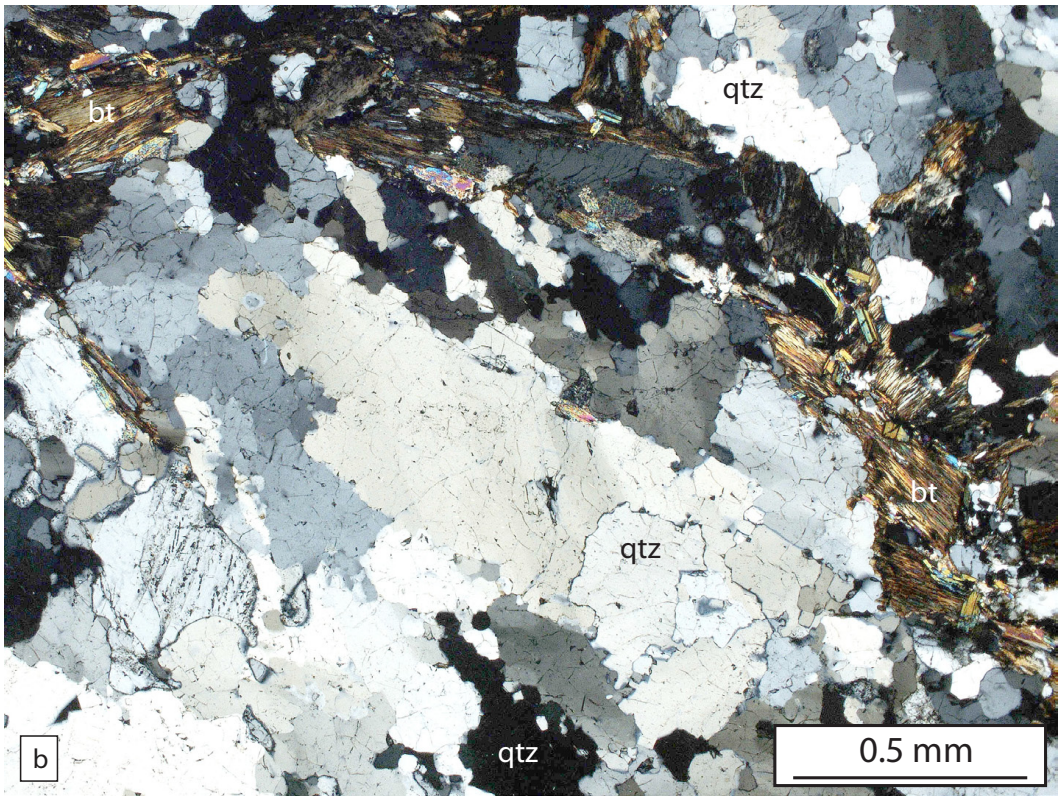
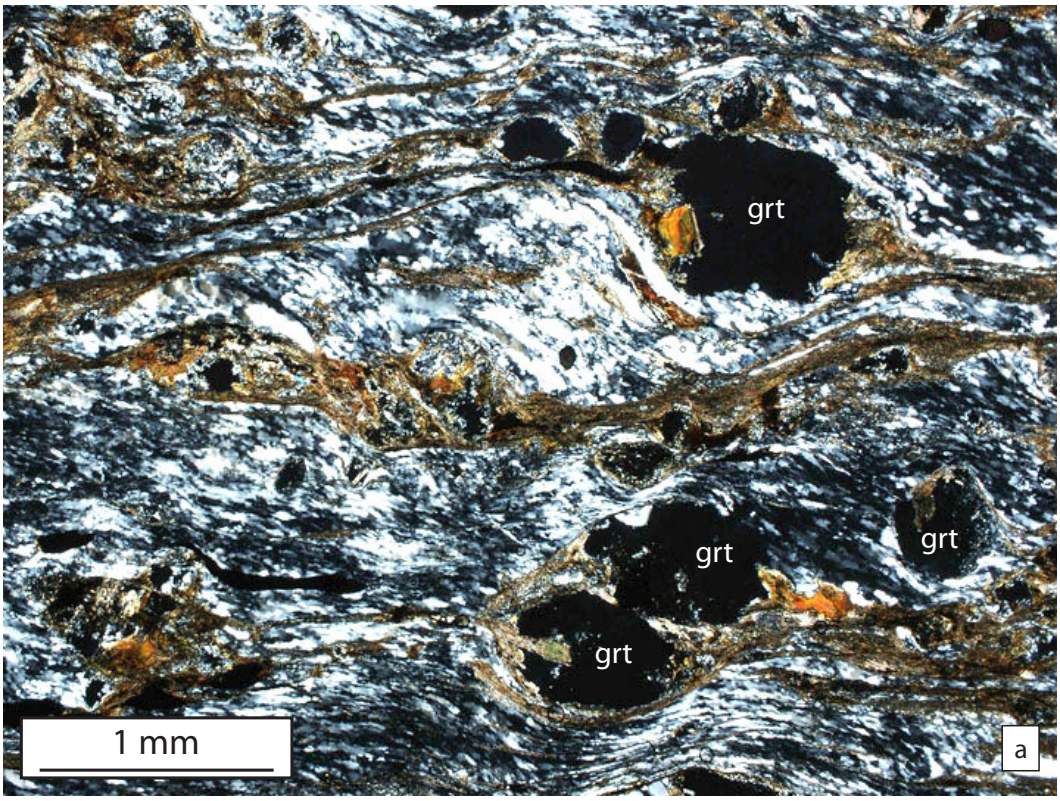
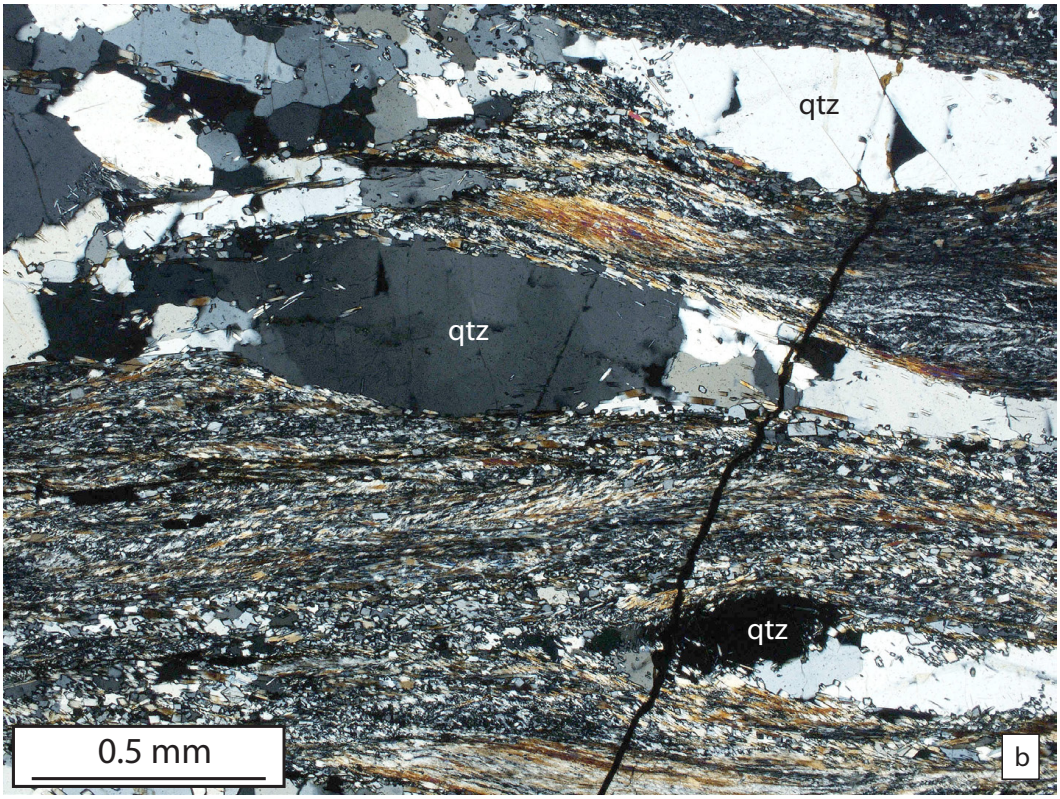

bt
qtz
bt
qtz
qtz
b
0.5 mm

Figure 5-15. (a) Thin section of Towaliga mylonite from a swamp along the Little Towaliga River ~1.5 km west of Harmony Hill Ranch Road, Monroe County, Georgia. Strong mylonitic foliation is defined by compositional layering and the preferred orientation of elongate quartz crystals. Feldspar (highly weathered) and garnet σ porphyroclasts reveal top to the left shear sense. Thin section not oriented. (b) Thin section of high temperature mylonite from ~360 m east of Turner Road, Lamar County, Georgia. Fibrolitic sillimanite crystals parallel to foliation are visible in the matrix between dynamically recrystallized quartz ribbons. Prismatic sillimanite crystals are also visible in thin section, but are oriented with their C-axis perpendicular to the field of view. Muscovite, biotite, and recrystallized quartz make up the rest of the matrix material. Right of the center of the photomicrograph, a brittle fracture crosscuts and slightly offsets the mylonitic fabric. grt-garnet; qtz-quartz.


grt
grt
grt
grt
1 mm
a


qtz
qtz
qtz
0.5 mm
b

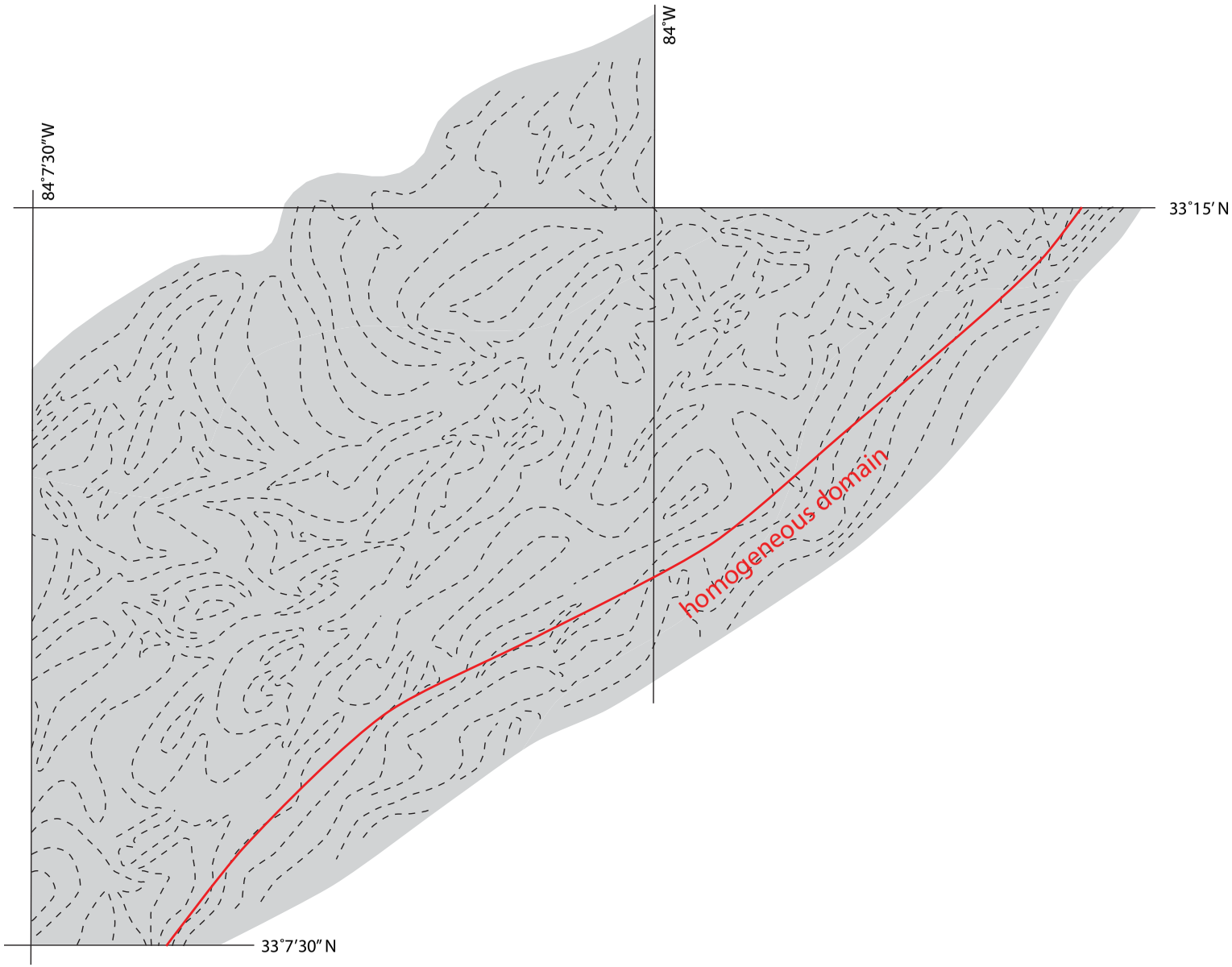


Figure 5-16. Form lines drawn from strike of foliation in the project area.

the trace of the fault zone. The dip angle and dip direction of foliation in this area are not nearly as consistent. Dip angles range from 28° to 68°, and direction of dip is southeast and northwest. Still, the consistency of the strike of foliation in this narrow band suggests that deformation along the Towaliga fault may have had a significant influence on rock fabric on either side of the fault zone. The lack of any recognizeable pattern in the form lines elsewhere is likely related to the abundance of High Falls Granite, which dominates the Cat Square terrane in the study area. Foliation is commonly discordant with the regional fabric in the High Falls Granite. Discordant foliation may be a relict magmatic fabric, or possibly a second regional foliation. There is no easy way to determine the source of the discordant foliation. The effect of this relict foliation cannot only be seen in the form-line diagram, but is also likely responsible for much of the scatter in data shown on the stereonet of poles to foliation (Fig. 5-10 a and b).

Many other workers who have mapped in the Inner Piedmont have used a framework that separates deformation into six distinct phases (Fig. 5-17) (Davis, 1993, Yanagihara, 1994; Bream, 1999; Giorgis, 1999; Hill, 1999; Williams, 2000; Bier, 2001; Kalbas, 2003; Merschat, 2003; Gatewood, 2007; Byars, 2010; Davis, 2010; Gilliam, 2010; Huebner and Hatcher, 2011). Observations made in the field are typically placed into the context of this framework in an attempt to associate structures with certain phases of deformation. Below is a discussion of how structures observed during field mapping may fit into the framework shown in Figure 5-17.

D_1

D_1 is the oldest deformation recognized in the study area and produced the first episode of deformation, forming penetrative S_1 foliation and F_1 folds. These structures were overprinted by more intense deformation associated with the Neoacadian orogeny. S_1 foliations and possibly a few tight folds can be seen in amphibolite boudins.

	FABRICS	FOLDS	FAULTS	METAMORPHIC CONDITIONS	REGIONAL EVENTS	OROGENIC EVENTS
D_1	S_1 Early foliation preserved in boudins	F_1 Intrafolial and isoclinal folds preserved in boudins	Initial development of the CPS	Rising temperature and pressure, amphibolite facies, kyanite grade	Initial collision and A-subduction of IP beneath Carolina superterrane	Pre- to Early Acadian 410-400 Ma
D_2	S_2 Penetrative regional foliation L_2 Mineral stretching lineations	F_2 Tight to isoclinal passive and flexural flow folds, macro scale sheath folds	SW-directed emplacement of ductile thrust sheets, movement along BCFZ, KCFZ, deflection and dextral strike-slip on BFZ	Peak IP metamorphism upper amphibolite facies, Sillimanite I and II grade	Dextral-oblique accretion and obduction of Carolina superterrane above IP, SW-directed extrusion of IP	Neoacadian orogeny 360-345 Ma
D_3	S_3 Rare secondary foliation	F_3 Reclined, open to tight folds	Continued ductile displacement along IP fault zones	Lower temperature and pressure	Continued subduction of IP, unroofing, and cooling of IP	Late Neoacadian orogeny 345-340 Ma
D_4	L_4 Dextral S-C fabrics in the BFZ, TFZ, and CPS, mineral stretching lineations in faults, low-temperature plastic deformation of quartz	F_4 Broad upright open folds	Dextral strike-slip on TFZ, dextral reactivation of the BFZ and CPS	Upper greenschist to lower amphibolite facies	Orogen-scale dextral activation of EPFS	Alleghanian orogeny 330-300 Ma
D_5	Joints		Brittle displacement along BFZ, sinistral reactivation of TFZ, development of ribbon quartz mylonites	Temperatures pass below brittle-ductile transition	Emplacement of BR-IP megathrust sheet and subsequent unrofing	Late Alleghanian 300-265 Ma
D_6	Joints		Movement on meso- and macroscale strike-slip faults	Brittle conditions	Regional uplift and rifting, intrusion of ~200 Ma diabase dikes, rift-drift transition	Mesozoic breakup of Pangea 230-200 Ma (Cenozoic uplift?)

Figure 5-17. Summary and relative timing of deformation events in the Inner Piedmont, central Georgia. Modified from Davis, 1993; Yanagihara, 1994; Bream, 1999; Giorgis, 1999; Hill, 1999; Williams, 2000; Bier, 2001; Kalbas, 2003; Merschat, 2003; Gatewood, 2007; Byars, 2010; Davis, 2010; Gilliam, 2010; Huebner and Hatcher, 2011. BCFZ=Brindle Creek fault zone; BFZ=Brevard fault zone; BR-IP=Blue Ridge-Inner Piedmont; CPS=Central Piedmont suture; EPFS=Eastern Piedmont fault system; IP=Inner Piedmont; KCFZ=Kinnard Creek fault zone; TFZ=Towaliga fault zone.

T.L. Davis (1993) identified preserved compositional layering in the Poor Mountain Formation of North Carolina that was attributed to D_1 deformation. B.A. Davis (2010) identified a similar style of folds to the northeast of the study area in the Farrar and Mansfield 7.5-minute quadrangles. Bodies of amphibolite in the study area are sparse, and no structures were identified that fit into this category.

D_2

The Neoacadian orogeny is the peak tectonothermal event recorded in the Inner Piedmont. Upper amphibolite facies metamorphism is thought to be the product of the oblique collision of the Laurentian-Taconian continental margin with the Carolina superterrane (Merschat et al., 2005). This event produced penetrative regional foliation (S_2) that transposed the majority of S_1 foliations. Any relict F_1 folds not occurring inside amphibolite boudins were completely overprinted during this phase of deformation.

S_2 foliation is the dominant rock fabric in the mapped area, and is normally defined by the orientation of platy and tabular minerals, and compositional layering, as described above (Figs. 5-11, 5-12, and 5-14). The fact that sillimanite crystals are typically oriented parallel to S_2 foliation (excluding exception noted in Fig. 5-15b) strongly suggests that this foliation formed during peak metamorphic conditions during the Neoacadian orogeny. The calculated beta (β) axis trends southwest with a shallow plunge (~12º) (Fig. 5-10b).

Lineations

L_2 lineations are defined by elongated grains of quartz, feldspar, muscovite, and biotite in all rock units as discussed above. In metasedimentary rocks it may also be defined by sillimanite, which indicates L_2 formed during the metamorphic peak. L_2 mineral stretching lineations formed as the entire Inner Piedmont was extruded to the

southwest by ductile motion (Merschat et al., 2005; Hatcher and Merschat, 2006).

Folds

F_2 folds are described in Figure 5-17 as “tight to isoclinal passive and flexural flow folds.” A calc-silicate layer that has buckled while muscovite-biotite schist has flowed around it can be seen in Figure 5-8a. Excellent examples of isoclinal passive to flexural flow folds can also be seen in Figure 5-8. Many similar folds in metasedimentary units in the field area are likely F_2 structures. Davis (2010) also concluded this style of fold formed during D_2 deformation. Some fold hinges (Fig. 5-13a) are parallel with L_2 mineral stretching lineation (Fig. 5-10 c and d).

Faults

Oblique-dextral strike-slip movement along the Brindle Creek fault zone likely occurred during the Neoacadian D_2 event. The transition from a shallow-dipping mylonite zone in the North Carolina Inner Piedmont to a steeply-dipping mylonite zone in central Georgia may be related to proximity to the Central Piedmont suture (Davis, 2010). In the study area, the Brindle Creek is a relatively narrow mylonite zone (<30 m) with a well-developed mylonitic fabric (Fig. 5-9). Metasedimentary rocks close to the Brindle Creek fault zone typically display intense migmatization (Davis, 2010), and this was observed in several locations in the mapped area (Fig. 4-2). Distinct lithologies on both sides of the Brindle Creek fault (Lithonia Gneiss and High Falls Granite) also help identify the trace. Structural data (strike and dip of mylonitic foliation, dextral shear sense indicators) from the Brindle Creek fault in the mapped area support the conclusion that the fault surface dips southeast and strike-slip motion is dextral. The sinuous trace of the Brindle Creek fault has two possible interpretations: (1) heterogeneities (asperities) in the rocks along the Brindle Creek fault forced

irregularities in the trace of the fault while it was developing; or (2) the Brindle Creek fault has been folded by deformation that occurred after the mylonite zone developed.

The Kinnard Creek fault (initially named the Rex Haven fault) is a narrow mylonite zone (~20 m) identified by Davis (2010) in the Farrar quadrangle. Shear-sense indicators and fabrics reveal that it is a high-temperature, low-angle (15-45º), dextral strike-slip fault that is thought to have formed during the Neoacadian orogeny. Additional geologic data have extended the trace of the Kinnard Creek fault zone as far southwest as the Forsyth quadrangle (Huebner et al., 2011; Hatcher, unpublished data).

One small (<10 m of exposure), high temperature shear zone was also identified during field mapping. It was initially concluded that the outcrop exposed a low-temperature ribbon quartz mylonite. However, analysis of a thin section proved that this is not the case (Fig. 5-15b). This mylonite is characterized by anastamosing quartz ribbons and the presence of fibrolitic and prismatic sillimanite crystals.

D_3

Subduction of the Inner Piedmont beneath the Carolina superterrane continued into the late Neoacadian orogeny; however, by this time pressures and temperatures in the orogenic belt began to decrease due to unroofing. F_3 folds are described as tight to open and upright or inclined. Davis (2010) concluded that F_3 folds are geometrically similar to F_2 folds except they fold the earlier S_2 foliation. Possible refolded F_2 folds were observed during field mapping (Fig. 5-11a) although, it is also possible that open folds in the field area formed during the later stages of D_2. Another possibility is that the fold pictured in Figure 5-11a is a Type 3 fold interference pattern (Ramsay and Huber, 1987) in which an early tight to isoclinal fold is folded about its own axis. In this case, no subsequent phase of deformation is necessary.

D_4

During the Alleghanian orogeny, faults bounding the Inner Piedmont (Brevard fault zone and the Central Piedmont suture) were reactivated dextrally in the ductile regime, producing S-C and mineral stretching lineations in the fault zones. The Towaliga fault zone formed as a dextral fault, producing a wide mylonite zone. Dextral shear sense indicators (σ, δ, and θ porphyroclasts; asymmetric folds) were observed in the Towaliga fault zone during this study (Fig. 5-15a). The Alleghanian orogeny also produced broad to open upright folds (F_4) (Fig. 5-17). The refolded fold illustrated in Figure 5-11a has a veritcal axis and could have been generated during D_4 deformation . Joints and quartz veins that formed ribbon quartz mylonite in D_5 (discussed below) may have formed in D_4.

D_5

The final stages of the Alleghanian orogeny emplaced the Blue Ridge-Piedmont megathrust sheet. Erosional unroofing for the megathrust sheet accompanied this uplift. This unroofing significantly lowered the pressure and temperature of Inner Piedmont rocks. Reduced temperatures and waning deformation may have produced ribbon-quartz mylonite in and around the Towaliga fault zone. Huebner and Hatcher (in review) estimated the temperature during formation of these isolated mylonite zones was ~400º C, bracketed by ribbon quartz microfabrics and the lack of ductile deformation in feldspar. Ribbon-quartz mylonite float was identified in several locations in the mapped area, and one inplace outcrop was located ~1.3 km northwest of the Towaliga fault zone. Shear-sense indicators in the outcrop of ribbon quartz mylonite indicate dextral movement. Other ribbon quartz layers in the Piedmont also record dextral displacement as summarized by Huebner and Hatcher (in review). Joints and unstrained quartz veins in the mapped area may have formed during D_5.

D_6

The final stage of deformation recorded in the mapped area is a result of Mesozoic extension related to the breakup of Pangea and includes joints, quartz veins, and brittle reactivation of the Towaliga fault. Brittle reactivation along the Towaliga fault is responsible for the bodies of siliceous cataclasite described above (Fig. 5-5). Joint sets attributed to D_6 deformation in the Farrar and Mansfield quadrangles strike N5ºW, N85ºE, N5ºE, and N45ºE (B.A. Davis, 2010).

Categorizing folds by style (see above) is a convenient way to organize data collected in the field; however, assigning entire classes of folds to a rigid framework of deformation in a region that has undergone multiple phases of deformation is difficult at best. It is possible to identify individual fold generations at a singe outcrop where exposure is good. It is difficult to confidently associate one fold style with a specific phase of deformation that has affected a large region where good exposures in the mapped area are separated by considerable distances (Williams, 1970, 1985). If good exposure is continuous throughout most of a mapped area and different generations of folds have similar syles, then associating particular styles of folds with specific phases of deformation can be done with a reasonable amount of confidence. In the study area, this association is made more difficult by the large amount of High Falls Granite. Since the High Falls Granite was emplaced while the Cat Square Terrane was being deformed during the Acadian/Neoacadian event in the southern Appalachians, foliation in the granite is not consistently concordant with regional foliation.

Chapter 6 - Conclusions

Synthesis of Structural, Geochronologic, and Geochemical Anlyses

The emplacement conditions of the High Falls Granite are crucial to understanding the middle Paleozoic history of the southern Inner Piedmont. Resolution of these conditions requires interpretation of several data sets. U-Pb isotope dating produced several critical pieces of evidence. First, different bodies of High Falls Granite crystallized over an extended period (~42 Ma) during the Silurian and Devonian. Also, the older (424-406 Ma) and southwesternmost samples of High Falls Granite (SWHFG) contain zircons with inherited cores. The inherited cores have a provenance identical to that of the metasedimentary rocks in the Cat Square terrane (Chapter 3).

This contrasts with the younger (383-382 Ma) northeasternmost samples (NEHFG), which contain only a single pan-African inherited core among them. The contrast in inheritance may be attributed to one of several factors: 1) SWHFG passed through and assimilated a significant amount of Cat Square terrane crust, whereas NEHFG either did not pass through as much crust or it simply did not assimilate as much material during emplacement; or 2) SWHFG melt was produced at a significantly lower temperature than NEHFG, thus allowing detrital zircons incorporated into SWHFG to not be resorbed during emplacement. Any inherited zircons that were assimilated by NEHFG were completely resorbed. Bulk geochemistry of High Falls Granite samples reveals lower Zr concentrations in SWHFG compared to NEHFG and indicates Zr saturation was not a controlling factor in zircon inheritance. NEHFG crystallization ages were closer to peak metamorphism in the Cat Square terrane, so elevated temperatures may be responsible for a lack of zircon inheritance in the northeastern part of the pluton. A similar contrast in zircon inheritance between the eastern Blue Ridge and western

Inner Piedmont was attributed to differences in magma temperatures (Mapes, 2002). Hatcher et al. (2007a) concluded that a lack of zircon inheritance in the Walker Top Granite in North Carolina either did not assimilate a significant amount of continental crust during emplacement, or thermal and chemical conditions in the melt caused any inherited zircon to be resorbed and completely recrystallized.

SWHFG samples plot in the volcanic-arc field on tectonic discrimination diagrams, which calls the anatectic origin into question. Samples of NEHFG plot in either the syn-collisional or within-plate granite fields. This suggests these portions of the pluton may have been produced in different tectonic settings; however, the discrimination diagrams may be affected by several factors. The Cat Square basin was filled with sediment derived from a volcanic arc complex as well as a relatively mature continental source. It seems highly unlikely that sediments derived from these sources were distributed evenly in the Cat Square basin. A melt derived from a heterogeneous mixture of continental and island-arc sediments may produce varied chemical signatures. There may be some significance in how the ages and trace element abundances of the High Falls Granite cluster, but it may also be coincidental.

Another possibility is that a portion of the High Falls Granite pluton was generated above a subduction zone that transitioned into collisional setting. If the SWHFG was generated above a subduction zone, the melt must have assimilated Cat Square terrane material as it was emplaced, as indicated by the provenance of inherited zircon cores. This would require that the Cat Square basin had already narrowed to receive sediment derived from Laurentian-Taconian margin and the Carolina superterrane. Subduction ceased in the Devonian; the Carolina superterrane was then obducted above the Cat Square terrane, thickening the crust and generating anatectic

melts that were incorporated into the High Falls pluton during Neoacadian peak metamorphism.

The middle Paleozoic granitoids in the Cat Square terrane were used as a proxy for the closure of the Cat Square remnant ocean basin (Merschat and Hatcher, 2007). Crustal thickening and anatexis caused by A-subduction of the Cat Square terrane beneath the Carolina superterrane is thought to be responsible for the generation of middle Paleozoic granitoids in the Inner Piedmont. However, this is difficult to reconcile with geochemical data from the Walker Top Granite in the northern Inner Piedmont, which indicate those plutons were produced in a mature volcanic arc or within-plate setting (Byars, 2010).

High Falls Granite U-Pb geochronologic data produced a spread of crystallization ages from 424 to 382 Ma in the central Georgia Inner Piedmont. If the High Falls Granite was entirely generated by crustal anatexis, this requires that the southwestern end of the Cat Square terrane be buried to depths of 15-20 km prior to 424 Ma. This would require the Carolina superterrane to obduct onto the Laurentian + Taconian margin before the beginning of the Acadian orogeny in the southern Appalachians (Fig. 5-13). If the oldest portions of the High Falls Granite were instead generated by a continental subduction zone, as geochemical data presented in Chapter 3 suggest, the intrusion of this portion of the pluton would not necessarily require a change in the hypothesized timing of obduction of the Carolina superterrane (beginning at 410 Ma) (Fig. 5-13).

Other important points from this study include the following:

1. Southwest of Jackson, Georgia, the High Falls Granite becomes the most abundant rock unit in the Cat Square terrane. The Pennsylvanian-Permian Indian Springs Granite and Siluro-Devonian sillimanite schist and biotite gneiss are other major units exposed in the Cat Square terrane in the mapped area. Minor units exposed in the Cat Square terrane include amphibolite, calc-silicate, and diabase.

2. Exposures of High Falls Granite cover over 230 km^2 in the central Georgia Inner Piedmont and may be a composite batholith that was formed by several phases of magmatism.

3. Similarities between the High Falls and Walker Top Granites include mineralogy, texture, age, and trace element abundances.

4. Chondrite-normalized Rare Earth Element abundances reveal a negative Eu anomaly in both the Walker Top and High Falls Granite likely due to fractional crystallization of feldspar. This anomaly is not observed in Indian Springs Granite samples.

5. Intense migmatization of metasedimentary rocks proximal to the Brindle Creek fault suggest the Brindle Creek thrust sheet was emplaced at a high temperature.

6. Sillimanite was commonly observed in Cat Square terrane metasedimentary rocks, indicating the entire terrane was exposed to upper amphibolite facies metamorphism.

7. Garnet-biotite geothermometry of a sample of the High Falls Granite revealed a

range of temperatures (690-770° C) using an assumed pressure of 5 kbar. It is unclear whether these results represent the temperature of emplacement or metamorphism.

8. Several large bodies of siliceous cataclasite were identified in the southern end of the High Falls quadrangle. These bodies are located in the northwestern edge of the Towaliga fault zone.

9. Foliation in the High Falls Granite is concordant with regional trends in many cases; however, in other cases the foliation is discordant. These discordant regions may preserve a relict magmatic foliation, or a foliation produced by a phase of deformation after the peak Neoacadian event.

10. Based on field observations, folding in metasedimentary units in the mapped area was a result of both passive and flexural flow.

11. Map patterns and outcrop relationships suggest the High Falls Granite is a catazonal pluton.

12. Discrete bodies of ribbon-quartz mylonite and a high-temperature mylonite were identified during field mapping, and both structures contain dextral shear-sense indicators.

REFERENCES CITED

Absher, S.B., and McSween, H.Y., Jr., 1985, Granulites at Winding Stair Gap, North Carolina: The thermal axis of Paleozoic metamorphism in the southern Appalachians: Geological Society of America Bulletin, v. 96, no. 5, p. 588-599.

Aleinikoff, J.N., Zartman, R.E., Walter, M., Rankin, D.W., Lyttle, P.T., and Burton, W.C., 1995, U-Pb ages of metarhyolites of the Catoctin and Mount Rogers Formations, central and southern Appalachians: Evidence for two pulses of Iapetan rifting: American Journal of Science, v. 295, p. 428-454.

Allmendinger, R.W., 2011, Stereonet v 7.3.0, computer program.

Altherr, R., Holl, A., Hegner, E., Langer, C., and Kreuzer, H., 2000, High-potassium, calc alkaline I-type plutonism in the European Variscides: northern Vosges (France) and northern Schwartzwald (Germany): Lithos, v. 50, p. 51-73.

Anderson, J.L., and Thomas, W.M., 1985, Proterozoic anorogenic two-mica granites: Silver Plume and St. Vrain batholiths of Colorado: Geology, v. 13, p. 177-180.

Atkins, R.L., and Lineback, J.A., 1992, Structural relations, origin and emplacement of granitic rocks in the Cedar Rock Complex, Georgia Piedmont: Georgia Geologic Survey Bulletin 115, 40 p.

Babaie, H.A., Babaei, A., and Hadizadeh, J., 1991a, Initiation of cataclastic flow and development of cataclastic foliation in nonporous quartzites from a natural fault zone: Tectonophysics, v. 200, p. 67-77.

Babaie, H.A., Hadizadeh, J., Babaei, A., and Ghazi, A.M., 1991b, Timing and temperature of cataclastic deformation along segments of the Towaliga fault zone, western Georgia, U.S.A.: Journal of Structural Geology, v. 13, no. 5, p. 579-586.

Barker, F., 1979, Trondhjemite: Definition, environment, and hypotheses of origin, *in* Barker, F., ed., Trondhjemites, Dacites, and Related Rocks: Amsterdam, Elsevier, p. 1-12.

Bateman, P.C., and Chappell, B.W., 1970, Variations of major chemical constituents across the central Sierra Nevada batholith: Geological Society of America Bulletin, v. 81, p. 409-420.

Bentley, R.D., and Neathery, T.L., 1979, Geology of the Brevard fault zone and related rock in the Inner Piedmont of Alabama: Alabama Geological Society Field Trip Guidebook, 119 p.

Best, M.G., 2003, Igneous and metamorphic petrology: Turin, Blackwell Science Ltd.,

729 p.

Bier, S.E., 2001, Geology of the southeastern South Mountains, North Carolina [M.S. thesis]: Knoxville, University of Tennessee, 162 p.

Bier, S.E., Bream, B.R., and Giorgis, S.D., 2002, Inner Piedmont stratigraphy, metamorphism, and deformation in the Marion-South Mountains area, North Carolina, *in* Hatcher, R.D., Jr., and Bream, B.R., eds., Inner Piedmont geology in the South Mountains-Blue Ridge Foothills and southwestern Brushy Mountains, central-western North Carolina: North Carolina Geological Survey, Carolina Geological Society annual field trip guidebook, p. 65-99.

Boynton, W.V., 1984, Geochemistry of the rare earth elements: meteorite studies. *in* Henderson, P., ed., Rare Earth Element Geochemistry: Elsevier, p. 63-114.

Bream, B.R., 1999, Geology of the Glenwood and Sugar Hill quadrangles, North Carolina, and the structure of the northeast end of the Henderson Gneiss [M.S. thesis]: Knoxville, University of Tennessee, 155 p.

Bream, B.R., 2003, Tectonic implications of para- and orthogneiss geochronology and geochemistry from the southern Appalachian crystalline core [Ph.D. dissertation]: Knoxville, University of Tennessee, 296 p.

Bream, B.R., Hatcher, R.D., Jr., Miller, C.F., and Fullagar, P.D., 2001, Geochemistry and provenance of Inner Piedmont paragneisses, NC and SC: Evidence for an internal terrane boundary?: Geological Society of America Abstracts with Programs, v. 33, no. 2, p. A-65.

Bream, B.R., Hatcher, R.D., Jr., Miller, C.F., and Fullagar, P.D., 2004, Detrital zircon ages and Nd isotopic data from the southern Appalachian crystalline core, GA-SC-NC-TN: New provenance constraints for part of the Laurentian margin, *in* Tollo, R.P., Corriveau, L., McLelland, J., and Bartholomew, M.J., eds., Proterozoic Evolution of the Grenville Orogen in North America: Geological Society of America Memoir 197, p. 459–475.

Byars, H.E., 2010, Tectonic evolution of the west-central portion of the Newton window, North Carolina Inner Piedmont: Timing and implications for the emplacement of the Paleozoic Vale charnockite, Walker Top granite, and mafic complexes [M.S. thesis]: Knoxville, The University of Tennessee, 248 p.

Chappell, B.W., and White, A.J.R., 1974, Two contrasting granite types: Pacific Geology, v. 8, p. 173-174.

Corfu, F., Hanchar, J.M., Hoskin, P.W.O., and Kinny, P., 2003, Atlas of zircon textures: Reviews in Mineralogy and Geochemistry, v. 53, p. 469-500.

Davis, B.A., 2010, Tectonic evolution of the southern Appalachian Inner Piedmont: Identification and Interpretation of crustal features from aeromagnetic data and detailed geologic mapping in central Georgia [M.S. thesis]: Knoxville, University of Tennessee, 262 p.

Davis, T.L., 1993, Lithostratigraphy, structure, and metamorphism of a crystalline thrust terrane, western Inner Piedmont, North Carolina [Ph.D. dissertation]: Knoxville, University of Tennessee, 245 p.

Duchesne, J.-C. and Wilmart, E., 1997, Igneous charnockites and related rocks from the Bjerkreim-Sokndal layered intrusion (southwest Norway): a jotunite (hypersthene monzodiorite)-derived A-type granitoid suite: Journal of Petrology, v. 38, p. 337-369.

Eckert, J.O., Jr., Hatcher, R.D., Jr., and Mohr, D.W., 1989, The Wayah granulite-facies metamorphic core, southwestern North Carolina; high-grade culmination of Taconic metamorphism in the southern Blue Ridge: Geological Society of America Bulletin, v. 101, p. 1434-1437.

Ellis, D.J., and Thompson, A.B., 1986, Subsolidus and partial melting reactions in the quartz-excess CaO + MgO + Al_2O_3 + SiO_2 + H_2O under water-excess and water-deficient conditions to 10 kb: some implications for the origin of peraluminous melts from mafic rocks: Journal of Petrology, v. 27, p. 91-121.

Frost, B.R., Barnes, C.G., Collins, W.J., Arculus, R.J., Ellis, D.J., and Frost, C.D., 2001, A geochemical classification for granitic rocks: Journal of Petrology, v. 42, no. 11, p. 2033-2048.

Frost, C.D., Frost, B.R., Chamberlin, K.R., and Edwards, B.R., 1999, Petrogenesis of the 1.43 Ga Sherman batholith, SE Wyoming: a reduced rapakivi-type anorogenic granite: Journal of Petrology, v. 40, p. 1771-1802.

Gardner, C. H., 1961, The geology of Central Newton County, Georgia [M.S. thesis]: Atlanta, Emory University, 53 p.

Gatewood, M.P., 2007, Tectonics of the northeastern Inner Piedmont, northwestern NC, from detailed geologic mapping, geochronologic, geochemical, and petrologic studies with structural analyses of ductile fault zones [M.S. thesis]: Knoxville, University of Tennessee, 263 p.

Gilliam, W.G., 2010, Structural and metamorphic evolution of the west-central Newton

window, eastern Inner Piedmont, Burke, Catawba, and Lincoln counties, North Carolina [M.S. thesis]: Knoxville, University of Tennessee, 156 p.

Giorgis, S.D., 1999, Inner Piedmont geology of the northwestern South Mountains near Morganton, North Carolina [M.S. thesis]: Knoxville, University of Tennessee, 191 p.

Glazner, A.F., Bartley, J.M., Coleman, D.S., Gray, W., and Taylor, R.Z., 2004, Are plutons assembled over millions of years by amalgamation from small magma chambers?: GSA Today, v. 14, no. 4/5, p. 4-11.

Graybill, E., 2012, Evidence for post-Grenville rifting at ~960 Ma in the Sams Creek volcanics/Wakefield carbonates complex, Western Piedmont, MD: Geological Society of America Abstracts with Programs, v. 44, no. 4, p. 64.

Griffin, V.S., Jr., 1974, Analysis of the Piedmont in northwest South Carolina: Geological Society of America Bulletin, v. 85, p. 1123-1138.

Hadizahdeh, J., Babaie, H.A. and Babaie, A., 1991, Development of interlaced mylonites, cataclasites and breccias: example from the Towaliga fault, south central Appalachians: Journal of Structural Geology, v. 13, no. 1, p. 63-70.

Hanchar, J.M., and van Westrenen, W., 2007, Rare earth element behavior in zircon-melt systems: Elements, v. 3, p. 37-42.

Hanchar, J.M., and Watson, E.B., 2003, Zircon saturation thermometry: Reviews in Mineralogy and Geochemistry, v. 53, p. 89-112.

Harris, N.B.W., Pearce, J.A., and Tindle, A.G., 1986, Geochemical characteristics of collision-zone magmatism, *in* Coward, M.P., and Reis, A.C., eds., Collision tectonics: Geological Society, London, Special Publication 19, p. 67-81.

Haslam, H.W., 1968, The crystallization of intermediate and acid magmas at Ben Nevis, Scotland: Journal of Petrology, v. 9, p. 84-104.

Hatcher, R. D., Jr., 1986, Interpretation of seismic reflection data in complexly deformed terranes: A geologist's perspective: American Geophysical Union, Geodynamics Series v. 14, p. 912.

Hatcher, R.D., Jr., 1971a, Geology of Rabun and Habersham Counties, Georgia: A reconnaissance study: Georgia Department of Mines, Mining, and Geology Bulletin 83, 48 p.

Hatcher, R.D., Jr., 1971b, Structural, petrologic, and stratigraphic evidence favoring a

thrust solution to the Brevard problem: American Journal of Science, v. 270, p. 177-202.
Hatcher, R.D., Jr., 1990, Structural geology, principles, concepts, and problems: New York, Merrill Publishing Company, 531 p.

Hatcher, R.D., Jr., 2001, Rheological partitioning during multiple reactivation of the Paleozoic Brevard Fault Zone, Southern Appalachians, USA, *in* Holdsworth, R.E., Strachan, R.A., Macloughlin, J.F., and Knipe, R.J., eds., The nature and significance of fault zone weakening: Geological Society of London Special Publication 186, p. 255-269.

Hatcher, R.D., Jr., 2002, The Alleghanian (Appalachian) orogeny, a product of zipper tectonics: Rotational transpressive continent-continent collision and closing of ancient oceans along irregular margins, *in* Martínez Catalán, J.R., Hatcher, R.D., Jr., Arenas, R., and García, F.D., eds., Variscan-Appalachian Dynamics: The Building of the Late Paleozoic Basement: Geological Society of America Special Paper 394, p. 199-208.

Hatcher, R.D., Jr., 2004, Southern Appalachian crustal transect: Day 2, The Neoacadian metamorphic core, large ductile thrust sheets, and a multiply reactivated crustal scale shear zone, *in* Merschat, A.J., and Hatcher, R.D., Jr., eds., Trans Appalachians Internides Geotraverse: 17th International Basement Tectonics Association Field Trip Guidebook, p. 29-60.

Hatcher, R.D., Jr., 2010, The Appalachian orogen: A brief summary, *in* Tollo, R.P., Bartholomew, M.J., Hibbard, J.P., and Karabinos, P.M., eds., From Rodinia to Pangea: The Lithotectonic Record of the Appalachian Region: Geological Society of America Memoir 206, p. 1–19.

Hatcher, R.D., Jr., and Hooper, R.J., 1992, Evolution of crystalline thrust sheets in the internal parts of mountain chains, *in* McClay, K.R., ed., Thrust tectonics: London, Chapman and Hall, p. 217-234.

Hatcher, R.D., Jr., and Merschat, A.J., 2006, The Appalachian Inner Piedmont: An exhumed strike-parallel, tectonically forced orogenic channel, *in* Law, R. D., Searle, M., and Godin, L., eds., Channel flow, ductile extrusion, and exhumation of lower-mid crust in continental collision zones: Geological Society of London Special Publication 268, p. 517-541.

Hatcher, R.D., Jr., Bream, B.R., and Merschat, A.J., 2007a, Tectonic map of the southern and central Appalachians: A tale of three orogens and a complete Wilson cycle, *in* Hatcher, R.D., Jr., Carlson, M.P., McBride, J.H., and Martínez Catalán, J.R., eds., 4-D Framework of Continental Crust: Geological Society of America Memoir 200, p. 1-19.

Hatcher, R.D., Jr., Lemiszki, P.J., and Whisner, J.B., 2007b, Boundaries and internal deformation in the curved southern Appalachian foreland fold-thrust belt, *in* Sears, J.W., Harms, T., and Evenchick, C., eds., Whence the Mountains? Inquiries into the Evolution of Orogenic Systems: A Volume in Honor of Raymond A. Price: Geological Society of America Special Paper 433, p. 243-276.

Hatcher, R.D., Jr., Howell, D.E., and Talwani, P., 1977, Eastern Piedmont fault system: Speculations on its extent: Geology, v. 5, p. 636-640.

Hatcher, R.D., Jr., Thomas, W.A., and Viele, G.W., 1989, The Appalachian-Ouachita orogen in the United States, *in* Hatcher, R.D., Jr., Thomas, W.A., and Viele, G.W., eds., The Appalachian–Ouachita orogen in the United States: Boulder, Colorado, Geological Society of America, The Geology of North America, v. F-2, p. 25-51.

Heatherington, A.L., Mueller, P.A., Kamenov, G., Steltenpohl, M.G., Hanley, T.B., and Wooden, J.L., 2006, Pine Mountain terrane: Geochemistry and geochronology of basement gneisses and xenoliths: Geological Society of America Abstracts with Programs, v. 38, no. 3, p. 63.

Higgins, M.W., Atkins, R.L., Crawford, T.J., Crawford, R.F., III, Brooks, R., and Cook, R.B., 1988, The structure, stratigraphy, tectonostratigraphy and evolution of the southernmost part of the Appalachian orogen: U.S. Geological Survey Professional Paper 1475.

Hill, J.C., 1999, Stratigraphy, structure, and tectonics of part of the southern Appalachian Inner Piedmont, near Marion, North Carolina [M.S. thesis]: Knoxville, The University of Tennessee, 188 p.

Hoffman, P.F., 1988, United plates of America: The birth of a craton—Early Proterozoic assembly and growth of Laurentia: Annual Review of Earth and Planetary Sciences, v. 16, p. 542-603.

Hooper, R. J., 1986, Geologic studies at the east end of the Pine Mountain window and adjacent Piedmont, central Georgia [Ph.D. dissertation]: Columbia, University of South Carolina, 322 p.

Hooper, R.J., and Hatcher, R.D., Jr., 1988a, Mylonites from the Towaliga fault zone, central Georgia: products of heterogeneous non-coaxial deformation: Tectonophysics, v. 152, p. 1-17.

Hooper, R.J., and Hatcher, R.D., Jr., 1988b, Pine Mountain terrane, a complex window in the Georgia and Alabama Piedmont; evidence for the eastern termination: Geology, v. 16, p. 307-310.

Hopson, J.L., Hatcher, R.D., Jr., and Stieve, A.L., 1989, Geology of the eastern Blue Ridge, northeastern Georgia and the adjacent Carolinas, *in* Fritz, W.J., Hatcher, R.D., Jr., and Hopson, J.L., eds., Geology of the eastern Blue Ridge of northeast Georgia and the adjacent Carolinas: Georgia Geological Society Guidebooks, v. 9, p. 1-40.

Hoskin, P.W.O., and Ireland, T.R., 2000, Rare earth element chemistry of a zircon and its use as a provenance indicator: Geology, v. 28, no. 7, p. 627-630.

Hoskin, P.W.O., and Schaltegger, U., 2003, The composition of zircon and igneous and metamorphic petrogenesis, *in* Zircon, Reviews in Mineralogy and Geochemistry, v. 53, p. 27-62.

Huebner, M.T., and Hatcher, R.D., Jr., 2011, Evidence for sinistral Mesozoic inversion of the dextral Alleghanian Towaliga fault, *in* Huebner, M.T., and Hatcher, R.D., Jr., eds., The geology of the Inner Piedmont at the northeast end of the Pine Mountain window: Georgia Geological Society 16th Annual Field Trip, v. 31, no. 1, p. 55-72.

Huebner, M.T., Hatcher, R.D., Jr., and Howard, C.W., 2011, Insights into Paleozoic orogenesis and Mesozoic rifting from detailed mapping in the Georgia Inner Piedmont: Geological Society of America Abstracts with Programs, v. 43, no. 2, p. 68.

Hyndman, D.W., 1984, A petrographic and chemical section through the northern Idaho batholith: Journal of Geology, v. 92, p. 83-102.

Ingersoll, R.V., Graham, S.A., and Dickinson, W.R., 1995, Remnant ocean basins, *in* Busby, C.J., and Ingersoll, R.V., eds., Tectonics of sedimentary basins: Cambridge, Massachusetts, Blackwell Science, p. 363-392.

Janoušek, V., Farrow, C.M. and Erban, V., 2006, Interpretation of whole-rock geochemical data in igneous geochemistry: introducing Geochemical Data Toolkit (GCDkit): Journal of Petrology, v. 47, p. 1255-1259.

Johnson, K., Barnes, C.G., and Miller, C.A., 1997, Petrology, geochemistry, and genesis of hi-Al tonalite and trondhjemites of the Cornucopia stock, Blue Mountains, northeastern Oregon: Journal of Petrology, v. 38, p. 1585-1611.

Jones, D. D., Jr., 1970, Petrofabric and movement study of faults in Newton and Walton Counties, Georgia [M.S. thesis]: Atlanta, Emory University, 28 p.

Kalbas, J.L., 2003, Geology of part of the southwestern Brushy Mountains, Inner Piedmont [M.S. thesis]: Knoxville, University of Tennessee, 208 p.

King, P.B., 1970, Epilogue, *in* Fisher, G.W., Pettijohn, F.J., Reed, J.C., Jr., and Weaver, K.N., eds., Studies in Appalachian Geology: central and southern: New York, Wiley-Interscience, p. 437-439.

King, P.B., and Ferguson, H.W., 1960, Geology of northeasternmost Tennessee: U.S. Geological Survey Professional Paper 311, 136 p.

King, P.L., White, A.J.R., Chappell, B.W., and Allen, C.M., 1997, Characterization of origin of aluminous A-type granites from the Lachlan fold belt, southeastern Australia: Journal of Petrology, v. 38, p. 371-391.

Kohn, M.J., and Spear, F.S., 1989, Empirical calibration of geobarometers for the assemblage garnet+hornblende+plagioclase+quartz: American Mineralogist, v. 74, p. 77-84.

Kohn, M.J., and Spear, F.S., 1990, Two new barometers for garnet amphibolites, with applications to southeastern Vermont: American Mineralogist, v. 75, p. 89-96.

Ludwig, K.R., 2001, SQUID v. 1.02, computer program.

Ludwig, K.R., 2003, Isoplot/Ex v. 3.00, computer program.

Mapes, R.W, 2002, Geochemistry and geochronology of mid-Paleozoic granitic plutonism in the southern Appalachian Piedmont terrane, North Carolina-South Carolina-Georgia [M.S. thesis]: Nashville, Tennessee, Vanderbilt University, 140 p.

McBride, J.H., Hatcher, R.D., Jr., Stephenson, W.J., and Hooper, R.J., 2005, Integrating seismic reflection and geological data and interpretations across an internal basement massif: The southern Appalachian Pine Mountain window, USA: Geological Society of America Bulletin, v. 117, no. 5/6, p. 669-686.

McConnell, K.I., and Abrams, C.E., 1984, Geology of the greater Atlanta region: Georgia Geologic Survey Bulletin, no. 96, 127 p.

McSween, H.Y., Jr., and Harvey, R.P., 1997, Concord plutonic suite: Pre-Acadian gabbro-syenite intrusions in the southern Appalachians, *in* Sinha, A.K., Wahlen, J.B., and Hogan, J.P., eds., The Nature of Magmatism in the Appalachian Orogen: Boulder, Colorado, Geological Society of America Memoir 191, p. 221-234.

Merschat, A.J., 2003, Inner Piedmont tectonics in the southwestern Brushy Mountains, North Carolina: Field and laboratory data revealing a 3-D crustal flow and sillimanite I and II metamorphism [M.S. thesis]: Knoxville, University of Tennessee, 199 p.

Merschat, A.J., 2009, Assembling the Blue Ridge and Inner Piedmont: Insights into the nature and timing of terrane accretion in the southern Appalachian orogen from geologic mapping, stratigraphy, kinematic analysis, petrology, geochemistry, and modern geochronology [Ph.D. dissertation]: Knoxville, University of Tennessee, 455 p.

Merschat, A.J., and Hatcher, R.D., Jr., 2007, The Cat Square terrane: Possible Siluro-Devonian remnant ocean basin in the Inner Piedmont, southern Appalachians, *in* Hatcher, R.D., Jr., Carlson, M.P., McBride, J.H., and Martinez Catalan, J.R., eds., The 4D Framework of Continental Crust: Boulder, Colorado, Geological Society of America Memoir 200, p. 553-565.

Merschat, A.J., and Hatcher, R.D., Jr., and Davis, T.L., 2005, The northern Inner Piedmont , southern Appalachians, USA: kinematics of transpression and SW-directed mid-crustal flow: Journal of Structural Geology, v. 27, p. 1252-1281.

Merschat, A.J., Hatcher, R.D., Jr., Bream, B.R., Miller, C.F., Byars, H.E., Gatewood, M.P., and Wooden, J.L., 2010, Detrital zircon geochronology and provenance of southern Appalachian Blue Ridge and Inner Piedmont crystalline terranes, *in* Tollo, R.P., Bartholomew, M.J., Hibbard, J.P., and Karabinos, P.M., eds., From Rodinia to Pangea: The Lithotectonic Record of the Appalachian Region: Geological Society of America Memoir 206, p. 661-699.

Miller, C.F., 1985, Are strongly peraluminous magmas derived from sedimentary sources?: Journal of Geology, v. 93, p. 673-689.

Miller, C.F., McDowell, S.M., and Mapes, R.M., 2003, Hot and cold granite? Implications of zircon saturation temperatures and preservation of inheritance: Geology, v. 31, no. 6, p. 529-532.

Mirante, D.C., and Patino-Douce, A.E., 2000, Melting and migmatization in the southern Appalachian Inner Piedmont of northeast Georgia; the Athens gneiss: Geological Society of America Abstracts with Programs, v. 33, p. 297.

Mukasa, S.B., and Henry, D.J., 1990, The San Nicolas batholith of coastal Peru: early Paleozoic continental arc or continental rift magmatism?: Journal of the Geological Society, London, v. 147, no. 1, p. 27-39.

Nash, W.P., and Wilkinson, J.F.G., 1970, Shonkin Sag laccolith, Montana 1. Mafic minerals and estimates of temperature, pressure, oxygen fugacity, and silica activity: Contributions to Mineralogy and Petrology, v. 25, p. 241-269.

O'Connor, J.T., 1965, A classification of quartz-rich igneous rocks based on feldspar ratios: U.S. Geological Survey Professional Paper 525B, p. B79-B84.

Pearce, J.A., Harris, N.B.W., and Tindle, A.G., 1984, Trace element discrimination diagrams for the tectonic interpretation of granitic rocks: Journal of Petrology, v. 25, p. 956-983.

Pownceby, M.I., Wall, V.J., and O'Neill, H. St.C., 1987, Fe-Mn partitioning between garnet and ilmenite: experimental calibration and applications: Contributions to Mineralogy and Petrology, v. 97, p. 116-126.

Ramsay, J.G., and Huber, M.I., 1987, The techniques of modern structural geology, Vol. 2: Folds and fractures: London, Academic Press, 392 p.

Reade, E. H., Jr., 1960, The geology of a portion of Newton and Walton Counties, Georgia [M.S. thesis]: Atlanta, Emory University, 65 p.

Rollinson, H.R., 1993, Using geochemical data: Evaluation, presentation, and interpretation: John Wiley and Sons, Inc., 352 p.

Roy, S., and Purkait, P.K., 1968, Mineralogy and genesis of the metamorphosed manganese silicate rocks (gondite) of Gowari Wadhona, Madhya Pradesh, India: Contributions to Mineralogy and Petrology, v. 20, no. 1, p. 86-114.

Schamel, S., Hanley, T.B., and Sears, J.W., 1980, Geology of the Pine Mountain window and adjacent terranes in the Piedmont province of Alabama and Georgia: Geological Society of America, Southeastern Section Guidebook, 69 p..

Sheraton, J.W., Black, L.P., and Tindle, A.G., 1992, Petrogenesis of plutonic rocks in a Proterozoic granulite facies terrane; the Bunger Hills, Antarctica: Chemical Geology, v. 97, p. 163-198.

Sinha, S.P., 1983, The europium anamoly, in Sinha, S.P., ed., Systematics and the properties of the lanthanides: D. Reidel Publishing Company, p. 550-553.

Sloss, L.L., 1988, Tectonic evolution of the craton in Phanerozoic time, *in* Sloss, L.L., ed., Sedimentary cover—North American craton, U.S.: Boulder, Colorado, Geological Society of America, The Geology of North America, v. D-2, p. 25-51.

Smith, D.R., Noblett, J., Wobus, R.A., Unruh, D., Douglass, J., Beane, R., Davis, C., Goldman, S., Kay, G., Gustavson, B., Saltoun, B., and Stewart, J., 1999, Petrology and geochemistry of late-stage intrusions of the A-type, mid-Proterozoic Pikes Peak batholith (Central Colorado, USA): implications for petrogenesis models: Precambrian Research, v. 98, p. 271-305.

Sneyd, D., 1995, Geology of the Barnesville hydrologic research site, Lamar County, Georgia: Georgia Geologic Survey Information Circular 98, 27 p.

Spear, F.S., and Kohn, M.J., 1999, Geothermobarometry, v. 2.1, computer program.

Steltenpohl, M.G., 1988, Kinematic of the Towaliga, Bartletts Ferry, and Goat Rock fault zones, Alabama: The late Paleozoic dextral shear system in the southernmost Appalachians: Geology, v. 16, p. 852-855.

Steltenpohl, M.G., Heatherington, A., Mueller, P., and Wooden, J.L., 2004, Pre-Appalachian tectonic evolution of the Pine Mountain window in the southernmost Appalachians, Alabama and Georgia: Geological Society of America Memoir 197, p. 633-646.

Steltenpohl, M.G., Hatcher, R.D., Jr., Mueller, P.A., Heatherington, A.L., and Wooden, J.L., 2010, Geologic history of the Pine Mountain window, Alabama and Georgia: Insights from a new geologic map and U-Pb isotopic dates, *in* Tollo, R.P., Bartholomew, M.J., Hibbard, J.P., and Karabinos, P.M., eds., From Rodinia to Pangea: The lithotectonic record of the Appalachian region: Geological Society of America Memoir 206, p. 1-21.

Sun, S.S., and McDonough, W.F., 1989, Chemical and isotopic systematics of ocean basalts: implications for mantle compositions and processes, *in* Saunders, A.D., and Norry, M.J., eds., Magmatism in the Ocean Basins: Geological Society of America Special Publication 42, p. 313-345.

Thomas, W.A., 2006, Tectonic inheritance at a continental margin: GSA Today, v. 16, no. 2, p. 4-11, doi: 10.1130/1052-51.

Vinson, S., 1999, Ion probe geochronology of granitoid gneisses of the Inner Piedmont, North Carolina and South Carolina [M.S. thesis]: Nashville, Tennessee, Vanderbilt University, 84 p.

Walawender, M.J., Gastel, R.G., Clinkenbeard, J.P., McCormick, W.V., Eastman, B.G., Wernicke, R.S., Wardlaw, M.S., Gunn, S.H., and Smith, B.M., 1990, Origin and evolution of the zoned La Posta-type plutons, eastern Peninsular Ranges batholith, southern and Baja California, *in* Anderson, J.L., ed., The Nature and Origin of Cordilleran Magmatism: Geological Society of America Memoir 174, p. 1-18.

Wark, D.A., and Miller, C.F., 1993, Accessory mineral behavior during differentiation of a granite suite: monazite, xenotime and zircon in the Sweetwater Wash pluton, southeastern California, U.S.A.: Chemical Geology, v. 110, p. 49-67.

Watson, E.B., and Harrison, T.M., 1983, Zircon saturation revisited: Temperature and composition effects in a variety of crustal magma types: Earth and Planetary Science Letters, v. 64, p. 295-304.

Watson, T.L., 1902, A preliminary report on a part of the granites and gneisses of Georgia: Georgia Geologic Survey Bulletin 9-A, 367 p.

West, T. E., Jr., 1994, Field evidence that the Appalachian décollement is exposed in central Georgia at the east end of the Pine Mountain terrane [M.S. thesis]: Columbia, South Carolina, University of South Carolina, 26 p.

Williams, P.F. 1970, A criticism of the use of style in the study of deformed rocks: Geological Society of America Bulletin, v. 81, p. 3283-3296.

Williams, P.F., 1985, Multiply deformed terrains-problems of correlation: Journal of Structural Geology, v. 7, p. 269-280.

Williams, S.T., 2000, Structure, stratigraphy, and migmatization in the southwestern South Mountains, North Carolina [M.S. thesis]: Knoxville, University of Tennessee, 111 p.

Wilson, C.G., 2006, Origin and tectonic evolution of the southern Appalachian Neoacadian crystalline core: Evidence from the geology of the Gilreath 7.5-minute quadrangle, North Carolina [M.S. thesis]: Knoxville, University of Tennessee, 219 p.

Yanagihara, G.M., 1994, Structure, stratigraphy, and metamorphism of a part of the Columbus Promontory, North Carolina [M.S. thesis]: Knoxville, University of Tennessee, 214 p.

Yardley, B.W.D., 1989, An Introduction to Metamorphic Petrology: Essex, Longman Scientific and Technical, 248 p.

Zhao, J.-X., Shiraishi, K., Ellis, D.J., and Sheraton, J.W., 1995, Geochemical and isotopic studies of syenites from the Yamato magmas: Geochimica et Cosmochimica Acta, v. 59, p. 1363-1382.

APPENDICES

APPENDIX 1
Station Data

Abbreviations
Indian Springs Granite - ISG
High Falls Granite - HFG
Biotite gneiss - Bg
Schist - Sch
Calc-silicate - C-sil
Pegmatite – Peg
Amphibolite – Amp
Granitic orthogneiss – Go
Gondite – gd
Migmatite – Mig
Woodland gneiss – Yw

					Foliation		Lineation		Fold Hinge		Axial Surface		IL Angle	Vergence	Joint	
Quad	Station	Lithology	Minerals	Grain Size	Strike	Dip	Trend	Plunge	Trend	Plunge	Strike	Dip			Strike	Dip
HF	1	Bg			45	45										
HF	2	Bg	bt,qtz	Med-Coarse	6	72										
HF	3	Bg	bt,qtz	Med-Coarse	45	49										
HF	4	HFG		Med-Coarse	14	90										
HF	5	HFG		Med-Coarse	169	52										
HF	6	HFG		Med-Coarse	190	72										
HF	7	Sch		Medium	154	63										
HF	8	HFG		Med-Coarse												
HF	9	Sch		Med-Coarse	65	71										
HF	9	Sch		Med-Coarse											310	37
HF	10	Sch		Med-Coarse	326	63										
HF	10	Sch		Med-Coarse					306	33						
HF	10	Sch		Med-Coarse	326	64										
HF	11	Bg		Med-Coarse	40	59										
HF	12	Sch		Med-Coarse	43	53										
HF	13	Bg	bt,qtz	Med-Coarse	39	57										
HF	14	Sch		Med-Coarse	22	75										
HF	15	Bg		Med-Coarse	18	61										
HF	16	ISG	plg,qtz	Med-Fine												
HF	17	ISG		Med-Fine	19	56										
HF	18	Bg	bt,qtz	Medium							211	78	60	SW		
HF	18	Bg	bt,qtz	Medium					226	40						
HF	18	Bg	bt,qtz	Medium	214	78										
HF	18	Bg	bt,qtz	Medium			221	34								
HF	19	ISG		Med-Fine												
HF	20	Bg	bt,qtz	Med-Coarse												
HF	21	Bg	bt,qtz	Medium	158	69										
HF	22	HFG		Med-Coarse	155	41										
HF	22	HFG		Med-Coarse	206	69										
HF	23	HFG		Med-Coarse	0	0										
HF	24	HFG		Med-Coarse	50	48										
HF	25	ISG		Med-Fine												
HF	26	HFG		Coarse	226	46										
HF	27	Bg		Med-Coarse												
HF	28	HFG		Med-Coarse	216	44										
HF	29	Sch		Med-Coarse	227	58										
HF	30	HFG		Med-Coarse	228	68										
HF	31	HFG		Med-Coarse	73	42										
HF	32	Bg		Med-Coarse												
HF	33	Bg	bt,qtz	Med-Coarse	38	52										
HF	34	HFG		Med-Coarse	95	57										
HF	35	HFG		Med-Coarse	0	0										
HF	36	Sch		Med-Coarse	201	74										
HF	37	Sch		Med-Coarse							76	78	65	NW		
HF	37	Sch		Med-Coarse					84	11						
HF	37	Sch		Med-Coarse	66	68										
HF	38	Sch		Med-Coarse	54	75										
HF	39	Sch		Med-Coarse	69	42										
HF	40	Sch		Med-Coarse											201	90
HF	41	Sch		Medium							104	76	60	NE		
HF	41	Sch		Medium					103	68						
HF	42	Sch		Medium	60	54										
HF	43	Sch		Medium	64	36										
HF	44	Sch		Medium	47	68										
HF	45	Sch		Medium	100	51										
HF	46	Sch		Medium											324	65
HF	46	Sch		Medium											346	77
HF	47	Sch			105	60										
HF	48	ISG		Med-Fine							216	78	50	SW		
HF	48	ISG		Med-Fine					231	36						
HF	48	ISG		Med-Fine	156	51										
HF	49	Sch		Med-Coarse	49	28										
HF	50	ISG		Med-Fine	0	0										
HF	51	Sch		Medium	112	39										
HF	52	Sch		Medium	86	47										
HF	53	Sch		Medium	102	67										
HF	54	Sch		Medium	80	40										
HF	55	Bg		Med-Coarse												
HF	56	Bg		Med-Coarse												
HF	57	Bg		Med-Coarse	134	66										
HF	58	Bg		Med-Coarse												
HF	59	HFG		Med-Coarse												
HF	60	HFG		Med-Coarse												
HF	61	HFG		Med-Coarse												

HF	62	HFG		Med-Coarse	66	54										
HF	63	HFG		Med-Coarse												
HF	64	HFG		Med-Coarse	211	71										
HF	65	HFG		Med-Coarse												
HF	66	HFG		Med-Coarse	226	64										
HF	67	HFG		Med-Coarse	211	70										
HF	68	HFG		Med-Coarse	233	51										
HF	69	HFG		Med-Coarse												
HF	70	HFG		Med-Coarse	220	51										
HF	71	HFG		Med-Coarse												
HF	72	HFG		Med-Coarse	57	47										
HF	73	HFG		Med-Coarse												
HF	74	HFG		Med-Coarse	53	64										
HF	75	Bg														
HF	76	HFG		Med-Coarse												
HF	77	HFG		Med-Coarse												
HF	78	HFG		Med-Coarse	255	46										
HF	79	HFG		Med-Coarse												
HF	80	Bg	qtz,bt	Medium												
HF	81	Qv														
HF	82	ISG		Medium												
HF	83	Sch	sil	Med-Coarse					215	63						
HF	84	Sch	sil	Med-Coarse			247	45								
HF	85	Sch	sil	Med-Coarse							211	66	150	SW		
HF	85	Sch	sil	Med-Coarse					215	40						
HF	85	Sch	sil	Med-Coarse	188	52										
HF	86	ISG		Med-Coarse	144	72										
HF	87	ISG		Med-Coarse	69	67										
HF	88	HFG		Med-Coarse	55	57										
HF	89	ISG		Medium												
HF	90	HFG		Med-Coarse	186	54										
HF	91	HFG		Med-Coarse												
HF	92	Sch		Med-Coarse	341	34										
HF	93	HFG		Med-Coarse	178	76										
HF	94	HFG		Med-Coarse	32	72										
HF	95	HFG		Med-Coarse	198	76										
HF	96	HFG		Med-Coarse	170	41										
HF	97	Peg	ms	Coarse												
HF	98	HFG		Med-Coarse	193	61										
HF	99	HFG		Med-Coarse	36	65										
HF	100	HFG		Med-Coarse	171	55										
HF	101	HFG		Med-Coarse												
HF	102	HFG		Med-Coarse	24	64										
HF	103	HFG		Med-Coarse	76	65										
HF	104	HFG		Med-Coarse	79	56										
HF	105	HFG		Med-Coarse	76	63										
HF	106	HFG		Med-Coarse	44	82										
HF	107	HFG		Med-Coarse	78	59										
HF	108	HFG		Med-Coarse	77	67										
HF	109	HFG		Med-Coarse	210	67										
HF	110	HFG		Med-Coarse	4	70										
HF	111	ISG		Medium	183	82										
HF	112	ISG		Medium	176	74										
HF	113	ISG		Medium	8	76										
HF	114	Bg		Med-Coarse	122	24										
HF	115	Bg		Medium												
HF	116	Bg		Medium												
HF	117	Bg		Med-Coarse	21	66										
HF	118	Bg		Medium												
HF	119	Bg		Coarse												
HF	120	Bg		Med-Coarse	65	62										
HF	121	Sch		Med-Coarse	213	38										
HF	122	Sch		Medium	60	78										
HF	123	Sch		Medium	82	69										
HF	124	Sch		Medium	76	76										
HF	125	Sch		Medium	72	64										
HF	126	Sch		Medium	96	63										
HF	127	Bg		Med-Coarse												
HF	128	Sch		Medium												
HF	129	Sch		Medium												
HF	130	Sch		Medium	55	68										
HF	131	Sch		Medium												
HF	132	Sch		Medium												
HF	133	Bg		Medium												
HF	134	Bg		Medium												
HF	135	Sch		Med-Coarse	171	33										

HF	136	Sch		Med-Coarse	69	45										
HF	137	Sch		Med-Coarse							252	75	155	SW		
HF	137	Sch		Med-Coarse					250	46						
HF	138	Sch		Med-Coarse	86	70										
HF	139	Sch		Med-Coarse	75	58										
HF	140	ISG		Medium	193	81										
HF	141	Sch		Medium												
HF	142	Bg		Med-Coarse												
HF	143	Bg	ms,bt	Med-Coarse												
HF	144	Bg	ms,bt	Med-Coarse												
HF	145	Bg	bt,ms	Med-Coarse												
HF	146	Bg	ms,bt	Medium	260	70										
HF	147	Bg	bt,ms	Medium												
HF	148	Bg		Coarse												
HF	149	Bg	bt,ms	Medium	231	66										
HF	150	Sch		Medium	92	64										
HF	151	Sch		Medium	246	76										
HF	152	Sch		Med-Coarse												
HF	153	Sch		Medium												
HF	154	Qv		Medium												
HF	155	Sch		Med-Coarse												
HF	156	Sch		Med-Coarse												
HF	157	Sch		Med-Coarse												
HF	158	Bg		Med-Fine	48	66										
HF	159	Sch		Med-Coarse												
HF	160	Bg	bt,ms	Medium	60	64										
HF	161	Bg	bt	Med-Coarse	120	28										
HF	161	Bg	bt	Med-Coarse			238	14								
HF	162	Bg	bt	Med-Coarse							170	65	160	NE		
HF	162	Bg	bt	Med-Coarse					268	54						
HF	162	Bg	bt	Med-Coarse	169	12										
HF	163	Bg	bt	Med-Coarse	131	32										
HF	164	Bg	bt,qtz	Med-Coarse	170	30										
HF	164	Bg	bt,qtz	Med-Coarse			230	28								
HF	165	Bg	bt,qtz	Med-Coarse							85	65	160	NW		
HF	165	Bg	bt,qtz	Med-Coarse					125	45						
HF	166	Bg	bt,qtz	Med-Coarse	136	38										
HF	167	Bg	bt,qtz	Med-Coarse	195	26										
HF	168	Bg	bt,qtz	Med-Coarse	220	30										
HF	169	Bg	bt,qtz	Med-Coarse	215	32										
HF	170	Go		Med-Coarse	54	66										
HF	171	Go		Med-Coarse	122	64										
HF	172	Sch		Med-Coarse	103	58										
HF	173	Sch		Med-Coarse	99	59										
HF	174	Sch		Med-Coarse	112	32										
HF	175	C-Sil		Med-Fine												
HF	176	Sch		Med-Coarse	114	46										
HF	177	HFG		Med-Coarse	255	67										
HF	178	HFG		Med-Coarse	48	64										
HF	179	HFG		Med-Coarse	54	49										
HF	180	HFG		Med-Coarse	18	62										
HF	181	HFG		Med-Coarse	175	52										
HF	182	HFG		Med-Coarse	185	62										
HF	183	Bg		Medium	176	56										
HF	184	Bg		Medium	333	32										
HF	184	Bg		Medium	238	72										
HF	184	Bg		Medium	195	74										
HF	185	Sch		Med-Coarse	149	53										
HF	186	Sch		Med-Coarse	108	67										
HF	187	Sch		Med-Coarse	192	42										
HF	188	ISG		Medium	184	33										
HF	188	ISG		Medium	204	32										
HF	189	Si-C		Med-Coarse	227	44										
HF	190	Si-C		Med-Coarse			6	30								
HF	191	Bg		Medium												
HF	192	ISG		Med-Coarse	85	79										
HF	193	ISG		Med-Coarse	180	65										
HF	194	Bg		Medium	243	61										
HF	195	Bg	bt	Med-Coarse	196	64										
HF	196	Qv		Medium	231	42										
HF	197	ISG		Medium	218	42										
HF	198	Qv			210	28										
HF	199	HFG		Med-Coarse												
HF	200	HFG		Med-Coarse												
HF	201	HFG		Med-Coarse	185	57										
HF	202	ISG		Medium	35	50										

HF	203	HFG		Med-Coarse	214	21										
HF	204	HFG		Med-Coarse												
HF	205	Bg		Medium												
HF	206	ISG		Medium												
HF	207	ISG		Medium												
HF	208	ISG		Medium												
HF	209	Bg		Medium												
HF	210	Sch		Med-Coarse												
HF	211	Sch		Med-Coarse												
HF	212	Sch		Med-Coarse												
HF	213	Sch		Med-Coarse												
HF	214	Sch		Medium												
HF	215	Bg		Medium												
HF	216	Sch		Medium												
HF	217	Bg	bt,ms	Med-Coarse	50	54										
HF	218	Bg		Med-Coarse												
HF	219	Bg		Med-Coarse	51	38										
HF	220	Bg		Medium												
HF	221	Bg		Medium												
HF	222	Bg		Medium	115	74										
HF	223	Bg		Medium												
HF	224	Bg	bt,ms	Med-Coarse												
HF	225	Peg		Coarse												
HF	226	Bg		Med-Coarse												
HF	227	Bg	bt,ms	Med-Coarse	74	46										
HF	228	ISG		Medium	100	71										
HF	229	Bg		Med-Coarse												
HF	230	Bg	bt,ms	Med-Coarse	81	65										
HF	231	Bg	bt,ms	Med-Coarse												
HF	232	Bg	ms	Med-Coarse												
HF	233	Sch		Med-Coarse	219	86										
HF	234	Bg		Medium												
HF	235	Bg	ms	Med-Coarse												
HF	236	Bg	ms,bt	Med-Coarse												
HF	237	Bg			65	71										
HF	238	ISG		Medium	53	72										
HF	239	ISG		Medium	64	81										
HF	240	ISG		Medium	218	60										
HF	241	Bg	bt,ms	Coarse	36	78										
HF	242	ISG		Medium	129	71										
HF	243	ISG		Medium	48	75										
HF	244	ISG		Medium	203	84										
HF	245	ISG		Medium	293	58										
HF	246	ISG		Medium	224	70										
HF	247	Bg	bt,ms	Medium	233	72										
HF	248	Bg	bt,ms	Medium												
HF	249	HFG	bt	Med-Coarse	266	71										
HF	250	HFG	bt,ms	Medium	54	56										
HF	251	HFG	bt	Medium	239	58										
HF	252	HFG	bt	Med-Coarse												
HF	253	ISG	bt	Med-Coarse												
HF	254	HFG	bt	Medium	221	47										
HF	255	Bg	bt	Medium												
HF	256	Qv			330	80										
HF	257	HFG	bt	Medium	154	44										
HF	257	HFG	bt	Medium			240	38								
HF	258	HFG	bt	Medium												
HF	259	HFG	bt	Med-Coarse	75	59										
HF	260	HFG	bt	Med-Coarse												
HF	261	HFG	bt	Med-Coarse	257	72										
HF	262	Bg	bt,ms	Medium	120	38										
HF	263	HFG	bt	Medium												
HF	264	Bg	ms,bt	Medium	74	40										
HF	265	HFG	bt	Medium												
HF	266	HFG		Med-Coarse	131	74										
HF	267	Si-C														
HF	268	Si-C														
HF	269	Si-C														
HF	270	Si-C														
HF	271	Si-C														
HF	272	Si-C														
HF	273	Si-C														
HF	274	Si-C														
HF	275	Si-C	py													
HF	276	Si-C														
HF	277	Si-C														

HF	278	Si-C														
HF	279	Si-C														
HF	280	Si-C														
HF	281	Si-C														
HF	282	Si-C														
HF	283	Si-C														
HF	284	Si-C														
HF	285	Si-C														
HF	286	Si-C														
HF	287	Si-C														
HF	288	Si-C														
HF	289	Si-C														
HF	290	Si-C														
HF	291	ISG		Medium												
HF	292	HFG		Med-Coarse	19	65										
HF	293	ISG		Medium												
HF	294	HFG		Med-Coarse												
HF	295	HFG		Med-Coarse	168	38										
HF	296	HFG		Med-Coarse	189	26										
HF	296	HFG		Med-Coarse			255	16								
HF	297	HFG		Med-Coarse	154	28										
HF	298	HFG		Med-Coarse	180	24										
HF	299	ISG		Medium	54	61										
HF	300	HFG		Med-Coarse	150	65										
HF	300	HFG		Med-Coarse	164	74										
HF	301	HFG		Med-Coarse	180	61										
HF	302	HFG		Med-Coarse	215	44										
HF	303	HFG		Med-Coarse	190	49										
HF	304	HFG		Med-Coarse												
HF	305	HFG		Med-Coarse												
HF	306	HFG		Med-Coarse												
HF	307	HFG		Med-Coarse	26	46										
HF	308	HFG		Med-Coarse	173	47										
HF	309	HFG		Med-Coarse	225	76										
HF	310	HFG		Med-Coarse	208	59										
HF	311	Sch		Med-Coarse												
HF	312	Bg		Medium												
HF	313	HFG		Med-Coarse	157	54										
HF	314	HFG		Med-Coarse	219	59										
HF	315	HFG														
HF	316	HFG		Med-Coarse												
HF	317	HFG		Med-Coarse												
HF	318	HFG		Med-Coarse												
HF	319	HFG		Med-Coarse	126	60										
HF	320	HFG		Med-Coarse												
HF	321	HFG		Med-Coarse	32	69										
HF	322	HFG		Med-Coarse	290	67										
HF	323	Si-C														
HF	324	HFG		Med-Coarse												
HF	325	HFG		Med-Coarse	89	59										
HF	326	HFG		Med-Coarse												
HF	327	HFG		Med-Coarse	44	50										
HF	327	HFG		Med-Coarse			170	27								
HF	328	Si-C		Coarse												
HF	329	HFG		Med-Coarse												
HF	330	Qv		Med-Coarse	239	53										
HF	331	Yw														
HF	332	Bg		Medium												
HF	333	Bg		Med-Coarse	289	52										
HF	333	Bg		Med-Coarse			348	61								
HF	334	Bg														
HF	335	Bg		Med-Coarse												
HF	336	Bg		Med-Coarse												
HF	337	Bg		Med-Coarse												
HF	338	Bg		Coarse	229	36										
HF	339	Bg		Med-Coarse												
HF	340	Bg		Med-Coarse												
HF	341	Qv		Fine												
HF	342	Bg		Med-Coarse												
HF	343	Bg		Med-Coarse												
HF	344	C-Sil		Fine												
HF	345	Qv		Med-Coarse												
HF	346	Si-C		Fine												
HF	347	HFG		Med-Coarse												
HF	348	Qv		Fine												
HF	349	Qv		Fine												

HF	350	Sch		Med-Coarse												
HF	351	Yw	qtz	Med-Fine												
HF	352	Si-C		Med-Coarse												
HF	353	HFG	plg	Fine												
HF	354	HFG	plg	Fine												
HF	355	Si-C		Medium												
HF	356	Qv		Fine												
HF	357	Si-C		Med-Fine												
HF	358	Qv		Medium												
HF	359	HFG		Med-Fine	216	33										
HF	360	HFG		Med-Coarse	72	27										
HF	361	ISG		Med-Fine												
HF	362	ISG	ms,grt	Fine												
HF	363	HFG		Med-Coarse	152	64										
HF	364	HFG		Med-Coarse	233	56										
HF	365	HFG		Med-Coarse	204	60										
HF	366	HFG		Med-Coarse	172	54										
HF	367	HFG		Med-Coarse	148	58										
HF	368	HFG		Med-Coarse	186	55										
HF	369	Peg		Coarse	268	72										
HF	370	HFG		Med-Coarse	172	59										
HF	370	HFG		Med-Coarse	148	69										
HF	371	ISG		Med-Coarse	182	61										
HF	372	HFG		Med-Coarse	54	59										
HF	373	ISG		Medium	173	68										
HF	374	ISG		Medium												
HF	375	HFG		Med-Coarse	58	68										
HF	376	HFG		Med-Coarse	86	81										
HF	376	HFG		Med-Coarse	79	70										
HF	377	HFG		Med-Coarse												
HF	378	Qv		Medium												
HF	379	HFG		Med-Coarse	224	65										
HF	380	HFG		Med-Coarse	244	73										
HF	381	HFG		Med-Coarse	271	74										
HF	382	HFG		Med-Coarse	291	72										
HF	383	HFG		Med-Coarse	99	64										
HF	384	HFG		Med-Coarse	277	64										
HF	385	HFG		Med-Coarse	274	65										
HF	386	Qv		Medium												
HF	387	HFG		Med-Coarse												
HF	388	HFG		Med-Coarse												
HF	389	HFG		Med-Coarse	229	75										
HF	390	HFG		Med-Coarse	240	73										
HF	391	HFG		Med-Coarse												
HF	392	HFG		Med-Coarse	241	71										
HF	393	HFG		Med-Coarse	220	71										
HF	394	HFG		Med-Coarse	196	67										
HF	395	HFG		Med-Coarse	270	50										
HF	396	HFG		Med-Coarse	244	54										
HF	397	HFG		Med-Coarse	231	66										
HF	398	HFG		Medium	241	56										
HF	399	Qv		Fine	242	30										
HF	400	HFG		Med-Coarse	242	55										
HF	401	HFG		Med-Coarse	267	67										
HF	402	HFG		Med-Coarse	136	62										
HF	403	Sch	sil	Med-Coarse	261	48										
HF	403	Sch	sil	Med-Coarse			275	38								
HF	404	Si-C		Fine												
HF	405	Si-C		Fine												
HF	406	Si-C		Fine												
HF	407	Sch	grt	Medium	210	27										
HF	408	Sch		Med-Fine												
HF	409	Qv		Coarse												
HF	410	HFG		Med-Coarse												
HF	411	HFG		Med-Coarse	206	62										
HF	411	HFG		Med-Coarse			250	34								
HF	412	HFG		Med-Coarse	206	27										
HF	412	HFG		Med-Coarse			331	18								
HF	413	HFG		Med-Coarse	174	33										
HF	414	HFG		Med-Coarse	229	49										
HF	415	HFG		Med-Coarse												
HF	416	HFG		Med-Coarse	144	81										
HF	417	ISG		Medium	68	73										
HF	418	HFG			129	79										
HF	419	HFG		Med-Coarse												
HF	420	HFG		Med-Coarse												

HF	421	Bg		Med-Fine	14	76										
HF	422	Sch		Medium	94	84										
HF	423	Sch		Medium							122	78	140	NE		
HF	423	Sch		Medium					296	51						
HF	423	Sch		Medium	157	75										
HF	424	Sch		Medium	214	59										
HF	425	Sch		Medium	55	76										
HF	426	Sch		Medium	40	79										
HF	427	Sch		Medium	35	85										
HF	428	Sch	sil	Medium	222	86										
HF	429	Sch		Medium	210	80										
HF	430	Sch	sil	Medium	223	84										
HF	431	Sch	sil	Medium	211	79										
HF	432	Sch	sil	Medium	61	67										
HF	433	Sch		Medium	296	80										
HF	434	Sch		Medium	58	62										
HF	434	Sch		Medium			89	33								
HF	435	Sch	sil	Medium	169	69										
HF	436	Sch		Medium	110	63										
HF	437	Sch	sil,bt	Medium	165	65										
HF	438	Sch		Medium	87	58										
HF	439	Sch		Medium	29	64										
HF	440	Sch	sil	Medium	254	74										
HF	441	Sch		Medium												
HF	442	ISG		Med-Fine	44	70										
HF	442	ISG		Med-Fine	86	44										
HF	443	HFG		Med-Coarse												
HF	444	Sch		Medium	124	35										
HF	444	Sch		Medium			178	43								
HF	445	Bg		Medium	35	34										
HF	446	Sch	sil	Medium	232	34										
HF	446	Sch	sil	Medium	247	37										
HF	447	Sch	sil	Med-Fine												
HF	448	Bg		Medium	138	66										
HF	449	ISG		Medium	84	70										
HF	450	ISG		Medium	224	75										
HF	451	HFG		Med-Coarse	34	66										
HF	452	ISG	ms,bt	Medium												
HF	453	ISG		Medium												
HF	454	Sch		Medium												
HF	455	ISG		Med-Fine												
HF	456	HFG		Med-Coarse												
HF	457	HFG		Med-Coarse												
HF	458	Sch	bt,grt	Medium												
HF	459	Sch	bt,grt	Medium	29	54										
HF	460	Sch	bt,grt	Medium												
HF	461	Sch	bt,grt	Medium	16	43										
HF	462	Sch	bt,grt	Medium	332	49										
HF	462	Sch	bt,grt	Medium			208	32								
HF	463	HFG		Med-Coarse												
HF	464	Dd		Med-Fine												
HF	465	Dd		Med-Fine												
HF	466	Bg		Medium												
HF	467	Bg	bt	Med-Fine												
HF	468	ISG		Medium												
HF	469	Go		Med-Coarse												
HF	470	Dd		Med-Fine												
HF	471	Go		Med-Coarse	247	37										
HF	472	Amp		Med-Fine												
HF	473	Go		Med-Coarse	144	32										
HF	474	Amp		Med-Fine												
HF	475	Bg	bt	Medium	108	29										
HF	476	HFG		Med-Coarse	155	26										
HF	477	Sch	grt,sil	Med-Fine												
HF	478	ISG		Med-Fine	64	37										
HF	478	ISG		Med-Fine			166	28								
HF	479	ISG		Medium	226	68										
HF	480	HFG		Med-Coarse												
HF	481	Sch		Med-Fine	76	68										
HF	481	Sch		Med-Fine			242	32								
HF	482	Sch		Med-Fine												
HF	483	Bg		Med-Fine												
HF	484	ISG	ms	Medium												
HF	485	Bg		Medium												
HF	486	HFG		Med-Coarse	25	67										
HF	487	HFG		Med-Coarse	238	57										

HF	488	ISG		Medium	203	40										
HF	489	ISG		Medium												
HF	490	Sch		Med-Coarse												
HF	491	Sch		Medium												
HF	492	ISG		Medium												
HF	493	Sch		Medium												
HF	494	Sch		Medium							100	84	145	NE		
HF	494	Sch		Medium					104	68						
HF	494	Sch		Medium	84	76										
HF	495	HFG		Med-Coarse												
HF	496	C-Sil		Med-Fine												
HF	497	Sch		Medium												
HF	498	Sch		Medium												
HF	499	Sch		Medium												
HF	500	Sch		Medium												
HF	501	Sch		Medium												
HF	502	Sch		Medium												
HF	503	Sch		Medium												
HF	504	Sch		Medium												
HF	505	Sch		Medium												
HF	506	Sch		Medium												
HF	507	ISG		Medium	248	64										
HF	508	Sch		Medium												
HF	509	HFG		Med-Coarse	225	66										
HF	510	ISG		Medium	190	75										
HF	511	Sch		Medium	131	24										
HF	512	Sch		Medium	87	64										
HF	513	Sch		Medium	212	57										
HF	513	Sch		Medium			271	37								
HF	514	Sch		Medium	147	31										
HF	514	Sch		Medium			243	15								
HF	515	Sch		Medium	246	86										
HF	516	Sch		Medium	147	34										
HF	516	Sch		Medium			264	27								
HF	517	Sch		Medium	61	35										
HF	518	Bg		Medium	282	12										
HF	519	ISG		Medium												
HF	520	Bg	bt	Medium												
HF	521	HFG		Med-Coarse	114	59										
HF	522	HFG	grt,sil	Med-Coarse	140	59										
HF	522	HFG	grt,sil	Med-Coarse			261	26								
HF	523	HFG		Med-Coarse	243	34										
HF	523	HFG		Med-Coarse			84	22								
HF	524	HFG		Med-Coarse	46	51										
HF	525	HFG		Med-Coarse												
HF	526	HFG		Med-Coarse	298	76										
HF	527	Bg		Medium												
HF	528	HFG		Med-Coarse												
HF	529	HFG		Medium												
HF	530	HFG		Medium												
HF	531	HFG		Med-Coarse												
HF	532	HFG		Med-Coarse	91	64										
HF	533	HFG		Medium												
HF	534	HFG		Med-Coarse												
HF	535	HFG		Med-Coarse	86	65										
HF	536	HFG		Medium												
HF	537	HFG		Medium												
HF	538	HFG		Medium	264	57										
HF	539	Sch		Medium												
HF	540	HFG		Med-Coarse	35	56										
HF	541	Sch		Medium												
HF	542	Sch		Medium												
HF	543	Sch		Medium	182	67										
HF	543	Sch		Medium			302	51								
HF	544	Sch		Medium	195	63										
HF	545	Sch	qtz	Medium												
HF	546	Sch		Medium												
HF	547	Bg	bt,ms	Medium												
HF	548	Bg	bt,ms	Medium												
HF	549	Bg	bt,ms	Medium												
HF	550	Sch		Medium												
HF	551	Bg	ms	Medium												
HF	552	Bg	ms	Medium												
HF	553	Bg		Medium												
HF	554	Bg		Medium												
HF	555	Bg		Medium												

HF	556	Bg		Medium												
HF	557	Sch		Medium	218	60										
HF	557	Sch		Medium			287	51								
HF	558	HFG		Med-Coarse												
HF	559	HFG		Med-Coarse												
HF	560	HFG		Med-Coarse	197	68										
HF	561	HFG		Med-Coarse	191	70										
HF	562	ISG		Medium	219	76										
HF	563	HFG		Med-Coarse												
HF	564	HFG		Med-Coarse	211	71										
HF	565	HFG	grt	Med-Coarse	216	80										
HF	565	HFG	grt	Med-Coarse	190	80										
HF	566	Sch		Medium	237	53										
HF	566	Sch		Medium			35	32								
HF	567	HFG		Med-Coarse	340	61										
HF	568	HFG		Med-Coarse												
HF	569	Sch		Medium	201	71										
HF	570	HFG		Med-Coarse												
HF	571	HFG		Med-Coarse												
HF	572	HFG		Med-Coarse	140	60										
HF	573	ISG		Medium	160	68										
HF	574	HFG		Med-Coarse												
HF	575	HFG		Med-Coarse	253	72										
HF	576	HFG		Med-Coarse	330	64										
HF	577	HFG		Med-Coarse	167	67										
HF	578	Sch		Medium	77	46										
HF	578	Sch		Medium			278	42								
HF	579	Sch		Medium												
HF	580	ISG		Medium	92	59										
HF	581	Sch		Medium												
HF	582	Sch		Medium												
HF	583	HFG		Med-Coarse												
HF	584	Sch		Medium	41	72										
HF	585	Sch		Medium	234	73										
HF	586	Sch		Medium												
HF	587	Sch		Medium	38	68										
HF	588	Sch														
HF	589	Sch		Medium	212	63										
HF	590	Sch		Medium												
HF	591	Sch	sil	Medium												
HF	592	HFG		Med-Coarse												
HF	593	HFG		Med-Coarse	203	50										
HF	594	Sch	sil	Medium	103	34										
HF	594	Sch	sil	Medium			37	24								
HF	595	Sch		Medium	29	66										
HF	596	gd		Medium												
HF	597	Bg	grt	Medium												
HF	598	Bg									104	70	140	NE		
HF	598	Bg							92	64						
HF	599	HFG		Med-Coarse	238	43										
HF	600	Bg		Medium												
HF	601	HFG		Med-Coarse												
HF	602	HFG		Med-Coarse	222	69										
HF	603	Bg		Medium												
HF	604	ISG		Medium												
HF	605	Bg		Medium												
HF	606	Bg		Medium												
HF	607	ISG		Medium												
HF	608	HFG		Med-Coarse												
HF	609	Bg		Medium												
HF	610	ISG		Medium												
HF	611	Bg		Medium												
HF	612	Bg		Medium												
HF	613	Bg		Medium												
HF	614	Sch		Medium	66	79										
HF	615	Sch		Medium												
HF	616	HFG		Med-Coarse	137	38										
HF	617	Sch		Medium	64	46										
HF	618	Sch		Medium												
HF	619	Sch		Medium												
HF	620	Sch		Medium	122	34										
HF	621	Sch		Medium	103	59										
HF	621	Sch		Medium			200	36								
HF	622	Sch	sil	Medium	53	65										
HF	623	Sch	sil	Medium							104	66	30	NE		
HF	623	Sch	sil	Medium					276	63						

HF	624	Sch	sil	Medium	104	73										
HF	624	Sch	sil	Medium	344	0										
HF	625	Sch	sil	Medium	79	66										
HF	626	Sch	sil	Medium	54	84										
HF	627	Sch		Medium												
HF	628	Sch	sil	Medium												
HF	629	Sch	sil	Medium	266	88										
HF	630	Sch		Medium												
HF	631	Bg	ms	Medium												
HF	632	Bg	ms,bt	Medium	202	72										
HF	633	Bg	ms,sil	Medium												
HF	634	Bg	ms,sil	Medium												
HF	635	ISG		Medium												
HF	636	HFG		Med-Coarse												
HF	637	HFG		Med-Coarse												
HF	638	HFG		Med-Coarse												
HF	639	Bg	ms,sil	Medium	149	73										
HF	640	Bg	ms,sil	Medium												
HF	641	ISG		Medium												
HF	642	ISG		Medium	63	75										
HF	643	HFG		Med-Coarse	157	60										
HF	643	HFG		Med-Coarse	286	51										
HF	643	HFG		Med-Coarse			311	24								
HF	644	Si-C		Medium	200	67										
HF	645	Si-C		Med-Fine	239	71										
HF	646	HFG		Med-Coarse												
HF	647	Bg		Med-Coarse												
HF	648	HFG		Med-Coarse	247	65										
HF	649	HFG		Med-Coarse	324	63										
HF	650	HFG		Med-Coarse												
HF	651	Sch		Medium												
HF	652	Sch		Medium												
HF	653	HFG		Med-Coarse	234	75										
HF	654	Sch		Medium												
HF	655	Sch		Medium	175	66										
HF	656	Sch		Medium												
HF	657	HFG		Med-Coarse												
HF	658	HFG		Med-Coarse	56	72										
HF	659	HFG		Med-Coarse												
HF	660	HFG		Med-Coarse												
HF	661	HFG		Med-Coarse	212	55										
HF	662	HFG		Med-Coarse	130	67										
HF	663	Sch	sil	Medium	226	45										
HF	664	Sch		Medium												
HF	665	Sch		Medium												
HF	666	Sch		Medium												
HF	667	Sch		Medium												
HF	668	HFG		Med-Coarse												
HF	669	Sch		Medium	72	61										
HF	670	Sch		Medium												
HF	671	HFG		Medium	126	41										
HF	672	Sch		Medium												
HF	673	HFG		Med-Coarse	51	78										
HF	674	HFG		Med-Coarse	216	65										
HF	675	Si-C		Fine												
HF	676	Si-C		Medium	346	70										
HF	677	Si-C														
HF	678	Si-C		Med-Coarse	16	64										
HF	679	Si-C		Med-Fine	233	73										
HF	680	Si-C		Fine	16	88										
HF	681	Si-C		Fine	326	47										
HF	681	Si-C		Fine			49	23								
HF	682	Si-C		Med-Fine	234	77										
HF	683	Si-C		Med-Fine	276	54										
HF	684	HFG		Med-Coarse	79	69										
HF	685	Sch		Medium												
HF	686	HFG		Med-Coarse												
HF	687	HFG		Med-Coarse												
HF	688	Bg		Coarse												
HF	689	HFG		Med-Coarse	200	51										
HF	690	HFG		Med-Coarse	223	58										
HF	691	HFG		Med-Coarse												
HF	692	HFG		Med-Coarse	206	75										
HF	693	HFG		Med-Coarse	25	68										
HF	694	HFG		Med-Coarse	217	80										
HF	695	HFG		Med-Coarse	40	66										

HF	696	HFG		Med-Coarse	47	81										
HF	697	HFG		Med-Coarse	28	77										
HF	698	HFG														
HF	699	HFG		Med-Coarse												
HF	700	HFG		Med-Coarse												
HF	701	HFG		Med-Coarse	216	77										
HF	702	HFG		Med-Coarse	204	84										
HF	703	HFG		Med-Coarse												
HF	704	HFG		Med-Coarse	54	68										
HF	705	HFG		Med-Coarse	216	84										
HF	706	HFG		Med-Coarse	217	70										
HF	707	HFG		Med-Coarse	343	71										
HF	708	HFG		Med-Coarse	47	67										
HF	709	HFG		Med-Coarse	150	76										
HF	710	HFG		Med-Coarse	142	64										
HF	711	HFG		Med-Coarse												
HF	712	HFG		Med-Coarse	189	80										
HF	713	HFG		Med-Coarse	216	64										
HF	714	HFG		Med-Coarse	202	76										
HF	715	HFG		Med-Coarse	34	72										
HF	716	HFG		Med-Coarse												
HF	717	HFG		Med-Coarse	204	77										
HF	718	HFG		Med-Coarse	194	74										
HF	719	HFG		Med-Coarse	4	78										
HF	720	HFG		Med-Coarse	99	66										
HF	721	HFG		Med-Coarse												
HF	722	HFG		Med-Coarse												
HF	723	Si-C		Fine												
HF	724	HFG		Med-Coarse	246	83										
HF	725	Sch		Medium												
HF	726	HFG		Med-Coarse												
HF	727	HFG		Med-Coarse	86	69										
HF	728	HFG		Med-Coarse	141	63										
HF	729	Bg	bt,ms	Medium												
HF	730	Bg		Medium												
HF	731	Bg		Medium												
HF	732	Bg	ms	Medium												
HF	733	Bg	bt,ms	Medium												
HF	734	HFG		Med-Coarse												
HF	735	HFG		Med-Coarse												
HF	736	Sch		Medium												
HF	737	HFG		Med-Coarse												
HF	738	HFG		Med-Coarse												
HF	739	HFG		Med-Coarse	14	69										
HF	740	HFG		Med-Coarse												
HF	741	Sch		Medium												
HF	742	Bg		Med-Coarse												
HF	743	HFG		Med-Coarse	219	78										
HF	744	Bg	ms	Med-Coarse												
HF	745	Bg	ms,sil	Medium												
HF	746	Bg	ms,sil	Medium	9	70										
HF	747	Sch	sil	Medium	187	67										
HF	748	ISG		Medium	279	69										
HF	749	Bg	ms,sil	Medium												
HF	750	Sch	sil	Medium												
HF	751	HFG		Med-Coarse	164	69										
HF	752	Bg	ms,bt	Medium												
HF	753	Sch	sil	Medium												
HF	754	Sch	sil	Medium	138	39										
HF	754	Sch	sil	Medium			250	38								
HF	755	Sch	sil	Medium	133	72										
HF	756	Sch	sil	Medium	67	69										
HF	757	HFG		Med-Coarse	246	80										
HF	758	Sch	sil	Medium												
HF	759	Sch	sil	Medium	171	43										
HF	759	Sch	sil	Medium			225	24								
HF	760	Sch	sil	Medium	130	34										
HF	760	Sch	sil	Medium			265	14								
HF	761	Sch	sil	Medium												
HF	762	Sch	sil	Medium	181	33										
HF	763	Sch	qtz	Medium	156	21										
HF	764	HFG		Med-Coarse	134	68										
HF	765	HFG		Med-Coarse	262	57										
HF	766	HFG		Med-Coarse	294	62										
HF	767	HFG		Med-Coarse	251	68										
HF	768	HFG		Med-Coarse												

HF	769	HFG		Med-Coarse	186	69										
HF	770	HFG		Med-Coarse												
HF	771	HFG		Med-Coarse	176	65										
HF	772	ISG		Medium												
HF	773	Bg		Medium												
HF	774	HFG		Med-Coarse												
HF	775	Bg		Medium												
HF	776	Bg		Medium												
HF	777	Bg		Medium	1	64										
HF	778	Bg	ms	Medium												
HF	779	Sch		Medium												
HF	780	Sch		Medium												
HF	781	Sch	qtz	Medium												
HF	782	Sch	qtz	Medium												
HF	783	Sch	qtz	Medium												
HF	784	Sch	qtz	Medium												
HF	785	Bg		Med-Coarse												
HF	786	Amp		Med-Fine												
HF	787	Bg		Medium	48	52										
HF	788	Bg		Medium												
HF	789	Bg		Medium												
HF	790	Bg		Medium												
HF	791	Bg		Medium	169	72										
HF	792	Bg		Medium												
HF	793	Amp		Med-Fine												
HF	794	Bg		Medium												
HF	795	Bg		Medium												
HF	796	Bg		Medium	219	50										
HF	797	HFG		Med-Coarse												
HF	798	HFG		Med-Coarse	178	71										
HF	799	HFG		Med-Coarse	225	75										
HF	800	HFG		Med-Coarse												
HF	801	Sch	sil	Medium												
HF	802	HFG		Med-Coarse												
HF	803	HFG		Med-Coarse	49	68										
HF	804	HFG		Med-Coarse	34	59										
HF	805	HFG		Med-Coarse												
HF	806	HFG		Med-Coarse												
HF	807	HFG		Med-Coarse												
HF	808	Sch		Medium	202	55										
HF	809	HFG		Med-Coarse												
HF	810	HFG		Med-Coarse												
HF	811	HFG		Med-Coarse	54	55										
HF	812	HFG		Med-Coarse	40	62										
HF	813	HFG		Med-Coarse	65	50										
HF	814	HFG		Med-Coarse	52	54										
HF	815	Bg		Medium												
HF	816	HFG		Med-Coarse												
HF	817	HFG		Med-Coarse	179	63										
HF	818	HFG		Med-Coarse												
HF	819	HFG		Med-Coarse	73	68										
HF	820	Bg	ms,bt	Medium												
HF	821	HFG		Med-Coarse												
HF	822	Bg		Medium												
HF	823	HFG		Med-Coarse	119	51										
HF	824	HFG		Med-Coarse	145	55										
HF	825	HFG		Med-Coarse	217	50										
HF	826	HFG		Med-Coarse												
HF	827	HFG		Med-Coarse												
HF	828	HFG		Med-Coarse												
HF	829	HFG		Med-Coarse	146	60										
HF	830	HFG		Med-Coarse												
HF	831	HFG		Med-Coarse												
HF	832	ISG		Medium												
HF	833	HFG		Med-Coarse												
HF	834	HFG		Med-Coarse	149	68										
HF	835	HFG		Med-Coarse	120	73										
HF	836	Bg		Medium												
HF	837	HFG		Med-Coarse												
HF	838	HFG		Med-Coarse												
HF	839	HFG		Med-Coarse	43	71										
HF	840	HFG		Med-Coarse												
HF	841	HFG		Med-Coarse												
HF	842	HFG		Med-Coarse												
HF	843	HFG		Med-Coarse												
HF	844	HFG		Med-Coarse												

HF	845	HFG		Med-Coarse												
HF	846	HFG		Med-Coarse												
HF	847	HFG		Med-Coarse												
HF	848	ISG		Medium												
HF	849	HFG		Med-Coarse												
HF	850	HFG		Med-Coarse												
HF	851	ISG		Medium												
HF	852	ISG		Medium												
HF	853	HFG		Med-Coarse												
HF	854	HFG		Med-Coarse												
HF	855	Go		Med-Coarse	218	43										
HF	856	HFG		Med-Coarse	113	34										
HF	857	HFG		Med-Coarse	86	32										
HF	858	HFG		Med-Coarse	75	60										
HF	859	HFG		Med-Coarse	248	81										
HF	860	HFG		Med-Coarse	235	26										
HF	861	HFG		Med-Coarse	248	79										
HF	862	HFG		Med-Coarse	297	78										
HF	863	HFG		Med-Coarse	277	77										
HF	864	HFG		Med-Coarse	215	51										
HF	865	HFG		Med-Coarse	234	47										
HF	866	HFG		Med-Coarse												
HF	867	HFG		Med-Coarse												
HF	868	HFG		Med-Coarse	46	70										
HF	869	HFG		Med-Coarse	42	56										
HF	870	HFG		Med-Coarse	231	70										
HF	871	HFG		Med-Coarse	346	69										
HF	872	Sch		Medium												
HF	873	HFG		Med-Coarse												
HF	874	HFG		Med-Coarse	146	53										
HF	875	HFG		Med-Coarse	174	65										
HF	876	HFG		Medium	217	62										
HF	877	HFG		Med-Coarse												
HF	878	HFG		Med-Coarse												
HF	879	Amp		Med-Fine												
HF	880	Sch	sil	Medium	183	31										
HF	880	Sch	sil	Medium			242	26								
HF	881	Bg		Med-Coarse	201	47										
HF	881	Bg		Med-Coarse			253	43								
HF	882	Sch		Medium	198	33										
HF	883	Bg		Medium	69	49										
HF	884	Amp		Med-Fine												
HF	885	Bg	bt	Med-Coarse	237	72										
HF	885	Bg	bt	Med-Coarse			253	25								
HF	886	Amp		Med-Fine												
HF	887	Bg	bt	Med-Coarse	62	52										
HF	888	Bg		Medium	49	76										
HF	889	Bg		Medium	70	65										
HF	890	gd		Med-Fine												
HF	891	Bg		Med-Coarse	197	44										
HF	892	Bg		Med-Coarse	200	43										
HF	893	Bg		Med-Coarse	196	37										
HF	894	HFG		Coarse	130	37										
HF	895	HFG		Med-Coarse	209	72										
HF	896	Sch		Medium												
HF	897	Sch		Medium												
HF	898	HFG		Med-Coarse												
HF	899	Sch		Medium												
HF	900	HFG		Med-Coarse												
HF	901	HFG		Med-Coarse												
HF	902	Sch	sil	Medium	81	69										
HF	903	HFG		Med-Coarse	255	71										
HF	904	HFG	bt	Med-Coarse	228	32										
HF	905	Sch		Medium	139	60										
HF	906	HFG		Med-Coarse												
HF	907	ISG		Medium												
HF	908	ISG		Medium	129	73										
HF	909	HFG		Med-Coarse												
HF	910	HFG		Med-Coarse												
HF	911	HFG		Med-Coarse	46	68										
HF	912	HFG		Med-Coarse												
HF	913	HFG		Med-Coarse												
HF	914	HFG		Med-Coarse												
HF	915	HFG		Med-Coarse	0	59										
HF	916	Sch		Medium												
HF	917	HFG		Med-Coarse	113	66										

HF	918	HFG		Med-Coarse												
HF	919	HFG		Med-Coarse												
HF	920	HFG		Med-Coarse												
HF	921	HFG		Med-Coarse												
HF	922	HFG		Med-Coarse												
HF	923	Sch		Medium	62	44										
HF	924	HFG		Med-Coarse	96	70										
HF	925	HFG		Med-Coarse	91	73										
HF	926	HFG		Med-Coarse	104	69										
HF	927	Sch	sil	Medium	62	75										
HF	928	HFG		Med-Coarse	45	44										
HF	929	HFG		Med-Coarse												
HF	930	Sch		Medium	54	29										
HF	931	Sch	sil	Medium	128	33										
HF	932	HFG		Med-Coarse	154	53										
HF	933	Sch		Medium	143	41										
HF	934	HFG		Med-Coarse	53	59										
HF	935	HFG		Med-Coarse												
HF	936	HFG		Med-Coarse												
HF	937	HFG														
HF	938	Sch		Medium												
HF	939	HFG		Med-Coarse												
HF	940	HFG		Med-Coarse												
HF	941	Sch		Medium												
HF	942	HFG		Med-Coarse												
HF	943	Sch		Medium												
HF	944	Bg		Medium												
HF	945	HFG		Med-Coarse												
HF	946	HFG		Med-Coarse	139	68										
HF	947	HFG		Med-Coarse												
HF	948	HFG		Med-Coarse												
HF	949	Bg		Medium	159	42										
HF	950	Bg		Medium	149	41										
HF	951	Bg		Med-Coarse	56	72										
HF	952	Bg		Med-Coarse							226	78	150	SW		
HF	952	Bg		Med-Coarse					228	66						
HF	953	Bg		Medium	81	81										
HF	954	Bg		Medium	76	75										
HF	955	Bg		Med-Coarse												
HF	956	Bg		Med-Coarse	230	76										
HF	957	Bg	bt	Medium												
HF	958	Bg	bt	Medium												
HF	959	Bg	bt	Med-Coarse	214	37										
HF	960	Sch		Medium												
HF	961	Bg	bt	Med-Coarse												
HF	962	Bg		Med-Coarse	205	24										
HF	963	Bg	bt	Medium												
HF	964	Bg	bt	Medium	128	31										
HF	965	Bg		Medium	149	23										
HF	966	Bg	bt	Medium												
HF	967	Bg		Medium												
HF	968	Bg	bt	Medium	43	66										
HF	969	Sch		Medium												
HF	970	Bg	bt	Medium	247	77										
HF	971	Bg		Medium												
HF	972	Bg	bt	Medium												
HF	973	Bg	bt	Med-Coarse												
HF	974	Bg	bt	Medium												
HF	975	Bg	bt	Med-Coarse	350	77										
HF	976	Bg	bt	Med-Coarse	64	77										
HF	977	Bg	bt	Med-Coarse	206	65										
HF	978	Go		Med-Coarse	227	32										
HF	979	Bg	bt	Med-Coarse	64	49										
HF	980	Bg		Med-Coarse	200	45										
HF	981	Bg	bt	Med-Coarse	198	23										
HF	982	Go		Med-Coarse	180	53										
HF	983	Bg		Medium	270	48										
HF	984	Go		Med-Coarse												
HF	985	Bg		Med-Coarse	208	24										
HF	986	Bg	bt	Med-Coarse	193	23										
HF	987	Bg	bt	Med-Coarse	189	33										
HF	988	Bg	bt	Med-Coarse	146	54										
HF	989	Go		Med-Coarse	230	72										
HF	990	Bg	bt	Medium												
HF	991	Sch	bt	Medium	139	48										
HF	992	Sch	sil	Medium	154	56										

HF	992	Sch	sil	Medium			239	45									
HF	993	Sch	bt	Medium	129	31											
HF	993	Sch	bt	Medium			242	22									
HF	994	Go		Med-Coarse	66	78											
HF	995	Sch		Medium	151	31											
HF	995	Sch		Medium			235	19									
HF	996	HFG	ms,bt	Med-Coarse													
HF	997	HFG	ms,bt	Med-Coarse													
HF	998	HFG	ms	Med-Coarse	116	29											
HF	999	Sch		Medium	114	35											
HF	999	Sch		Medium			206	23									
HF	1000	ISG	ms	Medium	179	31											
HF	1001	ISG	ms	Medium	183	36											
HF	1002	ISG	ms	Medium	188	50											
HF	1003	Sch		Medium													
HF	1004	ISG	ms	Medium	163	52											
HF	1005	HFG		Med-Coarse													
HF	1006	HFG		Med-Coarse													
HF	1007	HFG		Med-Coarse	153	32											
HF	1008	HFG		Med-Coarse													
HF	1009	HFG		Med-Coarse													
HF	1010	HFG		Med-Coarse													
HF	1011	HFG		Med-Coarse	80	47											
HF	1012	HFG		Med-Coarse													
HF	1013	HFG		Med-Coarse	183	60											
HF	1014	HFG		Med-Coarse													
HF	1015	HFG	ms	Med-Coarse	113	61											
HF	1016	HFG		Med-Coarse	111	56											
HF	1017	HFG		Med-Coarse	84	67											
HF	1018	Bg	bt	Medium													
HF	1019	HFG		Med-Coarse													
HF	1020	HFG		Med-Coarse	247	70											
HF	1021	HFG		Med-Coarse	213	64											
HF	1022	Bg	bt	Medium	136	40											
HF	1023	Bg	bt	Med-Coarse	111	45											
HF	1024	HFG		Med-Coarse													
HF	1025	Bg	bt	Medium	164	33											
HF	1026	Bg		Med-Coarse													
HF	1027	Bg		Medium	166	40											
HF	1028	HFG		Med-Coarse	136	69											
HF	1029	HFG		Med-Coarse	18	81											
HF	1030	HFG		Med-Coarse													
HF	1031	HFG		Med-Coarse	203	57											
HF	1032	HFG		Med-Coarse													
HF	1033	HFG		Med-Coarse	158	67											
HF	1034	HFG		Med-Coarse	213	77											
HF	1035	HFG		Med-Coarse	202	60											
HF	1036	Sch		Medium	211	79											
HF	1037	Sch		Medium	204	82											
HF	1038	Sch		Medium	134	63											
HF	1039	Sch		Medium	195	26											
HF	1040	Bg		Medium	158	68											
HF	1041	Bg	bt	Medium	329	75											
HF	1042	Bg		Medium	299	64											
HF	1043	Sch		Medium	219	66											
HF	1043	Sch		Medium			239	33									
HF	1044	Sch		Medium	109	61											
HF	1045	Bg		Medium	152	61											
HF	1046	Bg		Medium	284	69											
HF	1047	Sch		Medium	190	75											
HF	1048	Sch		Medium	201	68											
HF	1048	Sch		Medium			221	28									
HF	1049	Bg		Med-Coarse	167	19											
HF	1050	Bg		Med-Coarse	54	31											
HF	1050	Bg		Med-Coarse			149	22									
HF	1051	Bg		Med-Coarse	217	75											
HF	1052	Bg		Med-Coarse	241	42											
HF	1053	Bg		Med-Coarse	81	11											
HF	1054	Sch		Medium	128	62											
HF	1055	Sch		Medium	9	48											
HF	1055	Sch		Medium			164	31									
HF	1056	Qv		Med-Fine													
HF	1057	Bg	bt	Med-Fine	249	76											
HF	1058	Bg		Med-Coarse	257	36											
HF	1059	Bg		Med-Coarse	345	39											
HF	1060	Bg		Med-Coarse	324	26											

HF	1061	Bg		Med-Coarse	225	28										
HF	1062	Bg		Med-Coarse	258	28										
HF	1063	Bg		Med-Coarse	116	52										
HF	1064	Bg		Med-Coarse	175	58										
HF	1065	Bg		Med-Coarse	323	19										
HF	1065	Bg		Med-Coarse			169	11								
HF	1066	Bg		Med-Fine	211	12										
HF	1066	Bg		Med-Fine			339	7								
HF	1067	Bg		Med-Coarse	209	19										
HF	1068	Bg		Med-Coarse	336	73										
HF	1069	Sch		Medium	26	21										
HF	1069	Sch		Medium			156	10								
HF	1070	Bg		Medium	20	21										
HF	1070	Bg		Medium			171	13								
HF	1071	Bg		Medium	230	11										
HF	1071	Bg		Medium			330	6								
HF	1072	Bg		Med-Coarse	218	26										
HF	1072	Bg		Med-Coarse			348	4								
HF	1073	Sch		Medium	68	38										
HF	1073	Sch		Medium			147	23								
HF	1074	Sch	grt	Medium	34	20										
HF	1074	Sch	grt	Medium			96	14								
HF	1075	Sch		Medium	116	23										
HF	1076	Sch		Medium	49	29										
HF	1077	Sch		Medium	34	26										
HF	1078	Bg		Medium	33	28										
HF	1078	Bg		Medium			176	30								
HF	1079	Sch		Medium	28	17										
HF	1079	Sch		Medium			152	18								
HF	1080	Bg		Medium	354	44										
HF	1080	Bg		Medium			145	38								
HF	1081	Bg	ms	Medium	305	16										
HF	1081	Bg	ms	Medium			328	8								
HF	1082	Sch		Medium	27	11										
HF	1082	Sch		Medium			155	4								
HF	1083	Bg		Med-Coarse	249	12										
HF	1083	Bg		Med-Coarse			149	9								
HF	1084	Sch		Medium	54	14										
HF	1085	Bg		Med-Coarse	341	31										
HF	1086	Sch		Medium	39	21										
HF	1086	Sch		Medium			141	18								
HF	1087	Sch		Medium	35	38										
HF	1087	Sch		Medium			162	26								
HF	1088	Bg		Med-Coarse	359	75										
HF	1089	Bg	grt	Med-Coarse	346	36										
HF	1089	Bg	grt	Med-Coarse			336	9								
HF	1090	Sch		Medium	22	24										
HF	1090	Sch		Medium			165	17								
HF	1091	Bg		Medium												
HF	1092	Bg		Medium												
HF	1093	Sch		Medium	172	46										
HF	1093	Sch		Medium			238	21								
HF	1094	Bg		Medium												
HF	1095	HFG		Med-Coarse	76	21										
HF	1096	Sch		Medium	209	32										
HF	1096	Sch		Medium			229	38								
HF	1097	Bg		Medium	209	29										
HF	1098	Bg		Medium	109	32										
HF	1099	Bg		Med-Fine	235	63										
HF	1100	Bg		Medium												
HF	1101	Bg		Medium												
HF	1102	Mig		Medium	189	51										
HF	1103	Bg		Medium	202	45										
HF	1104	Bg		Medium	206	46										
HF	1105	Bg		Medium	203	57										
HF	1106	Sch		Medium												
HF	1107	Sch	sil	Medium	249	39										
HF	1108	Sch		Medium												
HF	1109	Amp		Med-Fine												
HF	1110	Bg		Medium	206	41										
HF	1111	Sch		Medium												
HF	1112	Bg		Medium	274	66										
HF	1113	Bg		Med-Coarse	223	35										
HF	1114	Bg		Medium	40	14										
HF	1115	Bg		Medium												
HF	1116	Bg		Medium	286	36										

HF	1117	Sch		Medium	218	12										
HF	1118	HFG		Med-Coarse	52	68										
HF	1119	Sch	sil	Medium	85	35										
HF	1120	Sch	sil	Medium	98	38										
HF	1121	Sch	sil	Medium	111	44										
HF	1121	Sch	sil	Medium			273	25								
HF	1122	Sch	sil	Medium	81	42										
HF	1123	Sch	sil	Medium							78	87	35	NW		
HF	1123	Sch	sil	Medium					259	37						
HF	1124	Bg		Medium	216	38										
HF	1125	Sch		Medium	78	59										
HF	1126	Sch		Medium	141	57										
HF	1127	Sch	ms	Medium	121	55										
HF	1128	Sch	sil	Medium	196	72										
HF	1129	Sch		Medium	279	74										
HF	1130	Sch	ms	Medium	58	50										
HF	1131	Sch	sil	Medium	53	57										
HF	1132	Sch	sil	Medium	82	56										
HF	1133	HFG		Med-Coarse	70	65										
HF	1134	HFG		Med-Coarse	131	31										
HF	1135	HFG		Med-Coarse	101	34										
HF	1136	Sch		Medium												
HF	1137	HFG		Med-Coarse	130	62										
HF	1138	HFG		Medium												
HF	1139	Bg		Medium	103	13										
HF	1140	HFG		Med-Coarse												
HF	1141	Bg		Med-Coarse	143	48										
HF	1142	HFG		Med-Coarse												
HF	1143	Bg		Med-Coarse												
HF	1144	HFG		Med-Coarse												
HF	1145	HFG		Med-Coarse												
HF	1146	HFG		Med-Coarse	145	67										
HF	1147	HFG		Med-Coarse	138	60										
HF	1148	HFG		Med-Coarse	128	54										
HF	1149	Bg	bt,ms	Medium	134	44										
HF	1150	HFG		Med-Coarse	209	40										
HF	1151	ISG		Medium	153	59										
HF	1152	ISG		Medium	216	78										
HF	1153	ISG		Medium	55	76										
HF	1154	Bg		Medium	65	50										
HF	1155	HFG		Med-Coarse	220	61										
HF	1156	Sch		Medium	53	45										
HF	1157	Sch		Medium	107	66										
HF	1158	Sch		Medium												
HF	1159	Bg		Medium	175	47										
HF	1160	Bg		Medium	166	60										
HF	1161	Bg	ms	Medium	100	31										
HF	1162	Sch		Medium												
HF	1163	Bg		Medium												
HF	1164	HFG		Med-Coarse												
HF	1165	HFG		Med-Coarse	121	66										
HF	1166	Sch		Medium												
HF	1167	Sch		Medium	14	76										
HF	1168	Sch	grt	Medium	42	71										
HF	1169	Sch	grt,sil	Medium	64	70										
HF	1170	Sch	grt	Medium	145	71										
HF	1171	Sch		Medium												
HF	1172	Bg		Medium												
HF	1173	Bg		Medium	53	71										
HF	1174	Sch		Medium												
HF	1175	Sch		Medium	82	58										
HF	1176	ISG		Med-Fine	198	50										
HF	1177	ISG		Med-Fine	149	60										
HF	1178	ISG		Medium	84	38										
HF	1179	ISG		Medium	184	76										
HF	1180	HFG		Med-Coarse	64	83										
HF	1181	HFG		Med-Coarse	344	77										
HF	1182	ISG		Medium	115	44										
HF	1183	HFG		Med-Coarse	75	58										
HF	1184	HFG		Med-Coarse												
HF	1185	HFG		Med-Coarse	51	65										
HF	1186	HFG		Med-Coarse												
HF	1187	ISG		Medium	113	75										
HF	1188	ISG		Medium												
HF	1189	ISG		Medium	68	70										
HF	1190	Bg		Medium												

HF	1191	ISG		Medium	58	41										
HF	1192	Bg		Medium	57	43										
HF	1193	Bg		Medium	70	50										
HF	1194	Bg		Medium	67	46										
HF	1195	Sch		Medium												
HF	1196	Sch		Medium												
HF	1197	HFG		Medium	104	66										
HF	1198	Sch		Medium	189	44										
HF	1199	HFG		Med-Coarse												
HF	1200	HFG		Med-Coarse	323	71										
HF	1201	ISG		Medium	333	72										
HF	1202	HFG		Med-Coarse												
HF	1203	ISG		Medium	178	63										
HF	1204	HFG		Med-Coarse												
HF	1205	Bg		Medium												
HF	1206	Sch		Medium												
HF	1207	Bg	sil	Medium	137	26										
HF	1208	Sch		Medium												
HF	1209	Bg	sil	Medium	128	22										
HF	1210	HFG		Med-Coarse												
HF	1211	Bg		Med-Coarse	124	38										
HF	1212	Bg		Med-Coarse	153	32										
HF	1213	Bg		Med-Coarse												
HF	1214	Bg		Med-Coarse	136	22										
HF	1214	Bg		Med-Coarse			154	10								
HF	1215	Bg		Med-Coarse	14	24										
HF	1215	Bg		Med-Coarse			0	11								
HF	1216	Bg		Med-Coarse	193	23										
HF	1217	Bg		Med-Coarse	155	14										
HF	1218	Bg		Med-Coarse	171	21										
HF	1219	Bg		Med-Coarse	145	22										
HF	1220	Bg		Med-Coarse	313	13										
HF	1221	Bg		Med-Coarse	16	22										
HF	1222	HFG		Med-Coarse	36	42										
HF	1223	HFG		Med-Coarse	233	30										
HF	1224	HFG		Med-Coarse	223	49										
HF	1225	HFG		Med-Coarse	112	34										
HF	1226	HFG		Med-Coarse	192	67										
HF	1227	Bg		Medium	123	65										
HF	1228	ISG	plg	Medium												
HF	1229	ISG		Medium												
HF	1230	Sch		Medium	185	81										
HF	1231	ISG		Medium												
HF	1232	Bg		Medium												
HF	1233	Bg	bt	Medium												
HF	1234	Bg		Medium												
HF	1235	Bg		Medium												
HF	1236	Bg		Medium	209	56										
HF	1237	Bg		Medium	114	24										
HF	1238	Bg		Medium	134	41										
HF	1239	Bg		Medium	204	71										
HF	1240	Bg		Medium	221	75										
HF	1241	Bg		Medium	233	84										
HF	1242	Bg		Medium												
HF	1243	Bg		Medium												
HF	1244	Bg		Medium												
HF	1245	Bg		Medium	225	74										
HF	1246	Bg		Medium	215	40										
HF	1247	Bg		Medium	227	78										
HF	1248	Bg		Medium	42	86										
HF	1249	Bg		Medium												
HF	1250	Sch		Medium	2	60										
HF	1251	Bg		Medium							186	66	155	SW		
HF	1251	Bg		Medium					182	54						
HF	1252	Bg		Medium	209	69										
HF	1253	Bg		Medium												
HF	1254	Bg		Medium												
HF	1255	Bg		Medium												
HF	1256	Sch	sil	Medium												
HF	1257	Sch	sil	Medium	5	75										
HF	1258	Bg		Medium												
HF	1259	Bg		Medium	358	54										
HF	1260	Sch		Medium	38	74										
HF	1261	Bg		Medium	208	68										
HF	1262	Bg		Medium	49	56										
HF	1263	Bg		Medium	199	71										

HF	1264	Sch	sil	Medium	46	64										
HF	1265	Sch	sil	Medium	36	65										
HF	1266	Bg		Medium	144	61										
HF	1267	Sch		Medium	133	25										
HF	1268	Bg		Medium	150	37										
HF	1269	Bg		Medium	194	44										
HF	1270	Bg		Medium	187	41										
HF	1271	Bg		Medium												
HF	1272	Bg		Medium	100	72										
HF	1273	Bg		Medium	211	74										
HF	1274	Sch	sil	Medium	164	29										
HF	1275	Bg		Medium												
HF	1276	Sch		Medium	38	56										
HF	1277	Bg		Medium												
HF	1278	Bg		Medium												
HF	1279	Bg		Medium												
HF	1280	Bg		Medium												
HF	1281	Bg		Medium	119	44										
HF	1282	Sch		Medium												
HF	1283	Bg		Medium												
HF	1284	Bg		Medium												
HF	1285	Sch		Medium												
HF	1286	Sch	grt	Medium												
HF	1287	Sch	sil	Medium	174	44										
HF	1288	Sch		Medium												
HF	1289	Bg		Medium												
HF	1290	Bg		Medium	56	65										
HF	1291	Sch		Medium	101	24										
HF	1292	Sch		Medium	111	21										
HF	1293	Sch	sil	Medium	210	50										
HF	1294	Sch		Medium	216	74										
HF	1295	Sch		Medium												
HF	1296	Sch		Medium												
HF	1297	Sch		Medium												
HF	1298	Sch	sil	Medium	70	59										
HF	1298	Sch	sil	Medium			236	14								
HF	1299	Sch		Medium												
HF	1300	Sch		Medium												
HF	1301	Sch	sil	Medium	41	76										
HF	1302	Sch	sil	Medium	74	69										
HF	1303	Sch	sil	Medium	37	75										
HF	1304	Sch	grt	Medium												
HF	1305	Sch		Medium												
HF	1306	ISG		Medium	209	81										
HF	1307	Bg		Medium	239	86										
HF	1308	ISG		Medium												
HF	1309	Sch		Medium												
HF	1310	Sch		Medium												
HF	1311	Sch		Medium	74	41										
HF	1312	Sch		Medium	74	69										
HF	1313	Sch		Medium	91	42										
HF	1314	Sch		Medium												
HF	1315	Sch		Medium	59	82										
HF	1316	Sch		Medium	69	20										
HF	1317	HFG		Med-Coarse												
HF	1318	Sch		Medium												
HF	1319	Sch		Medium	81	68										
HF	1320	Sch		Medium							33	89	150	NE		
HF	1320	Sch		Medium					215	82						
HF	1320	Sch		Medium	209	74										
HF	1321	HFG		Med-Coarse	212	68										
HF	1322	Sch		Medium	199	32										
HF	1323	Sch		Medium	74	46										
HF	1324	Sch		Medium	57	61										
HF	1325	HFG		Med-Coarse	249	61										
HF	1326	Sch		Medium												
HF	1327	Sch		Medium	157	44										
HF	1328	Sch		Medium												
HF	1329	HFG		Med-Coarse	124	74										
HF	1330	HFG		Med-Coarse												
HF	1331	HFG		Med-Coarse	90	67										
HF	1332	HFG		Med-Coarse	216	66										
HF	1333	HFG		Med-Coarse	84	46										
HF	1334	HFG		Med-Coarse	220	48										
HF	1335	Sch		Medium												
HF	1336	Sch		Medium												

HF	1337	Sch		Medium												
HF	1338	Sch	sil	Medium	73	44										
HF	1339	HFG		Med-Coarse												
HF	1340	HFG		Med-Coarse												
HF	1341	Sch		Medium												
HF	1342	HFG		Med-Coarse												
HF	1343	HFG		Med-Coarse	228	50										
HF	1344	HFG		Med-Coarse												
HF	1345	HFG		Med-Coarse												
HF	1346	Bg		Med-Coarse	197	42										
HF	1347	Amp		Medium												
HF	1348	Amp														
HF	1349	Amp		Medium												
HF	1350	Bg		Med-Coarse	175	40										
HF	1351	Amp		Medium												
HF	1352	Sch	sil	Medium	209	44										
HF	1353	Amp		Medium												
HF	1354	Bg		Medium												
HF	1355	Bg		Medium	211	39										
HF	1356	Bg		Med-Coarse												
HF	1357	Bg		Medium												
HF	1358	Bg	bt	Medium												
HF	1359	Bg		Medium												
HF	1360	Bg	bt	Medium												
HF	1361	Sch	sil	Medium	174	54										
HF	1362	Bg	bt	Med-Coarse												
HF	1363	Bg	bt	Medium												
HF	1364	Sch	sil	Medium	141	36										
HF	1365	Bg	bt	Med-Coarse												
HF	1366	Bg	bt	Medium												
HF	1367	Bg		Medium	324	60										
HF	1368	Bg		Med-Coarse	137	44										
HF	1369	Bg		Medium	262	37										
HF	1370	Bg		Medium	104	29										
HF	1371	Bg		Medium	174	10										
HF	1372	Bg	bt	Medium	128	21										
HF	1373	Bg		Medium	101	32										
HF	1374	Bg		Medium	222	39										
HF	1375	Bg		Medium	119	21										
HF	1376	Bg		Medium	198	11										
HF	1377	Bg		Medium	143	22										
HF	1378	Sch		Medium	152	18										
HF	1379	Bg		Medium	129	16										
HF	1380	Sch		Medium												
HF	1381	Sch	sil	Medium												
HF	1382	ISG		Medium	54	78										
HF	1383	Sch		Medium												
HF	1384	Sch		Medium	228	56										
HF	1385	Sch		Medium	69	59										
HF	1386	Sch		Medium	109	35										
HF	1387	Sch		Medium												
HF	1388	Sch		Medium												
HF	1389	ISG		Medium												
HF	1390	Sch		Medium												
HF	1391	Sch		Medium	156	36										
HF	1392	Dd														
HF	1393	Sch		Medium												
HF	1394	Sch		Medium	29	74										
HF	1395	Sch		Medium	86	32										
HF	1396	Sch		Medium	310	19										
HF	1397	Sch		Medium	80	38										
HF	1398	Go		Med-Coarse	44	74										
HF	1399	Sch		Medium	221	44										
HF	1400	ISG	chl	Medium	171	54										
HF	1400	ISG	chl	Medium											242	60
HF	1401	Sch	chl	Medium	220	29										
HF	1401	Sch	chl	Medium			4	19								
HF	1402	Si-C		Medium												
HF	1403	Sch		Medium	199	78										
HF	1404	Bg		Med-Coarse												
HF	1405	Bg		Med-Coarse												
HF	1406	Bg		Med-Coarse	247	26										
HF	1407	Bg		Med-Coarse	265	39										
HF	1408	Bg		Med-Coarse	184	22										
HF	1409	Sch		Medium	39	56										
HF	1410	Sch		Medium	111	42										

HF	1410	Sch		Medium			151	26								
HF	1411	Sch		Medium	64	46										
HF	1411	Sch		Medium			134	34								
HF	1412	Sch		Medium	150	34										
HF	1413	Bg		Med-Coarse	146	60										
HF	1414	Sch		Medium	134	40										
HF	1415	Sch		Medium	84	21										
HF	1416	Bg		Med-Coarse	344	85										
HF	1417	Bg		Med-Coarse	176	65										
HF	1418	Bg		Med-Coarse	145	31										
HF	1418	Bg		Med-Coarse			167	13								
HF	1419	Bg		Med-Coarse	228	3										
HF	1420	Bg		Med-Coarse	277	66										
HF	1421	Bg		Med-Coarse	219	29										
HF	1422	Bg		Med-Coarse	241	31										
HF	1423	Bg		Med-Coarse	334	32										
HF	1424	Bg		Med-Coarse	170	16										
HF	1425	Bg		Med-Coarse	106	23										
HF	1426	Bg		Med-Coarse	269	35										
HF	1427	HFG														
HF	1428	ISG		Medium												
HF	1429	Sch		Medium	271	38										
HF	1430	Sch		Medium	214	71										
HF	1431	Sch		Medium	191	64										
HF	1432	HFG		Med-Coarse												
HF	1433	Sch		Medium							214	82	150	SW		
HF	1433	Sch		Medium					218	18						
HF	1434	Sch		Medium	249	46										
HF	1434	Sch		Medium	131	55										
HF	1435	Sch		Medium							213	80	140	SW		
HF	1435	Sch		Medium					221	58						
HF	1436	Sch		Medium	112	47										
HF	1436	Sch		Medium			182	36								
HF	1437	Sch		Medium							107	85	40	NE		
HF	1437	Sch		Medium					278	49						
HF	1437	Sch		Medium			245	26								
HF	1438	Sch		Medium							86	84	30	NW		
HF	1438	Sch		Medium					101	71						
HF	1439	Sch		Medium	116	44										
HF	1439	Sch		Medium			216	26								
HF	1440	Sch		Medium	144	18										
HF	1440	Sch		Medium	262	44										
HF	1440	Sch		Medium			168	19								
HF	1441	Sch		Medium							124	44	140	NE		
HF	1441	Sch		Medium					203	35						
HF	1441	Sch		Medium	137	52										
HF	1442	Sch		Medium	122	50										
HF	1442	Sch		Medium			258	27								
HF	1443	Sch		Medium							18	82	160	NW		
HF	1443	Sch		Medium					194	34						
HF	1443	Sch		Medium			180	36								
HF	1444	Sch		Medium	91	38										
HF	1444	Sch		Medium	212	35										
HF	1445	Sch		Medium							122	76	35	NE		
HF	1445	Sch		Medium							14	86	145	NW		
HF	1445	Sch		Medium					171	63						
HF	1445	Sch		Medium					181	59						
HF	1445	Sch		Medium	85	81										
HF	1446	Sch		Medium							75	82	30	NW		
HF	1446	Sch		Medium							234	86	125	SW		
HF	1446	Sch		Medium					107	49						
HF	1446	Sch		Medium					154	46						
HF	1446	Sch		Medium			241	32								
HF	1447	Sch		Medium					184	46						
HF	1447	Sch		Medium	11	87										
HF	1448	Sch	sil	Medium							54	54	25	NW		
HF	1448	Sch	sil	Medium							239	84	130	SW		
HF	1448	Sch	sil	Medium					131	48						
HF	1448	Sch	sil	Medium					139	34						
HF	1448	Sch	sil	Medium			211	33								
HF	1449	Sch	sil	Medium							210	81	160	SW		
HF	1449	Sch	sil	Medium					206	26						
HF	1449	Sch	sil	Medium			216	31								
HF	1450	Sch		Medium	69	59										
HF	1451	Sch		Medium							103	59	35	NE		
HF	1451	Sch		Medium							84	64	40	NW		

HF	1451	Sch		Medium					179	61						
HF	1451	Sch		Medium					201	64						
HF	1452	Sch		Medium							175	78	150	NE		
HF	1452	Sch		Medium					178	41						
HF	1453	Sch		Medium							69	41	35	NW		
HF	1453	Sch		Medium					210	44						
HF	1453	Sch		Medium			171	50								
HF	1454	Sch		Medium					100	75						
HF	1454	Sch		Medium					96	68						
HF	1455	Sch		Medium							98	69	40	NW		
HF	1455	Sch		Medium							97	77	40	NE		
HF	1455	Sch		Medium					133	48						
HF	1455	Sch		Medium					262	49						
HF	1456	Sch		Medium							171	84	150	NE		
HF	1456	Sch		Medium					176	62						
HF	1457	Sch	sil	Medium	119	36										
HF	1457	Sch	sil	Medium			216	29								
HF	1458	Sch		Medium							88	80	30	NW		
HF	1458	Sch		Medium	247	62										
HF	1459	Sch		Medium							169	84	150	NE		
HF	1459	Sch		Medium					164	75						
HF	1460	Sch	sil	Medium							179	79	140	NE		
HF	1460	Sch	sil	Medium					180	68						
HF	1461	Sch		Medium	96	60										
HF	1461	Sch		Medium			217	55								
HF	1462	Sch	sil	Medium	72	76										
HF	1462	Sch	sil	Medium			197	67								
HF	1463	Sch		Medium							80	68	40	NW		
HF	1463	Sch		Medium					243	61						
HF	1464	Sch	sil	Medium	94	62										
HF	1464	Sch	sil	Medium			194	54								
IS	163	HFG		Med-Coarse	16	53										
IS	164	HFG		Med-Coarse	289	54										
IS	165	HFG		Med-Coarse												
IS	166	HFG		Med-Coarse	244	46										
IS	167	HFG		Medium												
IS	168	Sch		Medium												
IS	169	HFG		Med-Coarse												
IS	170	HFG		Med-Coarse												
IS	171	Sch														
IS	172	Bg		Med-Fine												
IS	173	HFG		Med-Coarse	350	57										
IS	174	HFG		Med-Coarse	182	62										
IS	175	HFG		Med-Coarse												
IS	176	HFG		Med-Coarse												
IS	177	Sch		Medium												
IS	178	Sch		Medium												
IS	179	HFG		Med-Coarse	22	63										
IS	180	Sch		Medium												
IS	181	Bg	bt,ms	Medium												
IS	182	Sch		Medium												
IS	183	Sch	bt	Medium	255	59										
IS	184	Sch	bt	Medium												
IS	185	Bg	bt	Medium	318	44										
IS	186	Sch		Medium												
IS	187	Sch	sil	Medium	225	54										
IS	188	Sch	bt	Medium												
IS	189	Bg	bt,grt	Medium	81	52										
IS	190	Sch		Medium							222	74	160	SW		
IS	190	Sch		Medium					16	33						
IS	191	Bg	bt	Medium	354	55										
IS	192	Bg		Medium	273	63										
IS	193	Bg		Med-Coarse	237	64										
IS	194	Bg		Medium	205	44										
IS	194	Bg		Medium			238	27								
IS	195	Bg	bt	Medium	249	65										
IS	196	Sch	bt	Medium	236	60										
IS	197	Bg	bt	Medium	264	66										
IS	198	ISG		Med-Fine	306	66										
IS	199	Bg	bt	Medium	235	58										
IS	200	ISG		Med-Fine	173	65										
IS	201	HFG		Medium	172	70										
IS	202	HFG		Med-Coarse	337	66										
IS	203	Bg	bt	Med-Coarse	246	65										
IS	204	Bg	bt	Med-Coarse	287	54										
IS	205	ISG		Medium	104	63										

IS	206	ISG		Medium	116	76										
IS	207	Bg	bt,ms	Medium	303	50										
IS	208	Sch		Medium												
IS	209	Sch		Medium												
IS	210	ISG		Medium												
IS	211	ISG		Medium												
IS	212	ISG		Medium												
IS	213	ISG		Medium												
IS	214	ISG		Medium												
IS	215	HFG		Med-Coarse												
IS	216	ISG		Medium												
IS	217	ISG			294	53										
IS	218	HFG		Med-Coarse	217	48										
IS	219	HFG		Med-Coarse	227	53										
IS	220	HFG		Med-Coarse												
IS	221	HFG		Med-Coarse	170	50										
IS	222	ISG		Medium	100	72										
IS	223	ISG		Medium												
IS	224	Sch		Medium	241	80										
IS	224	Sch		Medium			277	48								
IS	225	Sch		Medium												
IS	226	Sch		Medium	62	76										
IS	227	HFG		Med-Coarse	195	67										
IS	228	Sch		Medium												
IS	229	Sch		Medium												
IS	230	Sch		Medium												
IS	231	HFG		Med-Coarse												
IS	232	Bg	bt	Med-Coarse	214	66										
IS	233	Bg	bt,ms	Med-Coarse	213	65										
IS	234	Sch		Medium												
IS	235	Sch		Medium												
IS	236	Sch		Medium												
IS	237	Bg		Medium												
IS	238	HFG		Med-Coarse												
IS	239	Bg		Medium	245	80										
IS	240	Bg	bt	Med-Fine	241	79										
IS	241	Sch		Medium												
IS	242	HFG		Med-Coarse	252	84										
IS	243	Bg	bt	Med-Coarse	216	75										
IS	244	Sch		Medium												
IS	245	ISG	bt	Medium	240	88										
IS	246	ISG		Medium												
IS	247	Bg	bt	Medium	62	74										
IS	248	Bg	bt	Med-Coarse	66	76										
IS	249	Sch		Medium												
IS	250	Sch		Medium	238	87										
IS	251	Bg	bt	Med-Coarse	53	73										
IS	252	ISG	bt	Med-Fine	98	40										
IS	253	ISG	bt	Med-Fine	94	70										
IS	254	ISG		Medium	155	56										
IS	255	Sch		Medium	224	81										
IS	256	Sch		Medium												
IS	257	Sch		Medium	224	65										
IS	258	HFG		Med-Coarse	185	73										
IS	259	ISG		Med-Fine	10	70										
IS	260	HFG		Med-Coarse	55	76										
IS	261	ISG		Medium												
IS	262	Sch	sil,grt	Medium	153	65										
IS	263	Sch		Medium	221	66										
IS	264	Bg	bt	Med-Coarse	148	35										
IS	265	ISG		Medium												
IS	266	ISG		Medium												
IS	267	HFG		Med-Coarse	172	67										
IS	268	Sch		Medium	80	66										
IS	269	HFG		Med-Coarse												
IS	270	Sch		Medium	80	39										
IS	271	HFG		Med-Coarse												
IS	272	ISG		Medium												
IS	273	HFG		Med-Coarse	205	55										
IS	274	HFG		Med-Coarse												
IS	275	ISG		Medium												
IS	276	ISG		Medium												
IS	277	Sch		Medium												
IS	278	Sch		Medium	211	56										
IS	279	HFG		Med-Coarse	220	43										
IS	280	Sch		Medium												

IS	281	Sch		Medium												
IS	282	HFG		Med-Coarse												
IS	283	HFG		Med-Coarse	46	56										
IS	284	ISG		Medium												
IS	285	Sch		Medium												
IS	286	Sch		Medium												
IS	287	Sch		Med-Fine												
IS	288	Sch		Medium	224	33										
IS	289	Sch		Medium	176	46										
IS	290	Sch		Medium	174	57										
IS	291	Sch		Medium	195	51										
IS	292	HFG		Med-Coarse	103	73										
IS	293	HFG		Med-Coarse	300	81										
IS	294	Si-C		Med-Fine												
IS	295	ISG	bt	Med-Fine												
IS	296	Bg		Med-Fine	149	32										
IS	296	Bg		Med-Fine			158	14								
IS	297	Sch		Medium	172	70										
IS	298	Sch		Medium	196	71										
IS	299	Sch		Medium							156	88	160	NE		
IS	299	Sch		Medium					338	55						
IS	300	Sch		Medium	256	76										
IS	301	HFG		Med-Coarse	194	79										
IS	302	HFG	bt	Med-Coarse	195	65										
IS	303	Sch		Medium	100	26										
IS	304	Sch	sil	Medium	183	55										
IS	305	Sch		Medium	174	73										
IS	306	Sch		Medium	219	49										
IS	307	Sch		Medium	200	56										
IS	308	Sch		Medium	212	66										
IS	309	HFG		Med-Coarse	168	64										
IS	310	Sch		Medium	219	60										
IS	311	HFG		Med-Coarse												
IS	312	Sch		Medium	214	40										
IS	313	HFG		Med-Coarse	216	48										
IS	314	Sch		Medium	207	40										
IS	315	Sch		Medium	228	44										
IS	316	HFG		Med-Coarse												
IS	317	HFG		Med-Coarse	314	49										
IS	318	HFG		Med-Coarse	181	50										
IS	319	HFG		Med-Coarse	185	48										
IS	320	HFG		Med-Coarse	116	73										
IS	321	HFG		Med-Coarse	158	64										
IS	322	HFG		Med-Coarse												
IS	323	HFG		Med-Coarse	217	36										
IS	323	HFG		Med-Coarse	291	47										
IS	323	HFG		Med-Coarse	349	78										
IS	324	HFG		Med-Coarse	203	58										
IS	325	HFG		Med-Coarse												
IS	326	HFG		Med-Coarse	219	59										
IS	327	HFG		Med-Coarse												
IS	328	HFG		Med-Coarse	214	72										
IS	329	HFG		Med-Coarse	302	39										
IS	330	HFG		Med-Coarse	348	83										
IS	331	HFG		Med-Coarse	337	67										
IS	332	HFG		Med-Coarse	176	73										
IS	333	HFG		Med-Coarse	199	78										
IS	334	HFG		Med-Coarse	205	84										
IS	335	HFG		Med-Coarse	10	75										
IS	336	HFG		Med-Coarse	233	74										
IS	337	HFG		Med-Coarse	183	79										
IS	338	HFG		Med-Coarse	239	78										
IS	339	HFG		Med-Coarse	205	69										
IS	340	HFG		Med-Coarse	160	83										
IS	341	HFG		Med-Coarse	332	76										
IS	342	HFG		Med-Coarse												
IS	343	HFG		Med-Coarse												
IS	344	HFG		Med-Coarse	1	77										
IS	345	HFG		Med-Coarse												
IS	346	HFG		Med-Coarse												
IS	347	HFG		Med-Coarse												
IS	348	HFG		Med-Coarse												
IS	349	HFG		Med-Coarse	74	72										
IS	350	HFG		Med-Coarse												
IS	351	HFG		Med-Coarse												
IS	352	HFG		Med-Coarse	216	75										

IS	353	Dd		Medium												
IS	354	HFG		Med-Coarse												
IS	355	HFG		Med-Coarse	265	79										
IS	356	Bg		Medium												
IS	357	HFG		Med-Coarse												
IS	358	HFG		Med-Coarse												
IS	359	HFG		Med-Coarse												
IS	360	HFG		Med-Coarse												
IS	361	HFG		Med-Coarse												
IS	362	HFG		Med-Coarse												
IS	363	HFG		Med-Coarse	260	63										
IS	364	HFG		Med-Coarse												
IS	365	HFG		Med-Coarse												
IS	366	HFG		Med-Coarse												
IS	367	Bg		Medium												
IS	368	Sch		Medium												
IS	369	HFG		Med-Coarse												
IS	370	HFG		Med-Coarse	155	48										
IS	371	HFG		Med-Coarse												
IS	372	HFG		Med-Coarse												
IS	373	HFG		Med-Coarse												
IS	374	HFG		Med-Coarse	59	69										
IS	375	HFG		Med-Coarse	38	74										
IS	376	HFG		Med-Coarse												
IS	377	HFG		Med-Coarse	254	72										
IS	378	HFG		Med-Coarse	65	59										
IS	379	HFG	bt	Med-Coarse												
IS	380	Sch		Medium												
IS	381	Sch		Medium												
IS	382	HFG		Med-Coarse												
IS	383	Sch		Medium	253	65										
IS	384	HFG		Med-Coarse												
IS	385	HFG		Med-Coarse												
IS	386	HFG		Med-Coarse	214	68										
IS	387	HFG		Med-Coarse	128	60										
IS	388	HFG		Med-Coarse	67	68										
IS	389	Bg		Med-Coarse	71	70										
IS	390	ISG		Medium	270	82										
IS	391	Sch		Medium												
IS	392	Sch														
IS	393	Sch														
IS	394	ISG		Medium												
IS	395	Sch		Medium	213	68										
IS	396	Dd		Medium												
IS	397	Sch		Medium	234	65										
IS	398	Bg		Medium	255	47										
IS	399	Sch		Medium												
IS	400	Sch		Medium												
IS	401	Bg		Medium	204	29										
IS	402	Sch		Medium												
IS	403	ISG		Medium												
IS	404	ISG		Medium	205	58										
IS	405	Bg	bt	Medium	84	34										
IS	406	ISG		Medium												
IS	407	HFG		Med-Coarse												
IS	408	Sch		Medium												
IS	409	Sch		Medium	225	60										
IS	410	Sch		Medium												
IS	411	ISG		Medium												
IS	412	Sch		Medium												
IS	413	Sch		Medium	164	65										
IS	414	Sch		Medium	178	66										
IS	415	Sch		Medium												
IS	416	Sch		Medium												
IS	417	ISG		Medium	132	82										
IS	418	Sch		Medium												
IS	419	HFG		Med-Coarse												
IS	420	HFG		Medium	156	57										
IS	421	Sch		Medium												
IS	422	Sch		Medium												
IS	423	Sch		Medium												
IS	424	Sch		Medium	118	77										
IS	425	Sch		Medium												
IS	426	Sch		Medium												
IS	427	ISG		Medium	149	72										
IS	428	Bg	bt	Medium	144	51										

IS	429	ISG		Medium												
IS	430	Sch		Medium												
IS	431	Sch		Medium												
IS	432	Sch		Medium												
IS	433	ISG		Medium	143	50										
IS	434	Sch		Medium												
IS	435	Sch		Medium	68	55										
IS	436	ISG		Medium	258	62										
IS	437	Go		Med-Coarse												
IS	438	Bg		Med-Coarse												
IS	439	Go	amp	Medium	281	26										
IS	440	HFG		Medium	201	30										
IS	441	HFG		Med-Coarse	165	38										
IS	442	HFG		Med-Coarse												
IS	443	HFG		Med-Coarse	209	58										
IS	444	ISG		Med-Fine												
IS	445	ISG		Med-Fine												
IS	446	Bg		Med-Fine												
IS	447	Sch		Medium												
IS	448	Sch		Medium												
IS	449	Sch		Medium												
IS	450	Sch		Medium												
IS	451	Sch		Medium												
IS	452	Sch		Medium	103	49										
IS	452	Sch		Medium			256	22								
IS	453	HFG		Med-Coarse	95	82										
IS	454	HFG		Med-Coarse	74	72										
IS	455	ISG		Medium												
IS	456	HFG		Med-Coarse												
IS	457	Sch		Medium												
IS	458	Bg		Medium												
IS	459	HFG		Med-Coarse												
IS	460	Sch		Medium												
IS	461	Sch		Medium	127	54										
IS	462	Sch		Medium	63	56										
IS	463	Sch		Medium	83	56										
IS	464	Sch		Medium	121	56										
IS	465	Sch		Medium	107	37										
IS	465	Sch		Medium	120	31										
IS	466	HFG		Med-Coarse	91	65										
IS	467	ISG		Medium												
IS	468	HFG		Med-Coarse												
IS	469	Sch		Medium												
IS	470	ISG		Med-Fine												
IS	471	Sch		Medium	191	64										

APPENDIX 2
Electron Microprobe Data

Microprobe analysis of HF1467

Oxide Wt. %	Grt01 r01	Grt01 r02	Grt01 r03	Grt01 r04	Grt01 r05	Grt01 r06	Grt01 r07	Grt01 r08	Grt01 r09	Grt01 r010
SiO2	37.3628	37.5803	36.7266	36.7489	36.8338	37.4298	37.5842	37.3099	37.2303	37.125
TiO2	0.0186	0.1054	0.0675	0.0804	0.0512	0.0225	0.0226	0.1478	0	0.0212
Al2O3	21.2581	21.4084	20.9341	20.9514	20.9897	21.2431	21.5655	21.0395	20.9863	21.0626
Y2O3	0	0	0	0	0	0	0	0	0	0
MgO	1.5064	1.3852	1.395	1.3629	1.3456	1.648	1.8215	1.5234	1.6372	1.6352
CaO	5.201	5.2397	5.2402	5.2715	5.385	5.0057	4.7788	5.0236	5.2419	5.3079
MnO	4.4203	4.6246	4.5471	4.6589	4.7291	4.3605	4.3059	4.4319	4.3848	4.4975
FeO	31.2812	30.8673	31.2332	30.9632	31.1226	31.2459	31.2272	31.5056	31.3589	31.1239
Na2O	0.0045	0.0185	0.0212	0	0.0188	0.0166	0.0201	0.0166	0.0121	0.0126
Total	101.0548	101.2312	100.1648	100.045	100.4757	100.9721	101.3257	100.9985	100.8515	100.7859

Cation based on 12 oxygens										
Si	2.988	2.995	2.973	2.976	2.973	2.992	2.988	2.989	2.987	2.98
Ti	0.001	0.006	0.004	0.005	0.003	0.001	0.001	0.009	0	0.001
Al	2.003	2.011	1.997	2	1.997	2.001	2.021	1.986	1.984	1.993
Y	0	0	0	0	0	0	0	0	0	0
Mg	0.18	0.165	0.168	0.165	0.162	0.196	0.216	0.182	0.196	0.196
Ca	0.446	0.447	0.454	0.457	0.466	0.429	0.407	0.431	0.451	0.457
Mn	0.299	0.312	0.312	0.32	0.323	0.295	0.29	0.301	0.298	0.306
Fe	2.092	2.057	2.114	2.097	2.101	2.089	2.076	2.111	2.104	2.089
OH	0	0	0	0	0	0	0	0	0	0
Na	0.001	0.003	0.003	0	0.003	0.003	0.003	0.003	0.002	0.002
Total	8.01	7.995	8.026	8.019	8.027	8.007	8.002	8.011	8.022	8.023

Microprobe analysis of HF1467

Oxide Wt. %	Grt01 r011	Grt01 c01	Grt01 c02	Grt01 c03	Grt01 c09	Grt01 c10	Grt01 c11	Grt01 c12	Grt02 c01	Grt02 c02
SiO2	37.0555	37.1178	37.4355	37.1419	37.0087	37.291	36.7932	36.3243	36.8646	36.9241
TiO2	0.025	0.6895	0.6879	0.7482	0.4418	0.4065	1.2719	1.9363	0.3653	0.307
Al2O3	20.9228	20.9581	21.0729	20.7115	20.723	21.1524	20.4397	19.6948	20.9339	20.8222
Y2O3	0	0.0538	0.033	0.0484	0.0272	0.0675	0.0113	0.0368	0.0497	0.0556
MgO	1.6318	1.4401	1.5366	1.3941	2.467	1.5985	1.4432	1.4482	1.614	1.7119
CaO	5.1598	4.3503	4.34	4.344	3.8367	5.2182	5.9773	7.4892	4.7248	4.4858
MnO	4.411	4.5861	4.4149	4.6707	3.0509	4.1718	4.2105	3.901	4.1344	4.1522
FeO	31.3049	32.1531	32.1961	32.1766	33.069	31.2281	31.2871	30.142	31.7575	32.1075
Na2O	0.0171	0.0091	0.0071	0.0096	0.0212	0.0352	0.003	0.0327	0.0055	0.0096
Total	100.528	101.3584	101.7239	101.2844	100.6734	101.1869	101.4507	101.0052	100.467	100.5758

Cation based on 12 oxygens										
Si	2.984	2.97	2.979	2.977	2.972	2.977	2.944	2.923	2.971	2.976
Ti	0.002	0.041	0.041	0.045	0.027	0.024	0.077	0.117	0.022	0.019
Al	1.986	1.977	1.976	1.956	1.961	1.99	1.928	1.868	1.989	1.978
Y	0	0.002	0.001	0.002	0.001	0.003	0	0.002	0.002	0.002
Mg	0.196	0.172	0.182	0.167	0.295	0.19	0.172	0.174	0.194	0.206
Ca	0.445	0.373	0.37	0.373	0.33	0.446	0.513	0.646	0.408	0.387
Mn	0.301	0.311	0.298	0.317	0.208	0.282	0.285	0.266	0.282	0.283
Fe	2.108	2.152	2.143	2.157	2.221	2.085	2.094	2.028	2.141	2.164
OH	0	0	0	0	0	0	0	0	0	0
Na	0.003	0.001	0.001	0.001	0.003	0.005	0	0.005	0.001	0.001
Total	8.023	7.999	7.992	7.998	8.021	8.004	8.015	8.028	8.011	8.016

Microprobe analysis of HF1467

Oxide Wt. %	Grt02 c03	Grt02 c04	Grt02 c05	Grt02 c06	Grt02 c07	Grt02 c08	Grt02 c09	Grt02 c010
SiO2	36.8323	37.1027	37.5609	37.277	37.335	37.1009	37.0015	37.0638
TiO2	0.3697	0.1939	0.1812	0.171	0.5238	0.3708	0.4964	0.6101
Al2O3	20.8554	21.0328	21.3117	21.2	21.0413	21.0665	21.1031	20.9394
Y2O3	0.0825	0.1469	0.0828	0.0728	0.0911	0.0503	0.0335	0.0077
MgO	1.6863	2.3141	2.3723	2.3339	1.841	1.809	1.7813	1.4112
CaO	4.5278	4.088	3.9112	3.9918	4.3464	4.4599	4.448	4.6562
MnO	4.2066	3.1446	3.1718	3.1531	3.7941	3.9665	3.8868	4.5935
FeO	32.0148	32.6993	32.8888	32.9425	32.2107	32.1437	32.0703	31.7653
Na2O	0	0.0146	0.0167	0	0.0061	0.0071	0	0.0248
Total	100.5938	100.737	101.5332	101.1588	101.2284	100.9791	100.8209	101.0854

Cation based on 12 oxygens								
Si	2.969	2.975	2.983	2.975	2.98	2.973	2.968	2.972
Ti	0.022	0.012	0.011	0.01	0.031	0.022	0.03	0.037
Al	1.981	1.988	1.995	1.994	1.98	1.989	1.995	1.979
Y	0.004	0.006	0.004	0.003	0.004	0.002	0.001	0
Mg	0.203	0.277	0.281	0.278	0.219	0.216	0.213	0.169
Ca	0.391	0.351	0.333	0.341	0.372	0.383	0.382	0.4
Mn	0.287	0.214	0.213	0.213	0.257	0.269	0.264	0.312
Fe	2.158	2.193	2.184	2.199	2.15	2.154	2.151	2.13
OH	0	0	0	0	0	0	0	0
Na	0	0.002	0.003	0	0.001	0.001	0	0.004
Total	8.016	8.017	8.008	8.015	7.996	8.01	8.004	8.003

Microprobe analysis of HF1467

Oxide Wt. %	Grt01 bt01	Grt01 bt02	Grt01 bt03	Grt01 bt04	Grt01 bt05	Grt01 bt06	Grt01 bt07	Grt02 bt01	Grt02 bt02	Grt02 bt03
SiO2	29.9251	33.7706	32.6517	29.5091	29.8884	30.1354	29.1287	29.4836	29.929	29.4719
TiO2	1.2875	2.4139	1.322	0.747	1.0994	1.2181	1.2495	1.2048	1.1393	0.8493
Al2O3	16.5015	11.5577	11.9744	16.5604	16.5931	16.7725	16.3892	14.7883	16.2269	16.1289
MgO	9.2604	1.6118	1.1123	9.366	9.0769	8.944	8.7969	7.6261	8.7475	9.0408
CaO	0.5182	29.4116	30.3324	0.2825	0.1031	0.1097	0.1168	5.0112	0.0625	0.1309
MnO	0.1556	0.0939	0.1023	0.1514	0.1421	0.1213	0.1392	0.1125	0.1547	0.1366
FeO	31.5029	16.7851	15.414	31.9489	31.2754	31.2332	31.8823	30.593	31.8419	32.6591
H2O	3.6262	3.8074	3.6984	3.5792	3.6085	3.6275	3.5566	3.5538	3.597	3.5838
Na2O	0.0372	0.0133	0.0061	0.0365	0.0392	0.0426	0.046	0.027	0.0564	0.0206
K2O	1.881	0.0498	0.1259	1.1672	2.6086	2.5277	2.0428	1.5863	2.7933	2.627
Total	94.6958	99.515	96.7396	93.3482	94.4347	94.732	93.3479	93.9867	94.5486	94.6488

Cation based on 22 oxygens

Si	4.949	5.319	5.294	4.944	4.967	4.982	4.911	4.975	4.99	4.932
Ti	0.16	0.286	0.161	0.094	0.137	0.151	0.158	0.153	0.143	0.107
Al	3.216	2.145	2.288	3.27	3.25	3.268	3.257	2.941	3.188	3.181
Mg	2.283	0.378	0.269	2.339	2.249	2.204	2.211	1.918	2.174	2.255
Ca	0.092	4.963	5.27	0.051	0.018	0.019	0.021	0.906	0.011	0.023
Mn	0.022	0.013	0.014	0.021	0.02	0.017	0.02	0.016	0.022	0.019
Fe	4.357	2.211	2.09	4.477	4.347	4.318	4.496	4.317	4.439	4.57
OH	4	4	4	4	4	4	4	4	4	4
Na	0.012	0.004	0.002	0.012	0.013	0.014	0.015	0.009	0.018	0.007
K	0.397	0.01	0.026	0.249	0.553	0.533	0.439	0.341	0.594	0.561
Total	19.487	19.329	19.414	19.458	19.554	19.506	19.529	19.577	19.58	19.655

Microprobe analysis of HF1467

Oxide Wt. %	Grt01 amp02	Grt01 amp03	Grt01 amp04	Grt01 amp05	Grt01 amp06	Grt01 amp07	Grt01 amp08	Grt01 amp09	Grt01 amp08	Grt01 amp09
SiO2	42.0884	41.1168	44.1827	52.6912	42.5775	41.7302	51.7599	51.3044	42.1385	42.6845
TiO2	0.8748	0.2615	0.1896	0.1914	0.8592	0.9577	0.0412	0.0483	0.7471	0.6457
Al2O3	11.5653	14.2499	10.2038	8.3511	11.4377	11.9864	0.4926	0.6094	12.2597	13.3437
Cr2O3	0.0185	0.0086	0.006	0.0027	0	0.0027	0.0032	0.0164	0.002	0
MgO	5.7677	4.9694	6.7682	3.4116	6.147	5.8315	10.6937	10.6856	5.8673	5.6073
CaO	10.044	11.213	11.3124	7.0423	9.3402	10.4773	0.8464	0.9397	10.3716	10.4664
MnO	0.4605	0.3101	0.343	0.1869	0.5222	0.4244	1.1371	1.1038	0.3652	0.3385
FeO	25.0631	24.0234	23.7238	17.2959	25.3632	24.4543	33.0184	33.4287	23.5085	23.5256
H2O	1.9365	1.9487	1.9604	1.9377	1.9453	1.9389	1.9548	1.9517	1.9401	1.9747
Na2O	1.5814	1.5629	1.1951	0.7593	1.4784	1.633	0.074	0.1073	1.6704	1.7444
K2O	0.5408	0.5644	0.2906	0.3347	0.4685	0.5064	0.001	0.0024	0.472	0.5069
Total	99.9411	100.2288	100.1756	92.2048	100.1393	99.9429	100.0224	100.1977	99.3423	100.8377
Cation based on 23 oxygens										
Si	6.517	6.327	6.757	8.153	6.562	6.453	7.939	7.882	6.512	6.481
Ti	0.102	0.03	0.022	0.022	0.1	0.111	0.005	0.006	0.087	0.074
Al	2.11	2.584	1.839	1.523	2.078	2.185	0.089	0.11	2.233	2.388
Cr	0.002	0.001	0.001	0	0	0	0	0.002	0	0
Mg	1.331	1.14	1.543	0.787	1.412	1.344	2.445	2.447	1.352	1.269
Ca	1.666	1.849	1.854	1.168	1.542	1.736	0.139	0.155	1.717	1.703
Mn	0.06	0.04	0.044	0.024	0.068	0.056	0.148	0.144	0.048	0.044
Fe	3.245	3.091	3.034	2.238	3.269	3.163	4.235	4.295	3.038	2.987
OH	2	2	2	2	2	2	2	2	2	2
Na	0.475	0.466	0.354	0.228	0.442	0.49	0.022	0.032	0.501	0.514
K	0.107	0.111	0.057	0.066	0.092	0.1	0	0	0.093	0.098
Total	17.616	17.639	17.506	16.21	17.566	17.638	17.023	17.073	17.581	17.557

Microprobe analysis of HF1467

Oxide Wt. %	Grt01 amp010	Grt01 amp011	Grt01 amp012	Grt01 amp013	Grt01 amp014	Grt01 amp015
SiO2	42.1234	42.1545	42.0728	41.8244	41.0056	42.3635
TiO2	0.831	0.7943	0.9701	0.9444	0.5119	0.8527
Al2O3	12.1959	12.2796	11.9365	11.8817	13.8722	12.0609
Cr2O3	0.0007	0.0087	0.02	0	0.0027	0.0146
MgO	5.8263	5.7357	5.7243	5.8079	5.2479	5.8274
CaO	10.2496	10.086	9.9521	9.99	10.8563	10.4967
MnO	0.3965	0.4105	0.4402	0.4006	0.2802	0.3285
FeO	23.813	23.7205	24.1576	24.4139	23.9886	23.8034
H2O	1.9427	1.939	1.9376	1.9321	1.9414	1.9465
Na2O	1.7931	1.734	1.8453	1.7503	1.5576	1.6267
K2O	0.4796	0.4616	0.5293	0.4952	0.5462	0.4214
Total	99.6517	99.3244	99.5858	99.4404	99.8105	99.7423

Cation based on 23 oxygens						
Si	6.501	6.518	6.511	6.491	6.333	6.526
Ti	0.096	0.092	0.113	0.11	0.059	0.099
Al	2.218	2.238	2.177	2.173	2.525	2.19
Cr	0	0.001	0.002	0	0	0.002
Mg	1.341	1.322	1.321	1.344	1.208	1.338
Ca	1.695	1.671	1.65	1.661	1.796	1.732
Mn	0.052	0.054	0.058	0.053	0.037	0.043
Fe	3.074	3.067	3.126	3.169	3.098	3.066
OH	2	2	2	2	2	2
Na	0.537	0.52	0.554	0.527	0.466	0.486
K	0.094	0.091	0.104	0.098	0.108	0.083
Total	17.608	17.575	17.616	17.625	17.632	17.564

Microprobe analysis of HF1467

Oxide Wt. %	Grt01 il05	Grt01 il06	Grt01 il07	Grt01 il08	Grt01 il09	Grt01 il010	Grt01 il011	Grt01 il012	Grt02 il01	Grt02 il02
SiO2	1.7515	3.5119	0.0277	0.0072	0.0858	0.0184	0.013	0.0198	0.0246	0.0205
TiO2	46.1702	33.975	51.8879	51.8426	50.8719	51.6789	51.1277	51.4029	51.7673	51.1041
Al2O3	0.5699	0.5	0	0.0205	0.0749	0	0.0079	0	0.0122	0.0141
Cr2O3	0	0.0076	0.0175	0.0019	0.0056	0	0.0175	0.0069	0.0194	0
Y2O3	0	0	0	0	0	0	0	0	0.0042	0
MgO	0.0699	0.1108	0.0015	0.0015	0.0138	0	0.0315	0.001	0.0202	0.0163
CaO	0.6477	0.5999	0.0184	0.0598	0.0386	0.0686	0.2188	0.0634	0.0386	0
MnO	1.8889	1.8849	1.8194	1.7258	1.8812	1.7061	1.8057	1.9101	1.7755	1.8089
FeO	42.025	35.7516	46.0453	46.1153	45.3594	45.9266	46.0396	45.9387	46.2041	46.0719
Na2O	0.0234	0.0363	0	0	0	0	0.0199	0.0162	0	0
Total	93.1464	76.3778	99.8176	99.7745	98.3312	99.3986	99.2817	99.3589	99.866	99.0357

Cation based on 12 oxygens										
Si	0.188	0.461	0.003	0.001	0.009	0.002	0.001	0.002	0.002	0.002
Ti	3.736	3.356	3.962	3.961	3.944	3.963	3.934	3.948	3.953	3.941
Al	0.072	0.077	0	0.002	0.009	0	0.001	0	0.001	0.002
Cr	0	0.001	0.001	0	0	0	0.001	0.001	0.002	0
Y	0	0	0	0	0	0	0	0	0	0
Mg	0.011	0.022	0	0	0.002	0	0.005	0	0.003	0.002
Ca	0.075	0.084	0.002	0.007	0.004	0.007	0.024	0.007	0.004	0
Mn	0.172	0.21	0.156	0.149	0.164	0.147	0.156	0.165	0.153	0.157
Fe	3.782	3.927	3.91	3.918	3.91	3.916	3.939	3.924	3.924	3.951
OH	0	0	0	0	0	0	0	0	0	0
Na	0.005	0.009	0	0	0	0	0.004	0.003	0	0
Total	8.042	8.148	8.035	8.037	8.043	8.036	8.066	8.051	8.043	8.056

Microprobe analysis of HF1467

Oxide Wt. %	Grt02 il03	Grt02 il04	Grt02 il05	Grt02 il06	Grt02 il07	Grt02 il08	Grt02 il09	Grt02 il010	Grt02 il011	Grt02 il012
SiO2	0.012	0.0065	0.0168	0.0101	0.0182	0	0.0342	0.0367	0.0073	0.0355
TiO2	51.762	50.589	50.8946	51.0893	51.2493	51.0985	50.6521	49.7773	51.1039	51.1705
Al2O3	0	0.0274	0.0036	0.0037	0.0184	0.0069	0.0032	0.021	0.0216	0
Cr2O3	0.0025	0.0006	0.0193	0.0165	0	0.0151	0	0.0075	0.0235	0
Y2O3	0	0	0	0	0	0	0	0	0	0
MgO	0.0015	0.0123	0.0429	0.0466	0	0.0054	0	0.0124	0.0145	0
CaO	0.0087	0.0421	0.0173	0.0873	0.0156	0.048	0.0461	0.0278	0.0012	0.0161
MnO	1.7875	0.6527	0.6611	0.7436	1.9124	1.8527	1.8836	1.915	1.837	1.8491
FeO	45.8749	47.2245	47.269	47.1561	45.6857	45.4652	45.6875	45.2286	46.094	45.7634
Na2O	0.0006	0.01	0	0.007	0.0199	0.0187	0	0	0	0
Total	99.4498	98.5651	98.9247	99.16	98.9195	98.5105	98.3068	97.0263	99.1029	98.8346

Cation based on 12 oxygens										
Si	0.001	0.001	0.002	0.001	0.002	0	0.004	0.004	0.001	0.004
Ti	3.966	3.926	3.933	3.936	3.952	3.956	3.937	3.924	3.939	3.951
Al	0	0.003	0	0	0.002	0.001	0	0.003	0.003	0
Cr	0	0	0.002	0.001	0	0.001	0	0.001	0.002	0
Y	0	0	0	0	0	0	0	0	0	0
Mg	0	0.002	0.007	0.007	0	0.001	0	0.002	0.002	0
Ca	0.001	0.005	0.002	0.01	0.002	0.005	0.005	0.003	0	0.002
Mn	0.154	0.057	0.058	0.065	0.166	0.162	0.165	0.17	0.159	0.161
Fe	3.909	4.076	4.062	4.041	3.918	3.915	3.949	3.965	3.951	3.929
OH	0	0	0	0	0	0	0	0	0	0
Na	0	0.002	0	0.001	0.004	0.004	0	0	0	0
Total	8.032	8.072	8.065	8.062	8.047	8.045	8.06	8.071	8.058	8.046

Microprobe analysis of HF1467

Oxide Wt. %	Grt01 plg02	Grt01 plg03	Grt01 plg04	Grt01 plg05	Grt01 plg06	Grt01 plg07	Grt01 plg08	Grt01 plg09	Grt01 plg010
SiO2	61.3752	62.4509	61.0754	60.6452	61.4219	60.6004	60.7459	60.9388	60.4368
Al2O3	24.5826	23.8219	24.8908	24.579	24.4243	24.7931	24.9993	24.9338	24.9543
MgO	0	0.0059	0.0015	0	0.0125	0.0022	0	0	0.0125
CaO	5.724	5.1112	6.2353	6.1061	5.8415	6.3708	6.4848	6.168	6.2251
FeO	0.1865	0.2047	0.1024	0.1148	0.1409	0.0525	0.0457	0.1307	0.0494
Na2O	8.3783	8.675	8.0507	8.0225	8.3642	8.1123	8.1106	8.278	8.1366
K2O	0.0806	0.042	0.0967	0.0763	0.0582	0.0603	0.0275	0.048	0.0235
Total	100.3272	100.3115	100.4527	99.5441	100.2635	99.9916	100.4139	100.4974	99.8382

Cation based on 8 oxygens									
Si	2.718	2.759	2.703	2.707	2.721	2.696	2.692	2.697	2.692
Al	1.283	1.24	1.298	1.293	1.275	1.3	1.305	1.301	1.31
Mg	0	0	0	0	0.001	0	0	0	0.001
Ca	0.272	0.242	0.296	0.292	0.277	0.304	0.308	0.293	0.297
Fe	0.007	0.008	0.004	0.004	0.005	0.002	0.002	0.005	0.002
OH	0	0	0	0	0	0	0	0	0
Na	0.719	0.743	0.691	0.694	0.719	0.7	0.697	0.71	0.703
K	0.005	0.002	0.005	0.004	0.003	0.003	0.002	0.003	0.001
Total	5.003	4.994	4.996	4.996	5.002	5.005	5.005	5.009	5.005

Microprobe analysis of HFSP

Oxide Wt. %	HFSP r01	HFSP r02	HFSP r03	HFSP r04	HFSP r05	HFSP r06	HFSP r07	HFSP r08	HFSP r09	HFSP r010
SiO2	36.4723	36.3585	36.4195	36.9563	36.351	36.5865	36.6145	36.8874	34.3481	36.4897
TiO2	0.0025	0.0621	0	0.0044	0.0415	0.0051	0.0271	0.0102	3.2442	0.0283
Al2O3	20.831	20.6793	21.0088	21.2216	20.7844	20.8977	20.9542	21.0646	17.2618	20.8942
Cr2O3	0.0083	0.0327	0.0058	0	0	0.0179	0.0057	0	0.0175	0
Y2O3	0.057	0.0788	0.0114	0.0893	0.0118	0.031	0.0888	0.0804	0	0.0593
MgO	1.2804	1.1831	1.0749	1.5459	1.5585	1.3251	1.4641	0.943	6.1234	1.4616
CaO	1.9809	2.2947	1.9659	2.0299	1.8735	1.8695	2.5053	2.1872	0.0886	1.9818
MnO	11.4159	12.1826	12.3961	8.7818	8.6861	11.9758	10.9225	12.7249	0.5129	10.8669
FeO	27.502	26.2568	26.4495	29.927	30.1429	26.9824	27.4841	26.0426	23.9729	27.761
Na2O	0.0231	0.0153	0.0205	0.0183	0.0199	0.0189	0.037	0.0319	0.0552	0.0208
Total	99.5733	99.144	99.3524	100.5745	99.4695	99.7099	100.1033	99.9722	85.6246	99.5636

Cation based on 12 oxygens										
Si	2.986	2.989	2.986	2.987	2.979	2.989	2.978	3.002	3.079	2.984
Ti	0	0.004	0	0	0.003	0	0.002	0.001	0.219	0.002
Al	2.01	2.003	2.03	2.022	2.007	2.012	2.009	2.021	1.824	2.014
Cr	0.001	0.002	0	0	0	0.001	0	0	0.001	0
Y	0.002	0.003	0	0.004	0.001	0.001	0.004	0.003	0	0.003
Mg	0.156	0.145	0.131	0.186	0.19	0.161	0.178	0.114	0.818	0.178
Ca	0.174	0.202	0.173	0.176	0.164	0.164	0.218	0.191	0.009	0.174
Mn	0.792	0.848	0.861	0.601	0.603	0.829	0.753	0.877	0.039	0.753
Fe	1.883	1.805	1.814	2.023	2.066	1.844	1.87	1.773	1.797	1.898
OH	0	0	0	0	0	0	0	0	0	0
Na	0.004	0.002	0.003	0.003	0.003	0.003	0.006	0.005	0.01	0.003
Total	8.009	8.004	8	8.002	8.016	8.005	8.017	7.987	7.795	8.008

Microprobe analysis of HFSP

Oxide Wt. %	HFSP r011	HFSP r012	HFSP r013	HFSP r014	HFSP r015	HFSP r016	HFSP r017	HFSP r018	HFSP r019	HFSP r020
SiO2	36.8674	36.6543	36.7492	36.6693	36.4588	36.1064	36.4781	36.3453	36.4084	36.6374
TiO2	0.0396	0.0301	0	0.0587	0.0082	0.0203	0.0125	0.0289	0	0.0549
Al2O3	21.2372	20.9524	21.2185	21.0893	20.9768	20.9961	21.1239	21.0763	20.835	20.8817
Cr2O3	0.0178	0.0083	0	0	0.012	0.0083	0	0.0083	0	0.0102
Y2O3	0	0	0.0657	0.05	0.0398	0.053	0.0253	0.0185	0.0881	0.0376
MgO	1.041	0.9354	1.5381	1.4134	1.3843	1.7157	1.29	1.1646	1.2022	1.0652
CaO	2.105	2.0319	1.9617	1.9406	1.855	2.0717	1.8315	1.8815	2.5799	2.6523
MnO	12.9297	13.9252	8.7889	8.6536	8.7411	8.5565	11.9978	12.6405	12.0281	12.7907
FeO	26.0184	24.9496	30.2379	30.2873	30.3939	30.1672	26.9029	26.3477	26.1866	25.5422
Na2O	0.0142	0.0364	0.0277	0.0245	0.0066	0.0252	0.0117	0.0142	0.0319	0.0497
Total	100.2703	99.5236	100.5877	100.1867	99.8765	99.7202	99.6737	99.5258	99.3601	99.7221
Cation based on 12 oxygens										
Si	2.991	2.999	2.975	2.981	2.977	2.954	2.98	2.977	2.984	2.991
Ti	0.002	0.002	0	0.004	0.001	0.001	0.001	0.002	0	0.003
Al	2.031	2.02	2.025	2.02	2.019	2.024	2.034	2.034	2.013	2.009
Cr	0.001	0.001	0	0	0.001	0.001	0	0.001	0	0.001
Y	0	0	0.003	0.002	0.002	0.002	0.001	0.001	0.004	0.002
Mg	0.126	0.114	0.186	0.171	0.169	0.209	0.157	0.142	0.147	0.13
Ca	0.183	0.178	0.17	0.169	0.162	0.182	0.16	0.165	0.227	0.232
Mn	0.889	0.965	0.603	0.596	0.605	0.593	0.83	0.877	0.835	0.884
Fe	1.766	1.707	2.047	2.059	2.076	2.064	1.838	1.805	1.795	1.744
OH	0	0	0	0	0	0	0	0	0	0
Na	0.002	0.006	0.004	0.004	0.001	0.004	0.002	0.002	0.005	0.008
Total	7.991	7.992	8.013	8.006	8.012	8.034	8.003	8.005	8.01	8.004

Microprobe analysis of HFSP

Oxide Wt. %	HFSP r021	HFSP r022	HFSP r023	HFSP r024	HFSP c01	HFSP c02	HFSP c03	HFSP c04	HFSP c05	HFSP c06
SiO2	36.974	37.0622	35.6546	35.8474	36.866	36.7648	36.9015	36.8894	36.9051	36.8551
TiO2	0.0195	0.0276	0.0513	0.0264	0	0	0	0.0204	0	0
Al2O3	21.2663	21.3232	20.589	20.5996	21.1801	21.1358	21.2884	21.2076	21.2411	21.231
Cr2O3	0.0076	0	0.0051	0.0044	0	0	0.0089	0.0045	0.0108	0.0185
Y2O3	0.0535	0.0334	0.015	0.0181	0.1302	0.1025	0.0771	0.1023	0.1012	0.1287
MgO	0.9695	0.8599	1.2149	1.2424	1.9236	1.8227	1.9307	1.7361	1.8009	1.8281
CaO	1.7815	1.8381	2.3449	2.2961	1.9972	1.9575	2.0309	1.9365	1.9333	1.9161
MnO	12.7805	13.1283	12.1895	12.0317	8.8095	8.7712	8.5447	9.3972	9.1919	9.1447
FeO	26.3822	26.0786	26.5231	26.5196	29.5384	29.8066	29.5718	29.2187	29.2647	29.574
Na2O	0.0264	0.0319	0.0313	0.0102	0.0334	0.0173	0.0202	0.0246	0.0213	0.0349
Total	100.2612	100.3833	98.6188	98.5958	100.4783	100.3783	100.3741	100.5372	100.4704	100.7311
Cation based on 12 oxygens										
Si	3	3.003	2.958	2.969	2.979	2.978	2.981	2.982	2.982	2.975
Ti	0.001	0.002	0.003	0.002	0	0	0	0.001	0	0
Al	2.034	2.036	2.013	2.011	2.017	2.017	2.027	2.02	2.023	2.02
Cr	0	0	0	0	0	0	0.001	0	0.001	0.001
Y	0.002	0.001	0.001	0.001	0.006	0.004	0.003	0.004	0.004	0.006
Mg	0.117	0.104	0.15	0.153	0.232	0.22	0.233	0.209	0.217	0.22
Ca	0.155	0.16	0.208	0.204	0.173	0.17	0.176	0.168	0.167	0.166
Mn	0.878	0.901	0.856	0.844	0.603	0.602	0.585	0.643	0.629	0.625
Fe	1.79	1.767	1.84	1.837	1.996	2.019	1.998	1.975	1.978	1.996
OH	0	0	0	0	0	0	0	0	0	0
Na	0.004	0.005	0.005	0.002	0.005	0.003	0.003	0.004	0.003	0.005
Total	7.983	7.979	8.035	8.024	8.012	8.013	8.005	8.007	8.005	8.014

Microprobe analysis of HFSP

Oxide Wt. %	HFSP c07	HFSP c08	HFSP c09	HFSP c010	HFSP c011	HFSP c012
SiO2	36.9941	37.0939	37.0384	36.3705	36.7754	36.6226
TiO2	0.0146	0.0083	0	0.0334	0	0
Al2O3	21.1414	21.1595	21.0579	20.8213	21.068	21.1533
Cr2O3	0	0.021	0.0159	0.0222	0.0058	0.0025
Y2O3	0.1172	0.1256	0.1223	0.1078	0.1438	0.1208
MgO	2.3796	2.3959	2.3971	1.6381	1.7288	1.7212
CaO	2.4488	2.2565	2.3417	2.1083	1.9971	2.049
MnO	6.2966	6.2678	6.3991	9.9031	9.3623	9.4248
FeO	31.012	31.1458	31.0695	28.391	28.9322	28.9428
Na2O	0.0373	0.0041	0.0168	0.034	0.0215	0.0142
Total	100.4417	100.4785	100.4588	99.4297	100.0349	100.0512

Cation based on 12 oxygens						
Si						
Ti	2.98	2.986	2.984	2.978	2.986	2.975
Al	0.001	0.001	0	0.002	0	0
Cr	2.007	2.007	2	2.009	2.016	2.025
Y	0	0.001	0.001	0.001	0	0
Mg	0.005	0.005	0.005	0.005	0.006	0.005
Ca	0.286	0.287	0.288	0.2	0.209	0.208
Mn	0.211	0.195	0.202	0.185	0.174	0.178
Fe	0.43	0.427	0.437	0.687	0.644	0.649
OH	2.089	2.097	2.094	1.944	1.965	1.966
Na	0	0	0	0	0	0
Total	0.006	0.001	0.003	0.005	0.003	0.002
	8.016	8.007	8.014	8.016	8.004	8.01

Microprobe analysis of HFSP

Oxide Wt. %	HFSP bt01	HFSP bt02	HFSP bt03	HFSP bt04	HFSP bt05	HFSP bt06	HFSP bt07	HFSP bt08	HFSP bt09	HFSP bt010
SiO2	34.6507	34.9401	35.0045	35.0925	34.8088	34.8708	34.6216	35.2056	33.5004	34.9747
TiO2	2.3058	2.4319	2.6245	2.7412	3.0056	2.7885	2.8332	2.1253	3.2736	2.4011
Al2O3	18.0307	17.8051	18.4764	18.2786	17.8207	17.6765	17.4585	18.1157	17.2407	17.9833
MgO	6.4881	6.5522	6.6337	7.0926	8.0597	6.2526	6.3505	6.4681	6.1112	6.6173
CaO	0.0156	0.0054	0	0.0014	0.0592	0.0219	0.0196	0.0271	0.0921	0.0472
MnO	0.4287	0.4516	0.4715	0.2415	0.195	0.5485	0.4809	0.4902	0.559	0.4196
FeO	23.3464	23.8432	22.8679	22.5606	20.7346	23.9754	24.3203	23.9395	24.0978	23.8056
H2O	3.8312	3.8513	3.8776	3.8883	3.858	3.8518	3.8383	3.8709	3.7642	3.8618
Na2O	0.0855	0.0746	0.0624	0.0817	0.1228	0.0537	0.0586	0.0615	0.0476	0.0938
K2O	9.8006	9.5781	9.6597	9.8779	9.7049	9.7406	9.6493	9.7362	9.1101	9.4885
Total	98.9832	99.5337	99.6781	99.8564	98.3692	99.7804	99.6307	100.0402	97.7967	99.6927

Cation based on 22 oxygens										
Si	5.424	5.44	5.414	5.412	5.411	5.429	5.409	5.454	5.337	5.431
Ti	0.271	0.285	0.305	0.318	0.351	0.326	0.333	0.248	0.392	0.28
Al	3.326	3.267	3.368	3.322	3.265	3.243	3.215	3.308	3.237	3.291
Mg	1.514	1.521	1.529	1.631	1.868	1.451	1.479	1.494	1.451	1.532
Ca	0.003	0.001	0	0	0.01	0.004	0.003	0.005	0.016	0.008
Mn	0.057	0.06	0.062	0.032	0.026	0.072	0.064	0.064	0.075	0.055
Fe	3.056	3.105	2.958	2.91	2.695	3.122	3.178	3.102	3.211	3.091
OH	4	4	4	4	4	4	4	4	4	4
Na	0.026	0.023	0.019	0.024	0.037	0.016	0.018	0.018	0.015	0.028
K	1.957	1.903	1.906	1.943	1.924	1.935	1.923	1.924	1.852	1.88
Total	19.633	19.604	19.56	19.593	19.587	19.598	19.621	19.616	19.585	19.597

Microprobe analysis of HFSP

Oxide Wt. %	HFSP bt011	HFSP bt012	HFSP bt013	HFSP bt014	HFSP bt015	HFSP bt016	HFSP bt017	HFSP bt018	HFSP bt019	HFSP bt020
SiO2	34.9972	35.1087	34.9668	34.9397	35.0381	34.6102	34.2241	34.8422	34.7648	34.7994
TiO2	2.7311	2.5981	2.9872	2.9086	3.1917	3.0852	2.7341	2.7772	2.8765	2.925
Al2O3	18.5438	17.164	19.4399	19.8841	17.8655	17.8499	17.7357	17.6914	17.6696	17.7763
MgO	6.5176	6.5759	6.8428	6.5971	8.0739	7.7977	6.1724	6.3592	6.4227	6.3085
CaO	0.063	0.051	0.0661	0.0523	0.0627	0.0424	0.0952	0	0.095	0.0832
MnO	0.4594	0.5349	0.289	0.3011	0.2197	0.2334	0.5695	0.6471	0.4602	0.5332
FeO	23.1526	24.7192	21.5146	21.5027	20.8777	20.9215	24.5865	23.9713	24.4845	24.4939
H2O	3.8906	3.8646	3.9037	3.9043	3.884	3.8453	3.8133	3.8501	3.8628	3.8656
Na2O	0.0513	0.0494	0.1036	0.0885	0.1093	0.1444	0.0682	0.0576	0.0663	0.0539
K2O	9.8189	9.8442	9.1119	8.8063	9.6804	9.642	8.7289	9.3727	9.4298	9.2668
Total	100.2256	100.5099	99.2256	98.9847	99.0029	98.1719	98.728	99.5687	100.1321	100.1058
Cation based on 22 oxygens										
Si	5.394	5.448	5.371	5.366	5.41	5.397	5.382	5.427	5.397	5.398
Ti	0.317	0.303	0.345	0.336	0.371	0.362	0.323	0.325	0.336	0.341
Al	3.369	3.139	3.52	3.599	3.251	3.281	3.287	3.248	3.233	3.25
Mg	1.498	1.521	1.567	1.511	1.858	1.813	1.447	1.477	1.486	1.459
Ca	0.01	0.008	0.011	0.009	0.01	0.007	0.016	0	0.016	0.014
Mn	0.06	0.07	0.038	0.039	0.029	0.031	0.076	0.085	0.061	0.07
Fe	2.984	3.208	2.764	2.762	2.696	2.729	3.234	3.122	3.179	3.178
OH	4	4	4	4	4	4	4	4	4	4
Na	0.015	0.015	0.031	0.026	0.033	0.044	0.021	0.017	0.02	0.016
K	1.931	1.949	1.786	1.726	1.907	1.918	1.751	1.862	1.868	1.834
Total	19.578	19.661	19.432	19.374	19.564	19.581	19.537	19.564	19.595	19.56

Microprobe analysis of HFSP

	HFSP bt021	HFSP bt022	HFSP bt023	HFSP bt024
SiO2	35.244	35.4266	34.7369	35.9121
TiO2	2.1646	2.1591	3.0575	2.8134
Al2O3	18.1419	18.1362	16.6686	18.1971
MgO	6.6392	6.6777	6.526	7.0144
CaO	0.0487	0.0727	0.0543	0.0829
MnO	0.5144	0.494	0.6029	0.7479
FeO	23.8845	24.0637	24.0496	23.6405
H2O	3.8799	3.8916	3.8157	3.9535
Na2O	0.0665	0.067	0.0607	0.0371
K2O	9.5656	9.3557	9.3674	9.1382
Total	100.1493	100.3443	98.9396	101.5372
Cation based on 12 oxygens				
Si	5.447	5.459	5.459	5.447
Ti	0.252	0.25	0.361	0.321
Al	3.305	3.294	3.087	3.253
Mg	1.53	1.534	1.529	1.586
Ca	0.008	0.012	0.009	0.013
Mn	0.067	0.064	0.08	0.096
Fe	3.087	3.101	3.161	2.999
OH	4	4	4	4
Na	0.02	0.02	0.018	0.011
K	1.886	1.839	1.878	1.768
Total	19.602	19.574	19.584	19.495

Microprobe analysis of IS370

Oxide Wt. %	IS307 Grt04 r01	IS307 Grt04 r02	IS307 Grt04 r03	IS307 Grt04 r04	IS307 Grt04 r05	IS307 Grt04 r06	IS307 Grt04 r07	IS307 Grt04 r08
SiO2	0.0718	0.0624	0.2431	0.037	0.1703	0.0295	0.1243	0.0671
TiO2	0	0.0217	0.1195	0.0394	0	0	0	0.0656
Al2O3	0	0.005	0.102	0.0013	0.1348	0.0032	0.1879	0.1416
Cr2O3	0	0.0123	0.0015	0	0.0167	0	0	0
Y2O3	0.0499	0.0491	0.0351	0.0607	0.0837	0.0981	0.1185	0.1235
MgO	0.0162	0	0.017	0.0069	0.0343	0.0024	0.013	0.002
CaO	56.6038	55.8629	56.1625	55.8001	55.3743	55.6057	55.0273	55.062
MnO	0.0335	0.0259	0.0233	0.0483	0.1141	0.1045	0.0432	0.0466
FeO	0.243	0.1806	0.2578	0.1117	0.3589	0.2004	0.1504	0.1273
Na2O	0.0318	0.0162	0.0222	0.0559	0.0753	0.0603	0.0549	0.0419
Total	57.0501	56.2362	56.984	56.1613	56.3624	56.104	55.7195	55.6776
Cation based on 12 oxygens								
Si	0.014	0.012	0.048	0.007	0.034	0.006	0.025	0.013
Ti	0	0.003	0.018	0.006	0	0	0	0.01
Al	0	0.001	0.024	0	0.032	0.001	0.044	0.034
Cr	0	0.002	0	0	0.003	0	0	0
Y	0.005	0.005	0.004	0.006	0.009	0.01	0.013	0.013
Mg	0.005	0	0.005	0.002	0.01	0.001	0.004	0.001
Ca	11.908	11.919	11.773	11.924	11.765	11.908	11.818	11.845
Mn	0.006	0.004	0.004	0.008	0.019	0.018	0.007	0.008
Fe	0.04	0.03	0.042	0.019	0.06	0.033	0.025	0.021
Na	0.012	0.006	0.008	0.022	0.029	0.023	0.021	0.016
Total	11.989	11.983	11.925	11.994	11.959	12	11.957	11.961

Microprobe analysis of IS370

Oxide Wt. %	IS307 Grt04 r09	IS307 Grt04 c01	IS307 Grt04 c02	IS307 Grt04 c03	IS307 Grt04 r010	IS307 Grt04 r011	IS307 Grt04 r012	IS307 Grt04 r013
SiO2	3.5791	0.0204	0.046	0.0392	0.0248	0.0249	0.0168	0.0301
TiO2	0	0	0.0306	0	0.0138	0.0123	0	0.0262
Al2O3	0	0.0126	0	0.0062	0.0967	0.0119	0	0.0076
Cr2O3	0.005	0.0059	0.0058	0	0	0	0.0043	0.0321
Y2O3	0.1111	0.1082	0.1201	0.103	0.1202	0.1297	0.199	0.1162
MgO	1.1532	0	0	0.0105	0.0126	0	0	0.0024
CaO	48.3674	55.8317	56.5722	55.994	55.6906	55.1211	55.484	54.5578
MnO	0.0866	0.025	0.0216	0.0276	0.1022	0.1133	0.121	0.0681
FeO	4.975	0.0232	0.0224	0.0413	0.2263	0.2006	0.1862	0.3846
Na2O	0.0713	0.0482	0.0672	0.0377	0.0766	0.1048	0.0893	0.0898
Total	58.3486	56.0752	56.8859	56.2596	56.3639	55.7186	56.1005	55.3149
Cation based on 12 oxygens								
Si	0.66	0.004	0.009	0.008	0.005	0.005	0.003	0.006
Ti	0	0	0.005	0	0.002	0.002	0	0.004
Al	0	0.003	0	0.001	0.023	0.003	0	0.002
Cr	0.001	0.001	0.001	0	0	0	0.001	0.005
Y	0.011	0.012	0.013	0.011	0.013	0.014	0.021	0.013
Mg	0.317	0	0	0.003	0.004	0	0	0.001
Ca	9.553	11.951	11.933	11.944	11.86	11.888	11.892	11.855
Mn	0.014	0.004	0.004	0.005	0.017	0.019	0.02	0.012
Fe	0.767	0.004	0.004	0.007	0.038	0.034	0.031	0.065
Na	0.025	0.019	0.026	0.015	0.03	0.041	0.035	0.035
Total	11.347	11.998	11.993	11.993	11.99	12.005	12.003	11.998

Microprobe analysis of IS370

Oxide Wt. %	IS307 Grt04 r014	IS307 Grt04 r015	IS307 Grt04 r016	IS307 Grt04 r017	IS307 Grt04 r018	IS307 Grt04 c04	IS307 Grt04 c05	IS307 Grt04 c06
SiO2	0.0726	1.361	0.9287	0.0505	0.0684	0.0223	0.0189	0.0177
TiO2	0	0.0215	0.218	0.0259	0	0.0197	0	0
Al2O3	0.0069	0.8496	0.7917	0	0.005	0	0.0031	0
Cr2O3	0	0	0	0	0.0014	0	0	0.0159
Y2O3	0.1469	0.027	0.0443	0.0483	0.0406	0.181	0.1279	0.1724
MgO	0.0092	0.1803	0.2341	0.0056	0	0	0	0.0181
CaO	55.8266	49.3186	53.9337	55.9725	56.2292	55.2375	55.8096	54.9472
MnO	0.0848	0.0377	0.0399	0.0432	0.0507	0.0955	0.0864	0.1401
FeO	0.4434	3.8308	0.994	0.3038	0.2938	0.0148	0.0161	0.0727
Na2O	0.0679	0.0292	0.0335	0.0468	0.0436	0.105	0.1174	0.1111
Total	56.6583	55.6557	57.2179	56.4968	56.7327	55.6757	56.1793	55.4952
Cation based on 12 oxygens								
Si	0.014	0.269	0.178	0.01	0.014	0.004	0.004	0.004
Ti	0	0.003	0.031	0.004	0	0.003	0	0
Al	0.002	0.198	0.179	0	0.001	0	0.001	0
Cr	0	0	0	0	0	0	0	0.003
Y	0.015	0.003	0.005	0.005	0.004	0.019	0.014	0.019
Mg	0.003	0.053	0.067	0.002	0	0	0	0.005
Ca	11.842	10.455	11.068	11.896	11.899	11.917	11.931	11.898
Mn	0.014	0.006	0.006	0.007	0.008	0.016	0.015	0.024
Fe	0.073	0.634	0.159	0.05	0.049	0.002	0.003	0.012
Na	0.026	0.011	0.012	0.018	0.017	0.041	0.045	0.044
Total	11.99	11.633	11.705	11.993	11.992	12.003	12.012	12.008

Microprobe analysis of IS370

Oxide Wt. %	IS307 Grt04 r014	IS307 Grt04 r015	IS307 Grt04 r016	IS307 Grt04 r017	IS307 Grt04 r018	IS307 Grt04 c04	IS307 Grt04 c05	IS307 Grt04 c06
SiO2	0.0726	1.361	0.9287	0.0505	0.0684	0.0223	0.0189	0.0177
TiO2	0	0.0215	0.218	0.0259	0	0.0197	0	0
Al2O3	0.0069	0.8496	0.7917	0	0.005	0	0.0031	0
Cr2O3	0	0	0	0	0.0014	0	0	0.0159
Y2O3	0.1469	0.027	0.0443	0.0483	0.0406	0.181	0.1279	0.1724
MgO	0.0092	0.1803	0.2341	0.0056	0	0	0	0.0181
CaO	55.8266	49.3186	53.9337	55.9725	56.2292	55.2375	55.8096	54.9472
MnO	0.0848	0.0377	0.0399	0.0432	0.0507	0.0955	0.0864	0.1401
FeO	0.4434	3.8308	0.994	0.3038	0.2938	0.0148	0.0161	0.0727
Na2O	0.0679	0.0292	0.0335	0.0468	0.0436	0.105	0.1174	0.1111
Total	56.6583	55.6557	57.2179	56.4968	56.7327	55.6757	56.1793	55.4952

Cation based on 12 oxygens								
Si	0.014	0.269	0.178	0.01	0.014	0.004	0.004	0.004
Ti	0	0.003	0.031	0.004	0	0.003	0	0
Al	0.002	0.198	0.179	0	0.001	0	0.001	0
Cr	0	0	0	0	0	0	0	0.003
Y	0.015	0.003	0.005	0.005	0.004	0.019	0.014	0.019
Mg	0.003	0.053	0.067	0.002	0	0	0	0.005
Ca	11.842	10.455	11.068	11.896	11.899	11.917	11.931	11.898
Mn	0.014	0.006	0.006	0.007	0.008	0.016	0.015	0.024
Fe	0.073	0.634	0.159	0.05	0.049	0.002	0.003	0.012
Na	0.026	0.011	0.012	0.018	0.017	0.041	0.045	0.044
Total	11.99	11.633	11.705	11.993	11.992	12.003	12.012	12.008

Microprobe analysis of IS370

Oxide Wt. %	IS307 Grt01 r01	IS307 Grt01 r02	IS307 Grt01 r03	IS307 Grt01 r04	IS307 Grt01 r05	IS307 Grt01 r06	IS307 Grt01 r07	IS307 Grt01 r08
SiO2	36.783	36.798	36.7771	35.9571	36.1987	19.2036	37.0034	36.7668
TiO2	0.0128	0.0013	0.0215	0.0456	0	0.0236	0.0295	0.0702
Al2O3	21.2327	21.2581	21.3241	22.1198	21.132	15.249	21.4132	21.3835
Cr2O3	0.0095	0	0.0132	0.0038	0.0064	0.0055	0.0057	0.0278
Y2O3	0	0.0184	0.0046	0	0	0	0.0388	0.0295
MgO	2.5797	2.7258	2.6734	2.6467	2.7419	7.8749	3.6986	3.6771
CaO	1.4496	1.4431	1.4977	1.4516	1.506	0.1714	1.2401	1.3077
MnO	3.7399	3.6227	3.7985	4.076	3.7159	0.7959	2.1073	2.0279
FeO	34.0044	34.2868	34.0399	32.9795	34.0742	33.3359	34.507	34.8796
Na2O	0.0308	0	0	0.0092	0.0062	0.0048	0.0178	0.0066
Total	99.8423	100.1542	100.1499	99.2894	99.3813	76.6647	100.0615	100.1768

Cation based on 12 oxygens								
Si	2.979	2.973	2.97	2.923	2.953	2.176	2.971	2.956
Ti	0.001	0	0.001	0.003	0	0.002	0.002	0.004
Al	2.027	2.024	2.03	2.119	2.032	2.037	2.026	2.026
Cr	0.001	0	0.001	0	0	0	0	0.002
Y	0	0.001	0	0	0	0	0.002	0.001
Mg	0.311	0.328	0.322	0.321	0.333	1.33	0.443	0.441
Ca	0.126	0.125	0.13	0.126	0.132	0.021	0.107	0.113
Mn	0.257	0.248	0.26	0.281	0.257	0.076	0.143	0.138
Fe	2.303	2.316	2.299	2.242	2.324	3.159	2.317	2.345
Na	0.005	0	0	0.001	0.001	0.001	0.003	0.001
Total	8.009	8.015	8.013	8.016	8.032	8.804	8.014	8.026

Microprobe analysis of IS370

Oxide Wt. %	IS307 Grt01 r09	IS307 Grt01 c01	IS307 Grt01 c02	IS307 Grt01 c03	IS307 Grt01 c04	IS307 Grt03 r01	IS307 Grt03 r02	IS307 Grt03 r03
SiO2	36.853	36.8457	37.0626	36.85	24.5416	36.6958	36.8653	36.8741
TiO2	0	0.0404	0.0154	0.0109	0.0075	0.0083	0.0529	0
Al2O3	21.4459	21.3986	21.4654	21.3513	20.1351	21.2293	21.38	21.0463
Cr2O3	0.0044	0.0247	0.0127	0	0.0012	0.0152	0	0
Y2O3	0.0023	0	0.0143	0.061	0	0	0.0161	0
MgO	3.7399	3.8656	3.7297	3.5928	9.0873	3.3358	3.3218	3.2863
CaO	1.2732	1.2546	1.2743	1.3542	0.0559	1.207	1.2099	1.302
MnO	2.1129	1.9902	2.1275	2.2803	0.7872	2.8302	2.8991	2.8914
FeO	34.8906	34.7188	34.5928	34.5387	33.6974	34.6853	34.6243	34.5522
Na2O	0	0.0025	0.0143	0.0015	0	0	0.0148	0
Total	100.3221	100.1411	100.3091	100.0407	88.3132	100.007	100.3841	99.9523
Cation based on 12 oxygens								
Si	2.957	2.959	2.969	2.965	2.316	2.963	2.963	2.978
Ti	0	0.002	0.001	0.001	0.001	0.001	0.003	0
Al	2.028	2.025	2.027	2.025	2.24	2.02	2.025	2.003
Cr	0	0.002	0.001	0	0	0.001	0	0
Y	0	0	0.001	0.003	0	0	0.001	0
Mg	0.447	0.463	0.445	0.431	1.279	0.402	0.398	0.396
Ca	0.109	0.108	0.109	0.117	0.006	0.104	0.104	0.113
Mn	0.144	0.135	0.144	0.155	0.063	0.194	0.197	0.198
Fe	2.342	2.332	2.318	2.324	2.66	2.342	2.327	2.334
Na	0	0	0.002	0	0	0	0.002	0
Total	8.028	8.026	8.017	8.021	8.563	8.026	8.022	8.021

Microprobe analysis of IS370

Oxide Wt. %	IS307 Grt03 c01	IS307 Grt03 c02	IS307 Grt03 c03	IS307 Grt03 r04	IS307 Grt03 r05	IS307 Grt03 r06
SiO2	37.0292	36.9958	37.279	36.9796	37.1415	36.4263
TiO2	0.0559	0	0.032	0.0038	0	0.0208
Al2O3	21.3348	21.3945	21.3839	21.0997	21.0777	20.9681
Cr2O3	0.0204	0.0287	0	0	0	0.0208
Y2O3	0.0032	0	0.0074	0	0	0
MgO	3.1701	3.0745	3.0284	1.7386	0.1906	1.4552
CaO	1.3782	1.3662	1.4803	1.5393	1.4923	1.4983
MnO	3.2403	3.2729	3.3516	6.5523	3.1366	7.2109
FeO	34.6561	34.4424	34.4046	31.9955	29.0534	31.5995
Na2O	0.0113	0	0.0092	0.0103	0.8076	0.0103
Total	100.8995	100.575	100.9763	99.9191	92.8996	99.2102
Cation based on 12 oxygens						
Si	2.966	2.97	2.98	3.002	3.157	2.988
Ti	0.003	0	0.002	0	0	0.001
Al	2.014	2.024	2.014	2.019	2.112	2.027
Cr	0.001	0.002	0	0	0	0.001
Y	0	0	0	0	0	0
Mg	0.379	0.368	0.361	0.21	0.024	0.178
Ca	0.118	0.118	0.127	0.134	0.136	0.132
Mn	0.22	0.223	0.227	0.451	0.226	0.501
Fe	2.321	2.312	2.3	2.172	2.065	2.168
Na	0.002	0	0.001	0.002	0.133	0.002
Total	8.024	8.017	8.012	7.989	7.853	7.997

Microprobe analysis of IS370

Oxide Wt. %	IS307 Grt04 bt01	IS307 Grt04 bt02	IS307 Grt04 bt03	IS307 Grt04 bt04	IS307 Grt04 bt05	IS307 Grt04 bt06	IS307 Grt04 bt07	IS307 Grt04 bt08
SiO2	27.1706	26.7851	26.4509	24.9634	27.9217	26.2561	27.0618	27.2737
TiO2	0.8043	0.4972	0.4068	0.3243	0.8426	0.8802	0.3626	0.8767
Al2O3	17.8837	18.2835	17.7894	17.0769	18.5021	18.665	18.6978	18.1024
MgO	8.3461	8.4812	8.1076	7.7925	8.381	8.3349	8.8182	8.6014
CaO	0.1921	0.2537	0.2323	4.1975	0.4282	0.4532	0.4854	0.466
MnO	0.3786	0.3924	0.3571	0.3695	0.38	0.3714	0.38	0.3494
FeO	33.5559	33.782	34.494	31.5708	32.0771	31.9338	33.275	32.1644
H2O	3.5036	3.5006	3.452	3.3687	3.56	3.4686	3.5378	3.5153
Na2O	0.0086	0	0.0041	0.002	0.0237	0.0168	0.0197	0.0173
K2O	0.5179	0.4458	0.2989	0.2392	1.0365	0.7388	0.364	0.8845
Total	92.3613	92.4213	91.5931	89.9048	93.153	91.1188	93.0024	92.2512
Cation based on 22 oxygens								
Si	4.65	4.588	4.595	4.444	4.703	4.539	4.587	4.653
Ti	0.104	0.064	0.053	0.043	0.107	0.114	0.046	0.112
Al	3.608	3.691	3.642	3.583	3.673	3.803	3.735	3.639
Mg	2.13	2.166	2.1	2.068	2.105	2.148	2.228	2.187
Ca	0.035	0.047	0.043	0.801	0.077	0.084	0.088	0.085
Mn	0.055	0.057	0.053	0.056	0.054	0.054	0.055	0.05
Fe	4.803	4.84	5.011	4.7	4.519	4.617	4.717	4.589
OH	4	4	4	4	4	4	4	4
Na	0.003	0	0.001	0.001	0.008	0.006	0.006	0.006
K	0.113	0.097	0.066	0.054	0.223	0.163	0.079	0.192
Total	19.5	19.551	19.565	19.749	19.469	19.529	19.542	19.514

Microprobe analysis of IS370

Oxide Wt. %	IS307 Grt04 bt09	S307 Grt04 bt010	S307 Grt04 bt011	S307 Grt04 bt012	S307 Grt04 bt013	S307 Grt04 bt014	S307 Grt04 bt015	S307 Grt04 bt016
SiO2	10.3241	27.6562	28.4124	4.7014	27.1125	47.5637	28.6353	27.1706
TiO2	0.2159	1.4979	1.057	0.0836	0.8757	0.502	3.5321	1.0487
Al2O3	6.6745	17.3902	17.7844	2.5011	17.5839	32.1148	17.0648	17.4979
MgO	3.0501	8.2642	8.554	0.9122	8.3195	1.7052	7.8859	8.5086
CaO	36.2611	0.9504	0.4244	46.8157	0.2377	0.1004	2.8718	0.3087
MnO	0.1101	0.3994	0.3517	0.0987	0.3377	0.0219	0.3269	0.3774
FeO	13.2986	33.0313	32.8952	6.45	33.1138	3.8867	29.9703	32.1808
H2O	2.3864	3.5446	3.5889	1.9372	3.4797	4.5004	3.6357	3.4793
Na2O	0.0165	0.0102	0.002	0.0342	0.0118	0.1189	0	0
K2O	0.2329	0.6577	1.2459	0.1423	0.5981	10.0584	0.7145	0.856
Total	72.5703	93.402	94.3158	63.6765	91.6704	100.5725	94.6372	91.4279
Cation based on 22 oxygens								
Si	2.594	4.679	4.747	1.455	4.672	6.338	4.723	4.683
Ti	0.041	0.191	0.133	0.019	0.113	0.05	0.438	0.136
Al	1.977	3.467	3.502	0.912	3.571	5.043	3.317	3.554
Mg	1.143	2.084	2.131	0.421	2.137	0.339	1.939	2.186
Ca	9.763	0.172	0.076	15.527	0.044	0.014	0.508	0.057
Mn	0.023	0.057	0.05	0.026	0.049	0.002	0.046	0.055
Fe	2.795	4.673	4.597	1.67	4.773	0.433	4.134	4.638
OH	4	4	4	4	4	4	4	4
Na	0.008	0.003	0.001	0.021	0.004	0.031	0	0
K	0.075	0.142	0.266	0.056	0.131	1.71	0.15	0.188
Total	22.418	19.469	19.502	24.107	19.496	17.961	19.255	19.498

Microprobe analysis of IS370

Oxide Wt. %	S307 Grt04 bt017	S307 Grt04 bt018	IS307 Grt01 bt01	IS307 Grt01 bt02	IS307 Grt01 bt03	IS307 Grt01 bt04	IS307 Grt01 bt05	IS307 Grt01 bt06
SiO2	28.3676	28.1572	47.2466	44.1655	46.6806	43.3064	47.3848	47.2886
TiO2	1.216	1.0468	0.2827	0.8121	0.3065	0.2604	0.1213	0.135
Al2O3	17.613	17.6848	32.457	28.5336	33.1628	28.514	26.6692	32.9382
MgO	8.4716	8.3982	1.5643	2.9896	1.595	3.1206	1.0438	1.4529
CaO	0.266	0.2734	0.0637	0.0178	0	0.0482	0.7888	0.0659
MnO	0.2964	0.3443	0.0671	0.1076	0.0749	0.1448	0.0655	0.0917
FeO	31.6115	31.514	2.9672	8.215	3.1998	8.0308	2.1467	2.8529
H2O	3.5544	3.5316	4.4818	4.3213	4.4894	4.2452	4.2039	4.4916
Na2O	0	0.0066	0.3552	0.3009	0.2089	0.1126	3.4419	0.3969
K2O	1.7213	1.4791	10.7287	10.6738	10.8702	10.4688	7.1164	10.4838
Total	93.1178	92.4359	100.2142	100.1372	100.5881	98.2517	92.9821	100.1975
Cation based on 22 oxygens								
Si	4.786	4.781	6.322	6.129	6.235	6.117	6.759	6.313
Ti	0.154	0.134	0.028	0.085	0.031	0.028	0.013	0.014
Al	3.502	3.539	5.118	4.667	5.221	4.747	4.484	5.183
Mg	2.131	2.126	0.312	0.618	0.318	0.657	0.222	0.289
Ca	0.048	0.05	0.009	0.003	0	0.007	0.121	0.009
Mn	0.042	0.05	0.008	0.013	0.008	0.017	0.008	0.01
Fe	4.46	4.475	0.332	0.953	0.357	0.949	0.256	0.319
OH	4	4	4	4	4	4	4	4
Na	0	0.002	0.092	0.081	0.054	0.031	0.952	0.103
K	0.37	0.32	1.831	1.89	1.852	1.887	1.295	1.786
Total	19.494	19.477	18.053	18.438	18.077	18.44	18.109	18.026

Microprobe analysis of IS370

Oxide Wt. %	IS307 Grt01 bt07	IS307 Grt01 bt08	IS307 Grt01 bt09	IS307 Grt03 bt01	IS307 Grt03 bt02	IS307 Grt03 bt03	IS307 Grt03 bt04	IS307 Grt03 bt05
SiO2	88.914	45.5408	40.5007	28.481	29.0918	30.2593	47.1755	46.7506
TiO2	0.0295	0.2819	0.2547	0.3753	0.6483	0.4289	0.6801	0.3125
Al2O3	5.3451	30.1478	26.4099	17.4854	17.8448	17.1623	31.9915	29.9146
MgO	0.3274	2.7517	4.5248	8.3704	8.5678	7.4542	1.459	2.025
CaO	0.0288	0.0959	0.043	0.1156	0.1337	0.2109	0.0122	0.0551
MnO	0.0444	0.0541	0.1676	0.3113	0.3491	0.3687	0.0131	0.0722
FeO	0.996	5.9173	13.709	28.7929	29.2724	29.4755	2.9473	3.2277
H2O	5.1775	4.3689	4.1397	3.4699	3.5472	3.5473	4.4575	4.3479
Na2O	0.0278	0.127	0.1101	0.0315	0.0119	0.0407	0.1647	0.1282
K2O	1.8902	9.6526	8.3002	2.9577	2.7045	3.5995	10.6241	10.4918
Total	102.7808	98.9381	98.1597	90.3911	92.1714	92.5474	99.525	97.3254
Cation based on 22 oxygens								
Si	10.298	6.251	5.867	4.922	4.918	5.115	6.347	6.448
Ti	0.003	0.029	0.028	0.049	0.082	0.055	0.069	0.032
Al	0.73	4.877	4.509	3.561	3.555	3.419	5.072	4.863
Mg	0.057	0.563	0.977	2.156	2.159	1.879	0.293	0.416
Ca	0.004	0.014	0.007	0.021	0.024	0.038	0.002	0.008
Mn	0.004	0.006	0.021	0.046	0.05	0.053	0.001	0.008
Fe	0.096	0.679	1.661	4.161	4.139	4.167	0.332	0.372
OH	4	4	4	4	4	4	4	4
Na	0.006	0.034	0.031	0.011	0.004	0.013	0.043	0.034
K	0.279	1.69	1.534	0.652	0.583	0.776	1.823	1.846
Total	15.477	18.144	18.633	19.58	19.515	19.515	17.982	18.029

Microprobe analysis of IS370

Oxide Wt. %	IS307 Grt03 bt06	IS307 Grt03 bt07	IS307 Grt03 bt08	IS307 Grt03 bt09
SiO2	42.6704	33.8143	33.1394	32.3194
TiO2	0.3372	2.4214	2.7087	2.2949
Al2O3	29.6356	17.6767	17.3923	17.3517
MgO	3.1431	6.545	6.4567	6.8694
CaO	0.0531	0.0387	0.0144	0.0922
MnO	0.0896	0.3137	0.3607	0.3288
FeO	9.4937	25.1881	25.8924	26.9864
H2O	4.2672	3.7842	3.7598	3.7216
Na2O	0.186	0.0325	0.0346	0.0378
K2O	8.4224	8.0704	8.155	7.1255
Total	98.2982	97.8848	97.9139	97.1277
Cation based on 22 oxygens				
Si	5.996	5.359	5.286	5.208
Ti	0.036	0.289	0.325	0.278
Al	4.908	3.301	3.269	3.295
Mg	0.658	1.546	1.535	1.65
Ca	0.008	0.007	0.002	0.016
Mn	0.011	0.042	0.049	0.045
Fe	1.116	3.338	3.454	3.637
OH	4	4	4	4
Na	0.051	0.01	0.011	0.012
K	1.51	1.632	1.659	1.465
Total	18.294	19.523	19.59	19.605

VITA

Christopher Howard was born October 10th, 1978 in East Ridge, Tennessee. His interest in geology was kindled while working as a draftsman at a civil engineering firm (ARCADIS) in Chattanooga, Tennessee. While attending the University of Tennessee, Chattanooga he developed a passion for structural geology and geologic field work. Aside from geology he enjoys spending time with his family (Tonya, Torin, and Logan), brewing beer, and camping. Christopher is grateful to his mentors (especially Jonathan W. Mies and Robert D. Hatcher, Jr.) for their encouragement, patience, and support.